Life-Cycle Cost-Based Optimal Seismic Design of Structures with Energy Dissipation Devices

Hyun Shin

Dissertation submitted to the faculty of the
Virginia Polytechnic Institute and State University
in partial fulfillment of the requirements for the degree of

Doctor of Philosophy
in
Civil Engineering

Mahendra P. Singh, Co-Chair
Raymond H. Plaut, Co-Chair
Carin L. Roberts-Wollmann
Finley A. Charney
Rakesh K. Kapania

November 16, 2010
Blacksburg, Virginia

Keywords: Passive Device, Life-Cycle Cost, Structural Optimization

Life-Cycle Cost-Based Optimal Seismic Design of Structures with Energy Dissipation Devices

Hyun Shin

(ABSTRACT)

Seismic designs of building structures are currently made based on the design criterion of life-safety and this requires that the structures do not collapse to compromise safety of people in the structure, but they can be designed to experience some damage. However, this design approach has allowed large economic losses primarily due to the damage to the nonstructural components at relatively moderate levels of seismic intensities. This led to a new thinking about design approach called performance-based design approach that satisfies the life-safety objective at the same time, reduces the economic loss to an acceptable level. The performance-based design approaches are multi-level design that addresses several different levels of structural performances under different levels of seismic intensities. In this study, we have investigated the use of energy dissipating damping devices to achieve the performance of a building structure in a desirable manner over all levels of seismic intensity. Since the initial motivation of performance-based design was reducing economic loss, the life-cycle cost-based optimization is considered in this study to obtain the optimal designs with different damping devices. For the optimal design, three types of devices are used in this study: fluid viscous dampers, solid visco-elastic dampers, and yielding metallic dampers. The combinations of two different types of dampers are also examined in this study. The genetic algorithm (GA) approach is adopted as an optimizer that searches for the optimal solution in an iterative manner. Numerical results from the application of the optimal design to the selected model building are presented to demonstrate the

applicability of the developed approach and to estimate the effectiveness of the obtained optimal design with each device. It is shown in the results that the optimal design with each individual damping devices or the combination of two different types of damping devices are very effective in reducing the expected failure cost as well as the displacement response quantities and fragilities. The results also show that the optimal designs focus relatively more on reducing economic losses for the lower but more frequent excitation intensities as these intensities contribute most to the failure costs.

Acknowledgements

I would like to give special thanks my advisors Dr. M. P. Singh and Dr. Raymond H. Plaut for their patience and guidance throughout my time as a Ph.D. student. Their enthusiasm and interest in the work of all their students is encouraging.

I would like to express my appreciation to Dr. Carin L. Roberts-Wollmann, Dr. Finely A. Charney and Dr. Rakesh K. Kapania for serving on my graduate committee.

I would like to thank all the friends I have met in Blacksburg and this country during my life in America.

Brothers and sisters in Korean Baptist Church of Blacksburg deserve my thanks for their prayer and love.

I would like to thank my special friend Soonkie Nam for his help and friendship.

I would like to thank my sisters and brother in Korea for their love and encouragement.

I would like to express my love to my parents–in-law Moonsoo Park and Youngjo Koo for their love, support and encouragement.

I would like to express my deepest gratitude to my parents Sungkyun Shin and Panim Kim.

I would like to thank my wife, Yujin, for her encouragement, patience, and love.

Most importantly, I would like to give all my thanks to God who guides and loves me.

Contents

List of Tables

List of Figures

CHAPTER 1

Introduction

1.1 Background and Motivation for the Study

Seismic designs of building structures are currently made based on the design criterion of life safety. It requires that the structures do not collapse to compromise the safety of people living there, but they can be designed to experience some damage. Structural design and detailing for this selected design level is done such that collapse is prevented. The design could also be made such that there is no structural damage at the selected design level. However, such designs would become very costly to construct. Even these designs with strong structural members could experience nonstructural damage. So the codes only require that structures be designed with the philosophy such that they experience "no damage in minor intensity earthquake, some nonstructural damage in the moderate intensity earthquakes, and some structural damage but no collapse in the design level earthquake."

The structures designed according to this philosophy, meeting the code specified design and detailing criteria, have, indeed, performed very well in protecting human lives. The past several earthquakes tend to confirm this feeling that this design approach is working quite well to protect life. However, this design approach has also been associated with large economic losses, primarily due to the damage of nonstructural components at moderate levels of seismic intensity. This was observed in the seismic events such as the Loma Prieta Earthquake in 1989, the Northridge Earthquake in 1994 and the Kobe Earthquake in 1995, where the ground motion intensity was moderate but the level of economic damage was considered too large to be acceptable. So the current code-based designs were not found satisfactory from the standpoint of economic performance. This led to a new thinking about designing building structures for some more demanding criteria that specify some expected performances (such as less, or acceptable level of, economic losses), at the same time not compromising the life-safety objective. Since this approach addressed the issue of building performance, this design approach was called performance-based design. Economic losses and life safety are just two performance requirements, and there could be others. Thus, in earlier thinking in

the direction of performance-based design, four performance objectives were specified, giving four performance levels for four different levels of seismic intensity (SEAOC,1995): immediate occupancy for frequent earthquakes, operational for occasional earthquakes, life-safety for rare earthquakes and near collapse in very rare earthquakes. The four earthquake intensity levels are associated with approximate return periods of 43, 72, 475, and 970 years. The pairs of performance level and corresponding intensity levels are called the performance objectives. So the performance-based design criterion just mentioned above has four performance objectives.

Since the performance levels mentioned above are stated in qualitative terms, they cannot be utilized for the design of a building structure by an engineer. They need to be converted into criteria stated in terms of engineering response variables such as displacement, deformations or accelerations. These response variables are also called engineering demand parameters in the performance-based engineering community. In earthquake structural engineering, the performance of building structures is commonly measured in terms of the inter-story drifts or drift ratios. Therefore, the above mentioned performance levels were stated in terms of the inter-story drift values limits, keeping their design implementation in mind, by the SEAOC Vision 2000 Committee (SEAOC, 1995), FEMA publications on the topic of performance-based design (FEMA-273,1997; FEMA-274, 1997; FEMA-343, 1999; FEMA-356, 2000; FEMA-445, 2006), ATC-13 (1985), Kirchner et al (1997), etc. Here it is mentioned that earlier attempts to express the performance levels quantitatively in terms of story drift values were not for multi-objective performance-based designs but for the estimation of loss during an earthquake event (Whitman, et al., 1973; ATC-13, 1985; FEMA-178, 1992). For the design of acceleration sensitive items in a building, these performance levels also need to be defined in terms of acceleration values or floor response spectrum values. The acceleration sensitive items in a building are the mechanical and electrical components, water tanks placed on the roofs, suspended ceilings, water heaters, parapet walls, fire-place chimneys, air conditioning units on the roofs, data processing units, hospital equipment, etc.

The performance-based design mentioned above is, thus, a multi-level or multi-objective design. The concept of multi-level design has been around in the earthquake engineering community for several decades. In fact, it was common to use the multi-level design in the early 1970's and, thereafter, in the nuclear power plant design industry through the prescription of operating basis and design basis earthquakes. In

simple terms, the designs made (or checked) for the operation basis earthquake were to ensure continued operation of the facility (something like immediate occupancy level for a building), and the designs made for the design basis earthquake were to ensure public safety from an unacceptable event. For the building designs, the dual level design criteria were also investigated by Collins et al. (1996) and Wen and Foutch (1997).

While designing a structure for multiple performance objectives, one usually starts with a structural configuration which is then evaluated to check if it meets the prescribed design criteria. In such checking it is common to find that a structure may satisfy the life-safety design criteria but may not be good or may be under designed for other design criteria, say for example it may not satisfy the design criteria for the immediate occupancy objective. On the other hand, if one designs to meet the criteria for immediate occupancy, it may be over designed for life safety. This may be acceptable but such a design could be more costly than the life-safety criteria-based design. In such case one has to make a trade-off.

Such trade-offs can be based on some optimality condition, such as minimizing a measure of the departure from the prescribed design criteria. Minimization of such a measure can, in principle, be achieved by adjusting the structural member sizing and layout (topological optimization). However, since there are only limited choices in adjusting structural member properties, and there may be other minimum requirements such as carrying the dead and live loads, changing the section properties may not be a viable option. Thus other means must be available to adjust the performance of the structure. In this study, we have investigated the use of different damping and stiffening devices to adjust the performance of a building structure in a desirable manner. The question of desirableness will be addressed shortly.

The use of energy dissipating damping devices, base isolation, and tuned mass dampers are some of the well-known options that have been considered and used in practice to reduce the response of structures subjected to dynamic loads. For seismic loads, the use of base isolation and energy dissipation dampers such as viscous dampers, visco-elastic dampers, friction dampers, and yielding metallic dampers is now becoming quite popular. Viscous dampers dissipate energy through viscous friction by forcing a fluid through one or more narrow orifices. Visco-elastic dampers dissipate energy through cyclic shear deformations and hysteretic behavior. The yielding metallic devices

dissipate energy through cyclic yielding of metal plates causing hysteresis. Since they also add significant stiffness to the system where they are installed, they are often called added damping and stiffness (ADAS) devices.

The history and literature on the subject of how the energy dissipation devices work and on their characteristics is vast. The earlier studies were made on these devices to characterize their force deformation or force velocity characteristics for use in structural applications. Later the studies were conducted to see how they can be used in the design and analysis of structures subjected to dynamic loads such as earthquakes, wind loads and wave loads. For example, on these topics, see the studies on fluid viscous dampers by Zhang and Soong (1989, 1992), Makris and Constantinou (1991, 1993), Makris, et al. (1993, 1995); on solid visco-elastic dampers by Mahmoodi (1969), Keel and Mahmoodi, (1986), Chang, et al. (1992), Kasai, et al. (1993), Tsai (1993, 1994), Tsai and Lee (1993), Bergman and Hanson (1993), Chang et al. (1993), Chang et al. (1995), Aprile et al, (1997), Makris (1998a, b); on yielding metallic dampers by Kelly et al. (1972), Skinner et al. (1975), Aiken and Kelly (1990), Xia and Hanson (1992), Hanson (1993), Tsai and Tsai (1995), and Tsai, et al. (1993). For a study and comprehensive treatment of this topic, a reader is best advised to refer to the book by Soong and Dargush (1997). Some of the literature of direct relevance to the subject will be cited when the application of these devices is discussed in the later chapters.

In the last two decades, there have been several studies that have addressed the optimal sizing and placement of these devices in buildings and other structures. See, for example, the studies by Lunden (1980), Gurgoze and Muller (1992), Onoda and Hanawa (1993), Milman and Chu, (1994), Tsuji and Nakamura (1996), Takewaki (1997), Wu et al. (1997), Hadi and Arfiadi (1998), Takewaki, et al. (1999), Ribakov and Gluck, (1999), Shukla and Datta (1999), Singh and Moreschi (2001, 2002), Singh et al. (2003), Moreschi and Singh (2003), Wongprasert and Symans (2004), Park and Koh (2004), Wang et al. (2005), Lavan and Levy (2006), Chen and Chai (2008), Ha et al. (2009), Fujita et al. (2010), and Kargahi (2010). Most of these studies deal with minimizing quantities like norms of some response quantities such as inter-story drifts, floor acceleration, or maximize energy dissipation etc. However, this optimization can also be done to achieve the desired performance objectives in the context of performance based design. This is the primary focus of this study.

1.2 Life-Cycle Cost-Based Performance Optimization

The optimization objective defines the function that one needs to use to obtain the optimal design configuration of the dampers and any protective device. If the objective is simply to reduce the inter-story drifts because they affect the performance of a structure, then one could choose an optimization function defined in terms of the inter-story drifts such as mean square values of the inter-story drift in different stories. One could also weight individual story drifts to give more emphasis to one story over another. Similarly if one is more interested in the reducing the damage to acceleration sensitive equipment and components, then the function to be minimized can be stated in terms of the floor acceleration where the components are placed. However, since the initial motivation that prompted the performance-based design movement was economic, the question that naturally comes to one's mind is to minimize the cost of damage caused by an earthquake to obtain the optimal placement of dampers or protective devices. There may also be an overriding interest in minimizing the down time, or casualties, or direct dollar losses. However, all these factors are a part of, and contribute to, the life-cycle cost. Thus a most suitable and comprehensive measure of the damage, damage cost, lives lost, the unavailability of a facility or downtime is the life-cycle cost. This will thus be the primary objective of this study: to minimize the life-cycle cost of a building structure using the protective devices.

The earthquake engineering community is also thinking in this direction as some studies and recommendations have been made to bring this into design and evaluation practice (ATC-58 50% Draft). The biggest hurdle in implementation of the life-cycle cost based designs is the availability of the data to relate the different levels of structural response to the level of damage and the cost it will need to reinstate to the original function. One can conduct a very though analysis to estimate this damage by calculating accurately the response of the structure and components and items attached to it. This will also require a good data base about the capacity of various components. This will also have to be supplemented by thorough testing of various components to assess different levels of damage that the structure and components can experience and the cost it will take to reinstate them to their original function. This line of thinking was the basis of the assembly-based vulnerability estimation approach presented in a study by Porter and his associates (Porter, et al., 2001; Porter, et al., 2004; Porter, et al., 2006; Porter, 2007). Warszawski, et al. (1996) also proposed a method for the economic evaluation of seismic design considering life-cycle cost. An experimental study was undertaken to

relate the damage cost of reinforced concrete structures subjected to different levels of ground accelerations. Earlier studies done to estimate the damage by Whitman et al. (1973) which led to the ATC-13 report (1985) have laid the ground work for this. FEMA has also produced documents (FEMA-178, 1992; FEMA-227, 1992; FEMA-228, 1992) that can be used for reasonable or first estimate of the damage cost. In these life-cycle cost estimations for performance evaluation, it is necessary that the stochastic nature of the hazard in terms of its occurrence rates and intensities be explicitly considered (Beck et al., 1999).

Wen and Kang's (2001 a,b) study utilized these methods for damage estimation in life-cycle cost estimation to determine the most appropriate level of seismic intensity for design of structures. In the absence of the availability of any more accurate data or method to estimate the damage costs associated with different levels of seismic response, this study has also used this approach to estimate the damage costs. The approach is based on the data provided in ATC-13(1985) and FEMA-227 (1992) of items such as damage factors, loss of use, loss of rent, minor and serious injuries and casualties that can be expected. The details of this approach are given in Chapter 2.

1.3 Objective and Scope of the Study

Realizing that energy dissipation devices can very effectively reduce the response of a structure and that an excellent assessment of the overall and long-term performance of a building structure can be measured in terms of its life-cycle cost, the focus of this study is on the optimal design of energy dissipation systems by minimizing the life-cycle cost. The energy dissipation systems that have been considered are: (a) fluid viscous dampers, (b) solid visco-elastic dampers, and (c) yielding metallic dampers. A study on the combination of these dampers has also been conducted. For life-cycle cost estimation, the cost of failure data based on the inter-story drifts given in ATC-13 (1985) and FEMA-227 and 228 (1992) and some other FEMA published documents are used. These documents are used to calculate the limit state costs, which are the cost of damage if the structure happens to be in the limit state. The random occurrences of the earthquakes defined in terms of the USGS's hazard curve are used. The stochastic nature of the earthquake ground motions causing the variability in the calculated response is included. Thus, the stochastic considerations are included to calculate the probability that the structure will be in the different limit states. These probabilities are used to calculate

the failure costs from the limit state costs. The total life-cycle cost includes the initial cost, cost of failure corrected for time value of the money, and the cost of devices. The initial cost is considered fixed. No optimization in the selection of the structural member sizes, etc. of the initial structure is done. The cost of failure includes the replacement cost for structural and non-structural components, cost of loss of business, down time cost, rent loss, cost of minor and serious injuries and casualty losses. The analysis procedure includes the effect of yielding if one is expected. For the yielding metallic dampers, nonlinear step-by-step time history analysis is used to calculate the structural response. Optimization is done using Genetic Algorithms to ensure that the results converge to a global minimum. For a system that can be analyzed in an elastic manner, one can use gradient based methods. In such a case it also becomes difficult to converge to an optimum solution. In this study therefore the genetic algorithm is used. Except for the metallic dampers or combination of metallic dampers with another damper, the GA is reasonably fast. For the non linear case, the GA is slow, but can still be carried out with a stand-alone PC.

1.4 Thesis Organization

This thesis consists of seven chapters. The first chapter describes the background and motivation for this study. It also defines the scope of the study that is covered in the following chapter. The following chapters have been organized to address the various issues that arise in implementation of the life-cycle cost-based optimal design of the energy dissipation devices. Each chapter also presents numerical results pertaining to the topic it covers. A brief description of each chapter is as follows:

Chapter 2: This chapter is the backbone of this study. It clearly defines the elements of the life-cycle cost that are relevant to the study. It presents the rationale for "why cost minimization?" It describes the hazard input and the seismic inputs that can be used for analyses. The formulation for calculating includes the failure cost considering the uncertainty in the hazard description, limit states, and limit state probabilities. It provides a methodology for calculating various cost estimates using RS Means Data, location index and time index. It describes the motivation for using the genetic algorithm and what genetic algorithm involves in very simple terms. The building models that are used in following chapters for numerical studies are presented. The numerical results of their limit state costs, failure cost, and fragility are presented. These

numerical results define the baseline and are repeatedly used in the following chapter to evaluate the performance and cost improvement that is obtained by optimal installation of different energy dissipation devices.

Chapter 3: This chapter is focused on the use of fluid visco-elastic dampers for cost minimization. It briefly describes the characteristics of the viscous dampers and how one can calculate response of a structure installed with them considering the non-classically damped nature of the problem. How one can handle the issue of nonlinearity in a simple manner if the structural elements are expected to yield is addressed. Numerical results for optimal designs are obtained for the two example building models. The reductions in the failure cost, object cost and life cycle costs are calculated. The fragility functions and the response quantities of some engineering design parameters of interest are obtained and compared with those of the original building to evaluate the improvement in the performance.

Chapter 4: This chapter is focused on the use of the solid visco-elastic dampers. This chapter follows the same format as chapter 3. The issue of dependence of the damper properties on frequency and temperature is addressed. Numerical results similar to those obtained in chapter 3 are also obtained for the visco-elastic dampers.

Chapter 5: This chapter deals with the yielding metallic devices. It presents the basic preliminaries that are needed to use these dampers. It develops the argument to choose the design variables that one needs to consider in optimization. Numerical results are obtained by time history analysis using step by step time integration method. Extensive numerical results similar to those obtained in the earlier chapters are also obtained to assess the improvement in the performance and reductions in the failure costs.

Chapter 6: This chapter considers combinations of different types of dampers to see if any further improvements can be obtained. The numerical results for different damper configurations are obtained and compared with the original building as well as with the results obtained in the previous chapters for single damper cases.

Chapter 7: This chapter summarizes the study and presents concluding remarks. Recommendations for future research studies are also presented.

CHAPTER 2

Life-Cycle Cost Analysis

2.1 Introduction

In the design of many engineering systems such as buildings and bridge structures, the life-cycle cost analysis (LCCA) is becoming an important approach for comparing design alternatives and making design decisions by explicitly considering the initial and the future cost of the facility. The life-cycle cost is the discounted total cost that would be needed to have a building or other facility in working condition to provide the services for which it was designed throughout the lifespan of the facility. It, thus, consists of several cost components such as the initial cost of construction and the discounted values of the cost of operating the facility, maintenance costs, cost of consequences (such as repairs, relocation, loss of business, injuries, deaths, and other cost of failures) that may follow the overloads and damages caused by the occurrences of extreme natural events such as earthquakes that can occur during the life time of structures, and the final disposal of the facility.

In the context of the present study, the life-cycle cost analysis can also be used as an important tool in evaluating and comparing the effectiveness of different protective devices that could be used to improve the seismic performance of a building structure. Furthermore, it can also be used as an important tool to optimize the use of one or more protective systems such as the damping or energy dissipation devices by minimizing the life cycle cost. As this is the primary focus of this study, in the following we develop a framework for using this approach for optimal designs with different types of damping devices. This chapter focuses on establishing a methodology for calculating various components of the life-cycle cost. Since the occurrences of earthquakes as well as the ground motion characteristics are random quantities, it is important that these random characteristics and uncertainties associated with the hazard be included in the life-cycle cost analyses. The framework developed in the following sections shows how the hazard uncertainties can be included in the life-cycle cost analysis. The application of this methodology for optimal configuration of different damping devices is then presented in the following chapter. This chapter thus provides the basic foundation for

the following chapters.
In various sections of this chapter, we expand on some elements of the life-cycle cost, optimality consideration, damage estimation and limit states, life-cycle cost and hazard uncertainties, optimization problem and methodology, chosen building structures, calculation of damage costs of chosen building structures, and finally the seismic hazard description for the site and analyses of the structures.

2.2 Life-cycle Cost Preliminaries

The life-cycle cost of a building structure with supplementary damping devices can be assumed to be broken down into the following three partial costs.

1. Initial cost
2. Failure cost
3. Cost for supplementary damping devices

Each of these partial costs consists of several specific costs. We elaborate on this further in the following.

Initial Cost

Initial cost can be considered to be a fixed cost for the life-cycle cost analysis in this study since it is assumed to be incurred at the beginning of the period at time 0. It is the cost required to construct the building structure but without supplementary damping device. This cost can be divided into the following three specific costs:

1. Cost for structural elements including material, fabrication and installation
2. Item and installation costs of
   - Basic non-structural elements
   - Optional non-structural elements
3. Indirect cost

Structural elements include all the elements that are required to resist and carry the dead, live and extreme loads on a structure. This cost includes the cost for columns, beams (girders), and slabs of a building structure. This cost is directly affected by the loading condition for which the structure is designed, the type of material used, and the design criteria.

As the name implies, the non-structural elements are not supposed to carry the loads. They can be divided into two categories: basic elements and optional elements. The basic elements are necessary to maintain the basic function of the building. They include the architectural elements, mechanical systems and electrical systems. The architectural elements are separation walls, filler walls, windows and their glazings, doors, false ceilings, dry walls, façade, stairwells, chimneys, parapets, etc. Mechanical components include elevators, water tanks, heaters, plumbing, etc. The electrical components are the power supply systems, lighting, electrical and telecommunication circuits, smoke detectors, etc. The optional nonstructural components are the ones chosen by the facility users and may include the smoke detector, carpets, furniture, appliances, sound system etc. The cost for the construction work at site such as labor cost, and lease cost of construction machines are also included in both cost for structural elements and non-structural elements.

Indirect cost is the cost that is not directly related to the construction of building structure. Contractor fees, architect fees and overheads and profits can be included here.

Failure Cost

The failure cost is associated with damage or failure of the building structure and its contents. In the context of our problem, this failure can be caused by an expected extreme event such as an earthquake. These damage costs include the direct cost of repair or the structural and nonstructural elements to regain the original function of the building. This also includes the indirect costs associated with the consequence of the damage such as the lost of rent, relocation cost, loss of business, litigation, etc. Since the load demand and corresponding system capacities are both uncertain quantities, the events of sustaining different levels of damage are associated with uncertainties. This introduces the element of uncertainty in the estimation of the failure costs. In the life-cycle cost estimation, it is common to work with the expected values of these quantities. Thus in the discussions dealing with the cost in the following, we will often be referring to expected failure costs.

For systematic estimation of these costs, the FEMA 227 (1992) and ATC-13 (1985) documents categorize these costs into primarily six elements as follows:

1. Damage/Repair cost
2. Cost for loss of contents

3. Relocation cost
4. Cost for economic loss
5. Injury cost
6. Human fatality cost

We expand on these as follows:

Damage/Repair cost is the expenditures on direct physical repairs needed to restore the structural and nonstructural damages. The partial or total demolition cost that may be necessary to carry out the repairs of the damaged elements is also included in this cost. While damage to structural components dominates the safety of buildings, damage to nonstructural components may dominate economic loss of the system. Typically, the worth of structural components is 25% of the total worth of the building. This means that the total life-cycle cost may be dominated by the damage cost of nonstructural components compared to the damage of the structural components. According to the study of Warszawski and Segal (1996) and ATC-13 (1985), damages of the structural components show different characteristics compared to those of the nonstructural components. For example, one can expect little or no damage of the structural components under the low intensity but frequent earthquakes, whereas there are always chances of some nonstructural component damage over the spectrum of earthquake intensities, even under low intensity events.

Cost for loss of contents includes the cost for the physical damages to the contents that are necessary to maintain the intended function of the structure. This cost will vary with the equipment in the building structure.

Relocation cost includes the cost which is required to replicate the function of the damaged structure during the repair or reconstruction.

Cost for economic loss is divided into two elements: rental loss and income loss. Building rental is one of the largest income sources of the commercial building. The amount of rental loss depends on the rental rate of the building, which varies widely with the classified social function of the building structure. The rental rate also varies with the economic conditions of the location where the building is located. This income is not available until the functionality of the damaged building is restored and this, thus, depends upon the restoration time. Income loss, on the other hand, is considered to represent the loss due to the disruption of the direct commercial activity in which the

building is used. The direct commercial activity represents all economic activities other than the building rentals. For a building that is only used for rent, this cost may not exist. The economical activity of the users of the structure also can be included in the direct commercial activity.

Injury cost means the cost associated with the injury to a person by the seismic loadings. For estimation purposes, this cost is often divided into minor and serious injury costs.

Human fatality cost is the cost associated with the loss of human life caused by the damage. Although the intent of the code is life safety, human casualties can occur. Actuarial costs are used to get a number for estimating this cost.

Cost for Supplementary Damping Devices

Since the focus of this study is on the use of supplementary damping and energy dissipation devices for building performance, we need to evaluate the effect of this investment on the life cycle cost and thus must include this cost in the analysis. This cost must include all costs needed to install and maintain the device in working condition. This cost thus includes:

1. Cost of damping devices
2. Installation cost
3. Maintenance cost

Cost of damping will vary with the type of device used and its capacity, with larger capacity devices costing more. The installation cost mainly consists of the cost of braces on which the device is placed and the labor cost of installation. The maintenance cost is to keep the device in working condition. It will depend on the type of device used; for example, an active or semi-active device will need higher maintenance than a passive device. Maintenance cost can be broken down into two categories: regular maintenance cost and special maintenance cost. Regular maintenance cost is cost that occurs every year over the span of the period. Special maintenance cost is cost that occurs due to a special event such as a strong earthquake. Among the passive devices, which are of interest in this study, the yielding metallic energy dissipation device may need a special maintenance cost to replace the seriously damaged components after a strong earthquake. This maintenance cost must be time amortized to reflect the time value of

the money. In this study we assumed the viscous dampers as leakage free, thus the regular maintenance cost for the selected passive devices is not necessary. However, the special maintenance cost for a yielding metallic energy dissipation device is considered.

2.3 Optimality in Life-Cycle Cost-Based Designs

As discussed in the previous section, the expected life-cycle cost of a structure designed for earthquake loads is a sum of three basic costs. Among these costs, the cost of failure depends upon the design of structural systems as well as the installation of protective damping systems. For a given structure, it is appropriate to assume that within reasonable limits an increased system performance caused by reduced dynamic response will require an increased investment in the installation of protective devices. It is also reasonable to assume that with increased performance, the structural system will experience smaller damage and thus that cost of failure will decrease. Figure 2.1 shows these variations in the failure costs and the cost of installing the protective devices as a function of the system performance in qualitative terms. The figure shows that the failure cost decreases as the performance increases. It also shows that the increased performance requires an increased investment in terms of installing damping devices. The figure also shows that the combined cost including the cost of failure and the cost of the damping devices attains a minimum at a certain performance level defined as the optimum performance with minimum life-cycle cost. The main focus of this study is to find this minimum cost and the configuration of damping devices which will lead to this life-cycle cost based optimal performance.

2.4 Damage Estimation and Limit States

The estimation of damage and its cost is a critical step in the life-cycle cost-benefit analysis. In the context of performance based design and optimization, a very accurate estimation of these will require a comprehensive dynamic analysis for the expected range of seismic intensities to establish the load/deformation demands on the structure. This will also require a large experimental program in which the structural and nonstructural components are subjected to a range of seismic demands to establish limit states which correspond to various degrees of damages. The experimental testing program will need to be validated with field data collected on damage in different

seismic events. The next step is the estimation of the direct and indirect costs for different levels of damage, considering all consequences such as demolition cost, direct repair cost, loss of rent and income, injuries and fatalities. Given that the seismic hazard and structural parameters are associated with significant uncertainties, this detailed process cannot be expected to cover all major damage scenarios and cost analyses, and thus simplified but realistic methods need to be established for the use in design practice.

The introduction of the performance-based design concept in earthquake engineering provided a strong motivation to develop a framework for such damage and cost estimation. The early efforts were focused on establishment of performance levels beyond the usual performance requirement of life safety. The four performance objectives that the facility; remains operational, can be occupied immediately, life safety and collapse prevention have been widely considered. For design purposes, quantitative guidelines expressed in terms of structural deformations have also been proposed. Under seismic loads, a structure deforms in various forms – joint rotation, shear deformation, axial and bending of structural members. If any of these deformations is large, it will lead to overstressing of the structural and nonstructural elements, and thus lead to damage. One could consider these in a detailed damage analysis, but for practical purposes in seismic building designs, the focus has been on the inter-story drift ratio. Thus, for the performance design purposes the above mentioned performance objectives have been expressed in terms of the limits on the inter-story drifts. There was a flurry of activity in the 1990s to quantify inter-story drift limits, and Table 2.1 provides this for three performance levels as given by various design provisions such as SEAOC Vision 2000 (1995), FEMA 273 (1997), and FEMA 356 (2000) as well as those suggested by Kirchner et al. (1997) based on their study of damage data in earthquakes. The table shows only three performance levels, but drift limits for the fourth performance level of the facility remaining in operation have also been proposed. The expected physical damage corresponding to these limit states, stated in qualitative terms, is given in Table 2.2.

The guidelines mentioned in the previous paragraphs were developed primarily to formulate performance based designs of building structures for which three to four performance levels were considered adequate. However, this information needs to be supplemented with damage quantifiers that can be used for damage cost estimations for cost benefit analyses of various retrofit strategies. These drift limit states also need to be further refined for more accurate damage cost estimations.

With the intent of estimating probable maximum loss in a region, Whiteman et al. (1973) proposed a damage probability matrix format giving various levels of damage, and a damage factor and the chances of occurrence of each level under different seismic intensity scenarios. This format was essentially adopted by ATC-13 (1985), but the numbers in the matrix were based on the expert opinions on the data of some 78 facilities which included 40 buildings. The report formed the basis for FEMA reports 227 and 228 (1992). ATC-13 and the FEMA reports used seven damage states and the corresponding range of damage factor as shown in Table 2.3. The damage factor is defined as the ratio of the expected damage to the replacement cost for the building. This factor will be used for calculating limit state cost and failure costs in the subsequent section. This table is, along with other tables given in Chapter 2, giving the loss of function duration, injury and death rates for the seven damage states, are considered to calculate failure cost in this study.

To use this valuable information provided in ATC-13 and FEMA 227 and 228 for individual buildings it is, however, necessary to correlate the damage states with building deformations expressed in terms of the story drift ratios in quantitative terms. For this, the data presented in Table 2.1 which defines the story drift ratios for various performance levels is used. The performance level of collapse is considered when the story drift ratio is higher than 5%. This corresponds to the last damage level of the building being destroyed. The life safety criterion, which has been considered to be associated with a story drift level of 2.5%, is herein associated with the damage level designated as “heavy” in Tables 2.3 and 2.4, following the interpretation by Maison and Bonowitz (1998). The light damage state, associated with immediate occupancy, herein is interpreted to correspond to an inter-story drift ratio of 0.7% in line with FEMA 356 (2000). Based on the above discussion and the information given in ATC-13 and FEMA 227, Table 2.4 now provides the chosen limit states expressed in terms of the inter story drifts and corresponding damage ratios. Table 2.4 also shows the inter-story drift ratio ranges and the damage factors for the damage states other than the immediate occupancy, life safety and collapse states. These damage states and associated inter-story drift ratios are in line with similar data used by Wen and Kang (2000 a,b) in their study conducted for selecting the optimum seismic design intensity level. These values are used in calculating the damage cost, as described in a later section.

2.5 Calculation of Expected Life-Cycle Cost

As indicated earlier, the expected life-cycle cost is the sum of initial cost, failure cost, and cost for supplementary damping devices. For a chosen framing system and loading on the structure, the initial cost can be treated as a fixed value as presented previously. In the calculation of the other two costs, the time value of the money must be considered. The expected failure cost value varies with time as it depends on when the damages occur during the life time. Cost for supplementary damping devices once installed will not vary with time. The time varying effect in the cost of damping devices occurs primarily because of the maintenance as some damping devices may require recurring maintenance or one-time maintenance, if the devices get damaged due to strong ground shaking.

Another factor that should be considered in the calculation of the expected life-cycle cost, especially the failure cost, is the frequency of occurrence of the earthquakes that can possibly occur at the building site. Although the structural designs are currently made only for one design level of seismic motion, in the calculation of the damage cost, all possible earthquake intensity levels that can occur at the site along with their frequencies of occurrence must be considered as there is always a possibility of the structural and nonstructural components of the building getting damaged. Furthermore, the uncertainties associated in the occurrences of the different intensity earthquakes must be included by using proper stochastic models.

2.5.1 Characterization of Input Ground Motion

As mentioned above, for life-cycle cost analysis, all significant earthquakes that can occur on the site must be considered. That is, we must consider all intensity ranges and their corresponding frequencies of occurrence. These can be determined by a seismic risk analysis considering the seismicity of all active faults that are around the site. For such a description, we have used the seismic hazard maps produced by United States Geological Survey (USGS) for various sites around the USA. The seismic hazard curve for a site is a plot of the earthquake intensity, *e,* versus the mean annual frequency of exceedance, λ, of all possible earthquakes. The inverse of this mean annual frequency of exceedance gives the return period of the earthquake of that intensity. For a building site in Los Angeles, California, the site chosen for the example problems in this study is at coordinates (34^{o}N, 118.2^{o}W), and this hazard curve is shown in Figure 2.2. This

curve was produced using the software developed by the USGS under their National Seismic Hazard Mapping Project (NSHMP). The information about the software is available on USGS URL http://earthquake.usgs.gov/research/software/#OpenSHA..

For the convenience of the numerical analyses, ATC-58 50% Draft (2009) suggests that such hazard curves can be divided into several discrete intervals along the intensity range values. The midpoint of each intensity interval, e_i^m (i = 1,…, n), is then taken to represent the range to obtain the discrete intensity values. The corresponding mean annual frequency of the event that the earthquake intensity will be in the intensity range of the interval is calculated as $\nu_i = \Delta\lambda_i = \lambda_{i+1} - \lambda_i$ where λ_i represents the mean annual frequency of exceedance. Thus, the whole hazard curve for the site is represented by n sets of discrete intensities e_i^m and frequencies of mean annual occurrences ν_i. This discrete representation of the hazard is used for calculating the numerical results in this study. In this study it is also assumed that the time occurrence of the earthquake in each intensity range can be represented by a Poisson process. For this process, the probability of getting exactly k earthquakes of intensity e_i^m in a time period t is defined by the following equation:

$$\Pr\left[N_i = k; t\right] = \frac{e^{-\nu_i t}(\nu_i t)^k}{k!}; k = 1, 2, .., \infty \qquad (2.1)$$

where ν_i is the mean frequency of occurrence of an earthquake.

We must also consider the fact that even for the same characteristic intensity (say the peak ground acceleration) there can be many different time histories of the motion. That is, we must consider the stochastic nature of the ground motion.

In the definition of the seismic hazard, the peak ground acceleration is usually defined in the range of 0.001g~5.0g. However, very small earthquakes are not of much interest and also very large earthquakes are too rare to be likely to occur during the life time of the structure. Actually, the acceptable range of the intensity for the discretization should be defined with respect to the site to get a more accurate discrete representation of the hazard curve. The lower limit is usually determined by the intensity value of interest and the upper limit by the annual frequency of exceedance. The lower limit of the hazard curve is usually selected such that an earthquake of intensity lower than that is not likely

to cause any structural or nonstructural damage. The upper limit of the intensity corresponds to the intensity of the earthquake above which the chances of their occurrences in the structure's lifetime are essentially zero. These boundaries also can be set by the user's interests.

Herein, the lower and upper boundaries of the intensity range are determined as per the recommendation of ATC-58 50% Draft (2009). The peak ground acceleration of 0.05g is recommended as the lower boundary by ATC-58 50% Draft for the given site. The annual frequency of exceedance of 2.0×10^{-4} is recommended as the upper boundary by ATC-58 50% Draft, as the earthquakes with annual frequency of exceedance less than 2.0×10^{-4} can be assumed not to occur during the lifetime of a structure. The selected intensity range between these limits is split into seven equal intervals and the corresponding range of the annual frequency of exceedance is also split into seven intervals for this study. The midpoint intensity of each interval and the corresponding mean annual frequency of occurrence are calculated with the procedure presented above. Table 2.5 shows these seven intensities and the corresponding mean annual occurrence frequencies. These values are then used to define the ground motion for the numerical calculation of limit state probabilities and failure costs.

The hazard curve provides information only about the intensity of motion and its return period or the mean annual probability of occurrence. For seismic analysis or evaluation of a structure, we need more information. Herein, we will use the design response spectra representation for linear analysis and time history representation for non-linear time history analyses.

Response Spectrum Input

The design response spectrum for this study is developed with the Newmark-Hall (1982) approach as described in the book by Chopra (2000). This design response spectrum for 5% damping ratio is similar to the design response spectrum used in the 2009 NEHRP provisions (2009). It is used here in place of the NEHRP spectrum as in this representation one can generate both mean and mean-plus-one-standard deviation response spectra. This information is helpful in estimating the standard deviation of the maximum response, which is required for calculating the probability of the response being in various limit states defined in Table 2.3 or Table 2.5. The peak ground accelerations of the expected earthquakes, which are necessary to develop the design

response spectrum, are given in Table 2.6.

It is usually assumed that the damping ratio of a normal building structure without supplementary damping devices is 3~5% of the critical damping, and the design response spectrum developed with the Newmark-Hall method is usually appropriate for a structural system with damping ratio less than or equal to 20% of the critical damping. However, with the installation of supplementary damping devices, the equivalent damping ratio of a structural system can be higher than 20% of the critical damping. One convenient way to obtain the response spectrum for the higher damping ratios is to use a scaling factor (or *damping reduction factor*) to the 5% damped spectrum ordinates as follows:

$$\mathrm{SD}(T,\xi) = \alpha_s \cdot \mathrm{SD}(T,5\%) \tag{2.2}$$

where SD is the elastic displacement response spectra and α_s is the scaling factor. Several different scaling factors have been proposed through many research studies after the initial study by Newmark and Hall (1982). Bommer et al. (2005) derived a scaling factor that is adopted by the current European Seismic Code (EC 8 EN 2004). This scaling factor is defined as a function of damping ratio only but is independent of the response period and the nature of the expected ground motion. Cardone et al. (2008) evaluated the effectiveness of several different scaling factors in their study and concluded that the scaling factor proposed by Bommer et al. (2005) probably represents the best compromise between the accuracy of results and simplicity of formulation. Not only the accuracy but also the simplicity is a very important factor for this study since the optimization process usually requires a large number of repeated response analyses. Thus, the scaling factor proposed by Bommer et al. (2005) is adopted in this study to develop the response spectra for high damping ratio. This scaling factor can be written in the following form:

$$\alpha_s = \sqrt{\frac{10}{5+\xi}} \tag{2.3}$$

The mean design response spectrum is used to get the mean response of the structure, and the *mean plus standard deviation* spectrum is used to get the mean plus one standard deviation response of the structure. The difference of the two values is used to obtain the standard deviation of the responses required in calculating the failure probability in the life-cycle cost analysis. The response spectra developed for use in this study are shown in Figure 2.3 for damping ratios up to 40% for the peak ground

acceleration of 0.56g, and the expected maximum considered earthquake (MCE) geometric mean peak ground acceleration of the given site in the 2009 NEHRP Provisions (2009).

Spectrum Compatible Time Histories as Seismic Inputs

The structural systems that show linear elastic behavior with and without damping devices can be analyzed by the response spectrum approach using the design spectrum as the seismic input. In some cases, the response spectrum method modified to include the yielding behavior through the use of the response modification factor, as suggested by the 2009 NEHRP Provisions (2009), can also be used for approximate estimation of drift response. However, if the system with or without damping devices behaves nonlinearly, then for accurate estimation of the system response, one needs to use the time history analysis to calculate the response.

For conducting time history analysis, we use the spectrum compatible synthetic ground acceleration time histories generated using the SIMQKE-1 program written by Gasparini and Vanmarcke (1976). SIMQKE-1 can simulate statistically independent accelerograms that are compatible with a given design spectrum for a site. The program first obtains the expected Fourier amplitudes or spectral density function equivalent to a given response spectrum. To generate time histories that have the same spectral representation, harmonics with random phasing and amplitude related to the ordinate of the spectral density function are added. The stationary versions of the time histories are then multiplied by an envelope function to represent the build-up and decaying phases that are commonly observed in recorded accelerograms. These synthesized time histories are then modified in an iterative manner to match a smooth target response spectrum. The envelope used in this study to generate the time histories is shown in Figure 2.4. In Figure 2.5, we show four samples of the synthetic ground motion accelerograms generated by SIMQKE-1 compatible with the design response spectrum developed for the peak ground acceleration of 0.56g. The acceleration values were generated at time intervals of 0.01 second for an earthquake duration of 20 seconds. For generation of these time histories, 50 iterations were specified for matching with the given response spectrum. The response spectra of these time histories are overlain on the Newmark-Hall spectrum for which these time histories were generated in Figure 2.6.

2.5.2 Time Value of Money and Discount Factor

As mentioned before, the failure costs are incurred at some future time whenever the structure experiences damage. These times of failure occurrences are usually random and are governed by the random occurrence model used to characterize the earthquake models. To compare the total cost for different design scenarios, the damage costs must be converted to a fixed time point. It is common to compare all costs at t=0 when the initial construction cost is incurred. This conversion of future cost to t=0 requires the use of the discount factor. In this section we briefly describe the calculation of this factor.

The time value varies according to the currency value, interest rate, and various other economical factors. The discount factor is a factor by which a future value must be multiplied to obtain the net present value (NPV). For a fixed discount rate r, continuously compounded over time t, the discount factor can be written as follows:

$$D(t) = \left\{ \lim_{n\to\infty} \left(1 - \frac{r}{n} \right)^{n} \right\}^{t} = e^{-rt} \tag{2.4}$$

Thus, in the context of our problem, the net present value of a repair or damage cost $C(t)$ made at a future time t can be obtained as follow:

$$\mathrm{NPV}(t) = C(t) \cdot D(t) = C(t) \cdot e^{-rt} \tag{2.5}$$

If these repair events happen to occur, say, N times at times t_i, i= 1, 2, .., N, caused by N earthquake events, then the total NPV associated with these occurrences can be written as follows:

$$\mathrm{NPV} = \sum_{i=1}^{N} C(t_i) e^{-rt_i} \tag{2.6}$$

This equation will be used in a later section when the formula for the total damage cost is developed considering all possible earthquake levels and their occurrence rates.

In such calculations a careful selection of the discount rate is necessary to get a realistic estimate of the failure cost. NPV varies with the discount rate and it is important to calculate the most appropriate discount rate. However, it is very complicate task to calculate the discount rate since it requires considering too many complicated factors, and it is not in our scope. According to FEMA 227 (1992), an annual discount rate of 0.03 or 0.04 is reasonable for public sector constructions. For private sector

considerations, a slightly higher factor of 0.04-0.06 is reasonable. In this study, the mean value 0.05 is used as the annual discount rate.

2.5.3 Expected Failure Cost

In this section we develop the formula that is used for calculating the failure cost. This approach is similar to the approach adopted in earlier studies by Wen and Ang (1991), Wen and Shinozuka (1994), Ang and Leon (1997) and Kang and Wen (2000 a, b), except that it is now developed for the hazard curve discretized as discussed earlier. This discretization approach affects the method for calculating the limit state probabilities.

Consider the occurrences of the earthquakes of a particular intensity defined by peak ground acceleration a_i and annual frequency of occurrence ν_i. Let there be exactly N_i occurrence of these earthquake of intensity a_i in the lifetime T of the structure. This number of occurrence N_i is a random quantity with random occurrence time. For this intensity earthquake, let the cost of damage due to the structural response being in the j^{th} limit state be denoted by C_{ij}. Let $P_{ij}(\boldsymbol{X})$ be the probability that the structural response will be in the j^{th} limit state due to the excitation of intensity, e_i, where $\boldsymbol{X}$ is the vector of design parameters on which the structural response depends. For a give structure, these design parameters in our study will be like the parameters of damping or energy dissipation devices. This vector, thus, could contain the parameters that define the strength of the damping devices, the number of such devices and where they are placed in the structure. In terms of these quantities, the expected cost of failure can be expressed as follows:

$$E\left[C_f(X)\right] = E\left(\sum_{i=1}^{N_e}\sum_{j=1}^{N_L}\sum_{k=1}^{N_i} e^{-rt_k} C_{ij} P_{ij}\left(X, t_k\right)\right) \tag{2.7}$$

Here, $E(.)$ is the expectation of quantity (.), N_e = the number of earthquake intensities used to define the hazard curve, N_L = the number of the mutually exclusive response limit states, N_i = the number of occurrences at time instances t_1, t_2, ... t_{Ni} of earthquakes of intensity e_i in the lifetime T, and r = the discount rate. In the above equation, the product of the damage cost C_{ij} (associated with the structural response due to the earthquake of intensity e_i being in the j^{th} limit state) with the probability $P_{ij}\left(\mathbf{X}, t_k\right)$ of the structural response being in that limit state gives the failure cost. The

discount factor e^{-rt_k} converts the failure cost incurred at time t_k to its net present value.

We observe that in this equation, the expectation is defined over the random variables representing the number of earthquake occurrences N_i and time instances t_k at which these earthquakes occur. This can thus be written in terms of the probability distributions of these variables as:

$$E\left[C_f(X)\right] = \sum_{i=1}^{N_e}\sum_{j=1}^{N_L} C_{ij}P_{ij}(X)\sum_{N_i=1}^{\infty}\left(\sum_{k=1}^{n_i}\int_0^T e^{-rt_k} f_{T_k}(t_k)\,dt_k\right) p_{N_i}(n_i) \tag{2.8}$$

where $p_{N_i}(n_i)$ is the probability mass function of the number of earthquake occurrences, and $f_{T_k}(t_k)$ is the probability density function of the time t_k. For the number of occurrences defined by a Poisson process, the probability mass function is as given in Eq. (2.1) which is repeated as follows:

$$p_{N_i}(n_i) = \Pr\left[N_i(t) = k\right] = \frac{e^{-\nu_i t}(\nu_i t)^k}{k!}; k = 1, 2, \ldots \tag{2.9}$$

Also, for the Poisson occurrences $f_{T_k}(t_k)$ is a uniformly distributed random variable in the range of *0-T* as,

$$f_{T_k}(t_k) = \frac{1}{T}; 0 \le t_k \le T\,. \tag{2.10}$$

Substituting Eqs. (2.9) and (2.10) in Eq. (2.8) and carrying out the simple integration and summation over the index k, we obtain the following for the expected value of the failure cost:

$$E\left[C_f(\mathbf{X})\right] = \sum_{i=1}^{N_e}\sum_{j=1}^{N_L} C_{ij}P_{ij}(\mathbf{X})\frac{\nu_i\left(1-e^{-rT}\right)}{r} \tag{2.11}$$

Cost of Supplementary Damping Devices Including Maintenance

For the cost benefit analysis of installing supplementary damping devices, we must include their installation and maintenance costs in the calculations. The initial cost of the damping devices is a constant cost that does not vary with time. It includes the cost for damping devices and the installation cost. The maintenance cost can be divided into the regular maintenance cost and the special maintenance cost. The regular maintenance represents the cost to keep the original function of the devices regardless of the occurrence of earthquake. It is usual that the passive damping devices do not require the regular maintenance cost. Special maintenance cost represents the cost to restore the original function of the devices after severe damage on the device by strong earthquakes. Special maintenance cost needs to be calculated considering the frequency of earthquake occurrences. Thus, the expected cost for supplementary damping devices can be estimated using the following equation:

$$\mathrm{E}\left[C^{\mathrm{d}}(\mathbf{X})\right] = C_{\mathrm{o}}^{\mathrm{d}}(\mathbf{X}) + \frac{e^{-rT}}{r} C^{\mathrm{r}} + \frac{1-e^{-rT}}{r} \sum_{i=1}^{N_e} \sum_{j=1}^{N_{LD}} \left\{ \nu_i C_{ij}^{\mathrm{s}}(\mathbf{X}) P_{ij}^{\mathrm{s}}(\mathbf{X}) \right\} \tag{2.12}$$

where $C_{\mathrm{o}}^{\mathrm{d}}$, C^{r}, and C^{s} represent the initial cost for devices, unit regular maintenance cost, and unit special maintenance cost for devices, respectively. $P_{ij}^{r}(X)$ represents the probability that the device will require special maintenance in j^{th} device limit state due to occurrences of earthquakes of intensity e_i. N_{LD} represents the number of device limit states.

2.5.4 Limit State Probabilities

We observe that in the calculation of the failure cost by Eq. (2.11), we need the probability of the response being in each limit state when an earthquake of intensity a_i occurs. In our case, the limit states are defined in terms of the maximum inter-story drifts of the buildings, as indicated in Table 2.4 or Table 2.5. These limit states could be the maximum values in any story of a multistory building. Usually the inter story drift is maximum in the first story, and if this first story drift is used in calculating the damage probability for each limit state, then the optimal damper design will be primarily governed by the first story deformation. In this study we, however, consider the damage in each story under each of these limit states and thus consider the effect of

distributed damage along the building height in calculating the total failure cost.

To calculate the probabilities $P_{ij}(X)$ in Equation (2.11) for each limit state, we need to conduct a dynamic analysis of the structure to define the statistics of the story drifts for calculating these probabilities. One way to calculate the failure cost is to conduct a detailed simulation in which a sample of ground motion time histories will be applied and the story drifts will be calculated for each motion. Corresponding to each story drift one could then calculate the damage using the damage factor and the cost of the story. This can be a cumbersome task, especially if one has to do several such analyses to search for an optimal solution. In our study thus a simpler approach is used. If the response of a structure with dampers can be considered to be linear, then one could do a response spectrum analysis using the response spectrum description of the ground motion. Use of a mean response spectrum will provide the mean of the inter-story drifts, and the use of the mean-plus-one-standard-deviation spectrum will provide a good estimate of the mean-plus-one-standard-deviation for the calculated story drift values. Several of the random vibration based studies conducted earlier (Singh,1980; Maldonado and Singh, 1991) provide a basis for this assertion. The difference of these two response values will then provide the standard deviation of the calculated response. To calculate the probability that the drift of a story will be in a pre-decided range defining the limit state can then be calculated using the lognormal distribution assumption for the story drift response. The assumption of lognormal distribution has been commonly made in several earlier studies including the study that formed the basis of defining mean and mean plus one standard deviation design spectra by Newmark and Hall (1982) and Newmark et al. (1973). Thus if (μ_k, σ_k), respectively, are the mean and standard deviation values for the drift Δ_{ik} in the k^{th} story when an earthquake of intensity a_i occurs, the probability of the drift being in the j^{th} limit state defined by limit state boundaries of (Δ_{j-1}, Δ_j) can be calculated using the following formulas for the lognormal distribution:

$$P_{ij}^k = P(\Delta_{j-1} < \Delta_{ik} < \Delta_j) = F_{i\Delta_k}(\Delta_j) - F_{i\Delta_k}(\Delta_{j-1}) \tag{2.13}$$

where $F_{i\Delta_k}(\Delta)$ is the cumulative distribution function of the story drift of the k^{th} story under an excitation of intensity a_i. Assuming that the story drifts are lognormally distributed, this distribution function can be written in terms of its parameters as

follows:

$$F_{i\Delta_k}(\Delta) = \Phi\left(\frac{\ln\Delta - \lambda_k}{\varsigma_k}\right) \tag{2.14}$$

where Φ(.) is the cumulative distribution function of the standard normal distribution with zero mean and standard deviation of 1. The parameters (λ_k, ζ_k) of the lognormal distributions are defined in terms of the mean and standard deviation of the story drift as:

$$\lambda_k = \ln(\mu_k) - \frac{1}{2}\ln\left(1 + \frac{\sigma_k^2}{\mu_k^2}\right) \tag{2.15}$$

$$\varsigma_k^2 = \ln\left(1 + \frac{\sigma_k^2}{\mu_k^2}\right) \tag{2.16}$$

For an accurate calculation of the story drifts and damage costs for structural systems that are likely to go into the inelastic range for any seismic hazard intensity level, one would need a detailed simulation with time histories. As mentioned earlier, this can be a cumbersome task especially for inelastic systems and more so for conducting a search for optimal solution requiring several trials. However, a reasonable estimate of the failure cost can also be made by using a simplified approach for calculating the story drifts. In this study, we have used the approach defined in 2009 NEHRP Provisions (2009) where the yielding effects are included through the use of the response modification factor and deflection amplification factor in the response spectrum methods.

The NEHRP approach consists of using the response spectrum methods, except that the response in each mode is modified through the use of the displacement amplification factor and the R-factor. The modal story drift, Δ_{km}, in mode *m* for k^{th} story is calculated as follows:

$$\Delta_{km} = \frac{C_d\left(\delta_{kem} - \delta_{(k-1)em}\right)}{I} \tag{2.17}$$

$$\delta_{kem} = \left(\frac{g}{4\pi^2}\right)\left(\frac{T_m F_{km}}{w_x}\right) \tag{2.18}$$

where,

C_d = the deflection amplification factor

δ_{kem} = the deflection for k^{th} story in the m^{th} mode at the center of the mass determined by an elastic analysis

g = acceleration due to gravity

I = the occupancy importance factor

T_m = the modal period of vibration of the m^{th} mode

F_{km} = the portion of the seismic base shear in the m^{th} mode, induced by the k^{th} mass

w_k = the portion of the total gravity load of the structure assigned to the k^{th} mass

The modal force, F_{km}, at each level shall be determined by the following equation:

$$F_{km} = C_{vkm} V_m \tag{2.19}$$

where C_{vkm} represents the vertical distribution factor in the *m-th* mode and can be calculated by the following equation:

$$C_{vkm} = \frac{w_k \phi_{km}}{\sum_{i=1}^{n} w_i \phi_{im}} \tag{2.20}$$

where ϕ_{im} represents the displacement amplitude at the i^{th} level of the structure when vibrating in its *m-th* mode. The portion of the base shear contributed by the m^{th} mode, V_m, shall be determined from the following equations:

$$V_m = C_{sm} W_m \tag{2.21}$$

$$W_m = \frac{\left(\sum_{i=1}^{n} w_i \phi_{im} \right)}{\sum_{i=1}^{n} w_i \phi_{im}^2} \tag{2.22}$$

where the modal seismic response coefficient, C_{sm}, shall be determined from the following equation:

$$C_{sm} = \frac{S_{am}}{R / I} \tag{2.23}$$

where S_{am} represents the design spectral response acceleration at period T_m determined from the input response spectrum. R represents the response modification factor. The 2009 NEHRP Provision (2009) recommend the use of R=3.5 and C_d=3.0 for the ordinary moment-resisting frame, and R=4.5 and C_d=4.0 for the intermediate moment resisting frame. These values can also be used to calculate other response quantities with appropriate substitution for building models used in this study. The modal responses calculated using the above approach for different modes are then combined by the square-root-of-the-sum-of-the-squares (SRSS) rule to obtain the total

response.

For the case of the structure provided with yielding metallic devices, however, time histories have been used.

2.6 Optimization Problem

2.6.1 Cost Function: Object Cost

The minimization of the life-cycle cost can be used for cost-effective designs of building structures. This can be used in selecting the most effective design configuration of a building including choice of material, energy management systems and structural performance enhancing systems.

In this study we just plan to focus on the control of the structural performance of building systems to minimize the life cycle cost. That is, we optimize only the energy dissipation system to minimize the life-cycle cost. No optimization in sizing of the elements of original structure or the integrated optimization of the elements of the structural system modified with dampers or energy dissipation is done. For performance control we plan to use the passive energy dissipation devices for an already configured building structure. Since the structural configuration and structural element have already been decided, the initial cost of construction is a fixed quantity. The only cost component that varies is the cost of damping devices and the failure cost which is a function of the damping devices. Thus, the main object of this study is to find the most cost-effective design of damping devices considering all the possible earthquakes during the lifetime of a structure.

This can be defined as an optimization problem which attempts to balance the reduction in the expected failure cost against the expected cost for the damping devices. The design parameters of the damping devices that affect these costs are: the type of damping device (that is, viscous, visco-elastic, or yielding metallic dampers), the damping or energy dissipation capacity of these devices (which are related to their sizes), and the placement locations of these devices in the building and numbers of them. All these design variables are designated by $\boldsymbol{X}$ in Eq. (2.11) and in the following.

Since the initial cost is not a function of these design variables, our objective here will be to minimize the expected value of the sum of the failure cost and the cost of installing the damping devices. Here we call this cost as the *object cost*. Here we choose to normalize this *object cost* by the expected value of the cost of failure of the original building without any damping devices to represent the cost function to be minimized by the optimization algorithm. Thus the normalized cost function or index function that we propose to minimize is defined as follows:

$$f_{index}(\mathbf{X}) = \frac{\mathrm{E}\left[\mathrm{C}^{\mathrm{object}}(\mathbf{X})\right]}{\mathrm{E}\left[\mathrm{C}_0^{\mathrm{object}}\right]} \tag{2.24}$$

We have introduced the vector of design variable $\mathbf{x}$ to indicate that the object cost and the cost function are functions of these variables. In the following chapters we minimize this function for different choices of damping devices subject to physical constraints that are imposed on the devices by the limits on their sizes, numbers, architectural considerations, code constraints, etc. Let these constraints be denoted by $g_j(\mathbf{m},\mathbf{n},\mathbf{l})$, $j = 1, 2, ..., m$, where m is the total number of constraints. In terms of the cost function and the constraints, the optimization problem can be stated as follows:

> Obtain the vector of design variables, $\boldsymbol{X}$
> to minimize, $f_{index}(\boldsymbol{X})$
> within the constraints, $g_j(\mathbf{m},\mathbf{n},\mathbf{l})$, $j = 1, 2, ..., m$

To solve this optimization problem, we have used the genetic algorithm described in the following section.

2.6.2 Genetic Algorithm

In this section we briefly describe the genetic algorithm that we have used for the optimum design search. There are now a large number of publications on genetic algorithms since its first proposal by Holland (1975). There are several books: Fogel (2006), Gen and Cheng (1997), Goldberg (1989 a,b), Michalewicz (1992), Stender et al. (1994), and Zalzala and Fleming (1997). There are also several papers that have explored its application in various fields of engineering including civil engineering: Camp et al. (1998), Chan (1997), Cheng and Li (1998), Furuya et al. (1998), Jenkins

(1997), Kim and Ghaboussi (1999), and Singh and Moreschi (1999 a,b). This brief description is not intended to provide an exhaustive account of the available literature, but just to present an introductory description of this method with focus on the application to select optimum placement of damping devices in a structure.

As the name indicates, the genetic algorithms try to imitate the workings of the process of natural selection in which stronger individuals in a species survive and evolve themselves through generations to have the best chances of survival in a competing natural environment. The primary reason for using this approach in our problem is that it can provide a globally optimal solution within the sample space of the design variables as against the gradient based approaches that often get trapped near a local optimum.

To avoid getting trapped near a local optimum, the genetic algorithm starts with several possible design options. Each design option is an individual. The collection of the selected design options (or individuals) is called the population of a generation. In this population, and the following generations of future populations, the best individual is the one which has the lowest (or highest) performance index. In our case, this performance index is the cost function described in the previous section. The search for the best design is accomplished by successively evolving each generation into a new generation with improved performance through mating of individuals for reproduction, with crossover, and mutations of the individual genes. The selection of pairs for mating exploits the characteristics of the individuals based on their fitness and some random scheme of pairing to encourage the propagation of better individuals (designs) and discouraging or dropping of poorer individuals. The mating of the pair produces new offspring which share the characteristics of the parents by some gene crossover schemes and some limited mutation. The new offspring define the new generation which further goes through the evolution process towards the new generation with improved performance till no further improvements are observed in the best individuals of the subsequent generations. Elitism schemes to give prominence to the best performing individuals and dropping of the worst performing individuals have also been used. In the following we describe various terms such as individuals, genes, crossover, mutation and elitism used in the previous paragraphs in the context of finding the best design with single or multiple types of dampers.

Our objective is to find the best combination of, say, three different types of dampers

(defined by their capacities and types): where and how many of them should be placed in the building to minimize the cost index defined in the previous section. So in this case there are three basic variable: (a) the type of damper (C_{D1}, C_{D2}, and C_{D3}), (b) the number of each damper type and (c) the story in which they needs to be placed. Also, let us say that there are N_s different stories or locations where they can be placed. A possible configuration of the damper placements is shown in Figure. 2.7. This configuration consists a string of $3N_s$ integer values N_{ij} with i=1, 2, and 3 and j=1, 2 .., N_s, representing the number of C_{di} dampers placed on the j^{th} location on the building. The length of an individual string, thus, would vary according to the number of different types of damping device we plan to use. This configuration of devices represents a possible design. In the terminology of a genetic algorithm it represents a chromosome defining an individual's characteristics. Each value in the string or the chromosome is a gene. A collection of such possible designs or individuals is called a population. The values of the genes in individual strings in a starting population are selected randomly from the possible values of the genes. That is, the numbers N_{ij} are randomly selected within reasonable ranges that do not violate the physical constraints of the building.

In an optimal search by a genetic algorithm, one starts with such a population that further evolves into future generations of populations according to a predefined scheme described in the following paragraphs. The size of population selected determines the speed with which the optimal selection process converges to the final value. There is, however, no set rule. Using a population with a large number of individuals will converge in fewer generations to the optimal values compared to a smaller size population. However, a large population will also require a longer time to evaluate the population performance.

The next step in the search for optimal solution is to evaluate the performance of each individual. In the context of our problem, it means the calculation of the cost function for each individual design. This requires the dynamic and cost analyses of the structure for calculating the limit states for all possible hazard intensities, limit state failure probabilities, and then the failure cost. An individual design with the lowest cost is the best individual design, and the one with the highest cost is the worst individual design. The individuals are then rank ordered from best to worst according to their calculated performance in terms of the failure costs.

To generate the next population of individuals using the mating of current population

individuals, first the following quantities are calculated for an i^{th} individual of the ordered set of individuals (Baker, 1985):

$$\Pr(i) = \frac{N_p - i + 1}{\sum_{i=1}^{N_p} i}; \quad \text{Fit}(i) = \sum_{k=1}^{i} \Pr(k) \quad where \sum_{i=1}^{N_p} \Pr(i) = 1.0 \tag{2.25}$$

where $\Pr(i)$ represents the relative probability of selecting the i^{th} ranked individual string in the population, $\text{Fit}(i)$ represents the fitness of the i^{th} ranked individual in the population and N_p is the total number of individuals in a population. We note that $\Pr(i) > \Pr(i-1)$. According to Eq. (2.25), we also note that a large value of the fitness function $\text{Fit}(i)$ is inversely associated with the performance of the individual. That is, the better individual has a lower $\text{Fit}(i)$ value.

Next a roulette wheel scheme is used for pairing of the individuals in the population for mating to create the next generation of the population. For this, a set of N_p random numbers is generated between the values of 0 and 1, and the individuals associated with the paired random numbers in sequence are selected for mating to create offspring. The individual corresponding to a random number is assigned based on the interval of fitness values in which the random number falls. Thus if a random number is in the k^{th} interval, then the k^{th} ranked individual in the population is associated with this random number. If two adjacent random numbers lead to the same individual, a new random number is generated to avoid mating of the two individuals with same genes.

Each consecutive pair of individuals selected according to the roulette scheme described above is then used to create two offspring through the process of crossover and mutation as follows. The idea behind the crossover is that all genes of an offspring come from its parents. Several variations of crossovers have been suggested and used. In a simple crossover, the genes of the parents above a randomly selected number between the first and the last gene are switched to create two off springs. In another crossover scheme, each gene in the parents is randomly switched to create the offspring. Yet in another scheme the genes of the offspring are an arithmetic combination of the parent genes as follows:

$$\begin{aligned} \bar{z}_i &= \alpha \bar{x}_i + (1-\alpha)\bar{y}_i \\ \bar{w}_i &= (1-\alpha)\bar{x}_i + \alpha \bar{y}_i \end{aligned} \tag{2.26}$$

where $\overline{x}_i$ and $\overline{y}_i$ are vectors containing the genes of the pair of the parents, and $\overline{z}_i$ and $\overline{w}_i$ are vectors of children produced by crossover. Also, for uniform arithmetical crossover, $0 \le \alpha \le 1$ should be picked randomly for each generation. This commonly used crossover scheme is adopted for this study.

Some genes of a fraction of individuals or chromosomes in the population are also mutated. Mutation is done to introduce new designs in the population. The fraction of the population to be mutated is usually kept at a low level, usually between 0.05~0.1, primarily to avoid too many offspring losing their ability to learn from their parents and also losing resemblance to their parents. A higher mutation rate may also delay the convergence to the optimal solution. This fraction value is decreased after a number of iterations in the search process to reduce the time of convergence. The mutation is applied to the worst 2*n* individual strings according to the ranking of each individual string, where 2*n* is the number to be mutated. Among the 2*n* individual strings, *n* individual strings are mutated with a Gaussian mutation operator and the remaining *n* individual strings are mutated with random mutation operator. Here 10% of the population was mutated according to the above scheme. The mean value of the Gaussian mutation operator is selected to be $\left(b_{\max} + b_{\min}\right)/2$ and the standard is usually selected to be about 10% of the range of the possible values of the genes as $\left(b_{\max} - b_{\min}\right)/10$, where $b_{\max}$ is the upper boundary and $b_{\min}$ is the lower boundary of possible values of the genes. In the random mutation operator one or more randomly selected genes are replaced by a random number within the possible range of the gene values.

Often, an elitist scheme is also adopted to retain the best features of the previous generation. For this a given number of the best performing individuals is retained for the next iteration in the searching process. In our search, first two best individual strings were selected for the next iteration without any mutation or crossover.

The process of rank-ordering, forming pairs for mating, reproduction through crossover and mutation, and elitist scheme are repeated for each generation to create a new generation till optimum results converge to a stable value.

2.6.3 Validation of Genetic Algorithm

As observed above, a genetic algorithm is a random search process which simultaneously considers many possible designs to avoid convergence to a local optimum. Based on the performances of individual designs, it iterates to create new populations of designs through the process of crossover, mutation and elitism. These processes use the random approaches to create diversity in the new population to look for better designs and at the same time retain the good features of the designs in the preceding population. As there are several variation that have been used to implement crossover, mutations and elitisms, it is necessary to test that a computer code written for an algorithm indeed converges to the optimum value sought. To test the algorithm code, a bench-mark test has been proposed by Ackley (1987) consisting of a function with many local minima and a global minimum value. Originally this function was defined for two dimensions, but it can be generalized to *N* dimensions. It consists of finding a string $\mathbf{x} = \{x1, x2, ..., xN\}$ within $xi \in (-32.768,\ 32.768)$ which minimizes the following equation;

$$F(\mathbf{x}) = -20 \cdot \exp\left(-0.2\sqrt{\frac{1}{n}\sum_{i=1}^{n} x_i^2} \right) - \exp\left(\frac{1}{n}\sum_{i=1}^{n} (2\pi \cdot x_i) \right) + 20 + e \qquad (2.27)$$

The theoretical optimal solution of this problem is the vector $\mathbf{v} = [0, 0, 0, ..., 0]$ that results in $F(\mathbf{v}) = 0$.

Figures 2.8 and 2.9 show the plots of this function for the one- and two-dimensional cases. The presence of several local minima is clearly seen, where a gradient based approach is likely to get trapped. The details of the validation of the code written in this study are shown in Appendix A, and they clearly show that the genetic algorithm written for this study works quite well for the optimization problem with multiple variables.

For calculation of optimal results in this study, the convergence to the final value was assumed to have been achieved when the maximum difference in the cost function value within a pre-decided number of iterations did not change more than 0.1% of the initial value. This pre-decided number of iterations was taken to be 10% of the population size. The population size in our study varied from 400 to 600 depending on the types of dampers considered in design.

2.7 Building Models – Example Problems

To generate numerical results in this study, two nine-story office buildings made of steel are selected as model buildings. It is assumed that they have the same plans, elevations, and architectural properties. However, they have different structural properties to represent two different building models: one is designed as an ordinary moment-resisting frame but with much stronger beam to weak column, so it behaves like a shear building and the other is designed as an intermediate steel moment-resisting framed (IMRF) building with fully restrained connections. Although, life-safety design criterion-based codes may allow the ordinary moment frame buildings in high seismicity regions only on a case by case basis, herein in this study the shear building with ordinary moment frame is included because it is more rigid than the IMRF buildings. Since shear building is more rigid, it is expected (and later it is, indeed, verified by this study) that it will have smaller inter-story deformations and thus lower failure costs than the IMRF building. Thus a study of the two buildings, one with already reduced failure cost than the other, may have relevance to development of the performance-based design concept where the one of the main focus has been to reduce the failure cost at moderate levels of seismic intensities.

The plan and elevation of the model building are shown in Figure 2.10. The main frame is constructed with ASTM A992 W-shape structural steel. It is assumed that the model buildings are located in downtown Los Angeles with 34.0^{o}N in latitude and 118.2^{o}W (-118.2^{o}) in longitude. At this location, the short period and 1 second period spectral response acceleration values are 17.06 m/sec^2 and 5.94 m/sec^2, respectively. Figure 2.11 shows the mean and mean plus one standard deviation Newmark-Hall spectra corresponding to the zero period acceleration value for this site.

For the functional category, both buildings are assumed to be commercial buildings for professional, technical, and business services. The exterior wall is brick faced with concrete block back-up. The inherent damping ratio of the model buildings is assumed to be 3% of critical damping.

The model buildings are designed to satisfy the limitation of drift ratio by 2009 NEHRP Provisions (2009) where the allowable story drift, Δ_a, is given as follows:

$$\Delta_a = 0.020 \cdot h_{sx} \tag{2.28}$$

where h_{sx} is the story height below level *x*.

Shear Beam Model: The shear building model is designed as a steel framed building with rigid beam-column connection with relatively strong girders and weak columns so that no rotational deformation is expected at the connection and floor system. The floor system of the shear building model is designed to have steel beams and a reinforced concrete slab that is connected to the main beams with shear studs. The thickness of the slab is $150mm$ and the yielding strength of concrete used for the slab is $f_c' = 25N/mm^2$. The concrete strength is used to calculate the stiffness of the slab. The stiffness and strength of the slab also can be included in the estimation of the stiffness of beam members if they are fully connected. It is expected that this composite floor system with steel beam and reinforced concrete slab will also increase the bending stiffness of the floor. Thus, the deep girders and composite floor with reinforced concrete slab would give relatively much larger stiffness to the beams compared to the columns, by which it would be possible to ensure the typical, so called, shear building behavior of the model building to the seismic loading. The estimated beam to column stiffness ratio in the mid-height of the shear building model is $\rho = 4.6$. The detailed structural properties of the structural members of the shear building model are given in Table 2.7, where girder means the lateral member that is connected to the columns and beam means a lateral member that is connected to the girders. Other data such as the dead load and live load needed to calculate the building weight for calculating the building response are given in Table 2.8. The mass matrix and stiffness matrix of the shear building model are listed in Tables 2.9 and 2.10, respectively. The stiffness also includes the contribution of other columns that are not directly related with the stiffness in the designated direction. Modal properties of the shear model building without dampers are given in Table 2.11.

MRF Model: The MRF building model is detailed as an intermediate moment resisting steel frame with relatively strong columns and weak beams that is expected to distribute the inelastic response relatively uniformly over several stories. This design is similar to the model structure that used by Kang and Wen (2001b) with some modifications. The estimated beam to column stiffness ratio in the mid-height of the MRF building model is $\rho = 0.38$. The detailed structural properties of the structural elements of the MRF building model are given in Table 2.12. Other data, such as the dead load and live load

needed to calculate the building weight for calculating the building response, are given in Table 2.13.

In the preparation of the analytical model of the MRF model, the following assumptions are made. The axial deformation in beams and columns of the moment frame is neglected. Each floor diaphragm is assumed to be rigid in its own plane but is flexible in bending in the vertical direction. It is assumed that the lateral deformations at each node at a floor level are the same. It is also assumed that the inertial effects associated with rotations of the nodes are zero. This model has 36 rotational degrees of freedom and 9 lateral degrees of freedom, with a total of 45 degrees of freedom.

The mass of the frame is assumed to be lumped at the global nodes at the floor level, thus rendering its mass matrix diagonal. Since the rotational inertia of the lumped nodal mass is neglected, the only non-zero terms of the mass matrix are those diagonal terms associated with in-plane translational degrees of freedom. Thus, the mass matrix can be expressed as a 9 by 9 diagonal matrix, where 9 is the story number of the model building.

For the stiffness matrix, the static condensation method is used to eliminate the 36 rotational degrees of freedom associated with zero mass, reducing the system to 9 degrees of freedom with the stiffness matrix condensed into a 9 by 9 matrix. Tables 2.14 and 2.15 show the mass matrix and stiffness matrix of the MRF building model. The modal properties of the MRF building model without damper are shown at Table 2.16

Table 2.17 provides the calculated story drifts according to 2009 NEHRP Provisions (2009) for the design seismic motion on the site. We note that the calculated story drifts satisfy the design criteria prescribed in the 2009 NEHRP Provisions (2009). In the calculation of the story drifts, the response modification coefficient and deflection amplification factor are applied if the story is assumed to yield. For the calculation of the story drift in the elastic range, those coefficient and factor are not applied. The yielding of the structural member is checked by calculating the ratio of maximum elastic stress in the member to the effective yield stress of the member in structural members. If more than 50% of the beams or columns at a given story yield, the story is assumed to have yielded. The effective yield strength of the structural members for A992 steel used with the R_y factor of 1.1 (FEMA 350, 2000) is taken to be 380MPa. Based on this stress analysis, it was observed that both the shear building and the MRF

building could be assumed to behave inelastically for seismic intensity levels of 4 and higher.

2.8 Initial Cost and Limit State Cost Estimation

The approach and data needed to calculate the initial cost and limit state cost for the building models considered in this study are described in this section. Although the cost function used in the optimization process does not need the initial cost explicitly, the calculation of the initial cost is needed in the calculation of the limit state costs and failure costs. The limit state cost is the expected failure cost if the response of a building is in a given limit state. The failure cost on the other hand also includes the chances of the response being in the limit state. Thus, the failure cost associated with a limit state is the limit state cost multiplied by the probability of the response being in that limit state. In this section we will provide the details for calculating the limit state costs for the seven limit states described in Table 2.5. This cost is calculated by multiplying the cost factor given in Table 2.5 by the replacement cost which is based on the initial cost. Thus in the following we describe the details of the procedure that we have used to calculate the initial cost.

Cost Adjustment Factors: The cost calculations are made for the year 2009 for the buildings that are assumed to be located in Los Angeles. For estimation of the construction cost, the data given in the RS Means cost documents is an excellent resource. Often the data is provided based on the national average costs. To use this data for specific sites around the country, the city index values are used to reflect the local variation in the labor and other costs. According to RS Means Construction Cost Data 2009 (2008), the recommended city cost index for the commercial building in Los Angeles is 108.3 relative to the national average of 100.0. Often the required cost data may be available for another city more conveniently. To convert this data for one city to that for another city, their cost index values can be used for the location adjustment as follows:

$$Cost\ in\ City\ \mathrm{A} = \frac{Index\ for\ City\ \mathrm{A}}{Index\ for\ City\ \mathrm{B}} \times Cost\ in\ City\ \mathrm{B} \tag{2.30}$$

All the costs in this study are estimated in terms of 2009 US dollars but sometimes the unit costs may be available as the average costs in years other than 2009. To use these values in different years, we use the historical cost index, also available in the RS

Means data. The recommended national average historical cost index for 2009 is 182.5 based on the value of 100 for January 1993. To convert the cost given in another year to the corresponding cost in 2009, we can use the following simple formula:

$$Cost\ in\ Year\ \mathrm{A} = \frac{Index\ for\ Year\ \mathrm{A}}{Index\ for\ Year\ \mathrm{B}} \times Cost\ in\ Year\ \mathrm{B} \tag{2.31}$$

These location and historical indices have been used in the cost estimations in this study.

2.8.1 Estimation of Initial Cost

As mentioned in section 2.1.1, the initial cost mainly consists of the cost for the structural elements and the cost for the non-structural elements. The cost for non-structural elements would vary with the dimensions of the building, class function, architectural decision and details, etc. As mentioned earlier, the two building models have the same dimensions and functional class. Therefore, the cost for non-structural elements of the two building models can be assumed to be the same.

The initial cost for non-structural elements is calculated using RS Means Square Foot Cost 2009 (2008) which gives the average construction cost per unit area of floor with respect to the functional class. According to RS Means Square Foot Cost, the model buildings are categorized as commercial office building with 5-10 stories. The exterior wall of the model buildings is assumed to have brick facade with concrete block back-up. The total floor area above the ground level of the model building is 7560m^2. The estimated unit construction cost for non-structural elements is \$1122.9/m^2. This unit cost includes the cost for all the basic non-structural elements, cost for substructures such as foundations (about 2.8%), and cost to set an elevator that is required for a 9 story building as a common additive. It also includes the 25% contractor fees, overhead and profits (O&P), and 10% architect fees. This unit cost also needs be adjusted for the variations in the story heights if the building story heights are different from the average height used in the estimation of this nominal cost.

The structural cost varies with the construction material used in the structural elements and the type of framing system. In this study, the model buildings are constructed of steel but have different framing systems. The initial cost for structural elements includes the material cost, labor cost of fabrication and installation, equipment cost, and 10% overhead and profit for columns, beams, and slabs.

Unit column cost and unit beam cost are estimated using 2009 National Construction Estimator (2008) and they are \$2.78/*kg* and \$2.93/*kg*, respectively. The total column weight needs to include the connection weight. For this, it is recommended to include 15% of the column weight as per 2009 National Construction Estimator (2008). The model buildings have different floor systems. The shear building model has 150*mm* cast-in-place reinforced concrete slab and the MRF building model has metal deck/concrete fill slab. Unit floor costs for the 150*mm* cast-in-place reinforced concrete slab and the metal deck with 76*mm* deep slab, estimated using RS Means Building Construction Cost Data 2009 (2008), are \$46.7/m^2 and \$41.3/m^2, respectively. Costs for the fireproofing of columns and beams are also included. The fireproofing cost is estimated based on the area of columns and beams to be covered using RS Means Building Construction Cost Data 2009 (2008). The estimated unit fireproofing costs for the columns and beams are 18.9/m^2 and 24.2/m^2, respectively.

Table 2.18 presents the initial cost data estimated for each story for the two building models used. The details of the basic data used for calculating these numbers and the formula for calculating the structural and nonstructural initial cost data are given in Appendix B. Based on these calculations, the estimated total initial costs of the shear building model and MRF building model are \$15,700,000 and \$12,900,000, respectively.

2.8.2 Estimation of Limit State Cost

To calculate the limit state cost, one needs to calculate the item costs that are associated with the calculation of the failure cost. These are: (1) cost associated with repairing the damage, (2) cost of loss and replacement of contents, (3) cost of loss of rental, (4) cost of relocation, (5) cost of economic loss, (6) cost of injury and (7) cost of human fatalities, all due to the structural response being in each limit state. To calculate these damages we use the damage factors proposed by ATC-13 (1985) and FEMA 227 (1992) given in Table 2.5, and the other data provided in Table 2.19 as explained below. As seen below, some of the available data may not pertain to the building sites or for the year 2009, for which both the time and location adjustments explained above are also applied.

Damage/repair cost is calculated using the damage factors and the replacement cost of the building. Replacement cost represents the cost to demolish and then dispose of the

damaged building and construct a new building. In terms of these items, the damage cost of the j^{th} story can be written as:

$$C_j^{\mathrm{d}} = (story\ initial\ cost + unit\ demolition\ cost \times floor\ area) \times damage\ factor \quad (2.32)$$

The unit demolition cost used in this calculation is \$285.3/m^2. This value is based on the value of \$201.2/m^2 provided by Whitney (2002), which is the average cost for Detroit in 2002, adjusted for the site chosen in Los Angeles using the location factor and for the year in 2009 using the time factor.

Cost for loss of contents is calculated using the unit contents cost per unit floor area, floor area and the damage factor as:

$$C_j^{\mathrm{loss}} = (floor\ area \times unit\ contents\ cost) \times damage\ factor \quad (2.33)$$

The unit contents cost depends upon the social and economical function of the building, and according to FEMA 227 (1992) the national average for a commercial office building can be taken to be \$310.9/m^2. This unit cost needs to be adjusted for the city of Los Angeles using the city cost index and historical cost index. This adjusted cost used in this study for Los Angeles in 2009 is \$616.5/m^2.

The relocation cost is calculated in terms of the unit relocation cost/unit area/unit time, the leasable area and the time it takes to restore the area to its original function as:

$$C_j^{\mathrm{relo}} = (leasable\ area \times unit\ relocation\ cost) \times restoration\ time \quad (2.34)$$

The restoration time would depend on the damaged floor area and the intensity of the damage in that area. ATC-13 (1985) proposed the weighted statistics for loss of function and restoration time with respect to the damage state as indicated in Table 2.5. As for estimating the leasable area, it is generally assumed that 55% of gross floor area is leasable for a commercial office building. FEMA handbook No. 178 (1989) suggested an amount of \$16.14/*month*/m^2 for the unit relocation cost. This when adjusted by the location and historical cost indices gives a value of \$34.5/*month*/m^2, which is used in this study.

The cost for economic loss consists of two parts: rental income loss and commercial income loss. Rental income is defined in terms of the rental rate and leasable area of the structure. The expected loss of function and restoration time from ATC-13 (1985) can be used to estimate rental loss of the building. For the rental loss cost, FEMA 228 (1992)

suggests a rate of \$6.56/*month*/m^2 for Seattle. This rate is adjusted to a value of \$11.4/*month*/m^2 for the location and time using the city cost and historical cost indices. Income loss is also proportional to the time of loss of function. FEMA 228 (1992) suggested \$89.7/*month*/m^2 as the rate of income loss for commercial, professional, and business services. This cost is also adjusted by the city cost and historical cost indices to a value of \$177.8/*month*/m^2. The time for rental loss and income loss is assumed as the same as the restoration time. The rental loss and income loss are estimated by the following equations:

$$C_j^{\text{renl}} = (\textit{leasable area} \times \textit{unit rental loss cost}) \times \textit{restoration time} \qquad (2.35)$$

$$C_j^{\text{incl}} = (\textit{leasable area} \times \textit{unit income loss cost}) \times \textit{restoration time} \qquad (2.36)$$

To calculate ***the expected injury cost*** one needs a good estimate of the number of people occupying the building, the rate at which the minor and major injuries are likely to happen and the cost of injury per person for minor and serious cases. ATC-13 (1985) suggests an occupancy rate of 4 persons/1000 sq. ft (4 persons/92.9m^2) for professional and business services. To calculate the number of injured persons, the number of occupants is multiplied by the rates at which the minor and serious injuries occur. The expected injury rate according to the damage state was suggested by FEMA 228 (1992). According to FEMA 228 (1992), the minor and major injury rates can be assumed to vary between the values of 0 to 0.4, depending upon the level of damage expected in the building. The level of damage is measured in terms of the limit states, and thus in this study the injury rates as assigned in Table 2.5 are assumed. FEMA 228 (1992) also suggests the values of \$1,000/*person* for a minor injury and \$10,000/*person* for a serious injury, and these values are used in this study. These costs adjusted for the city cost index and historical cost index are \$1,983/*person* and \$19,830/*person* for the minor injury and serious injury, respectively. Using the above discussed rates and unit costs, the injury cost can be calculated as follows:

$$C_j^{\text{inj}} = \textit{floor area} \times \textit{occupany rate} \times \textit{injury rate} \times \textit{unit injury cost} \qquad (2.37)$$

For the calculation of ***the cost of human fatalities***, assigning an economic value to a human life is a sensitive question. However, FEMA 228 (1992) suggested \$1,740,000/*person* in 1987 dollars which with historical cost adjustment index is \$3,620,000/*person*. The expected death rate, as suggested by FEMA 228 (1992), is assumed to vary between the values of 0 to 0.4 for different limit states, and these values are shown in Table 2.5. Using these values, the cost of fatalities is calculated as

follows:

$$C_j^{\text{fat}} = \textit{floor area} \times \textit{occupany rate} \times \textit{death rate} \times \textit{unit death cost} \qquad (2.38)$$

Table 2.19 summarizes the values of these different unit costs used in this study. The limit state costs calculated for each story of the shear building model and MRF building model on the basis of the above explanation are given in Tables 2.20 and 2.21. A part of these costs depends on the type of structure that is structural framing. However, a major part of these floor costs also consists of the cost of items such as relocation, rental, economic loss, injuries and fatalities which remain the same for each floor as they all depend upon the floor area which is the same at all floors. The breaking down of these floor area-dependent costs into these component costs is given in Table 2.22, both for the shear building model as well as the MRF building model. These component costs have been calculated as explained above.

2.9 Fragility Functions and Failure Costs of the Building Models

For each of the building models, we present the numerical results for the fragility functions corresponding to the three performance levels of (a) immediate occupancy, (b) life safety, and (c) collapse. The immediate occupancy limit state is defined by the story drift ratio limit of $\Delta \leq 0.7$, the life safety limit state is defined by the story drift ratio limit of $\Delta \leq 2.5$, and the collapse limit states defined by the story drift ratio limit of $\Delta \leq 5.0$. The fragility is defined as the probability of the story drift ratios exceeding these limits, and thus it is the conditional probability given that the earthquake of that intensity has occurred. The fragility function or curve is a plot of these probabilities at the given earthquake intensity. The seven earthquake intensities that are used to define the seismic hazard (Table 2.6) for the site are used. The mean and variances of the characteristics of the story drift ratios needed to calculate these probabilities are obtained as described in Section 2.5. In this chapter these results are obtained for the buildings without any supplementary damping devices. In the following chapters these results will be compared with the similar results for the buildings with optimally installed supplementary devices.

Figure 2.12a shows the plots of the fragility curves for the three limit states mentioned above both for the shear beam model and frame model buildings. These curves are based on the maximum value of the inter story drift ratio wherever it occurs irrespective

of the story. On this plot the fragility curves for the limit state of collapse do not appear as their probabilities are very low. Figure 12.2b is, thus, plotted on the log-scale to accommodate all curves in one plot. The log-scale plot covering a wide range of probability values also accentuates the differences between different curves. It is noted that the MRF building has higher probability of exceedance for each limit state than the shear building, primarily because it is relatively more flexible and thus experiences higher deformations.

In Figures 2.13-2.15, we show similar fragility curves but now for three different stories of the buildings. For the first story, the fragility curves shown in Figure 2.13a (plotted on natural scale) and Figure 2.13b (plotted on log-scale), for the two buildings are almost indistinguishable from each other. For higher stories, in Figure 2.14 and 2.15 which are now plotted on log-scale, the curves are different, with the MRF building showing higher vulnerability than the shear building.

From the presentations in the above set of curves we note that if the curves are plotted on the natural-scale some of the curves may not even show up because they are associated with low probability values. Whereas the curves plotted on the log-scale can cover wide range of cases especially if they are associated with low probability values. Thus in future presentations the fragility curves are only plotted on the log-scale to accentuate the differences between the curves for comparison of various cases.

In next set of figures we show the limit state costs for the two buildings. Figures 2.16 is the shear building, and Figure 2.17 is for the MRF building. They show the total limit state costs (top curves) as well as the limit state costs for two different floors. The costs are plotted on log scale to accommodate large differences for different stories and as a function of seismic intensity. It is interesting to note that for the MRF building, the limit state cost curves for the first story and the 9th story are almost the same, indicating that the damage and story drifts are more uniformly distributed over the height in the MRF building than in the shear building.

The limit state costs when multiplied by the probability that the response will be in that limit state will provide the variation of the failure costs. This variation for the two buildings for the total cost as well as failure costs associated with two particular stories are shown in the next two figures 2.18 and 2.19. A comparison of the total limit state cost and total failure cost for the two buildings, shown in Figures 2.20 and 2.21,

indicates that the MRF building has higher costs because of its being more flexible.

2.10 Chapter Summary

This chapter provides the basic framework for carrying out the life-cycle cost-based optimization of dampers for building structures exposed to the West Coast seismic environment. This framework forms the backbone of the studies reported in the following chapters for different types of dampers. The chapter briefly describes the elements of life-cycle cost, optimality consideration, damage estimation and limit state methodologies that have been considered in ATC and FEMA documents on loss estimation. Characterization of the seismic hazard that is appropriate for life-cycle cost estimation is defined, and use of this hazard information for dynamic analysis and for calculation of the limit state probabilities is described. The life-cycle cost estimation methodology considers all random occurrences of earthquakes of different intensities, stochastic characteristics of accelerograms, failure costs in different limit states, time value of money, and cost of dampers or energy dissipation devices. Basic elements of genetic algorithms, proposed to be used for the optimization search, are described in the context of this problem. Since a genetic algorithm requires multiple calculations of structural performance in terms of failure costs and improvement costs involving large number of trials, it is necessary that simple but adequate approaches be used for response analysis and limit state probability calculations. The calculation approach to be used for this are described in this chapter. Two structural models used with the same building configuration are selected for numerical investigation. One of them is a relatively rigid frame that can be characterized as a shear beam model. The other model is an intermediate moment resistant frame which is relatively more flexible. Both satisfy the inter-story drift limitations of the NEHRP design provisions. Both of them are assumed to be located in the Los Angeles area. The limit state costs and failure costs for these two building models are obtained and compared. Also obtained and compared are their fragility curves for three limit states of immediate occupancy, life-safety and collapse. The flexible moment resistant frame model is shown to be associated with higher failure costs and also higher vulnerability in all three limit states as expressed in terms of their fragility curves. In the following chapter, these models will be the subject of extensive numerical study wherein they will be improved with different types of dampers to minimize their life-cycle costs.

Tables 2

Table 2.1 Story-Drift Ratio Limits from Codes and Guidelines, Maison et al. (1999)

Reference	Structural Performance and Story-Drift Ratio Limit		
	Collapse Prevention	Life Safety	Immediate Occupancy
FEMA-356	5.0%	2.5%	0.7%
FEMA/NIBS	4.0%	1.5%	0.6%
SEAOC Vision 2000	2.5%	1.5%	0.5%
Kircher et. al	5.3%	2.0%	0.8%

Table 2.2 Proposed Damage States with the Performance Level in FEMA-356

	Performance Levels			
	Collapse Prevention	Life Safety	Immediate Occupancy	Operational
Damage State	Severe	Moderate	Light	Very Light
Structural	Little residual stiffness and strength, but load bearing columns and walls function. Large permanent drifts.	Some residual stiffness and strength left. Gravity-load-bearing elements function. No out of plane failure of walls. Some permanent drifts.	Structure substantially retains original strength and stiffness. Minor cracking of façades and partitions. No permanent drift.	All systems important to normal operation are functional. Minor cracking of façades and partitions. No permanent drift.
Nonstructural	Extensive damage	Many nonstructural systems are damaged	Equipment and contents are generally secure	Negligible damage occurs

Table 2.3 Damage State and Corresponding Central Damage Factor from ATC-13

Damage State	Damage Factor Range (%)	Central Damage Factor (%)
None	0	0
Slight	0~1	0.5
Light	1~10	5
Moderate	10~30	20
Heavy	30~60	45
Major	60~100	80
Destroyed	100	100

Table 2.4 Limit States and Drift Ratio Corresponding to the Damage Factor

Limit State	Damage State	Story Drift Ratio (%)	Damage Factor
1	None	$\Delta<0.2$	0.0
2	Slight	$0.2<\Delta<0.4$	0.005
3	Light	$0.4<\Delta<0.7$	0.05
4	Moderate	$0.7<\Delta<1.5$	0.2
5	Heavy	$1.5<\Delta<2.5$	0.45
6	Major	$2.5<\Delta<5.0$	0.8
7	Destroyed	$5.0<\Delta$	1.0

Table 2.5 Drift ratios, average damage factors, average loss of function, and percentage of minor and serious injuries and death per person occupancy as per ATC-13 and FEMA 227

Limit State	Damage State	Story Drift Ratio (%)	Damage Factor	Average loss of function (Days)	Minor injury (%)	Serious injury (%)	Death (%)
1	None	$\Delta<0.2$	0.0	0	0	0	0
2	Slight	$0.2<\Delta<0.4$	0.005	3.4	0. 003	0.0004	0.0001
3	Light	$0.4<\Delta<0.7$	0.05	12.08	0. 03	0.004	0.001
4	Moderate	$0.7<\Delta<1.5$	0.2	44.72	0. 3	0.04	0.01
5	Heavy	$1.5<\Delta<2.5$	0.45	125.66	3	0. 4	0. 1
6	Major	$2.5<\Delta<5.0$	0.8	235.76	30	4	1
7	Destroyed	$5.0<\Delta$	1.0	346.93	40	40	20

Table 2.6 Input Ground Motions and their annual frequencies of occurrence considered for numerical results in this study

Interval	Annual Occurrence Frequency	Intensity Range (g)	Midpoint Intensity (g)
$\Delta\nu_1$	0.10383	0.050 ~ 0.178	0.11
$\Delta\nu_2$	0.01109	0.178 ~ 0.306	0.24
$\Delta\nu_3$	0.00282	0.306 ~ 0.433	0.37
$\Delta\nu_4$	0.00114	0.433 ~ 0.561	0.50
$\Delta\nu_5$	0.00036	0.561 ~ 0.689	0.63
$\Delta\nu_6$	0.00028	0.689 ~ 0.817	0.75
$\Delta\nu_7$	0.00010	0.817 ~ 0.945	0.88

Table 2.7 Structural Property of Shear Building Model

Story	Members					
	Inner Columns	Outer Columns	Girders / Beams	Stiffness ($10^8 N/m$)	Weight ($10^6 N$)	
					Steel	Total
1	W14x398	W14x426	W44x335 / W16x77	8.09	2.45	6.30
2	W14x342	W14x370,	W44x335 / W16x77	8.68	2.35	6.15
3	W14x311	W14x342	W44x290 / W16x77	7.97	2.14	5.94
4	W14x311	W14x342	W44x290 / W16x77	7.97	2.12	5.92
5	W14x257	W14x311	W44x262 / W16x77	6.60	1.98	5.77
6	W14x257	W14x311	W44x262/ W16x773	6.60	1.94	5.74
7	W14x211	W14x257	W44x230 / W16x77	5.20	1.77	5.57
8	W14x176	W14x211	W44x230 / W16x77	4.14	1.67	5.47
9	W14x145	W14x145	W40x211 / W16x57	3.06	1.28	4.71

Table 2.8 Unit Dead Load for Shear Building Model

Load Factor	Unit Load (KN/m^2)	
	Floor	Roof
150*mm* Reinforced Concrete Slab	2.30	2.30
Insulation and Membrane	0.00	0.53
Ceiling	0.26	0.26
Mechanical and Electrical	0.19	0.19
Partition	0.96	0.00
Sub-Total	3.71	3.28
Exterior Wall	1.44	1.44
Live Load	2.15	0.77

Table 2.9 Mass Matrix of Shear Building Model (10^5 kg)

$$\begin{bmatrix} 6.42 & 0 & 0 & 0 & 0 & 0 & 0 & 0 & 0 \\ 0 & 6.24 & 0 & 0 & 0 & 0 & 0 & 0 & 0 \\ 0 & 0 & 6.01 & 0 & 0 & 0 & 0 & 0 & 0 \\ 0 & 0 & 0 & 5.99 & 0 & 0 & 0 & 0 & 0 \\ 0 & 0 & 0 & 0 & 5.85 & 0 & 0 & 0 & 0 \\ 0 & 0 & 0 & 0 & 0 & 5.83 & 0 & 0 & 0 \\ 0 & 0 & 0 & 0 & 0 & 0 & 5.68 & 0 & 0 \\ 0 & 0 & 0 & 0 & 0 & 0 & 0 & 5.60 & 0 \\ 0 & 0 & 0 & 0 & 0 & 0 & 0 & 0 & 4.80 \end{bmatrix}$$

Table 2.10 Stiffness Matrix of Shear Building Model (10^9 N/m)

$$\begin{bmatrix} 1.68 & -0.87 & 0 & 0 & 0 & 0 & 0 & 0 & 0 \\ -0.87 & 1.67 & -0.80 & 0 & 0 & 0 & 0 & 0 & 0 \\ 0 & -0.80 & 1.60 & -0.80 & 0 & 0 & 0 & 0 & 0 \\ 0 & 0 & -0.80 & 1.46 & -0.66 & 0 & 0 & 0 & 0 \\ 0 & 0 & 0 & -0.66 & 1.32 & -0.66 & 0 & 0 & 0 \\ 0 & 0 & 0 & 0 & -0.66 & 1.18 & -0.52 & 0 & 0 \\ 0 & 0 & 0 & 0 & 0 & -0.52 & 0.94 & -0.42 & 0 \\ 0 & 0 & 0 & 0 & 0 & 0 & -0.42 & 0.72 & -0.31 \\ 0 & 0 & 0 & 0 & 0 & 0 & 0 & -0.31 & 0.31 \end{bmatrix}$$

Table 2.11 Modal Properties of Shear Building Model

Mode	Frequency (Hz)	Damping Ratio
1	0.96	0.03
2	2.51	0.03
3	4.01	0.03
4	5.43	0.03
5	6.64	0.03
6	7.77	0.03
7	8.99	0.03
8	10.01	0.03
9	11.09	0.03

Table 2.12 Structural Property of MRF Building Model

Story	Members				
	Inner Columns	Outer Columns	Girders / Beams	Weight ($10^6 N$)	
				Steel	Total
1	W14x426	W14x500	W30x116 / W16x33	1.26	4.87
2	W14x370	W14x426	W30x116 / W16x33	1.15	4.71
3	W14x342	W14x398	W30x108 / W16x33	1.10	4.66
4	W14x342	W14x398	W30x108 / W16x33	1.06	4.62
5	W14x283	W14x342	W30x99 / W16x33	0.98	4.54
6	W14x283	W14x342	W30x99 / W16x33	0.95	4.50
7	W14x233	W14x283	W30x90 / W16x33	0.84	4.46
8	W14x233	W14x283	W27x84 / W16x33	0.74	4.30
9	W14x145	W14x145	W24x55 / W16x26	0.22	3.52

Table 2.13 Unit Dead Load for MRF Building Model

Load Factor	Unit Load (KN / m^2)	
	Floor	Roof
Concrete Slab with Metal Decking	2.01	2.01
Insulation and Membrane	0.00	0.53
Ceiling	0.26	0.26
Mechanical and Electrical	0.19	0.19
Partition	0.96	0.00
Sub-Total	3.42	2.99
Exterior Wall	1.44	1.44
Live Load	2.15	0.77

Table 2.14 Mass Matrix of MRF Building Model (10^5 kg)

$$\begin{bmatrix} 4.97 & 0 & 0 & 0 & 0 & 0 & 0 & 0 & 0 \\ 0 & 4.81 & 0 & 0 & 0 & 0 & 0 & 0 & 0 \\ 0 & 0 & 4.75 & 0 & 0 & 0 & 0 & 0 & 0 \\ 0 & 0 & 0 & 4.71 & 0 & 0 & 0 & 0 & 0 \\ 0 & 0 & 0 & 0 & 4.64 & 0 & 0 & 0 & 0 \\ 0 & 0 & 0 & 0 & 0 & 4.60 & 0 & 0 & 0 \\ 0 & 0 & 0 & 0 & 0 & 0 & 4.49 & 0 & 0 \\ 0 & 0 & 0 & 0 & 0 & 0 & 0 & 4.39 & 0 \\ 0 & 0 & 0 & 0 & 0 & 0 & 0 & 0 & 3.49 \end{bmatrix}$$

Table 2.15 Stiffness Matrix of MRF Building Model (10^9 N/m)

$$\begin{bmatrix} 1.447 & -0.921 & 0.247 & -0.045 & 0.008 & -0.002 & 0.000 & 0.000 & 0.000 \\ -0.921 & 1.348 & -0.852 & 0.231 & -0.039 & 0.007 & -0.001 & 0.000 & 0.000 \\ 0.247 & -0.852 & 1.271 & -0.797 & 0.203 & -0.036 & 0 .006 & -0.001 & 0.000 \\ -0.045 & 0.231 & -0.797 & 1.150 & -0.705 & 0.183 & -0.029 & 0.004 & -0.001 \\ 0.008 & -0.039 & 0.203 & -0.705 & 1.044 & -0.642 & 0.151 & -0.022 & 0.002 \\ -0.002 & 0.007 & -0.036 & 0.183 & -0.642 & 0.918 & -0.530 & 0.113 & -0.012 \\ 0.000 & -0.001 & 0.006 & -0.029 & 0.151 & -0.530 & 0.738 & -0.399 & 0.064 \\ 0.000 & 0.000 & -0.001 & 0.004 & -0.022 & 0.113 & -0.399 & 0.494 & -0.190 \\ 0.000 & 0.000 & 0.000 & -0.001 & 0.002 & -0.012 & 0.064 & -0.190 & 0.136 \end{bmatrix}$$

Table 2.16 Modal Properties of MRF Building Model

Mode	Frequency (Hz)	Damping Ratio
1	0.64	0.03
2	1.77	0.03
3	2.95	0.03
4	4.27	0.03
5	5.72	0.03
6	7.37	0.03
7	9.09	0.03
8	10.90	0.03
9	12.80	0.03

Table 2.17 Inter-Story Drift Limit Check with 2009 NEHRP Provision (2009) for Model Buildings

Story	Story-Drift Ratio (%)		
	Shear Building Model	MRF Building Model	Drift Ratio Limit
1	0.90	0.91	2.00
2	0.93	1.49	2.00
3	0.95	1.55	2.00
4	0.87	1.48	2.00
5	0.93	1.45	2.00
6	0.79	1.34	2.00
7	0.82	1.26	2.00
8	0.74	1.15	2.00
9	0.53	0.99	2.00

Table 2.18 Initial Cost of Each Story of the Model Buildings

Story	Initial Cost ($)	
	Shear Building Model	MRF Building Model
1	1,917,943	1,548,741
2	1,859,205	1,512,175
3	1,782,805	1,473,916
4	1,782,805	1,473,916
5	1,732,495	1,433,901
6	1,732,495	1,433,901
7	1,677,882	1,416,504
8	1,656,639	1,365,330
9	1,557,761	1,278,147
Sum	15,700,028	12,936,531

Table 2.19 Basic Cost to Estimate the Limit State Cost

Cost	Basic Cost ($)	Unit
Demolition	285.3	/m^2
contents cost	616.5	/m^2
relocation	34.5	/*month*/m^2
Rental Loss	11.4	/*month*/m^2
Income Loss	177.8	/*month*/m^2
Minor Injury	1,983	/*person*
Serious Injury	19,830	/*person*
Human Death	3,620,000	/*life*

Table 2.20 Limit State Cost of Shear Building Model at Each Story

Story	Limit State Cost (× $1,000)						
	1	2	3	4	5	6	7
1	0	25	176	698	1,762	4,292	30,314
2	0	25	173	686	1,736	4,245	30,255
3	0	24	169	671	1,702	4,184	30,179
4	0	24	169	671	1,702	4,184	30,179
5	0	24	167	661	1,679	4,144	30,129
6	0	24	167	661	1,679	4,143	30,128
7	0	24	164	650	1,654	4,100	30,074
8	0	24	163	646	1,645	4,083	30,053
9	0	23	158	626	1,600	4,004	29,954

Table 2.21 Limit State Costs of MRF Building Model at Each Story

Story	Limit State Cost (× $1,000)						
	1	2	3	4	5	6	7
1	0	23	157	624	1,596	3,997	29,945
2	0	23	155	617	1,579	3,967	29,909
3	0	23	153	609	1,562	3,937	29,869
4	0	23	153	609	1,562	3,937	29,869
5	0	23	151	601	1,544	3,905	29,829
6	0	23	151	601	1,544	3,905	29,829
7	0	23	150	598	1,537	3,891	29,812
8	0	22	148	587	1,514	3,850	29,761
9	0	22	143	570	1,474	3,780	29,674

Table 2.22 Each Component Cost of Limit State Cost at a Story of Model Building
(in USD)

Limit state	C^{loss}	C^{relo}	C^{ecol}		C^{inj}		C^{fat}
			C^{renl}	C^{incl}	minor	serious	
1	0	0	0	0	0	0	0
2	2,589	1,806	597	9,310	2	3	131
3	25,893	6,418	2,121	33,076	21	29	1,308
4	103,572	23,760	7,851	122,449	215	287	13,075
5	233,037	66,763	22,061	344,072	2,149	2,865	130,754
6	414,288	125,259	41,390	645,539	21,488	28,650	1,307,544
7	517,860	184,324	60,907	949,936	28,650	286,504	26,150,880

Table 2.23 Limit State Cost for Damage/Repair of Shear Building (× $1,000)

Story	Limit State						
	1	2	3	4	5	6	7
1	0	11	107	427	961	1,708	2,135
2	0	10	104	415	934	1,661	2,076
3	0	10	100	400	900	1,600	2,000
4	0	10	100	400	900	1,600	2,000
5	0	10	97	390	877	1,560	1,949
6	0	10	97	390	877	1,560	1,949
7	0	9	95	379	853	1,516	1,895
8	0	9	94	375	843	1,499	1,874
9	0	9	89	355	799	1,420	1,775

Table 2.24 Limit State Cost for Damage/Repair of MRF Building (× $1,000)

Story	Limit State						
	1	2	3	4	5	6	7
1	0	9	88	353	795	1,413	1,766
2	0	9	86	346	778	1,383	1,729
3	0	8	85	338	761	1,353	1,691
4	0	8	85	338	761	1,353	1,691
5	0	8	83	330	743	1,321	1,651
6	0	8	83	330	743	1,321	1,651
7	0	8	82	327	735	1,307	1,633
8	0	8	79	316	712	1,266	1,582
9	0	7	75	299	673	1,196	1,495

Figures 2

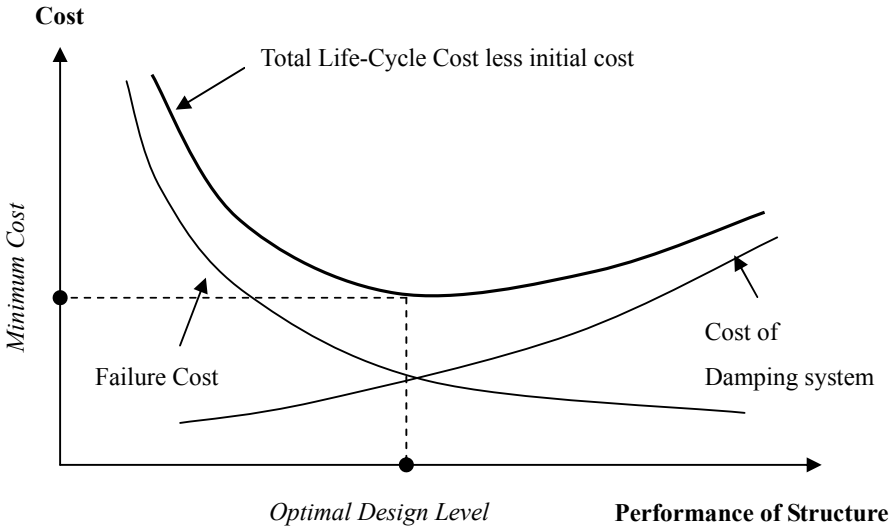

Figure 2.1 Qualitative Representation of the Variations in the Failure Cost, Cost of Damping System, and Total Cost as a Function of System Performance.

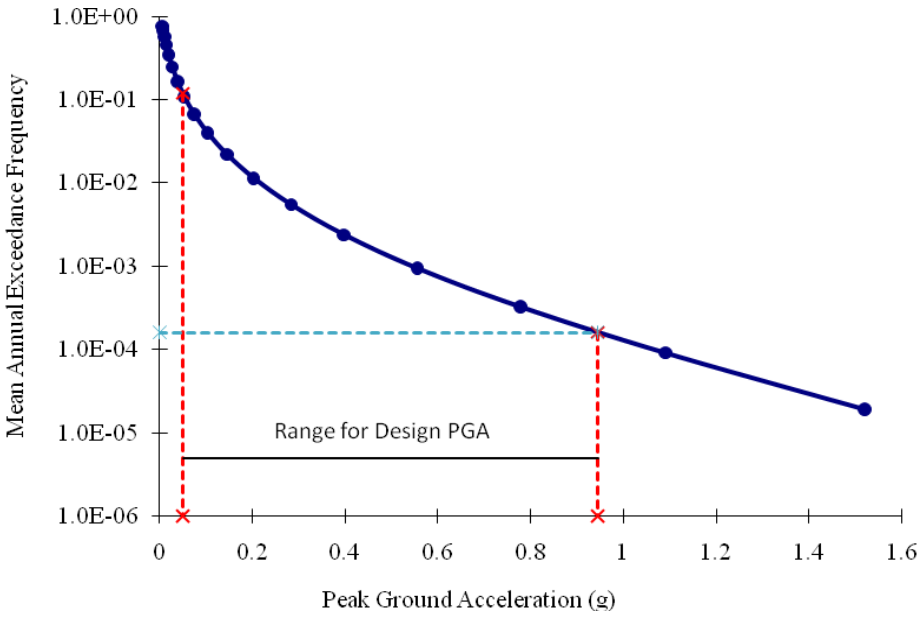

Figure 2.2 USGS Probabilistic Seismic Hazard Curve of the Model Building Site

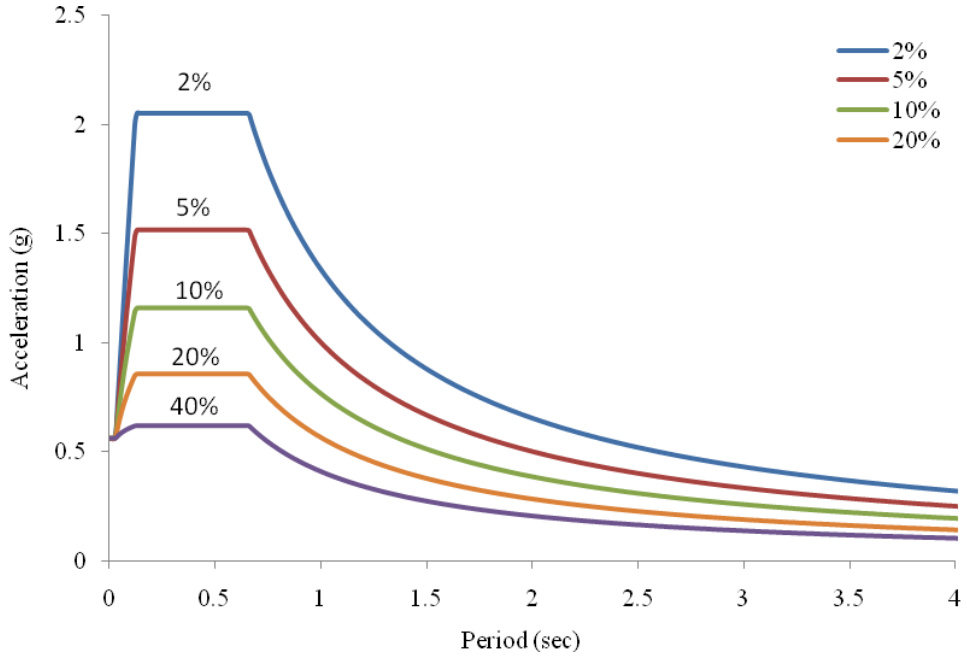

Figure 2.3 Mean Design Response Acceleration Spectra for Different Damping Ratios

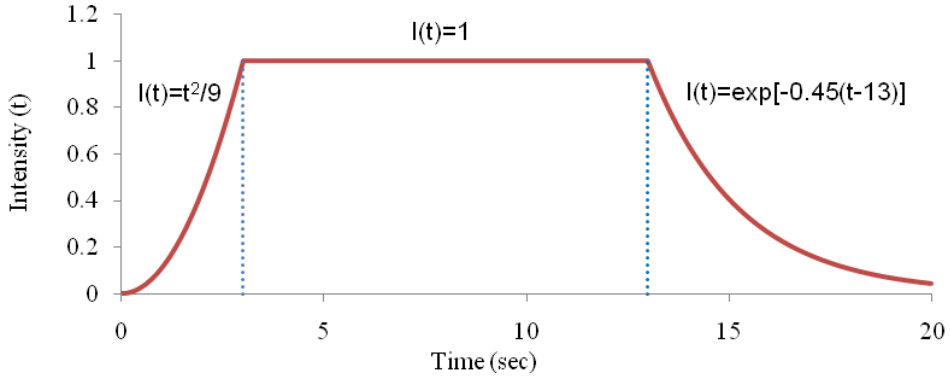

Figure 2.4 Envelope Function for the Generation of Synthetic Ground Motion

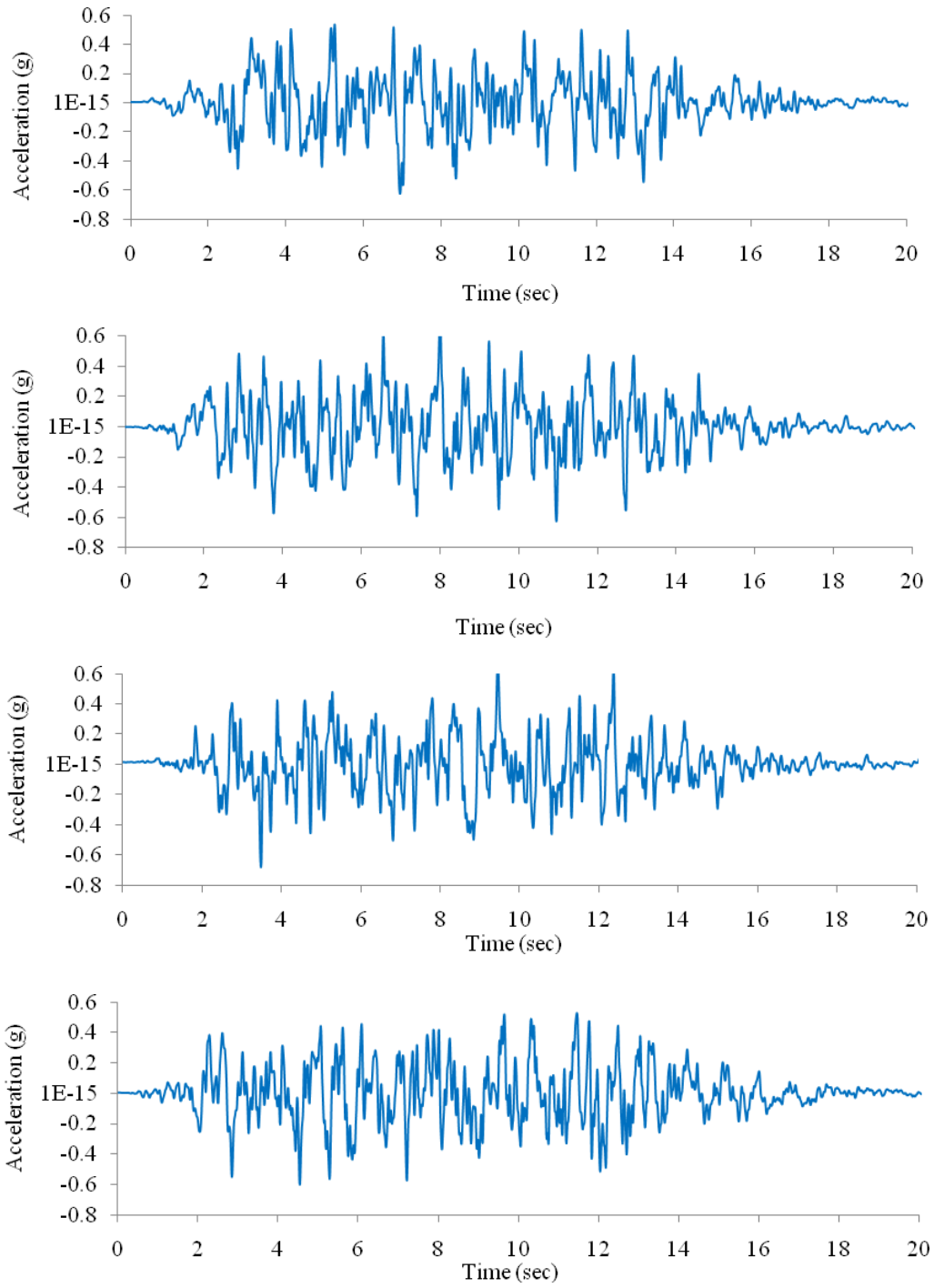

Figure 2.5 Four Sample Ground Motion Time histories generated by SIMQKE-1 (PGA=0.56g)

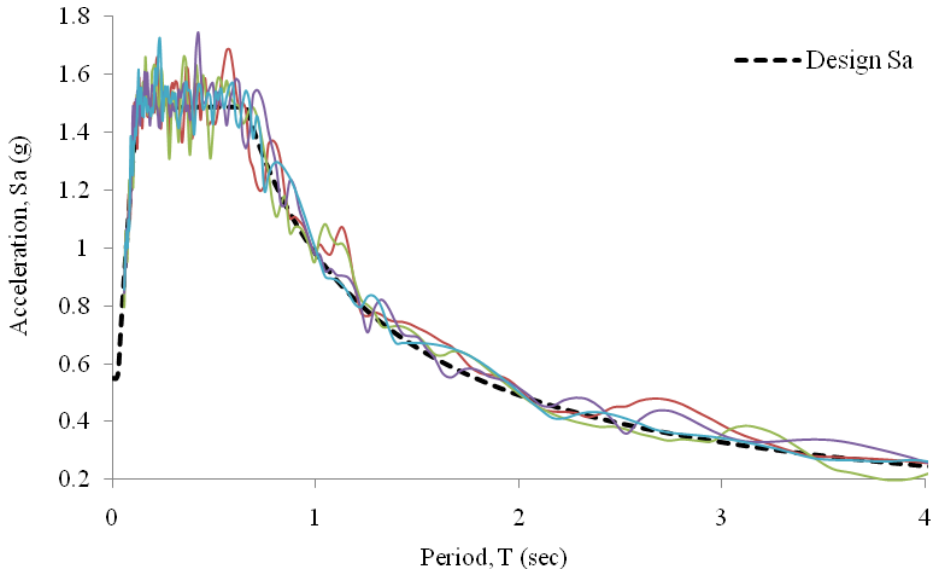

Figure 2.6 Newmark-Hall Acceleration Response Spectrum and Response Spectra of Four Synthetically Generated Sample Time histories (PGA=0.56g)

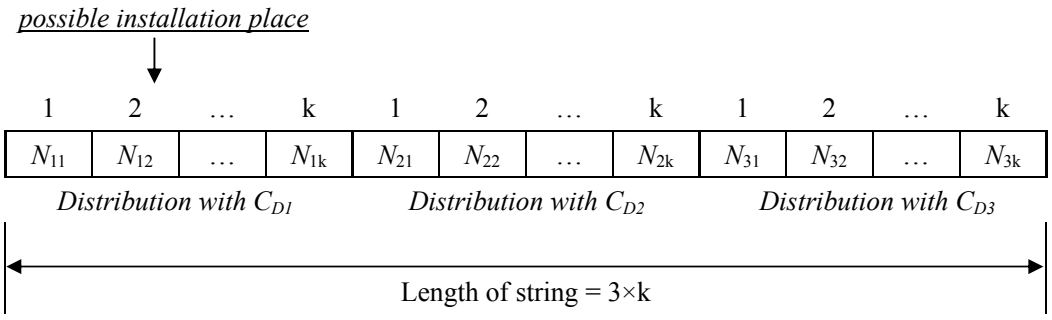

Figure 2.7 Example of an Individual String for Three Different Dampers

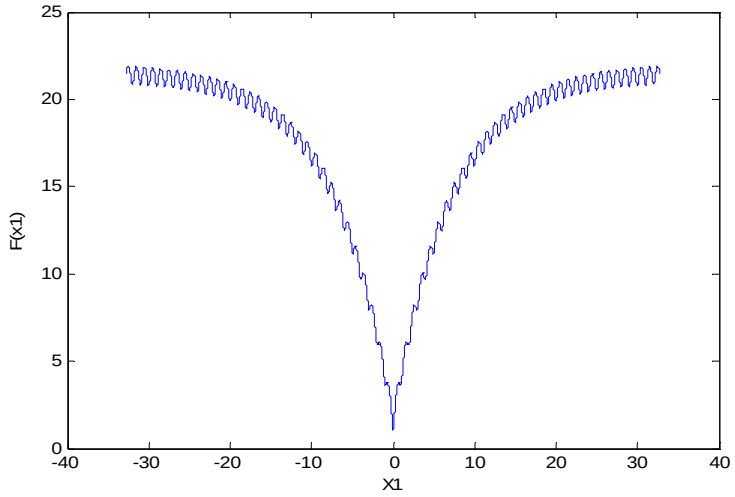

Figure 2.8 Ackley's Function with One Variable (X1)

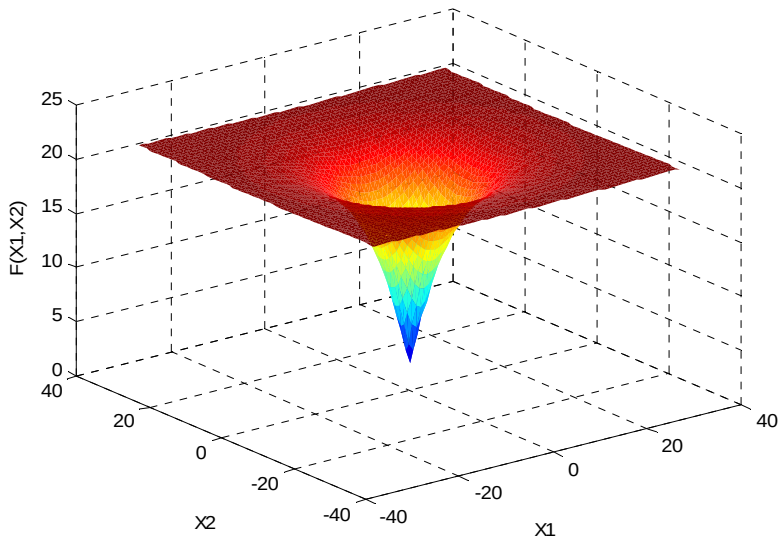

Figure 2.9 Ackley's Function with Two Variables (X1, X2)

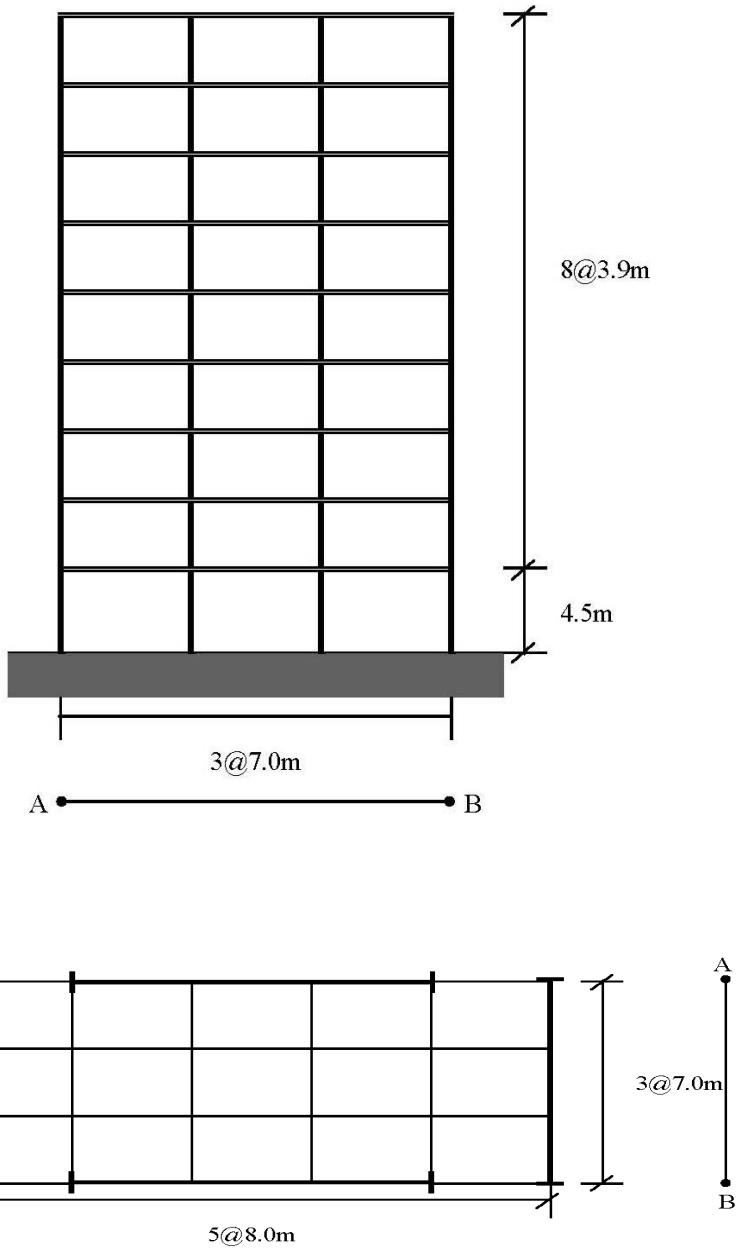

Figure 2.10 Elevation and Plan of Model Building

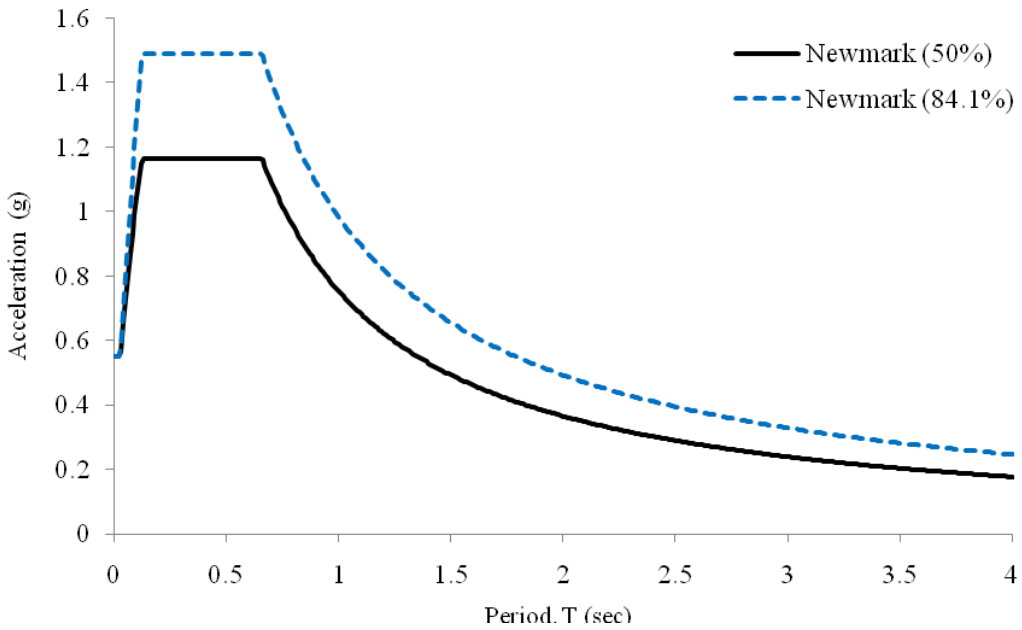

Figure 2.11 Design Response Spectra

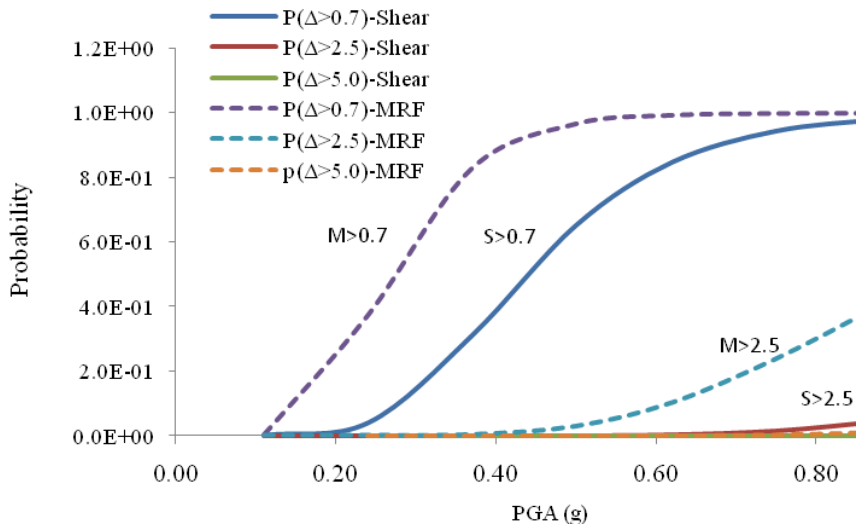

Figure 2.12(a) Fragility Curves at Three Limit States with Maximum Story Drift of the Model Buildings (Natural Scale)

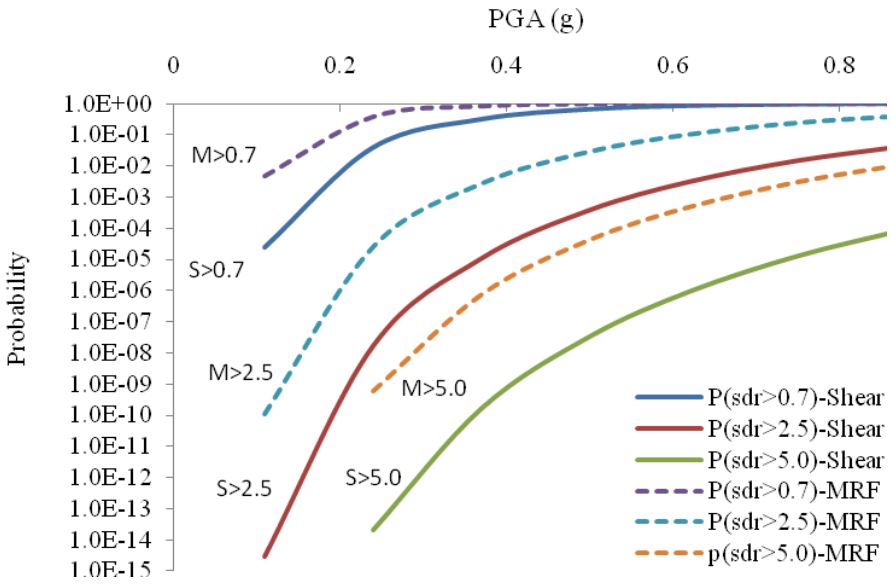

Figure 2.12(b) Fragility Curves at Three Limit States with Maximum Story Drift of the Model Buildings (Log Scale)

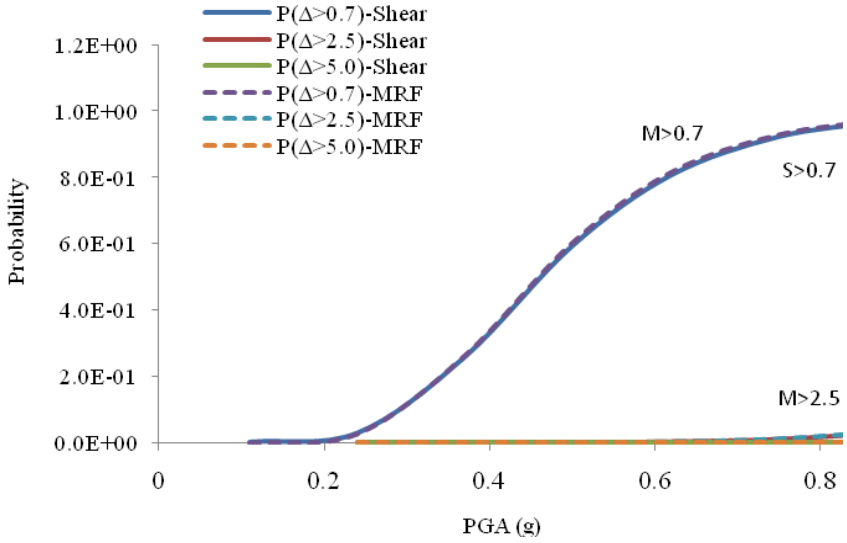

Figure 2.13(a) Fragility Curves for Three Limit States in 1st Story of the Model Buildings (Natural Scale)

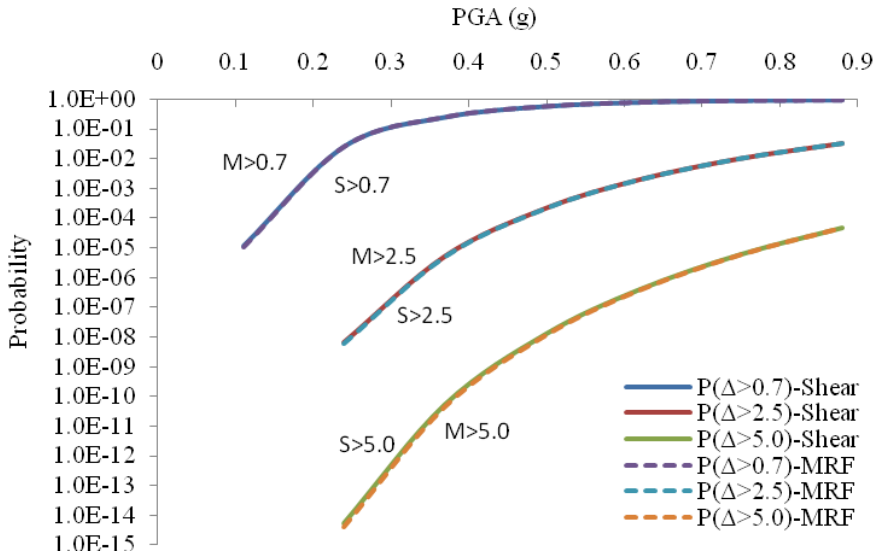

Figure 2.13(b) Fragility Curves for Three Limit States in 1st Story of the Model Buildings (Log Scale)

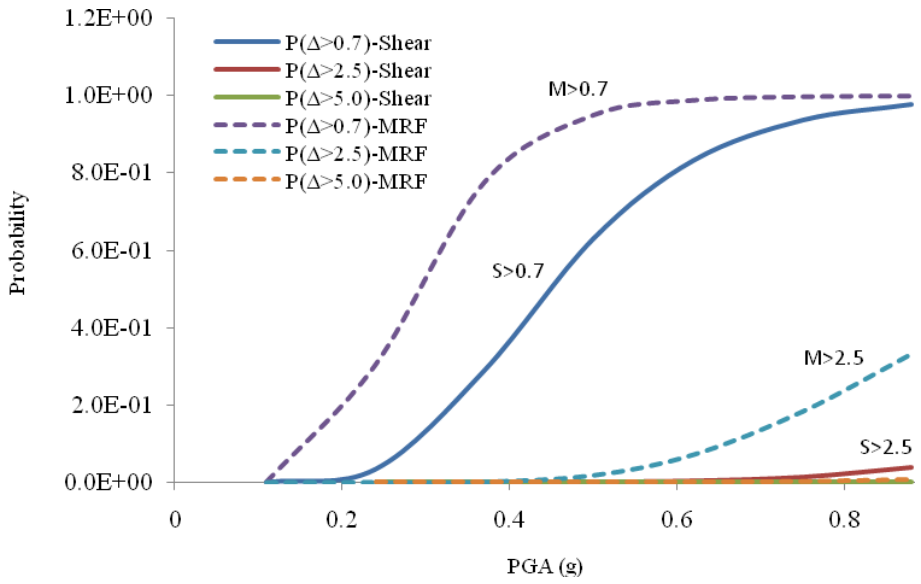

Figure 2.14(a) Fragility Curves for Three Limit States at the 5th Story of the Model Buildings (Natural Scale)

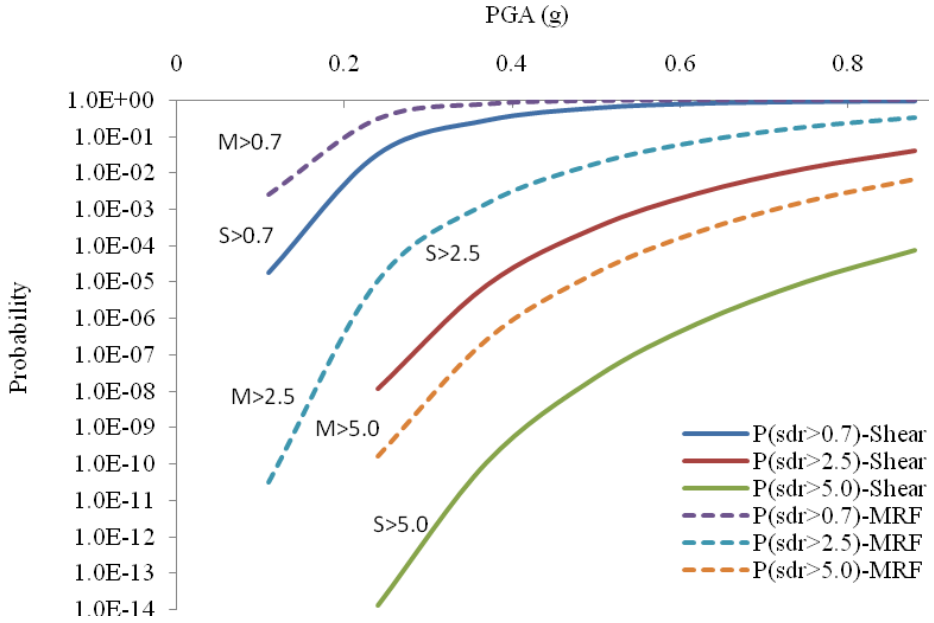

Figure 2.14(b) Fragility Curves for Three Limit States at the 5th Story of the Model Buildings (Log Scale)

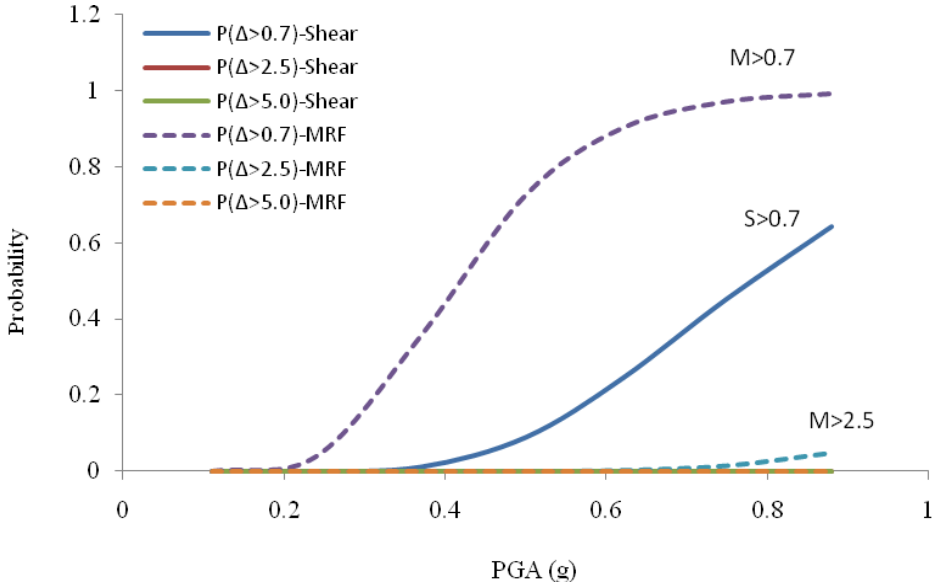

Figure 2.15(a) Fragility Curves for Three Limit States in the 9th Story of the Model Buildings (Natural Scale)

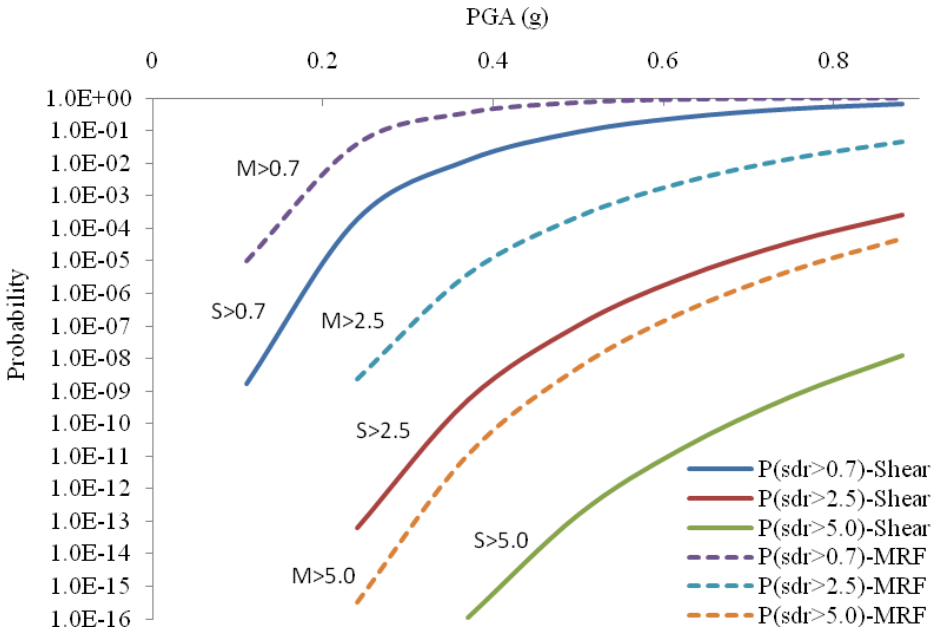

Figure 2.15(b) Fragility Curves for Three Limit States in the 9th Story of the Model Buildings (Log Scale)

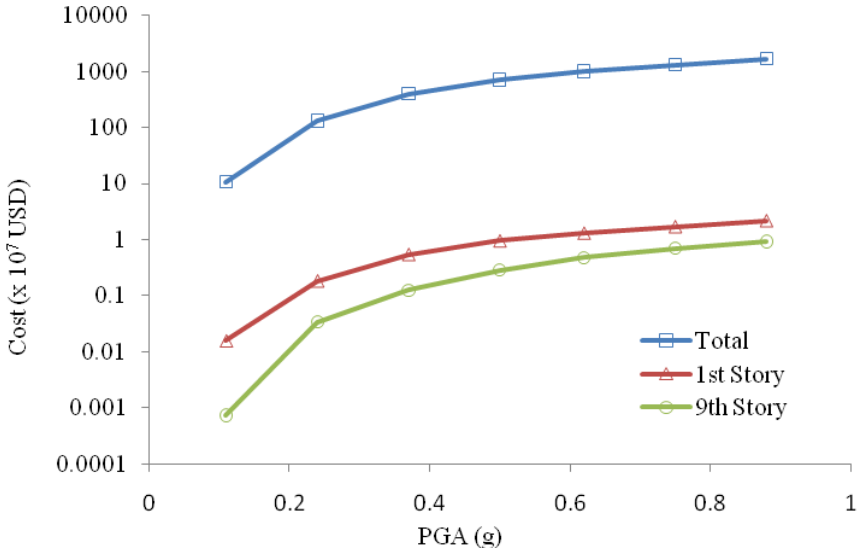

Figure 2.16 Limit State Cost of Shear Building Model at Different Story

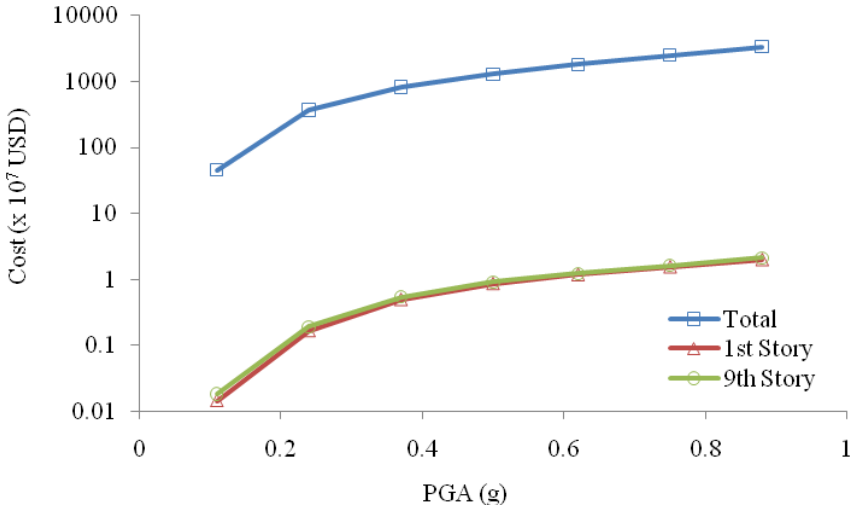

Figure 2.17 Limit State Cost of MRF Building Model at Different Story

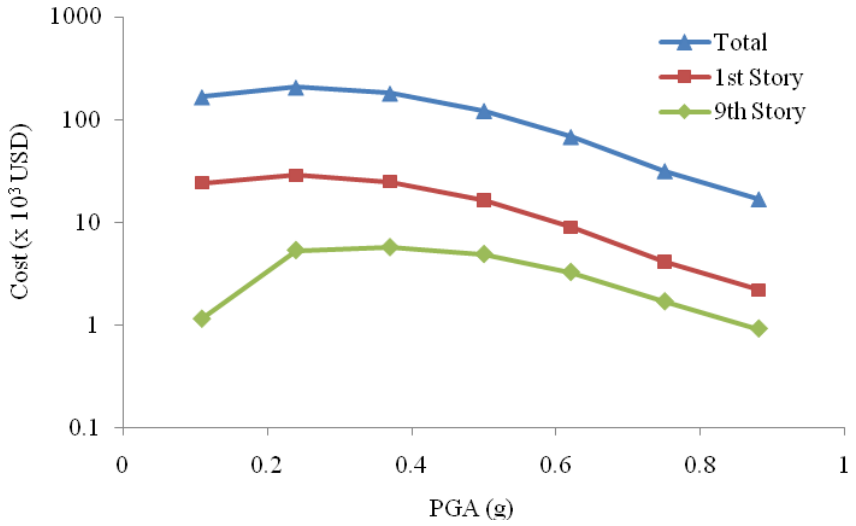

Figure 2.18 Expected Failure Cost of Shear Building Model

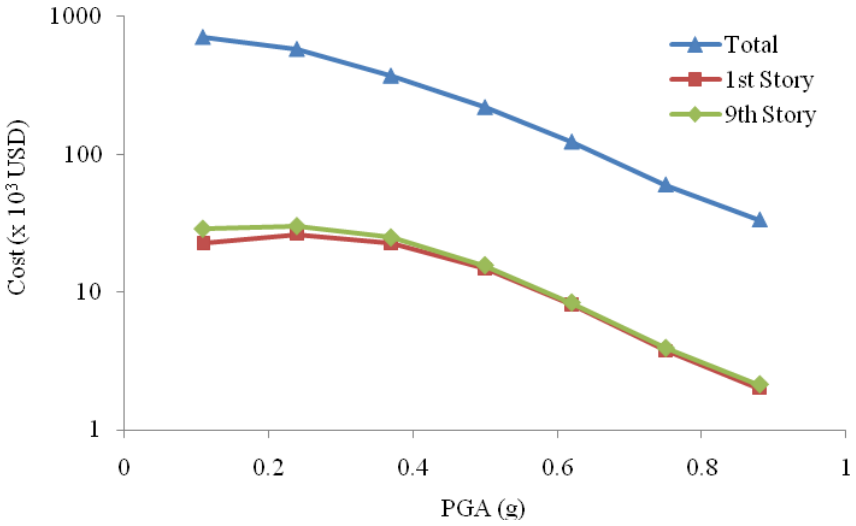

Figure 2.19 Expected Failure Cost of MRF Building Model

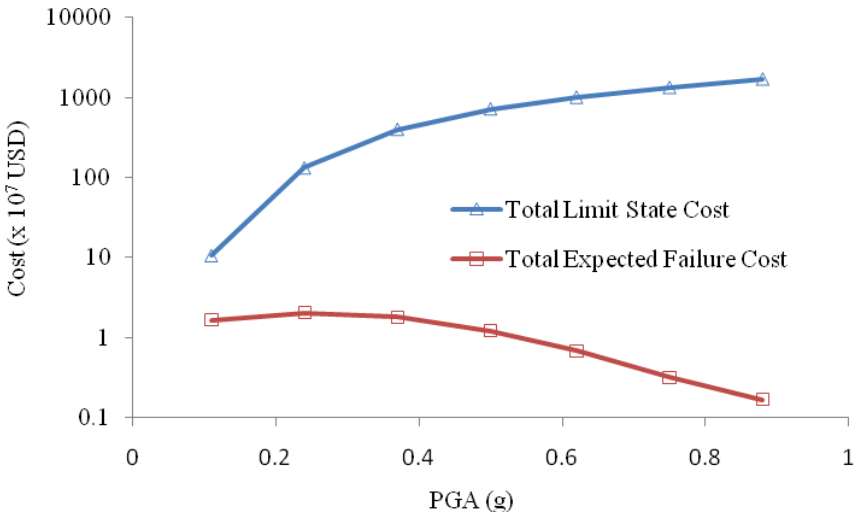

Figure 2.20 Comparison of Total Limit State Cost and Total Expected Failure Cost of Shear Building Model

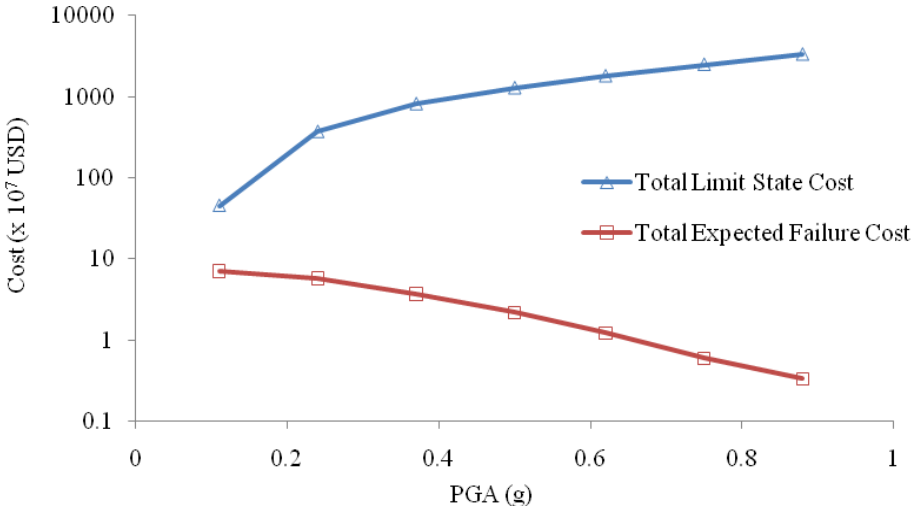

Figure 2.21 Comparison of Total Limit State Cost and Total Expected Failure Cost of MRF Building Model

CHAPTER 3

Optimal Design with Fluid Viscous Damping Devices

3.1 Introduction

A basic framework for carrying out the life-cycle-based optimal design with supplementary damping devices under seismic loading was presented in Chapter 2. In this chapter that framework is applied to obtain optimal designs for the two model structures with fluid viscous dampers. In the following chapters, other types of dampers will be considered. The various numerical results obtained for the designs with dampers are compared with the results without dampers.

As is well known, the fluid viscous dampers oppose the motion by creating a relative velocity dependent force, and dissipate seismic energy by heating of the fluid. They contain a cylindrical fluid chamber in which a piston with an orifice or orifices moves against the fluid. The two opposite ends of the device are attached at two different points on the structure which experience relative motion between them. In a building structure, these two ends could be on two adjacent floors of the building. The damper is attached to these two points either through a cross bracing or a Chevron-type brace. See Figure 3.17. A damper with such attachments will provide a force to oppose the relative motion between the floors. Such dampers are also commonly used in mechanical and aero structures primarily to reduce the motion and dissipate energy.

This velocity dependent force can be linearly or nonlinearly related to the relative velocity of the piston. The dampers can be manufactured to have both the linear or nonlinear damping force characteristics. In this study, we are assuming the classical representation of these dampers where the damping force is assumed linearly proportional to the relative velocity. This will allow us to use linear or modified linear response analysis methods. The design framework presented in the previous chapter, however, can also be applied to dampers with nonlinear behavior except that the linear analysis methods would not be applicable. Since the optimization process defined in the previous chapter requires a very large number of repeated calculations, the assumption of linearity for slightly nonlinear devices will also facilitate the optimal

design process, especially for preliminary investigation. This can be followed by more refined analyses where all the nonlinearities of the system can be included in the final evaluation of the optimal design obtained with the assumption of linearity.

In the following section we describe the analytical model of a building structure installed with linear viscous dampers and subjected to base excitation. This is followed by a brief description of an analytical approach that can be used to calculate the response of building structures. For the calculation of the failure costs, the responses of our interest are primarily the inter-story drifts. The approach is also used to calculate the other response quantities affected by the installation of dampers. Following this, the numerical calculation of the failure cost using the inter-story drifts and the optimization results are described.

3.2 Analytical Framework

Equations of Motion

The equations of motion of a structure installed with dampers at discrete locations and subjected to earthquake induced ground motion at its base can be written in the following form:

$$\mathbf{M}\,\ddot{\mathbf{u}}(t) + \mathbf{C}_s\dot{\mathbf{u}}(t) + \mathbf{K}\,\mathbf{u}(t) + \sum_{d=1}^{n_l}\mathbf{r}_d\, n_d\, F_d(t) = -\mathbf{M}\boldsymbol{\iota}\ddot{u}_g(t) \tag{3.1}$$

where **M, K** and $\mathbf{C}_s$ represent, respectively, the $N\times N$ mass, structural stiffness and inherent structural damping matrices; $\mathbf{u}(t)$ represents the relative displacement vector with respect to the base; a dot over a symbol indicates differentiation with respect to time; $\boldsymbol{\iota}$ is the vector of influence coefficients of ground motion to the structure; $\ddot{u}_g(t)$ = earthquake induced base acceleration. N is the number of dynamic degrees of freedom of the structure; $F_d(t)$, the local force applied by a passive damper installed at the d^{th} location, is considered through the N-dimensional influence vector $\mathbf{r}_d$, with n_d being the number of identical dampers at the location and n_l the number of possible locations for a device in the structure.

To define the local damper force, $F_d(t)$, for a viscous damper, several refinements can be considered. The first is to consider the frequency dependence of the damper force.

Several models have been suggested and used. The simplest is the classical visco-elastic Maxwell model in which the damping force is defined by the following differential equation:

$$F_d(t) + \frac{C_d}{K_d} \cdot \frac{dF_d(t)}{dt} = C_d \cdot \frac{d\Delta_d(t)}{dt} \tag{3.2}$$

where K_d is the stiffness of the damper at a very large frequency and C_d is the damping coefficient at zero frequency. The ratio, $\frac{C_d}{K_d}$, is referred to as the relaxation time constant in the literature on visco-elastic materials. Δ_d is the deformation of the damper. This model can be used in the analysis if desired. However, the high frequency effects are often not considered important and thus this model is further simplified by neglecting the derivative term on the left hand side of the above equation to produce the following popular classical model:

$$F_d(t) = C_d \cdot \frac{d\Delta_d(t)}{dt} \tag{3.3}$$

One can also include the effect of brace stiffness in this force model. Usually a damper will be installed either in a diagonal brace or a Chevron brace. Considering the brace stiffness along the damper, this effect can be incorporated through the following equation:

$$F_d(t) + \frac{C_d}{K_b} \cdot \frac{dF_d(t)}{dt} = C_d \cdot \frac{d\Delta_s(t)}{dt} \tag{3.4}$$

This equation is similar to Eq. (3.2) except now Δ_s is the relative displacement of the two points on the structure where the brace and the damper are connected. The stiffness of a brace is usually very large, which makes the brace deformation much smaller than the deformation of the damper, and thus the second term on the left hand side of the above equation associated with the brace deformation can be ignored. This simplifies the damper force equation to the following:

$$F_d(t) = C_d \cdot \frac{d\Delta_s(t)}{dt} \tag{3.5}$$

For a relatively rigid diagonal brace making an angle of θ_b with the horizontal, the local damper force in the horizontal direction can be modified using the following equation:

$$F_d(t) = C_d \cdot \frac{d\Delta_s(t)}{dt} \cos^2 \theta_d \tag{3.6}$$

The structural deformation Δ_s and its derivative in the above equation can be

expressed in terms of the global relative displacement vector $\mathbf{u}(t)$ as:

$$\Delta_d(t) = \mathbf{r}_d^T\, \mathbf{u}(t); \qquad \dot{\Delta}_d(t) = \mathbf{r}_d^T\, \dot{\mathbf{u}}(t) \tag{3.7}$$

With the substitution of Eq. (3.7) in Eq. (3.1) we obtain the following equation of motion:

$$\mathbf{M}\,\ddot{\mathbf{u}}(t) + \mathbf{C}_s\dot{\mathbf{u}}(t) + \mathbf{K}_s\,\mathbf{u}(t) + \sum_{d=1}^{n_l} n_d\, C_d \mathbf{r}_d\, \mathbf{r}_d^T \dot{\mathbf{u}}(t) = -\mathbf{M}\boldsymbol{\iota}\ddot{u}_g(t) \tag{3.8}$$

The last term of the right hand side gives the contribution of the supplementary dampers. Combining the two damping terms, we can write the equation in the following standard form:

$$\mathbf{M}\ddot{\mathbf{u}}(t) + \mathbf{C}\dot{\mathbf{u}}(t) + \mathbf{K}\mathbf{u}(t) = -\mathbf{M}\boldsymbol{\iota}\ddot{u}_g(t) \tag{3.9}$$

wherein now $\mathbf{C}$ is the combined damping matrix defined as:

$$\mathbf{C} = \mathbf{C}_s + \sum_{d=1}^{n_l} n_d C_d \mathbf{r}_d \mathbf{r}_d^{\mathrm{T}} \tag{3.10}$$

The objective of the design is to find the optimal values of the damper locations, *d*, the number of dampers at the location, n_d, and the size of the damper represented by the coefficient C_d such that the cost function defined in the previous chapter is minimized.

Response Analysis

To solve the equation of motion (3.9) for calculating the response, the following features of our problem must be considered: (a) the non-classical nature of the damping matrix and (b) nonlinearity of the structure if the seismic intensity is large and there is yielding in the structure. Since we need to calculate the response a large number of times for many different candidate designs in the design space for the genetic algorithm to converge to the optimal system, the response procedure must be efficient computationally. Keeping these objectives in mind, we have used an appropriate response spectrum method for linear analysis with the seismic input defined by response spectra for different seismic intensity levels of the hazard curve. This response spectrum method explicitly considers the non-classically damped nature of the system. Even if the original system is characterized by modal damping ratios (a common way to include the inevitable dissipation of energy in the system) and can be assumed classical, the system enhanced by installation of different numbers of supplementary dampers at different locations would induce non-classicality in the system. This non-classical feature prevents the use of the classical modal analysis method, and thus we have used a special

response spectrum method, briefly described below. To account for the nonlinearity caused by high intensity ground motions, we have modified this response spectrum method as per the 2009 NEHRP Provisions (2009) for these high intensity inputs. This response spectrum method also provides a workable approach in search of the optimal design as the computational time required here is relatively small compared to any other dynamic analysis approach.

The non-classical response spectrum method is based on the earlier work of Singh (1980) with further enhancements proposed by Maldonado and Singh (1991a,b). The earlier version of Singh's method did not consider the possibility of having large levels of damping in the system which can lead to over-damped modes. The study by Maldonado and Singh (1991a,b) used a rigorous approach to include the contributions of over-damped modes. This study also made an improvement to account for the missing mass effect caused by the truncation of modes, especially in stiffer systems. In the following we only describe the steps that are needed to use this response spectrum method for the sake of completeness of the work. These methods are based on the random vibration theory of structures and the theory behind the development of these methods is given in the cited references. The basic steps are as follows:

Uncoupling of Equations into Modal Equations: Since response spectrum methods are based on uncoupling of the coupled equations of motions into modal equations and then combination of the maximum modal response by a mode combination rule, basically the same process needs to be developed for the non-classical systems. For this, one re-states the equations of motion in state space and then uses the complex modes of the state space system to uncouple the equations with the following steps:

2N-dimensional State Equations*:* The equations of motion (3.8) can be written in the following form using auxiliary equations:

$$\mathbf{A}\dot{\mathbf{y}}(t) + \mathbf{B}\mathbf{y}(t) = -\mathbf{D}\ddot{u}_g(t) \tag{3.11}$$

where $\mathbf{y}(t)$ is the 2N-dimensional state vector whose upper half is the vector of relative velocity $\dot{\mathbf{u}}(t)$ and lower half is the vector of relative displacement $\mathbf{u}(t)$. The system matrices **A** and **B** are symmetric and 2N×2N dimensional. **D** is the 2N-dimensional system vector. The matrices and vectors of Eq. (3.11) can be defined in the following form:

$$\mathbf{A}=\begin{bmatrix}\mathbf{0} & \mathbf{M}\\ \mathbf{M} & \mathbf{C}\end{bmatrix};\quad \mathbf{B}=\begin{bmatrix}-\mathbf{M} & \mathbf{0}\\ \mathbf{0} & \mathbf{K}\end{bmatrix};\quad \mathbf{D}=\begin{Bmatrix}\mathbf{0}\\ \mathbf{M\iota}\end{Bmatrix};\quad \mathbf{y}(t)=\begin{Bmatrix}\dot{\mathbf{u}}(t)\\ \mathbf{u}(t)\end{Bmatrix} \tag{3.12}$$

Complex Eigenvalue Analysis: To uncouple the state equations, the eigenproperties of the following eigenvalue problem are used:

$$\mathbf{-pA\Phi = B\Phi} \tag{3.13}$$

where $\mathbf{p}$ is a diagonal matrix of eigenvalues p_j and $\mathbf{\Phi}$ is the matrix of mode shapes whose columns are the eigenvectors $\boldsymbol{\varphi}_j$.

Uncoupled equations of principle coordinates – complex-valued modal coordinates*:* Using the standard transformation, the state vector $\mathbf{y}(t)$ is expressed in terms of the vector of the modal coordinates $\mathbf{z}(t)$ as:

$$\mathbf{y}(t)=\mathbf{\Phi z}(t) \tag{3.14}$$

The uncoupled equation for the j^{th} modal coordinates $z_j(t)$ is then obtained as:

$$\dot{z}_j(t)-p_j z_j(t)=-F_j\ddot{u}_g(t);\qquad j=1,...,2N \tag{3.15}$$

where $z_j(t)$ and F_j, respectively, are the modal coordinate and the modal participation factor for the j^{th} mode. These equations occur in complex conjugate pairs for under-damped modes and appear as real equations for the over-damped modes. For the mode shapes normalized with respect to the state matrix, $\mathbf{A}$, the modal participation factor is defined as

$$F_f=\boldsymbol{\varphi}_j^T\mathbf{D} \tag{3.16}$$

Response quantity of interest*:* Using the modal solution of Eq. (3.15), a response quantity of interest such as displacement, velocity, acceleration, bending moment, story drift, etc, that can be expressed as a linear transformation of the state vector as follows:

$$r(t)=\sum_{j=1}^{2N}\rho_j\int_0^t\ddot{u}_g(\tau)e^{p_j(t-\tau)}d\tau \tag{3.17}$$

where ρ_j is the jth mode shape of the response quantity of interest obtained by linear transformation of the complex mode shape $\boldsymbol{\varphi}_j$ as:

$$\rho_j = \mathbf{T}^T \boldsymbol{\varphi}_j \; F_j \tag{3.18}$$

For a given time history of ground motion, Eq. (3.17) can be used to calculate the time history of any response quantity of interest, such as inter-story drift, using direct integration. For each time history one can then calculate the maximum value of the response quantity. Using these maximum values of the response for all the time histories, one can calculate the mean and standard deviation of the response quantity for later use in a probability analysis. This approach to calculate the mean and standard deviation of the story drifts, the quantities of our interest in calculating of the failure costs, can however be simplified significantly by using the response spectrum method. Eq. (3.17) can be used to develop a response spectrum method (Maldonado and Singh, 1991 a,b) to calculate the maximum value of the response quantity using a random vibration procedure as defined by the following equation:

$$\mathbf{R}(t) = \sqrt{\left(\mathbf{R}_1\right)^2 + \left(\mathbf{R}_2\right)^2 + \left(\mathbf{R}_3\right)^2} \tag{3.19}$$

where $\mathbf{R}(t)$ is the maximum response value of interest and terms $\left(\mathbf{R}_1\right)^2$, $\left(\mathbf{R}_2\right)^2$, and $\left(\mathbf{R}_3\right)^2$ are defined as follows:

$$\left(\mathbf{R}_1\right)^2 = \sum_{j=1}^{n_r} \rho_j^2 \left(L_j\right)^2 + 2\sum_{j=1}^{n_r-1} \sum_{k=j+1}^{n_r} \frac{\rho_j \cdot \rho_k}{\left(p_j + p_k\right)} \left\{ p_j \left(L_j\right)^2 + p_k \left(L_k\right)^2 \right\} \tag{3.20}$$

$$\left(\mathbf{R}_2\right)^2 = 2\sum_{j=1}^{n_r} \sum_{k=1}^{n_c} \rho_{jk} \left\{ A_{jk} \left(L_j\right)^2 + B_{jk} \left(\frac{A_k}{\left(\omega_k\right)^2} \right)^2 + C_{jk} \left(V_k\right)^2 \right\} \tag{3.21}$$

$$\left(\mathbf{R}_3\right)^2 = \sum_{k=1}^{n_c} \left[g_k^2 \left(\frac{A_k}{\left(\omega_k\right)^2} \right)^2 + 4a_k^2 \left(V_k\right)^2 \right] + 2\sum_{j=1}^{n_c-1} \sum_{k=j+1}^{n_c} \left[W_{jk} \left(\left(\frac{A_j}{\left(\omega_j\right)^2} \right)^2 - \frac{\left(A_k\right)^2}{\left(\omega_k\right)^4 \Omega^4} \right) + \right.$$

$$\left. Q_{jk} \left(\left(V_j\right)^2 - \left(V_k\right)^2 \right) + \frac{g_j \cdot g_k}{\Omega^2} \left(\frac{A_k}{\left(\omega_k\right)^2} \right)^2 + 4a_j a_k \left(V_k\right)^2 \right] \tag{3.22}$$

where the term $\mathbf{R}_1$ is the contribution of n_r of the real-valued over-damped modes; $\mathbf{R}_3$ is the contribution of n_c of the complex-valued under-damped modes; and $\mathbf{R}_2$ represents the contribution of the correlation between the real-valued and complex valued modes. The calculation of $\mathbf{R}_1$ requires the definition of the base input in term of the velocity response of a massless first order system. This form of the input can be generated using a large ensemble of recorded accelerograms in the same way as the design response spectra are developed, but this description is usually not available. The other two terms require the input defined in terms of the usual pseudo acceleration response spectra as well as relative velocity spectra. The pseudo acceleration spectra are very commonly used. The relative velocity spectra can also be defined in terms of the pseudo acceleration spectra with the help of the publications available in the open literature. To evaluate the relative importance of these various terms in the above equation, a small side study was conducted for an input defined by the spectral density function of Kanai-Tajimi form (Kanai, 1961; Tajimi, 1960). This study indicated that, the total contribution of the first two terms to the total response was not significant and thus these terms could be neglected. In this study these terms were thus not considered in the calculation of the story drift response by the response spectrum method. We now define various terms that are used in the calculation of $\mathbf{R}_3$ as follows:

$$p_j = -\beta_j\omega_j + i\left(\omega_d\right)_j = -\beta_j\omega_j + i\omega_j\sqrt{1-\beta_j^2};\ \ i=\sqrt{-1}; \qquad j=1,...,n_c$$

$$\text{Modal frequency} = \omega_j = \left|p_j\right|;$$

$$\text{Modal damping ratio } = \beta_j = -\frac{\text{Re}(p_j)}{\omega_j}$$

Modal response quantities:

$$\rho_j = a_j + ib_j \tag{3.23}$$

$$g_j = 2\omega_j\left[b_j\sqrt{1-\beta_j^2} - a_j\beta_j\right]$$

Input Spectrum Quantities:

A_j = pseudo acceleration response spectrum value at ω_j and β_j

V_j = relative velocity response spectrum value at ω_j and β_j

The other terms W_{jk} and Q_{jk} that appear in term $\mathbf{R}_3$ are the coefficients of partial fraction given in Maldonado and Singh, 1991 a,b. They are also provided in Appendix C in terms of the notations used here for ready availability and use, and also for

completeness sake. The relative velocity response spectrum is essentially the same as the pseudo velocity response spectrum for the lower ranges of frequencies. For frequencies higher that about 10 cps, the relative velocity response value decreases compared to the pseudo velocity spectrum. Gupta (1990) developed an approach to define the relative velocity response spectrum from the pseudo velocity response spectrum for use in his study on the seismic analysis of non-classically damped systems. He calculated four boundary frequencies from the pseudo response quantities of a structure and divided the possible frequency range of structure into four intervals with respect to the boundary frequencies and used different equations to develop the relative velocity response spectrum for each interval. This method is used for this study to get the relative velocity response spectrum value.

Response Spectrum Method and Inelastic Behavior

For the lower values of the ground motion intensities in the hazard curve, the structure remains elastic. The possibility of it remaining elastic is increased even for higher values of intensities with the installation of supplementary damping devices as they will reduce the response further. So for most values of the ground motion intensities, one can use the linear response spectrum method to calculate the inter-story drifts. For a few higher level ground motion intensities, however, the approach needs to be modified. The most accurate way is to conduct a time history analysis of the structure for several ground motion time histories representing the variability in ground motion. As mentioned earlier, this approach can become prohibitively costly especially for the purposes of finding optimal designs where many such analyses will be needed for a large population of possible designs in the search space. Also, as indicated earlier, although large intensity ground motions can cause large damage costs, the associated failure costs will not be significant because of the rarity of the occurrences of the large intensity earthquakes. For these reasons to get a reasonable estimate of the failure cost, we propose use of the response spectrum approach prescribed by 2009 NEHRP Provisions which considers the nonlinear effects in a simplified manner. As mentioned in Chapter 2, this approach consists of modifying each modal input response spectrum value by a factor expressed as $C_d / (R / I)$. Since this factor does not depend upon the modal frequency, one only needs to multiply the inter story-drift calculated by the linear response spectrum by this factor.

3.3 Optimal Design

In this section we outline the elements of the optimization approach that we have used to obtain the best design with minimum cost following the framework presented in Chapter 2. The objective is to minimize the combined cost of failure and cost of installing the damping devices. That is, we will be aiming at finding the least number of dampers placed at the best locations on the structure to get the desired reduction in the structural response to minimize the cost of failure enough to compensate for the cost of damper installation. In the market many different damper sizes are available to meet the industrial need. The cost of a damper increases with the size of the damper, but not necessarily in direct proportion. So another design variable could be the capacity damper one should choose to minimize the failure cost enough to be of benefit. In this study we considered the dampers manufactured by Taylor Devices, a leading manufacturer of the dampers for mechanical systems and now for building structure applications. Table 2.1 shows the seven types of dampers that they manufacture. We identify these seven dampers as $Fv1, Fv2..., Fv7$. The table provides their damping coefficients, costs and other physical parameters. The numbers in this table were obtained from the manufacturer and its website. With these different choices of available dampers, the optimization problem could be stated in the following form:

Obtain the design variables, $(N_{d1}, N_{d2}, .., N_{d7})$
To minimize the cost function, $f(N_{d1}, N_{d2}, .., N_{d7})$
Within the constraints, $g_j(N_{d1}, N_{d2}, .., N_{d7})$

where N_{di} is the vector containing the numbers of the dampers identified as Fvi placed in different stories of the building. The cost function $f(N_{d1}, N_{d2}, .., N_{d7})$ consists of the failure cost and cost of the devices and, thus, it depends on the design variables. As explained in Chapter 2, this function is normalized by the failure cost of the original building without any dampers, and a smaller value of this number indicates a better design. More will be said about the calculation of this function later.

The constraints $g_j(N_{d1}, N_{d2}, .., N_{d7})$ in the optimization problem define the limits on the number of dampers. This number is determined by their sizes and the number of available locations in the building. In the building models chosen for this study, there

are a total of 15 bays (Figure 2.10). Considering the size of the columns and the spacing between the columns, it was assumed that no more than two of the largest dampers can be installed in a bay. One could accommodate more than two of the small dampers, but based on the consideration of installing braces, this number was limited to two. Thus, with a limit of two dampers per bay and 15 bays, one could essentially install a total of 30 dampers per floor. In this study this number was, however, limited to 18 per floor as some bays may be needed for other purposes.

Reduction of Design Variables

To search for the optimum design, a genetic algorithm was used. As described in Chapter 2, we start with a population of possible designs. The size of the population depends on the number of design variables. A problem with large number of design variables will have a large design space, and thus it should have a large population to search for the optimal design with a genetic algorithm. In the optimization problem stated in Eq. (3.24) above, there are a total of 63 design variables: seven different dampers and nine different locations where they can be placed. Also, the total number of the dampers can vary between 0 and 18 divided into many possible combinations. That is, in a story these can be a maximum of 18 dampers. So the number of possible design combinations can be very large. So it was first considered necessary to reduce the number of different variables.

One variable that could be reduced is the number of damper choices. It is reasonable to assume that more damping in the structure is likely to improve its performance in terms of reduced failure cost. Table 2.1 lists seven different choices. From the cost values given in Table 2.1 for different dampers, one can see that we get most out of the large dampers in terms of damping coefficient per dollar. This will tend to favor larger dampers, especially for civil engineering applications where the demands on the capacity are large and constraints on the space needed for installation are not that severe as in mechanical applications. This assertion was validated by a preliminary optimization study in which the best design was found to be the one using the largest Fv7 dampers. However, there could be a situation where a smaller size damper may be sufficient according to the optimization algorithm and thus using a larger size may be a waste of money. Keeping this in mind, another optimization study was conducted where two dampers from the large capacity dampers were mixed, but there was no significant difference in the cost function to justify the use of another variable in the problem.

Herein, thus, the results of design using only Fv7 dampers are presented. In the calculating of the object cost, the cost of the Chevron brace was also included at $340/m length of the brace members for Fv7. The brace was designed to carry more than the damper capacity listed in Table 3.1. The actual force in the brace or damper varied with the seismic intensity and the maximum force induced was always less than the damper capacity. The brace size and its cost could be reduced, but brace was not re-sized. That is, no optimization on the brace cost was attempted and the cost of the original brace design was used in the object cost calculations.

Genetic algorithm (GA) requires a repeated calculation of performance index for each individual design in a population of a generation. These performance index values are then used in an evolutionary way to create successively new generations that tend to converge to the optimal performance. This optimal search requires a large computational effort. A large search space will require the use of a large population size and several generations and, thus, commensurately large computation time to converge to the optimal value. To reduce this effort, one effective method is to reduce the searching space of variables. To define an individual in a GA population, one generates a vector of genes the values of which are randomly generated within the expected range. However, one must have a good idea about this range in which various gene values need to be selected. In the context of our problem, we need to have some idea about what number of dampers we need to place on a floor to obtain a possible design. For this a preliminary study was conducted to estimate the total amount of damping one is likely to need to reduce the response by a certain amount. To estimate this value, an optimization study was conducted which estimated the damping coefficient value one would need in different stories to reduce the maximum story drift by 50% if a design level earthquake occurred. The design level earthquake was defined in Chapter 2 for the site in Los Angeles. In this preliminary study, no failure cost analysis was conducted as it takes much computational effort to do this. This study provided the range of values one needs to choose to create a potentially optimal design. Based on the values obtained in the preliminary design, the damping values at different floors between the range of 0 and 150% of the preliminary values were considered to form a possible design in the design space.

Failure Cost

The elements involved in the calculation of the failure cost were explained in Chapter 2.

For a design made with a given configuration of installed fluid viscous dampers, the following steps are implemented to calculate the failure cost in this chapter:

Step 1: Calculate the means and standard deviations of the inter-story drifts for all seven discrete values of hazard intensities defined in Chapter 2. For this, the seismic input is defined by response spectrum curves like the one shown in Figure 2.11. For these inputs the story drifts are calculated by using the response spectrum defined by Eq. (3.22). Only the $\mathbf{R}_3$ term is used in this study as the other terms were observed to be relatively insignificant. The response spectrum method was also used to calculate the stresses in the columns of the shear frame and the beams and columns of the moment resistant frame. If these elastically calculated stresses exceeded the yield stress at several locations in a story, the structure was assumed to behave nonlinearly. In that case the story drifts were calculated by using the modified response spectrum approach as described in 2009 NEHRP Provisions (2009).

Step 2: Calculate the probabilities of the story drift in all stories being in different limit states using Eq. (2.13) and the story drift parameters calculated for the each seismic intensity in Step 1.

Step 3: Calculate the expected failure cost using Eq. (2.11) with the damage costs developed in Chapter 2 for each building model, for different limit states, and the limit state probabilities calculated in Step 2 above.

Step 4: Calculate the total expected cost using the cost of dampers and their maintenance cost. Normalize this cost by the failure cost of the original building to define the cost function.

3.4 Numerical Results

In this section we present the numerical results obtained for the two building models using the approach described above and in Chapter 2. The results are obtained for the failure cost and the optimal distribution of dampers obtained by the GA approach. To start the GA approach, a population size of 400 designs was selected. These initial designs were changed using the evolutionary rules described in Chapter 2.

Figures 3.1 and 3.2 show evolutionary trends toward convergence to the optimal design for the two building models. It required 48 generations to converge for the shear building and 80 generations for the moment frame building. The convergence to the optimal design was assumed and the optimal search was stopped when the cost function value calculated in a generation did not change by 0.1% in the next 40 generations (10% of the population size.)

The results in Tables 3.2 and 3.3 show the total amount of damping and the distribution of the number of dampers and total damping coefficient in each story obtained by minimization of the cost functions. The effect of the installation of these dampers on the system frequencies and modal damping ratios is shown in Tables 3.4 and 3.5. From these tables we observe that the modal frequencies have changed only slightly but the modal damping ratios have increased significantly. Some of the modes have also become over-damped. This enhanced modal damping is primarily responsible for reducing the system response and consequently the failure cost.

Tables 3.2 and 3.3 also provide the percentages of the total damping coefficient value that are placed in different stories of the two buildings. For a better appreciation and comparison of the differences in these numbers for the two different building designs, Figure 3.3 compares the percentages of total damping coefficient at different stories in the two building models. Comparison of the results of the two systems indicates some differences (especially a large difference in the damping in the first story). However, the damping requirement as well as the distribution of the damping along the stories is more a function of the dynamics of the individual building and the models used, and based on the comparison of limited results, it is not possible to define any special trend as a function of the building characteristic (flexible or rigid) or its type (shear or MRF)

In Tables 3.6 and 3.7, we present the comparison of different costs for the two models. The tables give the initial costs, damper costs, failure costs, object costs (sum of the failure cost and damper cost) which were minimized, total life cycle cost (excluding building maintenance, etc.), and annualized value of the failure cost. Table 3.6 is for the shear building model and Table 3.7 for the MRF building model. For comparison purposes, each table gives these costs for the original building as well as for the building optimally configured with FVDs to minimize the object cost. Percent differences between the comparable costs are also given in the parentheses in the last columns of these tables.

One general observation that is common for both building types is that the failure cost can be significantly decreased by installation of the dampers. For both building models considered in this study, the failure costs are reduced by more than 85%. This reduction in the object cost, which now includes the cost of performance improvements (cost of damper), is about 58% for the shear building and about 76% for the MRF building. This difference in the level of reduction for the two building is dues to the fact that the original MRF building has a very large failure cost, and the damper installation brings a large drop in dollar figures for relatively the same level of damping addition. The reduction in the total life cycle cost is not much (3.3% for the shear Building and 11.4% for the MRF building), primarily because the failure costs are relatively small compared to the initial cost. Nonetheless, the MRF building seems to be more affected by the damper installation than the shear building. The last rows of these two tables indicate the reduction in the annual average cost of the failure to the building owner.

A point worth noting here is that these aforementioned reductions in the costs are achieved by a rather small investment in protective devices compared to the initial cost. For example, the cost of dampers as a percentage of the initial cost is about 1.6% in the shear building and about 2.1% in the MRF building.

The results in the next two Tables 3.8 and 3.9 show the distribution of the expected failure cost with the intensities of ground motion representing the seismic hazard at the site. Figures 3.4 and 3.5 also show the plots of these cost values for the two building models, and show more clearly in visual form their variations with intensities. First we observe, as also shown by the results presented in Chapter 2 for the original buildings, that total failure costs are much higher for the more frequent lower intensity ground motions than for the less frequent but high intensity ground motions. Of course, a high intensity ground motion, *if occurs*, will cause more damage than a low intensity ground motion. But when one considers the relatively small chances of experiencing a larger earthquake in the calculation of the expected failure cost, the cost value becomes smaller than that for the low intensity but more often occurring earthquakes. The optimal installation of the dampers that dissipate energy all the time at all intensities thus also focuses more on reducing these higher costs. We note from the numbers in the last columns of these two tables that the failure costs for the lower intensities are drastically reduced for both buildings, varying between 100% for the lowest intensity in the hazard model to about 60 to 70% for the high intensities. It is important to note that

this cost based optimization methodology directly deals with the issue of reducing the high economic losses that were observed due to the medium intensity seismic events in the Loma Prieta, Northridge and Kobe earthquakes which prompted the initiation of the performance based design thinking in the community.

Although the results in the tables can be compared to examine the differences in the results of the two buildings, Figure 3.6 compares these cost reductions graphically. The reductions are similar for the two models except for some large differences for the higher intensities. To some extent these differences will, of course, also depend on the building model.

Implications of the Nonlinearity of Structural Behavior on the Cost Analysis

In the cost analysis presented in this study, it was assumed that the structure satisfying the current design guidelines behaves linearly under the lower intensity motions. Thus the cost estimated for these motions were based on linear methods of analysis such as the response spectrum method. For the higher intensity ground motion, the designed structure could however yield, and thus the cost estimates based on the assumption of linearity may be different from those obtained with more accurate analysis with the realistic situation of the nonlinear structure. However, since the contribution of the less frequent higher intensity ground motion to the overall cost is relatively much smaller than those of the lower intensity and more frequent motions, error in this small contribution is not likely to alter significantly the final outcome of the optimization process.

To examine these observations, a small numerical study was conducted in which the cost for the shear building was estimated using the story drift responses calculated with three response analysis methods: (a) the elastic response spectrum approach presented in this study, (b) the modified response spectrum approach according to 2009 NEHRP Provisions (2009) to include the effect of yielding through R and C_d factors, and (c) a rigorous step-by-step time history analysis method considering the yielding of the structure with bilinear force deformation characteristics. Also, these cost analyses were made for only the last three hazard intensities where some stories of the structure yielded.

These cost analysis results are provided in Tables 3.10 and 3.11. The tables present the

failure cost values for the three highest intensity values calculated by the above three methods of response analysis. The next three rows of the tables provide: (a) combined cost for the three intensities, (b) total failure cost considering all intensities and (c) the total object cost which was minimized. The comparison of these cost results indicates some differences in the calculated values, although not much between the elastic and nonlinear time history approaches. (The larger difference between the NEHRP method and the nonlinear time history method is due to the use of the R and C_d prescribed by the 2009 NEHRP Provisions (2009) for the shear building model.) These differences in the cost values are reduced when we consider the total cost of failure, and more reduced when we consider the object cost – the item which was minimized.

The main conclusion one can draw from this discussion is that the use of one of the approximate methods of response analysis such as the one proposed in the 2009 NEHRP Provisions (which now represent best practices based on the current research and simplification need of the design community) for the calculation of the failure cost for optimal design of the damping configuration in a building is reasonably accurate.

Reductions in the Responses of Design Interest

The failure costs are reduced because the structural response is reduced. Although in the calculation of the failure cost we have only used the inter-story drifts, which are of course reduced by the installation of the dampers, other response quantities of design interest are also reduced significantly. These reductions are shown schematically in Figures 3.7 - 3.12 for the inter-story drifts, absolute accelerations of the floors, and story shear forces. The first three figures of this set (Figures 3.7-3.9) are for the shear building model and the next three (Figures 3.10-3.12) are for the MRF building. Both buildings show similar trends in the reduction of these response quantities. To compare the relative values of these reductions for the two models, we show Figures 3.13-3.15. Comparing the results in this set of figures, we observe that the story drifts and the story shears are reduced more in the MRF building than in the shear building. These results indicate that the flexible frame buildings are likely to benefit more from the optimal installation of the dampers than the stiffer frame buildings. The reductions in the absolute floor acceleration, which are of interest in the acceleration sensitive components, are sort of mixed in the two types of building, but here again the flexible moment resistant frame has higher reductions especially at higher levels of the building.

Effect of System Fragility

The reduction in the response of the structure due to installation of dampers has a huge impact on the fragility of the system across the hazard intensity values. This is clearly seen in the plots of the fragility curves shown for the limit state of immediate occupancy in Figure 3.16. The figure compares the probability of the maximum inter-story drift response in the buildings exceeding the value of 0.7% for the original buildings with those of the buildings installed with optimally configured dampers. The curves for both buildings are plotted together for comparison. The fragility values were also calculated for the other two limit states of life-safety and collapse, but they were nearly zero. Comparing the probability values for the original and damping enhanced buildings, we note a drastic reduction in the failure probabilities at the lower intensities for both buildings. The lower intensities are primarily responsible for contributing the most to the cost related to nonstructural component damage in the buildings. The optimal design reduces this cost drastically, thus achieving the primary objective of the performance-based design concept very well.

3.5 Chapter Summary

This chapter focused on the application of the life-cycle cost minimization framework presented in Chapter 2 for optimal design of fluid viscous dampers. First, the chapter presents a quick review of the analytical method for calculating the response of structures installed with these dampers, followed by the description of the optimization problem. Several choices that are available in the market to select the fluid viscous dampers to meet various damping needs from small mechanical systems to large civil engineering systems are considered. Preliminary analysis showed that it is best to select the largest available damper as the needs for the civil structures are usually very large. The numerical implementation of the optimization problem, specific to the use of the fluid viscous dampers, is discussed. The numerical results for the optimal distribution of the dampers in different stories, failure costs, level response reductions, and fragilities in different limit states are obtained for the two models of the structure. It is shown that optimally placed dampers drastically reduce the failure cost by reducing the building response. The failure costs are reduced for all seismic intensity levels, but the optimization algorithm focuses most in reducing the failure costs for the lower intensity levels which contribute the most to the total failure cost. This focus of the

optimization on reducing most the failure losses pertaining to the more frequent but low intensity level events directly addresses the core issue of the performance based design philosophy which was initially proposed to reduce large unexpected economic losses that were observed in the medium intensity Loma Prieta, Northridge and Kobe earthquakes. The reduction in the vulnerability of the structure is also drastic as indicated by the fragility studies for different limit states.

Tables 3

Table 3.1 Properties and Unit Cost of Fluid Viscous Damper (FVD) from Taylor Devices

Unit FVD	Capacity (KN)	Damping Coefficient ($\times 10^6$ N-sec/m)	Stroke (m)	Length (m)	Diameter (m)	Unit Cost ($)
Fv1	300	0.7	±0.08	0.85	0.08	2,000
Fv2	500	1.2	±0.10	1.04	0.11	3,200
Fv3	1000	2.5	±0.10	1.28	0.15	3,600
Fv4	1500	3.7	±0.10	1.42	0.19	4,400
Fv5	2000	4.9	±0.13	1.53	0.21	6,400
Fv6	2700	6.7	±0.13	1.62	0.24	8,600
Fv7	3900	9.8	±0.13	1.93	0.29	10,800

Table 3.2 Optimal Distribution of FVDs in Shear Building Model

Story	Number of Dampers	Total Damping	Distribution
	Fv7	($\times 10^6$ N-sec/m)	
1	5	49.3	26.3%
2	4	39.4	21.0%
3	4	39.4	21.0%
4	3	29.6	15.8%
5	2	19.7	10.5%
6	1	9.8	5.0%
7	0	0.0	0.0%
8	0	0.0	0.0%
9	0	0.0	0.0%
Total	19	187.2	100.0%

Table 3.3 Optimal Distribution of FVDs in MRF Building Model

Story	Number of Dampers	Total Damping	Distribution
	Fv7	($\times 10^6$ N-sec/m)	
1	1	9.8	4.7%
2	6	59.1	28.6%
3	4	39.4	19.0%
4	3	29.6	14.3%
5	3	29.6	14.3%
6	2	19.7	9.5%
7	2	19.7	9.5%
8	0	0.0	0.0%
9	0	0.0	0.0%
Total	21	206.9	100.0%

Table 3.4 Modal Properties of Shear Building Model

Mode	W/O Damper		Optimal FVD	
	Frequency (Hz)	Damping Ratio	Frequency (Hz)	Damping Ratio
1	0.96	0.03	0.97	0.14
2	2.51	0.03	2.62	0.17
3	4.01	0.03	3.69	1.00*
4	5.43	0.03	4.48	0.31
5	6.64	0.03	5.85	0.16
6	7.77	0.03	6.98	0.49
7	8.99	0.03	7.91	0.08
8	10.01	0.03	7.99	0.92
9	11.09	0.03	24.98	1.03*

* Indicates an over-damped mode.

Table 3.5 Modal Properties of MRF Building Model

Mode	W/O Damper		Optimal FVD	
	Frequency (Hz)	Damping Ratio	Frequency (Hz)	Damping Ratio
1	0.64	0.03	0.65	0.30
2	1.77	0.03	1.74	1.01*
3	2.95	0.03	2.44	0.28
4	4.27	0.03	3.12	0.47
5	5.72	0.03	3.95	1.01*
6	7.37	0.03	4.28	0.93
7	9.09	0.03	6.57	0.11
8	10.90	0.03	18.25	1.02*
9	12.80	0.03	43.03	1.03*

* Indicates an over-damped mode.

Table 3.6 Comparison of Different Costs of Shear Buildings With and Without FVD

Costs (× $1,000)	Seismic Designs	
	W/O Damper	Optimal FVD
Initial Cost	15,700	15,700
Damper Cost	0	248
Failure Cost	955	141 (85.3%)
Object Cost	955	389 (59.3%)
Life-Cycle Cost	16,655	16,089 (3.3%)
Mean Annual Failure Cost	50.0	7.4 (85.2%)

Table 3.7 Comparison of Different Costs of MRF Buildings With and Without FVD

Costs (× $1,000)	Seismic Design Approaches	
	W/O Damper	Optimal FVD
Initial Cost	12,900	12,900
Damper Cost	0	274
Failure Cost	2,255	254 (88.7%)
Object Cost	2,255	528 (76.6%)
Life-Cycle Cost	15,155	13,428 (11.4%)
Mean Annual Failure Cost	115.0	13.4 (88.4%)

Table 3.8 Expected Failure Costs of Shear Building Model With and Without FVD for Different Earthquake Intensities

PGA(g)	Expected Failure Cost (× $1,000)		Cost Reduction (%)
	W/O Damper	Optimal FVD	
0.11	246	0	100.0
0.24	275	40	85.5
0.37	213	33	84.5
0.50	113	36	68.1
0.62	64	18	71.9
0.75	30	8	73.3
0.88	16	6	62.5
Total	955	141	85.2

Table 3.9 Expected Failure Costs of MRF Building Model With and Without FVD for Different Earthquake Intensities

PGA(g)	Expected Failure Cost (× $1,000)		Cost Reduction (%)
	W/O Damper	Optimal FVD	
0.11	813	0	100.0
0.24	648	53	91.8
0.37	403	75	81.4
0.50	198	55	72.2
0.62	110	45	59.1
0.75	53	17	67.9
0.88	29	9	69.0
Total	2,255	254	88.7

Table 3.10 Effect of Yielding on the Failure Cost of Shear Building Model with Optimal FVDs

PGA (g)	Expected Failure Cost (× $1,000)			Difference (%)	
	Elastic	NEHRP	Time History	Ela-NEH	Ela-TH
0.63	21.3	17.7	20.9	16.9	1.9
0.75	13.6	8.3	11.2	39.0	17.6
0.88	8.7	5.7	6.5	34.5	25.3
Sub-Total	43.6	31.7	38.6	27.3	11.5
Total Failure	152.6	140.7	147.6	7.8	3.3
Object Cost	400.6	388.7	395.6	3.01	1.25

Table 3.11 Effect of Yielding on the Failure Cost of MRF Building Model with Optimal FVDs

PGA (g)	Expected Failure Cost (× $1,000)		Difference (%)
	Elastic	NEHRP	
0.75	21.0	16.7	20.5
0.88	9.5	8.8	7.4
Sub-Total	30.5	25.5	16.4
Total Failure	258.5	253.5	1.9
Object Cost	532.5	527.5	0.94

Figures 3

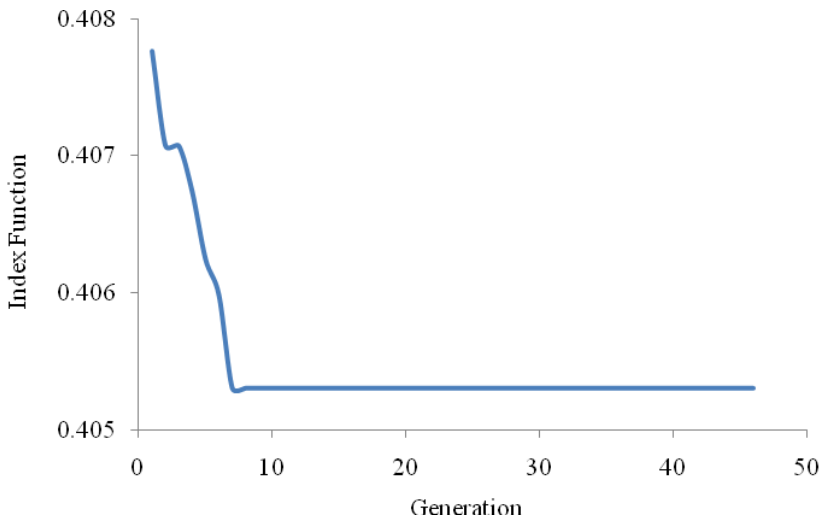

Figure 3.1 Convergence of GA for Shear Building Model with FVD

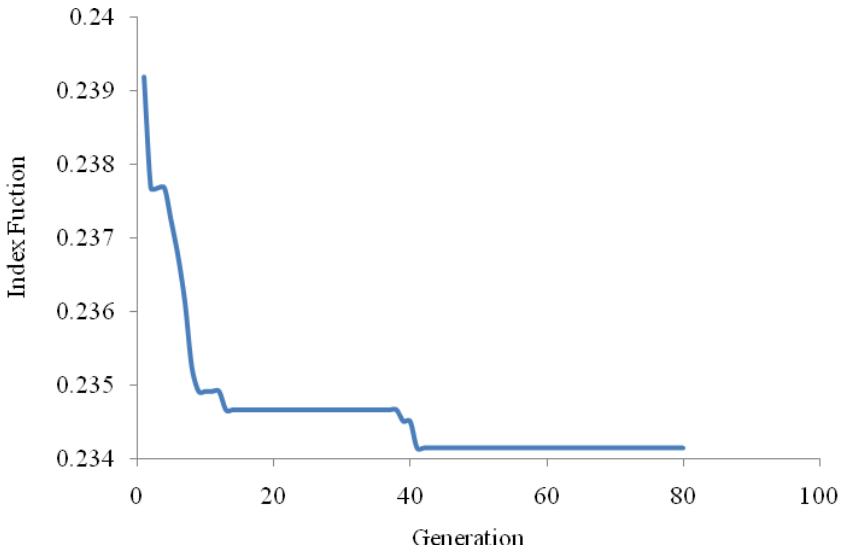

Figure 3.2 Convergence of GA for MRF Building Model with FVD

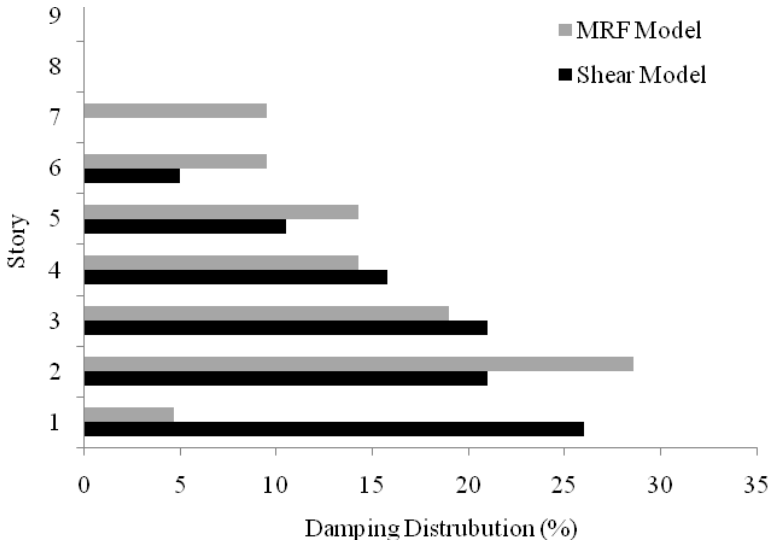

Figure 3.3 Comparison of the Percentage Distribution of Damping Coefficients

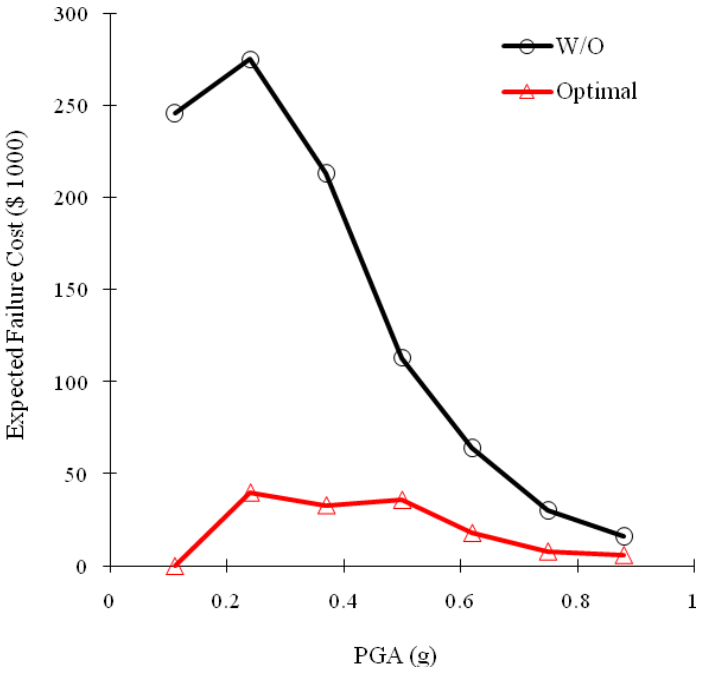

Figure 3.4 Expected Failure Costs of Shear Building Model with FVD under Various Earthquake Intensities

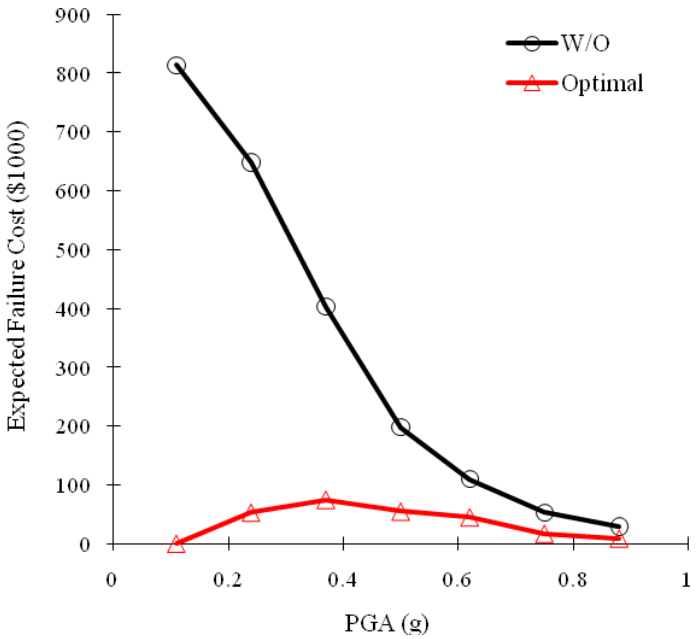

Figure 3.5 Expected Failure Costs of MRF Building Model with FVD under Various Earthquake Intensities

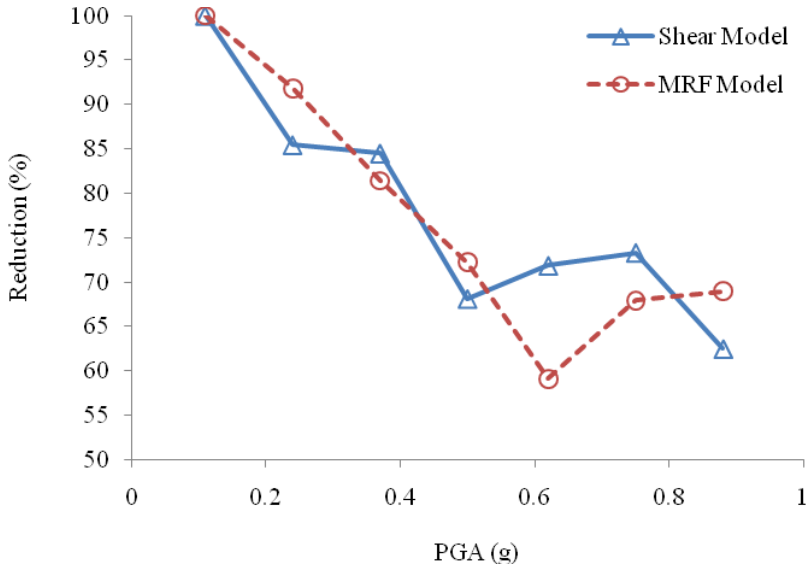

Figure 3.6 Percentage Failure Cost Reductions under Various Earthquake Intensities

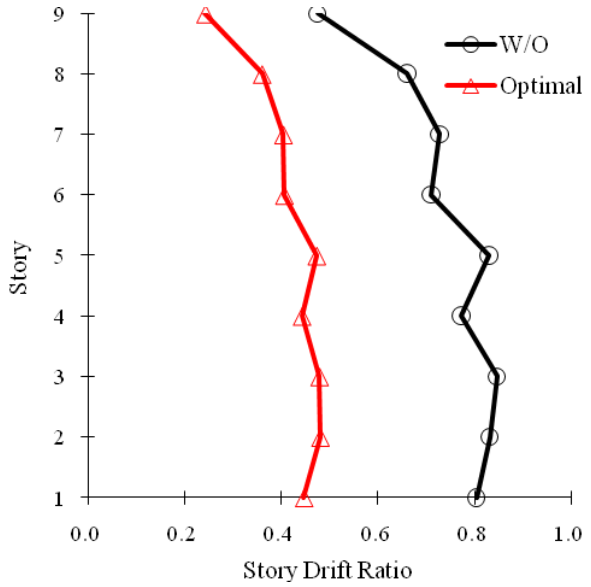

Figure 3.7 Comparison of the Mean Story Drift Ratios of the Original Shear Building and the Building with FVD (Earthquake Intensity = 0.50g)

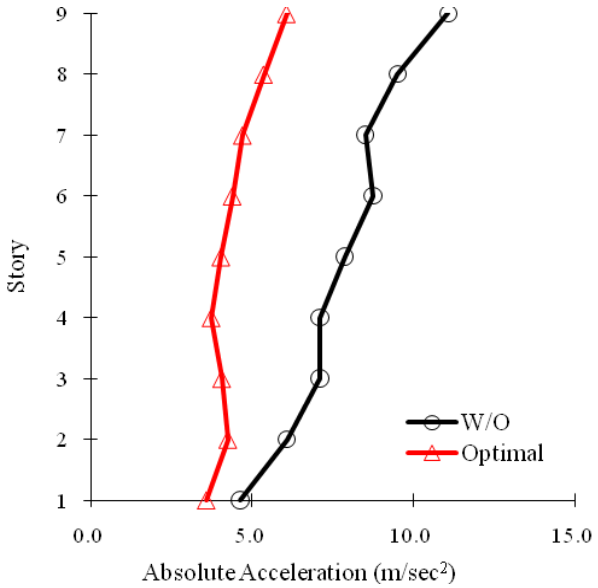

Figure 3.8 Comparison of the Average Floor Accelerations of the Original Shear Building and the Building with FVD (Earthquake Intensity = 0.50g)

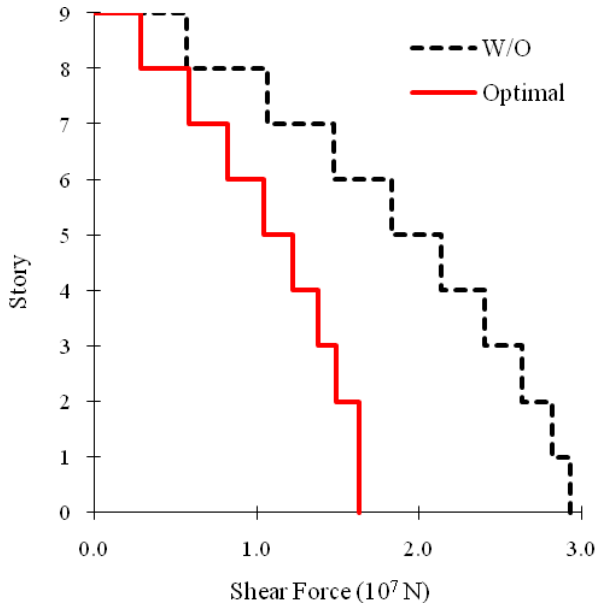

Figure 3.9 Comparison of the Mean Story Shear of the Original Shear Building and the Building with FVD (Earthquake Intensity = 0.50g).

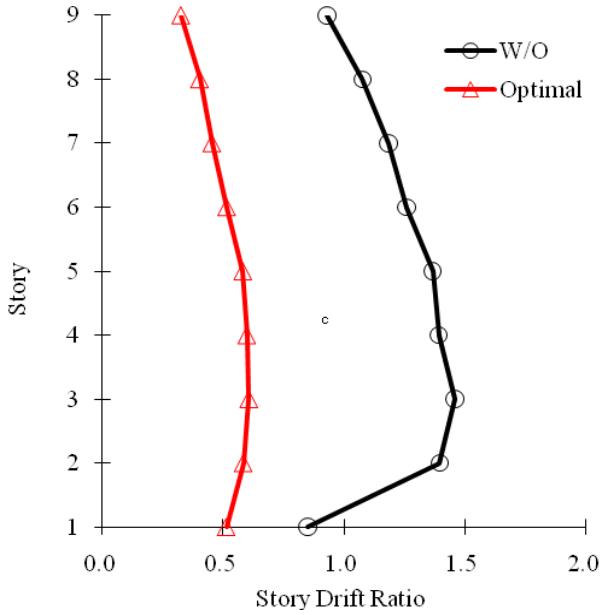

Figure 3.10 Comparison of the Mean Story Drift Ratios of the Original MRF Building and the Building with FVD (Earthquake Intensity = 0.50g)

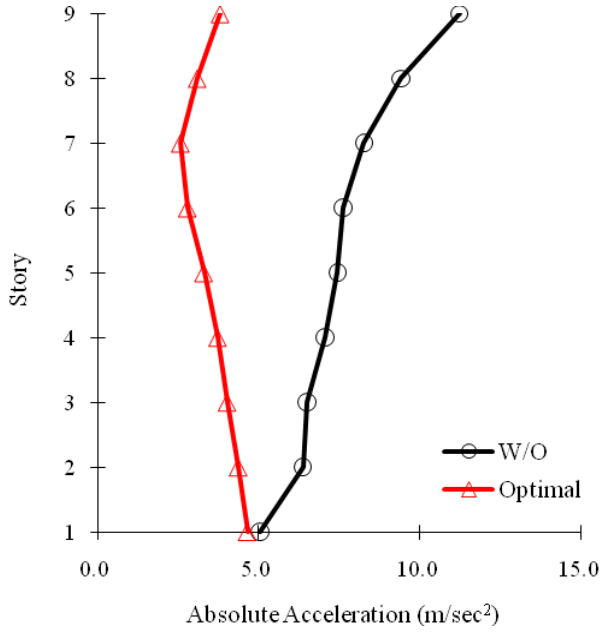

Figure 3.11 Comparison of the Average Floor Accelerations of the Original MRF Building and the Building with FVD (Earthquake Intensity = 0.50g)

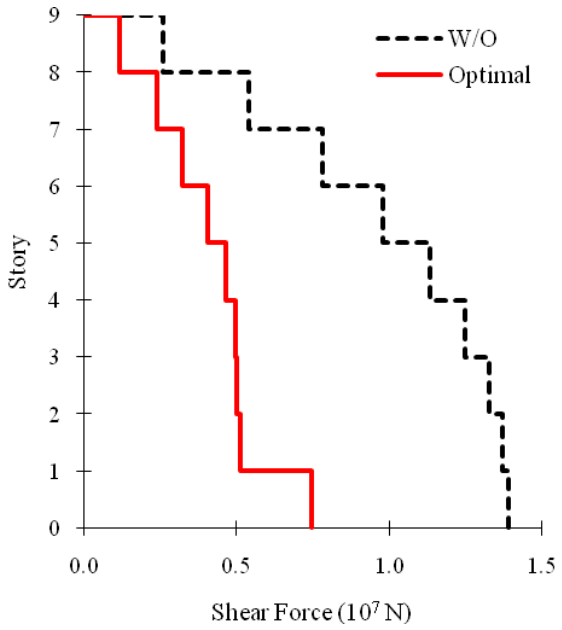

Figure 3.12 Comparison of the Mean Story Shear of the Original MRF Building and the Building with FVD (Earthquake Intensity = 0.50g)

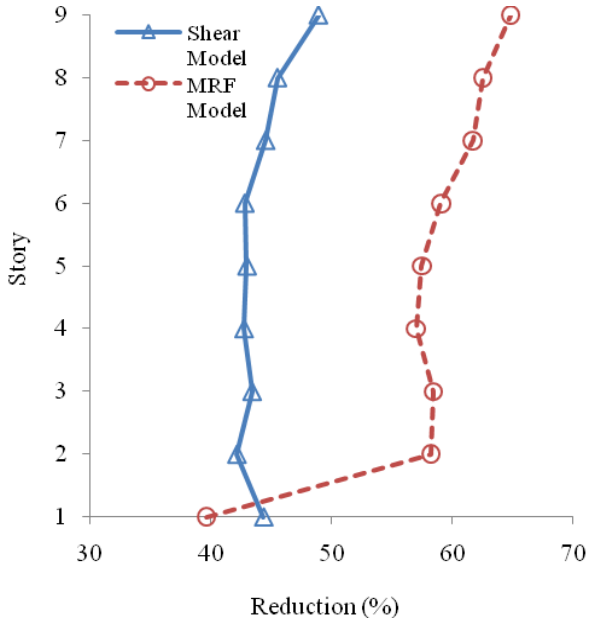

Figure 3.13 Percentage Story Drift Ratio Reductions under Various Earthquake Intensities

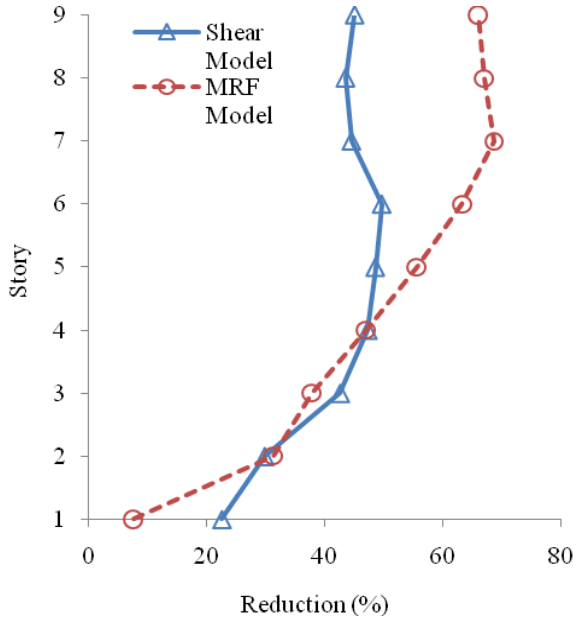

Figure 3.14 Percentage Absolute Acceleration Reductions under Various Earthquake Intensities

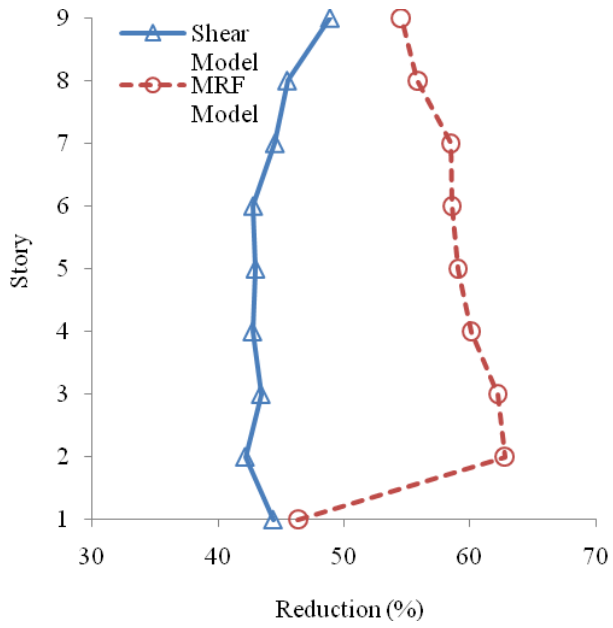

Figure 3.15 Percentage Shear Force Reductions under Various Earthquake Intensities

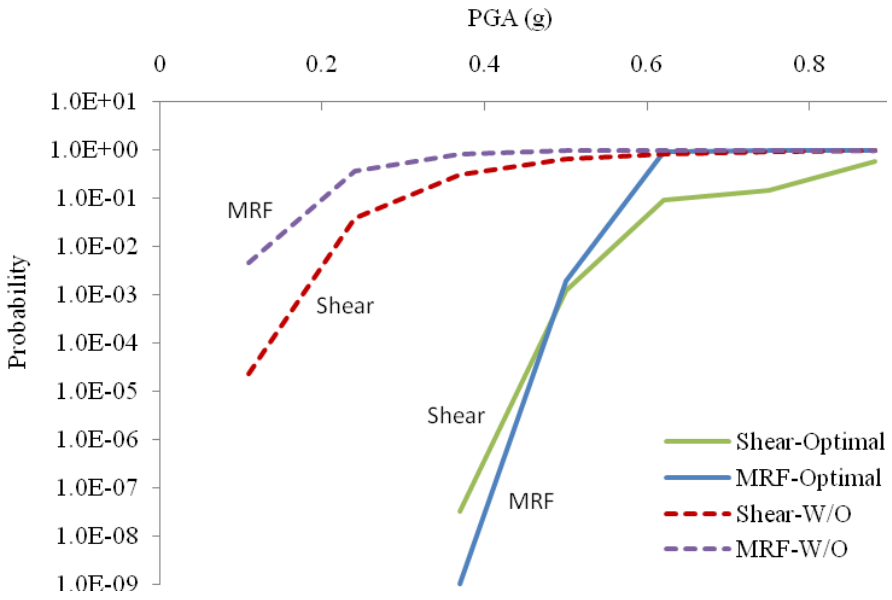

Figure 3.16 Fragility Curves Showing the Probabilities that the Maximum Story Drift Ratios in the Two Buildings Exceed the Immediate Occupancy Limit State, $P(\Delta > 0.7)$

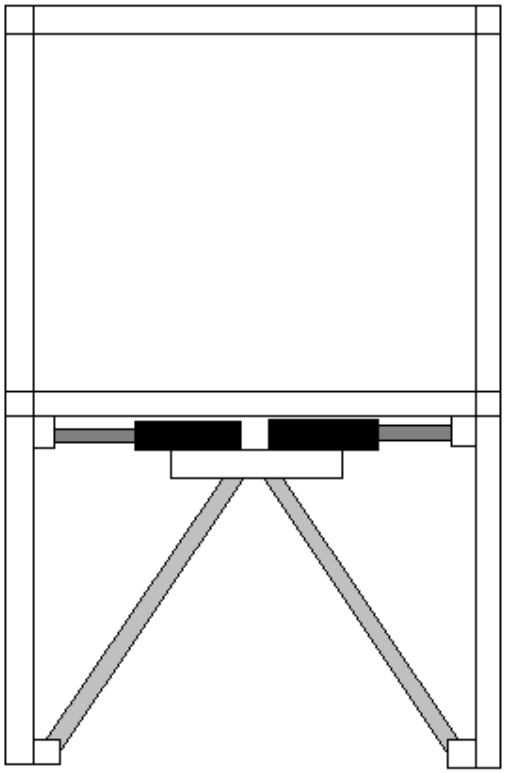

Figure 3.17 Typical Installation of Fluid Viscous Dampers with Chevron Braces

CHAPTER 4

Optimal Designs with Solid Visco-Elastic Dampers

4.1 Introduction

Solid visco-elastic dampers are among many energy dissipation devices that have been considered for reducing seismic vibrations in civil engineering structures. In this chapter, thus, we present the approach for optimal design of building structures using such dampers to minimize the expected life-cycle cost of a structure. The optimization framework developed in Chapter 2 is used again, as was done for the fluid viscous dampers in Chapter 3.

Solid visco-elastic dampers dissipate the vibration energy through hysteresis in shear deformations of a visco-elastic polymer. A common configuration of these dampers consists of one or two layers of a visco-elastic polymer glued to steel plates that move with respect to each other, applying shear deformation to the layers. Like a fluid viscous damper, they can also be installed in a diagonal brace or on a chevron brace in a bay of a building story. In many respects, the solid visco-elastic dampers are similar to the fluid viscous dampers. However, unlike fluid viscous dampers, solid visco-elastic dampers also provide stiffness along with damping to the structural system. Their performance in terms of energy dissipation characteristics are affected by variations in the material temperature. They are simpler to manufacture than the viscous dampers as they only require proper gluing of the visco-elastic polymers between two plates that can move relative to each other.

In the following, we briefly discuss the mechanical characteristics of these dampers from the perspective of their application in structures, the analytical models that can be used, and response analysis of structures with these dampers. In many respects this analysis is very similar to the one presented in Chapter 3. Numerical results for the optimal design of two building models described in Chapter 3, but now provided with solid visco-elastic dampers, are presented. The impact of the optimal installation of these dampers on the failure cost, object cost, and life-cycle cost of these two building models are evaluated. The effects on the fragility of the system and on the structural

response quantities of interest are also discussed.

4.2 Analytical Modeling of Solid Visco-Elastic Dampers

A large amount of literature is available on the properties and modeling of visco-elastic materials. Very sophisticated models have been proposed to describe the stress-strain relationships of these materials. In more refined application there is a need to use these models. However, for civil engineering applications of these materials in dampers, several simplified yet quite adequate models have been proposed and used. In this section, we briefly describe these models as they are applicable to our study. An excellent description about these dampers and their properties of civil engineering interest can be found in the book by Soong and Dargush (1997).

The mechanical characteristics of the visco-elastic polymer materials that are of our interest are the stiffness and damping properties. In engineering applications, these two characteristics for visco-elastic materials have been described in terms of the storage and loss moduli, here respectively denoted by $G'(\omega)$ and $G''(\omega)$. G' defines the stiffness characteristics and G'' defines the damping characteristics of the polymer. The energy dissipation capacity of a solid visco-elastic material is often characterized by the loss factor that is expressed in the following form:

$$\eta = \frac{G''(\omega)}{G'(\omega)} \tag{4.1}$$

These material parameters are dependent on the deformation frequency as well as temperature of the material. In simple terms, lowering of the material temperature increases its stiffness and damping capacity and vice-versa. To capture frequency dependence several advanced models have been proposed such as fractional derivative models, Maxwell ladders, Kelvin chains and a combinations of these (Flugge, 1967; Chang and Singh, 2009). For structural engineering applications, however, where we like to use stiffness and damping coefficients, these parameters can be assumed to be constant within a narrow band of frequency. Since the major contribution to dynamic response often comes from the fundamental mode (which is also a common assumption in the description of simplified formulas used for the calculation of story shears, etc., for the design of structures), the fundamental frequency of the structure is used to obtain the frequency dependent values of the storage and loss moduli for the calculation of

equivalent stiffness and damping coefficients for structural applications. In terms of these modulus values, the equivalent stiffness coefficient k_d and damping coefficient c_d for a layer of visco-elastic material in a damper are defined as follows (Singh and Moreschi, 2002):

$$k_d = \frac{A_s \, G'(\omega_1)}{h}, \qquad c_d = \frac{A_s \, G''(\omega_1)}{\omega_1 h} \tag{4.2}$$

where h is the thickness of the layer, A_s is the area of the layer, and ω_1 is the fundamental frequency of the building.

Inclusion of temperature dependence of these properties in the response analysis and in the calculation of failure cost in a sample manner is, on the other hand, quite difficult. For a given fixed temperature, these characteristics of the material can be assumed to be constant. However, the temperature of the material in a damper can change for two reasons: (a) accumulation of the dissipated vibration energy as heat in the material, (b) change in the environmental temperature around the damper. The first cause of increase in the material temperature is, however, not considered very significant, especially for earthquake induced vibrations which usually last only for a very short duration. The second cause for the change in the material temperature is associated with many factors. It is affected by the fluctuations in the environmental temperature, radiation, and convection, if the damper is directly exposed to outside elements of nature. However, the dampers in buildings, being inside, are most likely to be protected from the direct influence of the outside elements of nature. In some case they may even be located in a controlled temperature and humidity environment (e.g., air conditioning). Given all this variability, it is not possible to include this effect in a very accurate manner. In this study, however, to examine the impact of some possible temperature variations, a rather simplified approach is used.

Environmental temperature variations consist of the yearly (seasonal) and diurnal trends with superimposed faster random fluctuations. The inside temperatures near the dampers are, however, more likely to be most affected by the yearly trend and to a lesser extent by the daily variations. Thus, as a simplification we have assumed that our dampers are subjected to predominantly harmonic variations of yearly cycle. To define the amplitude of this cycle, we used the highest and the lowest monthly average values. Table 4.1 shows that average of the maximum temperature in each month in Los

Angeles. Based on this range the amplitude of the yearly harmonic is assumed to be 14-24^{o}C. To bring in the effect of the damper being inside, we further reduced the amplitude by 10%. The temperature range between these reduced amplitude values was divided into several equal intervals, and the probability of the temperature being in one of the ranges was calculated using the probability distribution for the temperature. If can be easily shown that the probability density function of the temperature varying harmonically with, say, a yearly trend can be defined as:

$$f_T(t) = \frac{1}{\pi} \frac{1}{\sqrt{\left(A_y^2 - t^2\right)}} \; ; -A_y \le t \le A_y \tag{4.3}$$

where T is the random variable of damper temperature and A_y is the amplitude of the assumed harmonic trend. With this probability density function, the probability of the temperature being in an interval (t_1, t_2) can be calculated by the following formula:

$$P(t_1 \le T \le t_2) = \frac{1}{2}\left[\sin^{-1}\left(\frac{t_2}{A_y}\right) - \sin^{-1}\left(\frac{t_1}{A_y}\right) \right] \tag{4.4}$$

To use these probabilities for different temperature intervals in the calculation of the total failure cost, we proceed as follows. We first divide the temperature range into N_I intervals and calculate the probabilities $p_i, i = 1, 2, ..., N_I$, using Eq. (4.3). Using the midpoint values of the temperature to represent the entire interval, we then find the temperature-dependent storage and loss modulus values and then equivalent stiffness and damping coefficient values from Eq. (4.2). The dynamic response quantities of interest (story drifts) are calculated for each stiffness and modulus value, which are then used in calculating the expected failure costs. These conditional expected failure costs – that is, the failure cost given that the temperature is within a certain range - are weighted by their respective probabilities to calculate the total failure cost. This total weighted failure cost is defined by the following formula:

$$C_F = \sum_{i=1}^{N_I} C_{Fi} P_i \tag{4.5}$$

where C_F is the weighted failure cost, C_{Fi} is the failure cost calculated with the stiffness and damping coefficient values for the average temperature in the i^{th} interval, and P_i is the probability that the damper temperature will be in the i^{th} interval. Using

this weighted failure cost, the cost function (object cost) is determined using the cost of the damper. The object cost is minimized using the GA to determine the optimal distribution of the dampers.

4.3 Responses Analysis

The equation of motion for an *N*-degree-of-freedom structure with added viscous damping devices was developed in Chapter 3. With the stiffness and damping coefficients of the visco-elastic damper defined by Eq. (4.2), the equation of motion for a structural system installed with such visco-elastic dampers can be expressed in the standard form as follows:

$$\mathbf{M}\ddot{\mathbf{u}}(t)+\mathbf{C}\dot{\mathbf{u}}(t)+\mathbf{K}\mathbf{u}(t)=-\mathbf{M}\mathbf{u}\ddot{u}_g(t) \tag{4.6}$$

where $\mathbf{C}$ is the total damping matrix and $\mathbf{K}$ is the total stiffness matrix of the structural system. FEMA 273 guidelines (1997) as well as other studies suggest that solid viscoelastic devices may be modeled by the classical Kelvin-Voigt model where the viscous dampers and elastic springs are connected in parallel. As mentioned earlier, other more sophisticated models have also been used to include frequency dependence more accurately, but the Kelvin-Voigt model has been considered adequate for most applications in civil engineering, primarily for its simplicity. For this model, the force-deformation relationship can be expressed in the following form (Soong and Dargush, 1993):

$$f_d(t)=k_d\delta_d(t)+c_d\frac{d\delta_d(t)}{dt} \tag{4.7}$$

where f_d is the damping force, δ_d is the local deformation on the damping device, and k_d and c_d are the stiffness and damping coefficient of the damping device, respectively. The local displacement and local velocity on the damping device can be directly related to the global displacement and velocity of the structural system. For example, for a damper installed in a diagonal brace making an angle of θ_d with the horizontal, the damper force in global coordinates can be expressed in terms of global deformation (inter-story drift) $\Delta_s(t)$ as:

$$F_d(t)=\cos^2\theta_d\cdot\left\{k_d\Delta_s(t)+c_d\frac{d\Delta_s(t)}{dt}\right\} \tag{4.8}$$

On the other hand, if the damper is installed in a Chevron brace constraining the deformation of the damper in horizontal direction, then $\delta_d(t) = \Delta_s$ and the global damper force is simply written as:

$$F_d(t) = k_d \Delta_s(t) + c_d \frac{d\Delta_s(t)}{dt} \tag{4.9}$$

The total damping matrix $\mathbf{C}$ and total stiffness matrix $\mathbf{K}$ of a structural system with additional solid visco-elastic damping devices can be written in terms of the damper force expressed by Equation (4.8) or (4.9) in the same way as for a fluid viscous damper in Chapter 3 as follows:

$$\begin{aligned} \mathbf{C} &= \mathbf{C}_{\mathrm{S}} + \sum_{i=1}^{N_d} \mathbf{r}_i \, n_i \, c_i \, \mathbf{r}_i^{\mathrm{T}} \\ \mathbf{K} &= \mathbf{K}_{\mathrm{S}} + \sum_{i=1}^{N_d} \mathbf{r}_i \, n_i \, k_i \, \mathbf{r}_i^{\mathrm{T}} \end{aligned} \tag{4.10}$$

where $\mathbf{C}_{\mathrm{S}}$ and $\mathbf{K}_{\mathrm{S}}$ are, respectively, the damping and stiffness matrices of the original structure without any dampers, and $\mathbf{r}_i$ is the influence vector (which depends on the degrees of freedom to which the opposite ends of the damper are attached) which permit the incorporation of the damping and stiffness contributions of the i^{th} damper to the corresponding system matrices, n_i is the number of dampers in the i^{th} story, and N_d is the number of different stories in which the dampers are installed.

As was the case with fluid viscous dampers in Chapter 3, the system of equations, (4.6), are linear with the assumed models of the dampers. Also, they are nonclassically damped because of the way the damping is introduced differently at different locations on the structure in the optimization process. Thus, their analysis needs to consider the nonclassically damped characteristic. For this, the approach described in Chapter 3 is entirely applicable. This non-classically damped system can also be over-damped in some modes, depending upon the amount of supplementary damping.

4.4 Input Data, Variables and Constraints Used in Optimization

In this section, some necessary data of the problem and optimization implementation are given. We have used two layers of 3M 112-viscoelastic damping polymer, bonded to the

steel plates in the damper. The classical damper configuration shown in Figure 4.1 is assumed. This polymer is designed to be used in damping applications to control the vibration and shock of machines and structures. The typical operating temperature range of this polymer is 0~60^{o}C. The mechanical properties of this material are defined in terms of the storage and loss moduli from the 3M website with URL http://solutions.3m.com/wps/portal/3M/en_US. The equivalent stiffness and damping coefficient for the damper were obtained using Eq. (4.2).

The storage modulus and loss modulus values needed in Eq. (4.2) were obtained at the fundamental frequencies of the two building models with their original properties. Although the frequencies of the systems change when the dampers are installed, as these dampers add some stiffness to the system, this change is not very large and was ignored in selecting the modulus values. To account for the change in the temperature of the damper, the approach described in Section 4.2 was used. The temperature range was divided into four intervals, and the storage and loss modulus values at the midpoint temperature of the interval were used in the calculations. Table 4.2 shows the four temperature intervals selected, the midpoint temperatures used, and the probability values of the temperature being in these four temperature ranges. The storage and loss modulus values obtained by this method for the two building models are given in Tables 4.3 and 4.4. The thickness of each visco-elastic layer was taken to be 3.2 cm. With this thickness and the maximum inter-story drift that could be expected to occur in the two structures with dampers, the shear strain in the visco-elastic material was within its allowable limit.

The volume of the visco-elastic material that will be strained to its full level determines its energy dissipation capacity. A damper using a larger volume will dissipate more energy than a smaller volume damper. Thus for the same amount of damping needed we will need fewer number of large dampers to be accommodated in the space available in a story. The maximum number that could be accommodated in a story was fixed at 18, as done for the fluid viscous dampers in Chapter 3. In the literature on the visco-elastic damper we were not able to find information on the different sizes that have been or can be manufactured and also on their unit cost like we were able to obtain for the fluid viscous dampers. We believe that a very large size damper may be difficult to manufacture. We assumed that a damper with a damping layer of 0.5 m^2 can be conveniently manufactured, and thus used this to present our numerical results. However, for comparative cost analysis and their relative effectiveness we also

considered two more damper sizes of 0.75 and 1.00 m^2 visco-elastic layers. The results shown later indicate that the large size dampers are slightly more efficient, but since they may be too large to fabricate, we focus on presenting the results only for the 0.5 m^2 layer dampers. Table 4.5 gives the unit cost used in this study for these three dampers. The bracing costs given in this table are for the brace which could carry the largest force expected to occur in the damper. Actual force in the brace for different intensities was always lower than the brace capacity, but no re-sizing of the brace for the reduced force was attempted.

4.4.1 Optimization Implementation Step.

The steps for implementing the optimization process to arrive at the optimal design for a minimum life-cycle cost are very similar to these given in Chapter 3 for the fluid viscous dampers. For a selected size of visco-elastic damper to be used, the objective is to determine the number of dampers we need in each story so that the cost function is minimized. The cost function is the normalized object cost which is the cost of failure plus the cost of the dampers used. As before, this object cost is normalized by the failure cost of the original building to define the cost function. The search for the optimal solution is made using the genetic algorithm. The basic steps involved in this process are as follows.

Step 1: Generate a population of feasible designs with the number of dampers on each story selected randomly within the limit determined by the available space. For the numerical results in this study, a population of 400 feasible designs was selected.

Step 2: For each feasible design, obtain the system stiffness and damping matrices for the four temperature intervals, as described before. For these system properties, calculate the inter-story drifts using the analytical approach described in Chapter 2. If the structure is known to yield in any story, use the modified spectrum approach per 2009 NEHRP Provisions (2009) using the appropriate C_d and R factors for the frames of the building models.

Step 3: For the calculated story drifts, calculate the probability of the drifts being in the seven limit states. Considering these limit state probabilities and the limit state costs defined in Chapter 2, calculate the failure costs.

Step 4: Obtain the total weighted failure cost using the failure costs for the four temperature intervals. Using the weighted failure cost, calculate the object cost and the cost function.

Step 5: Compare the cost functions of different feasible design in the population to determine the individual design for mating to produce the future generation of the designs considering the mutation and elitist scheme presented in Chapter 2. Repeat the steps for each future generation till the convergence in the cost function value is achieved according to the pre-decided convergence criteria.

4.5 Numerical Results

The numerical results obtained for the optimal designs for the shear building and the MRF building are presented. First the numerical results are presented for the selected size of the damper with 0.5 m^2 area of a visco-elastic layer, and the total visco-elastic area of 1.0m^2. Later the cost and response comparisons with larger dampers are also presented. Figures 4.2 and 4.3 show the convergence of the genetic algorithm to the optimal solutions for the two building models as a function of generations. The convergence was assumed to have been reached when the object cost did not change in the next 40 consecutive generations. As seen from these two figures, this required checking of 60 generations in the shear building and about 68 in the MRF building. Tables 4.6 and 4.7 present the final results of optimization for the two buildings. The MRF building, being more flexible, is seen to need more dampers to reduce the inter-story drifts to lower the failure cost. However, the additional damper cost also pays off in reducing the mean annual failure cost by almost 88%, whereas in the shear building this reduction is about 76%. However, these reductions per dollar of investment in damping in the two different buildings are almost the same (0.29% per $1000 of investment.)

The next two Tables, 4.8 and 4.9, show the distribution of dampers and the percentage of total damping along the building heights of the two models. In both models, the lower stories require the most dampers as the response of both buildings is most affected by the first few modes. We also note that the number of dampers in the lower stories reached its limiting value of 18. This limit, perhaps, also limited the reduction in the response that could be achieved. A later comparison shows that the larger size dampers are more effective, because with the limit of 18 maximum per story they provide more damping to reduce the overall response than the smaller dampers. As mentioned earlier, the MRF building, being flexible, demands higher supplementary damping than the shear building. Figure 4.4 compares the percentage distribution of

the damping along the story height in the two buildings.

Table 4.10 shows the modal properties of the two buildings. Both buildings experience an increase in the frequencies due to the contribution of the visco-elastic dampers to the system stiffness. This increase is about 5% in the shear building and about 15% in the MRF building. This increase was, however, not considered in changing the material properties for the GA optimization.

Tables 4.11 and 4.12 show how the failure costs are distributed in the different ranges of hazard intensities for the two buildings. The failure costs are drastically reduced for the lower hazard levels with overall reductions of 76% for the shear building and 88% for the MRF building. For a better visual presentation, Figures 4.5 and 4.6 show the plots of the failure costs for the two buildings for different hazard intensities. In Figure 4.7, the percent reductions in the costs for different intensities are compared for the two buildings. These relative reductions are functions of the building characteristics and, of course, depend on the details of the example problem chosen.

In the next set of six figures, Figures 4.8-4.13, we plot the story drifts, absolute floor accelerations, and story shear forces in the original and the damping enhanced buildings. The first three figures are for the shear building and the remaining three figures are for the MRF building. Large reductions, similar to those observed for the fluid viscous dampers are again observed for the visco-elastic dampers. In Figures 4.14-4.16 we compare these response reductions in the two buildings. The reductions in the story drifts and story shear are larger in the more flexible MRF building than those in the relatively rigid shear building. The reductions in the accelerations are somewhat less, especially at the lower floors. The floor acceleration reductions at lower floors are difficult to achieve as these accelerations have significant contributions from the higher modes.

Effect of Temperature Variations

In the calculation of the above results, the temperature range was divided into four intervals to facilitate the incorporation of the temperature dependence of the material properties. A particular form (yearly cycle) was assumed to represent the temperature variations. To examine if one need to consider such simplified variations or even worry about representing the variations more accurately, here we calculated the optimal

designs assuming only the average temperature value. For this average temperature value, the material properties (storage and loss modulus) used in this side study are shown in Table 4.13. Tables 4.14 and 4.15 compare the cost results obtained for the four-interval representation with those for the average temperature case. The difference in the results for the two temperature representations is not at all significant. The damper distribution values as well as the response calculated for the two temperature representations did not differ significantly. These results suggest that using the average temperature value in calculating the material property in designing buildings with visco-elastic dampers should be quite acceptable.

Effect of Using Larger Damper Size

The above results were obtained for a visco-elastic layer area of 0.5 m^2 providing a total area of 1.0 m^2 in each damper. The total supplemental damping of this size damper was limited by the restriction of 18 dampers in each story. To investigate the impact on the design of being able to use a larger size damper, with again the limitation of 18 dampers per story, numerical results have also been obtained for two larger size dampers that provide total areas of 1.5 m^2 and 2.0 m^2. Tables 4.16 and 4.17 compare the cost values for the three damper sizes for the shear building and MRF building, respectively. We observe that larger size dampers are relatively more effective than the smaller damper in the sense that they lead to lower damper costs, failure costs, object costs and annual failure cost. It is simply because within the limit of 18 dampers per story a larger damper can provide a higher level of supplemental damping. However, in this study it was subjectively felt that the dampers larger than 0.5 m^2 will be difficult to fabricate and are likely to be unwieldy to be accommodated in the braces.

Effect on the Limit State Fragilities

The next set of Figures, 4.17-4.20, shows the fragility curves for the two buildings. Figures 4.17 and 4.18 are for the overall fragility where the probabilities of the building going beyond the limit states of immediate occupancy and life safety are plotted against the ground motion intensity values. The next two figures show similar probabilities but now for an intermediate story, story no. 5. Figures 4.17 and 4.19 are for the shear building and Figures 4.18 and 4.20 for the MRF building. First we note that the fragilities are drastically improved with the use of visco-elastic dampers for both building models. The probabilities were also obtained to define the fragility curves for

the collapse limit state but they were so small both for the original building as well as the enhanced building to be outside the range of the probability scale shown in these figures.

4.6 Chapter Summary

This chapter describes the implementation of the life-cycle cost optimization procedure to obtain optimal distribution of the solid visco-elastic dampers. The mechanical properties of the material used in damper are reviewed with the point of their use in the optimization procedure. The dampers' properties depend upon the frequency of loading on the damper and temperature of the damper. The frequency dependence is considered through the usual procedure of using the properties corresponding to the fundamental frequency of the structure. For including the temperature-dependence, a new but simple approach that can be implemented for refined cost analysis is suggested. However, it is also observed that such refinements may not be necessary, especially for the dampers that are located in a controlled thermal environment.

The numerical results for the failure costs, object cost, distribution of dampers on the buildings, and the impact of damping on the other response quantities and the system fragility are obtained for the optimal configurations on the two building models. The calculated cost and response results are compared for the original and damping enhanced buildings to examine the level of improvement in the system performance. The results show drastic reductions in the failure costs and response quantities of design interest as well as significant improvements in the system performance measured in terms of the system fragility for different limit states.

Tables 4

Table 4.1 Monthly Average Temperature of Los Angeles (Model Building Site)

Month	Mean Temperature (^{o}C)
Jan.	14
Feb.	16
Mar.	16
Apr.	18
May	19
Jun.	22
Jul.	23
Aug.	24
Sep.	23
Oct.	21
Nov.	17
Dec.	15

Table 4.2 Design Ambient Temperatures for Visco-Elastic Damper

Interval	Temperature Range (^{o}C)	Midpoint Temperature (^{o}C)	Probability
ΔT_1	15.4 - 17.0	16.2	1/3
ΔT_2	17.0 - 18.5	17.7	1/6
ΔT_3	18.5 - 20.1	19.3	1/6
ΔT_4	20.1 - 21.6	20.8	1/3

Table 4.3 Property of Visco-Elastic Damping Polymer for Shear Building Model
(Frequency = 0.96 Hz)

Factors	Midpoint Temperature (^oC)			
	16.2	17.7	19.3	20.8
Shear Storage Modulus G'(Mpa)	0.28	0.25	0.21	0.18
Shear Loss Modulus G"(Mpa)	0.22	0.19	0.15	0.12
Loss Factor η	0.80	0.75	0.70	0.65

Table 4.4 Property of Visco-Elastic Damping Polymer for MRF Building Model
(Frequency = 0.58 Hz)

Factors	Midpoint Temperature (^oC)			
	16.2	17.7	19.3	20.8
Shear Storage Modulus G'(Mpa)	0.26	0.23	0.19	0.16
Shear Loss Modulus G"(Mpa)	0.20	0.16	0.12	0.10
Loss Factor η	0.75	0.70	0.65	0.60

Table 4.5 Unit Costs of SVD

Type	Small	Medium	Large
Total Shear Area (m^2)	1.0	1.5	2.0
Unit Cost ($)	1,440	2,000	2,400
Bracing Cost ($/$m$)	85	90	96

Table 4.6 Results from the Optimization of SVDs for Shear Building Model

Costs (× $1,000)	Seismic Design Approaches	
	W/O Damper	Optimal SVDs
Initial Cost	15,700	15,700
Damper Cost	0	261
Failure Cost	955	233
Object Cost	955	494
Life-Cycle Cost	16,655	16,194
Mean Annual Failure Cost	50.2	12.2

Table 4.7 Results from the Optimization of SVDs for MRF Building Model

Costs (× $1,000)	Seismic Design Approaches	
	W/O Damper	Optimal SVDs
Initial Cost	12,900	12,900
Damper Cost	0	301
Failure Cost	2,255	266
Object Cost	2,255	567
Life-Cycle Cost	15,155	13,467
Mean Annual Failure Cost	118.7	14.0

Table 4.8 Optimal Distribution of SVDs for Shear Building Model
(GA Uses Elastic Spectrum Analysis)

Mode	Number of Dampers	Added Mean Damping ($\times 10^7$ *N-sec/m*)	Added Mean Stiffness ($\times 10^8$ *N/m*)	Distribution (%)
1	18	1.59	1.29	16.1
2	18	1.59	1.29	16.1
3	18	1.59	1.29	16.1
4	15	1.32	1.08	13.4
5	18	1.59	1.29	16.1
6	9	0.79	0.65	8.0
7	10	0.88	0.72	8.9
8	6	0.53	0.43	5.4
9	0	0.00	0.00	0.0
Total	112	9.86	8.05	100.0

*Note: The optimal design of SVDs for the shear building model with the GA that uses the Modified Spectrum Analysis per 2009 NEHRP Provisions to account for the yielding of model building is exactly the same as the result in Table 4.6

Table 4.9 Optimal Distribution of SVDs for MRF Building Model
(GA Uses Modified Spectrum Analysis per 2009 NEHRP Provisions)

Story	Number of Dampers	Added Mean Damping ($\times 10^7$ *N-sec/m*)	Added Mean Stiffness ($\times 10^8$ *N/m*)	Distribution (%)
1	18	2.05	1.18	14.0
2	18	2.05	1.18	14.0
3	18	2.05	1.18	14.0
4	18	2.05	1.18	14.0
5	18	2.05	1.18	14.0
6	16	1.82	1.05	12.4
7	11	1.25	0.72	8.5
8	9	1.03	0.59	7.0
9	3	0.34	0.20	2.3
Total	129	14.71	8.47	100.0

4.10 Modal Properties of Model Buildings with Optimal Design of SVDs

Mode	Shear Building Model		MRF Building Model	
	Frequency (Hz)	Damping Ratio	Frequency (Hz)	Damping Ratio
1	1.01	0.09	0.74	0.14
2	2.63	0.13	2.00	0.26
3	4.24	0.17	3.33	0.36
4	5.65	0.18	7.98	0.42
5	6.95	0.23	6.18	0.52
6	8.00	0.34	7.98	0.59
7	9.45	0.35	9.53	0.62
8	10.48	0.45	11.41	0.70
9	11.73	0.49	13.30	0.71

Table 4.11 Expected Failure Costs of Shear Building Model with SVDs under the Earthquake with the Design Intensities

PGA (g)	Expected Failure Cost (× $1,000)		Cost Reduction Rate (%)
	W/O Damper	Optimal SVD	
0.11	246	9	96
0.24	275	61	78
0.37	213	69	68
0.50	113	44	61
0.62	64	27	58
0.75	30	15	50
0.88	16	8	50
Total	955	233	76

Table 4.12 Expected Failure Costs of MRF Building Model with SVDs under the Earthquake with the Design Intensities

PGA (g)	Expected Failure Cost (× $1,000)		Cost Reduction Rate (%)
	W/O Damper	Optimal SVD	
0.11	813	8	99
0.24	648	63	90
0.37	403	71	82
0.50	198	61	69
0.62	110	41	63
0.75	53	16	70
0.88	29	9	69
Total	2,255	267	88

Table 4.13 Properties of Visco-Elastic Damping Polymer for Each Building Model with Average Temperature of 18.5°C

Factors	Shear Building (Frequency = 0.96 Hz)	MRF Building (Frequency = 0.58 Hz)
Shear Storage Modulus G' (MPa)	0.23	0.21
Shear Loss Modulus G" (MPa)	0.17	0.14
Loss Factor η	0.73	0.68

Table 4.14 Results from the Optimization of SVDs for Shear Building Model with Different Ambient Temperature

Costs (× $1,000)	Design Ambient Temperature	
	Four Intervals	Average
Initial Cost	15,700	15,700
Damper Cost	261	263
Failure Cost	233	229
Object Cost	494	492
Life-Cycle Cost	16,194	16,192
Mean Annual Failure Cost	12.2	12.0

Table 4.15 Results from the Optimization of SVDs for MRF Building Model with Different Ambient Temperature

Costs (× $1,000)	Design Ambient Temperature	
	Four Intervals	Average
Initial Cost	12,900	12,900
Damper Cost	301	296
Failure Cost	267	274
Object Cost	568	570
Life-Cycle Cost	13,468	13,470
Mean Annual Failure Cost	14.0	14.4

Table 4.16 Results from the Optimization of SVDs for Shear Building Model

Costs (× $1,000)	Type of SVDs		
	Small	Medium	Large
Initial Cost	15,700	15,700	15,700
Damper Cost	261	265	262
Failure Cost	233	203	187
Object Cost	494	468	450
Life-Cycle Cost	16,194	16,168	16,150
Mean Annual Failure Cost	12.2	10.7	9.9

Table 4.17 Results from the Optimization of SVDs for MRF Building Model

Costs (× $1,000)	Type of SVDs		
	Small	Medium	Large
Initial Cost	12,900	12,900	12,900
Damper Cost	301	365	276
Failure Cost	267	162	180
Object Cost	568	527	456
Life-Cycle Cost	13,468	13,427	13,356
Mean Annual Failure Cost	14.0	8.5	9.6

Figures 4

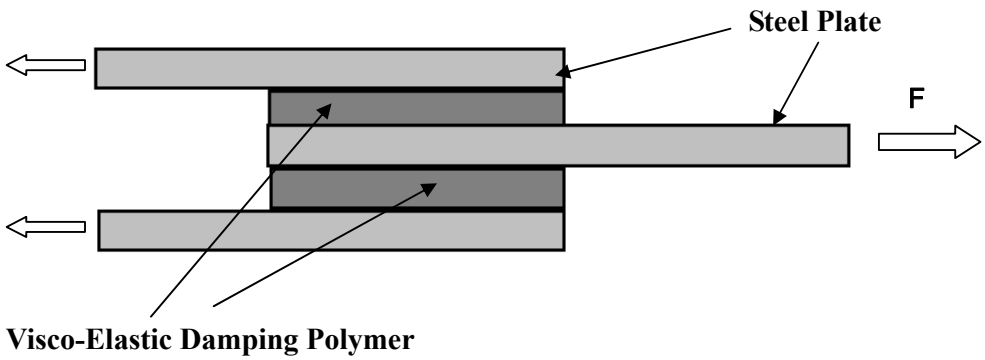

Figure 4.1 Typical Solid Visco-Elastic Device for Seismic Structure

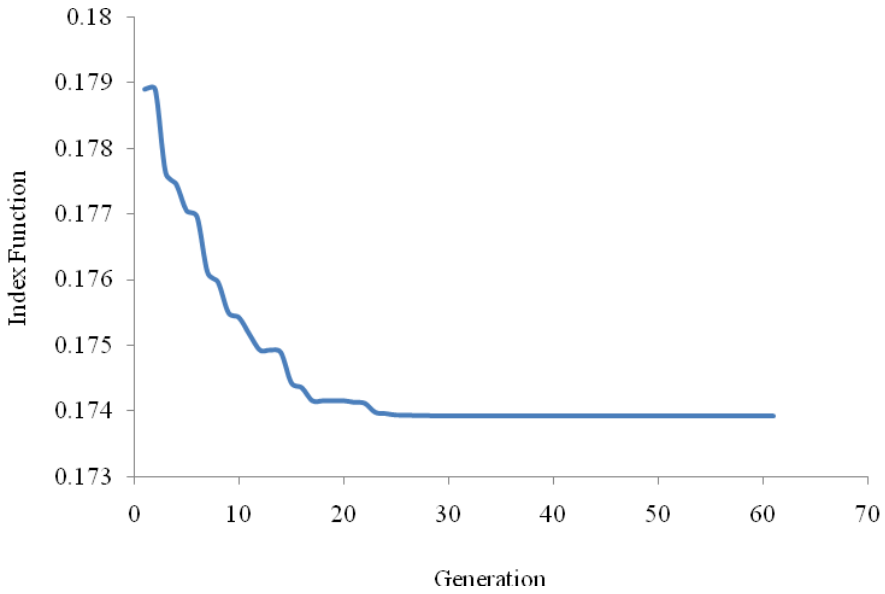

Figure 4.2 Convergence of GA for Shear Building Model with SVDs

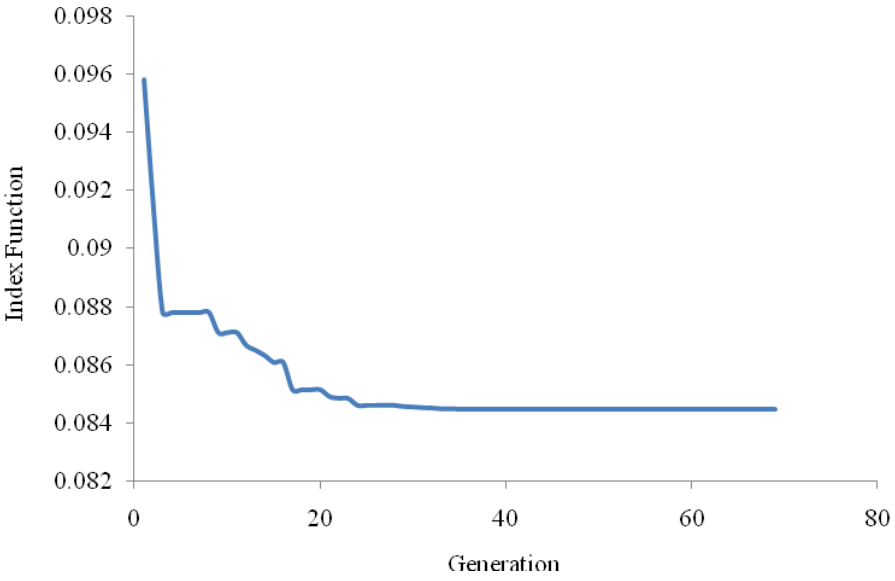

Figure 4.3 Convergence of GA for MRF Building Model with SVDs

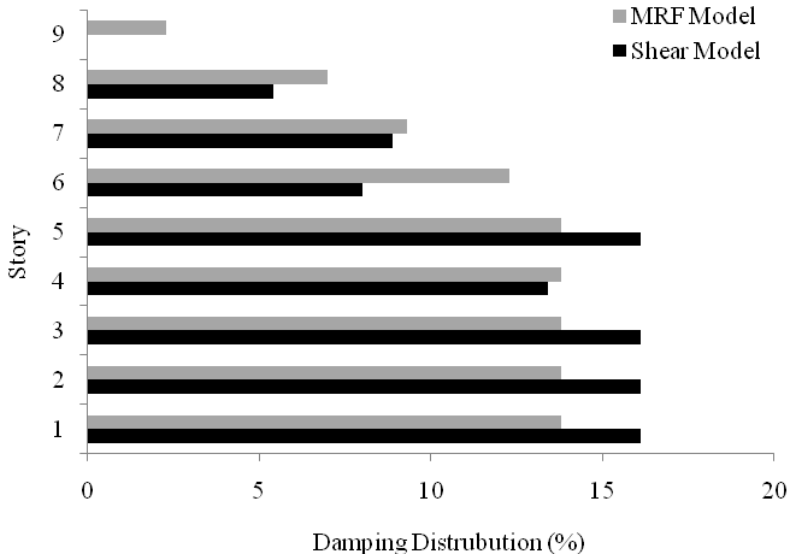

Figure 4.4 Comparison of the Percentage Distribution of Damping Coefficient

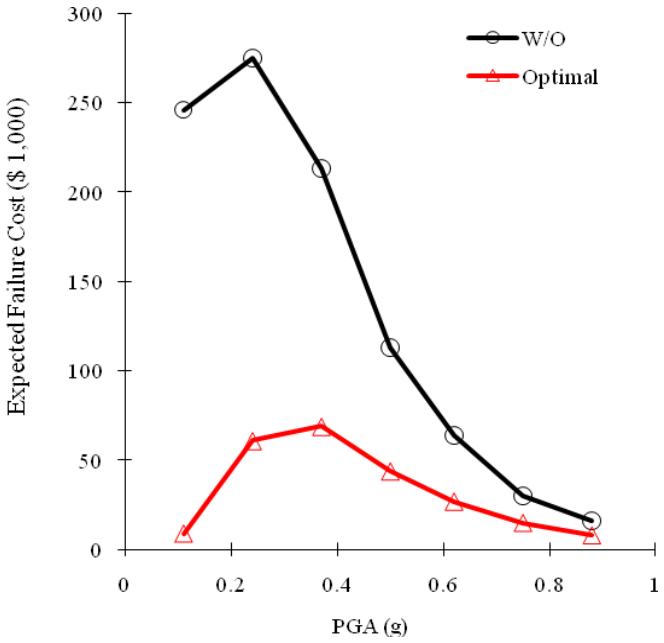

Figure 4.5 Expected Failure Costs of Shear Building Model with SVDs under Various Earthquakes Intensities

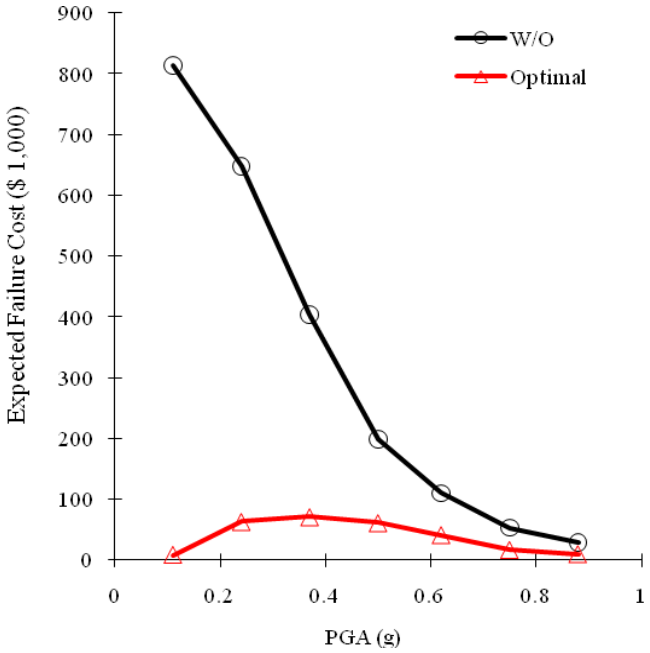

Figure 4.6 Expected Failure Costs of MRF Building Model with SVDs under Various Earthquakes Intensities

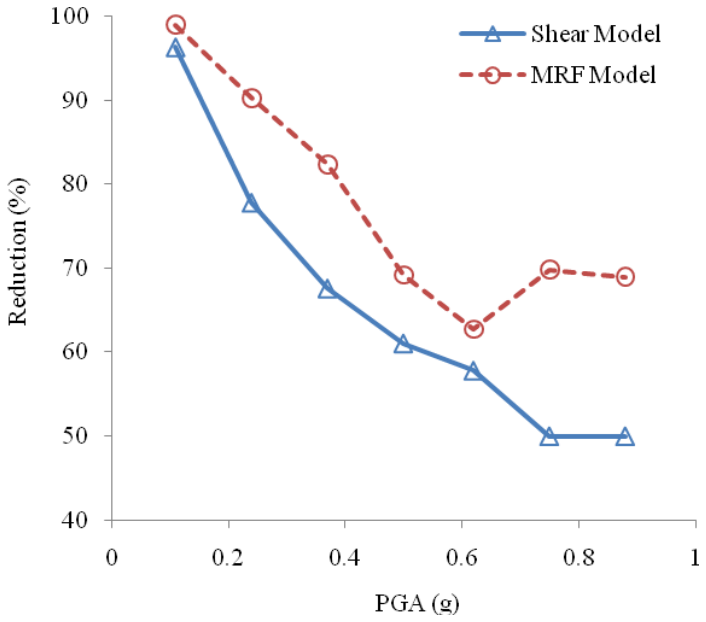

Figure 4.7 Percentage Cost Reduction Ratios under Various Earthquake Intensities

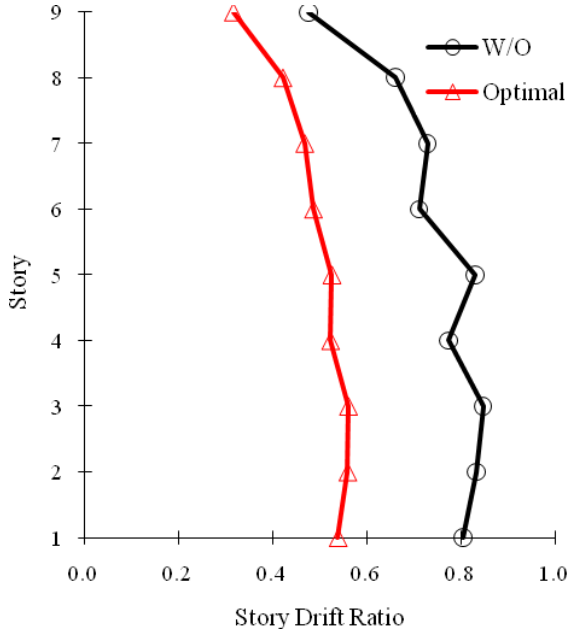

Figure 4.8 Comparison of the Mean Story Drift Ratios of the Original Shear Building and the Building with SVD (Earthquake Intensity = 0.50g)

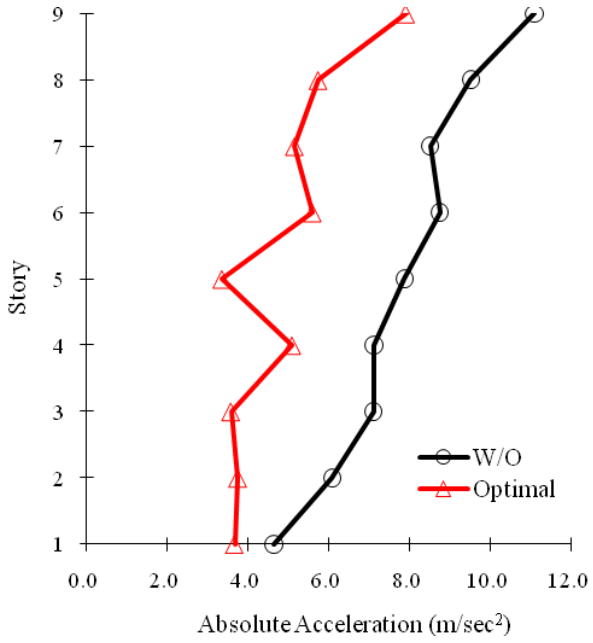

Figure 4.9 Comparison of the Average Floor Accelerations of the Original Shear Building and the Building with SVD (Earthquake Intensity = 0.50g).

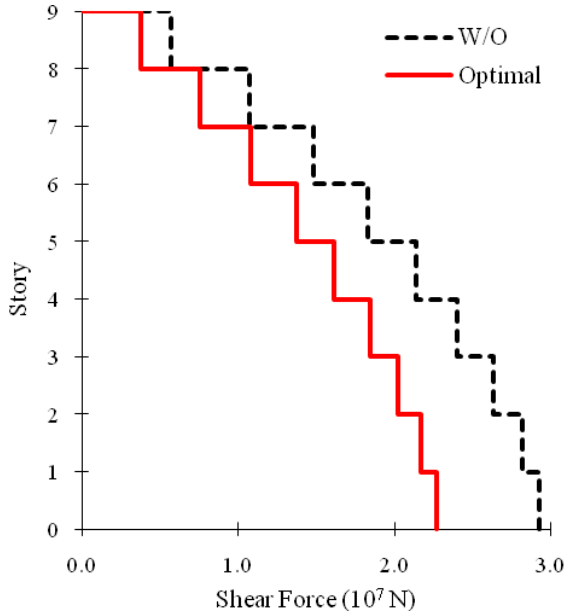

Figure 4.10 Comparison of the Mean Story Shear of the Original Shear Building and the Building with SVD (Earthquake Intensity = 0.50g).

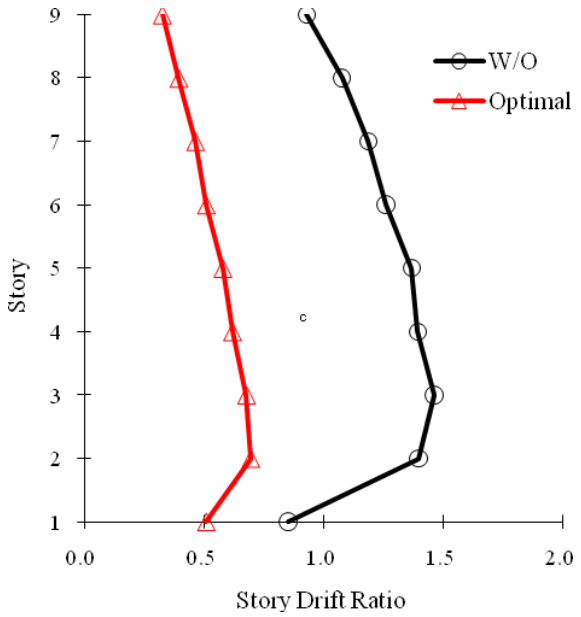

Figure 4.11 Comparison of the Mean Story Drift Ratios of the Original MRF Building and the Building with SVD (Earthquake Intensity = 0.50g)

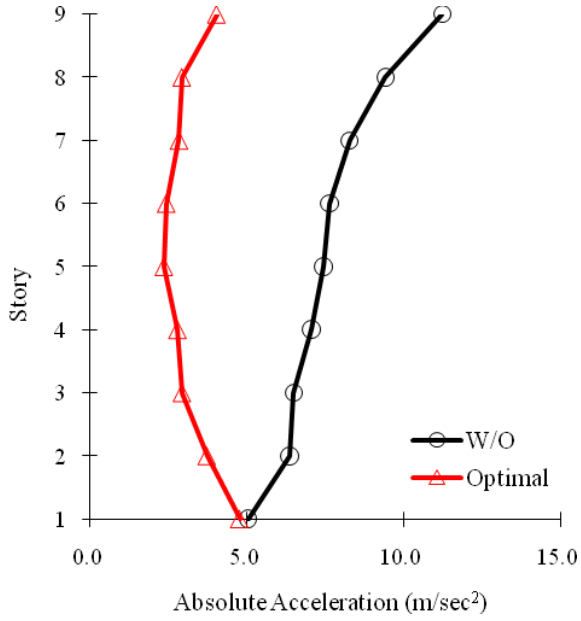

Figure 4.12 Comparison of the Average Floor Accelerations of the Original MRF Building and the Building with SVD (Earthquake Intensity = 0.50g).

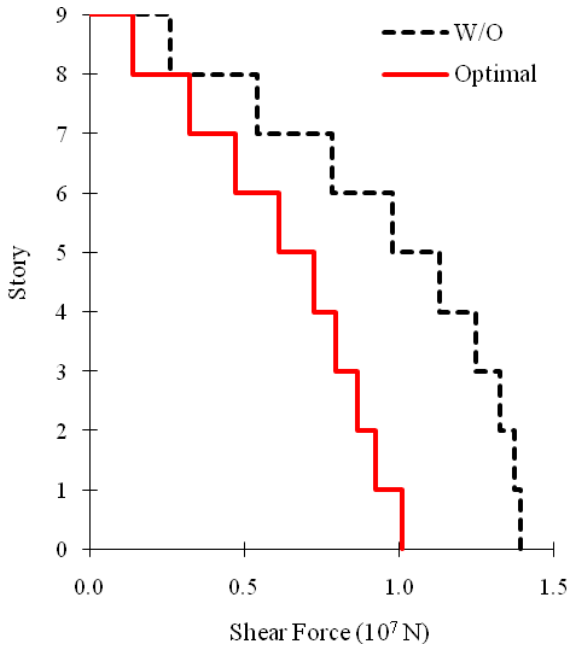

Figure 4.13 Comparison of the Mean Story Shear of the Original MRF Building and the Building with SVD (Earthquake Intensity = 0.50g).

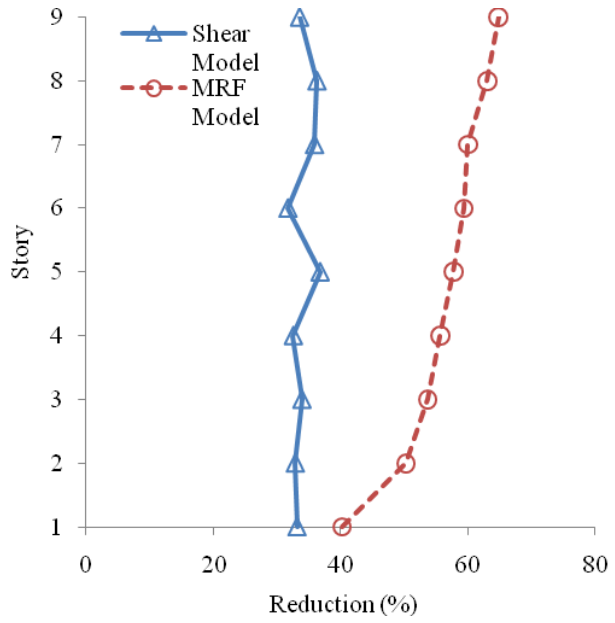

Figure 4.14 Percentage Story Drift Ratio Reductions under Various Earthquake Intensities

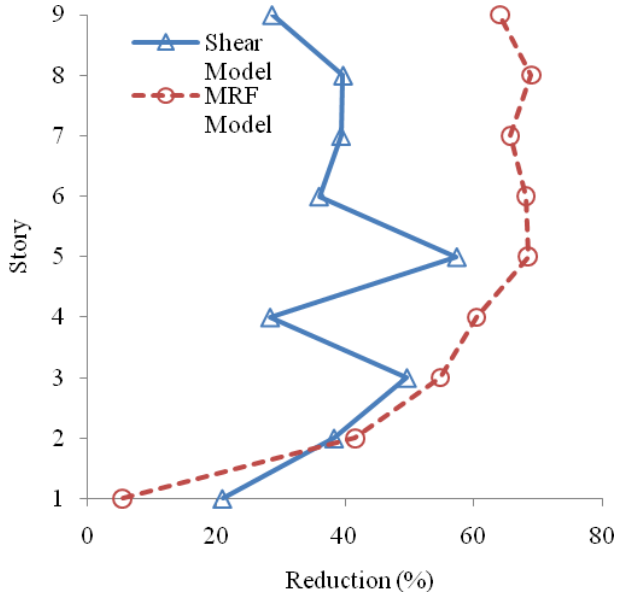

Figure 4.15 Percentage Absolute Acceleration Reductions under Various Earthquake Intensities

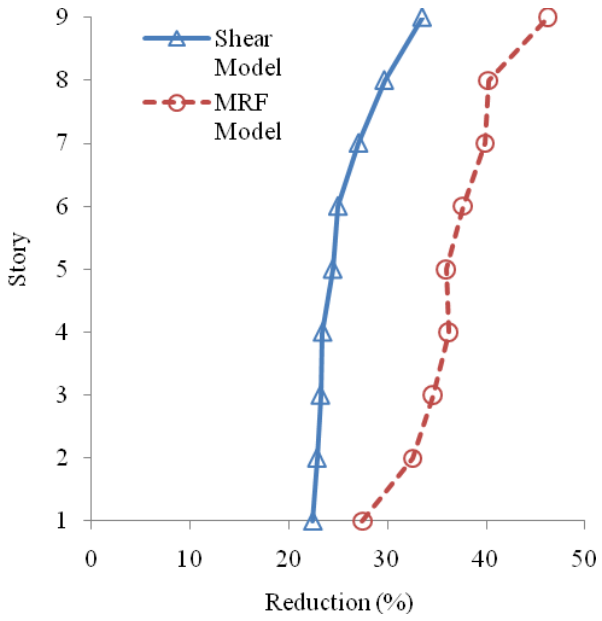

Figure 4.16 Percentage Shear Force Reductions under Various Earthquake Intensities

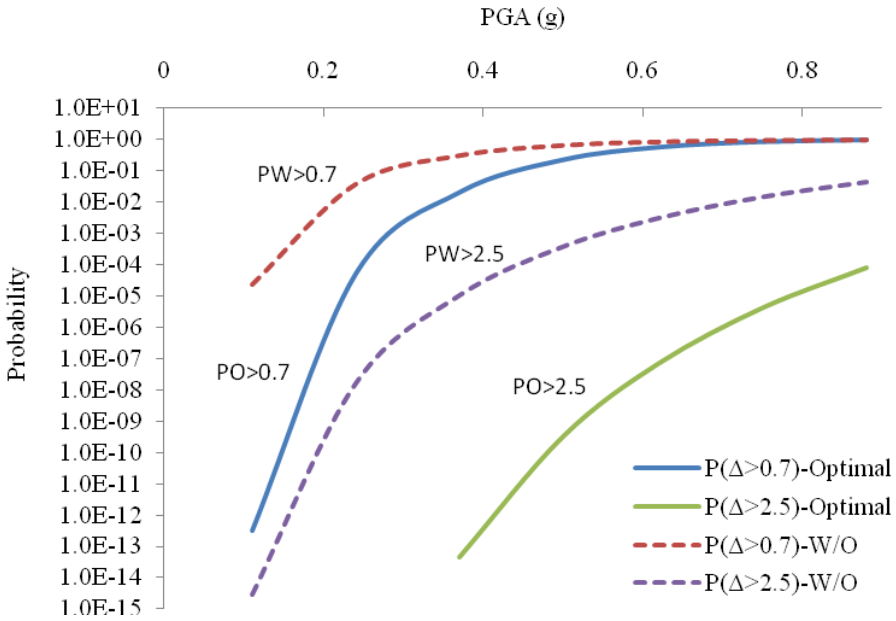

Figure 4.17 Fragility Curves with Maximum Story Drift Ratio of Shear Building Model

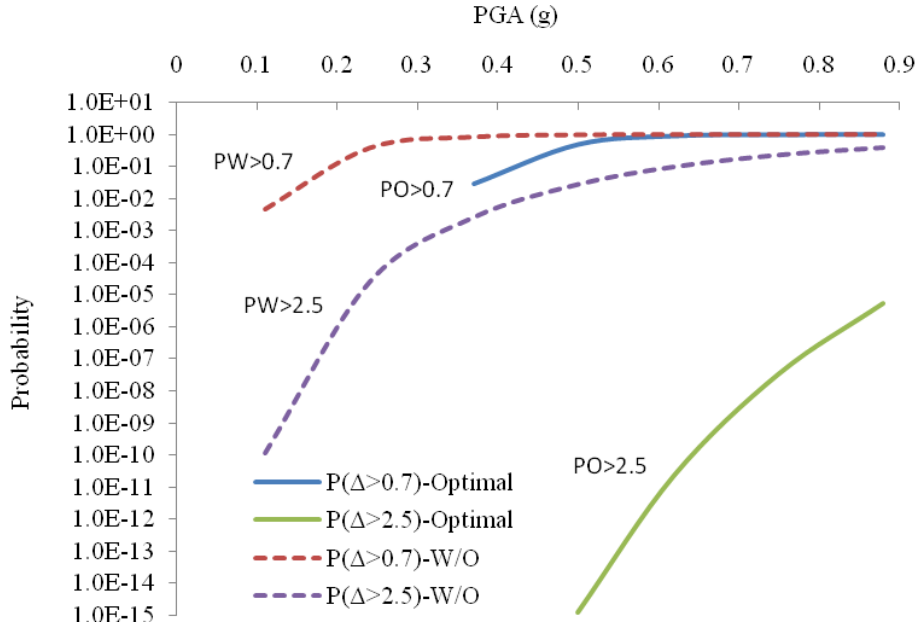

Figure 4.18 Fragility Curves with Maximum Story Drift Ratio of MRF Building Model

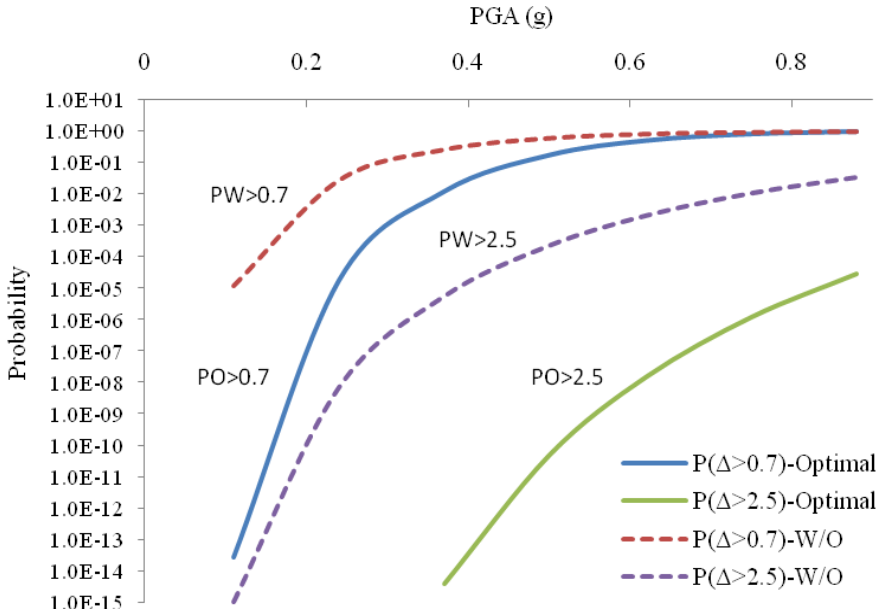

Figure 4.19 Fragility Curves with 1st Story Drift Ratio of Shear Building Model

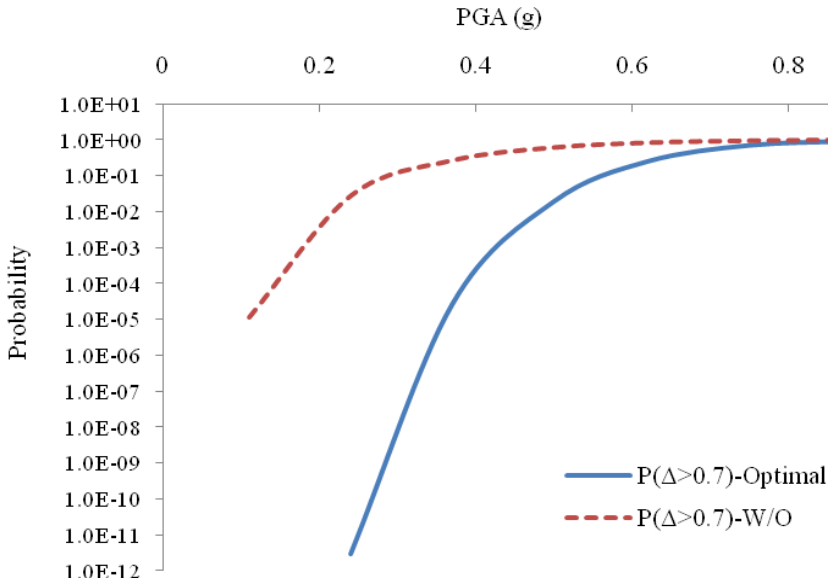

Figure 4.20 Fragility Curves with 1st Story Drift Ratio of MRF Building Model

CHAPTER 5

Design with Yielding Metallic Devices

5.1 Introduction

The presentations in previous chapters focused on the designs with viscous and visco-elastic damping devices to minimize the expected life-cycle cost. These damping devices dissipate the input seismic energy that was primarily proportional to their relative velocities. The response of the structures installed with these devices could be estimated with the assumption of linear behavior of the structure. This linear behavior assumption facilitated the optimization procedure greatly as the response quantities of interest could be easily calculated using the elastic design response spectra representation of earthquake input at different hazard intensities. As the optimization procedure required repeated response analyses for several feasible designs of a large population and then for several generations, the use of the response spectrum analysis resulted in immense saving in the computational effort.

In this chapter, we study the use of yielding metallic devices (YMD) in an optimal manner to reduce the failure cost of a structure. Yielding metallic devices behave quite differently from the visco-elastic damping devices in their principle of operation. Yielding metallic devices dissipate energy through the yielding of metal plates. When the yielding plates are subjected to cyclic loading, they create a hysteresis loop, and the area inside the loop represents the dissipated energy. This dissipation mechanism through hysteresis depends on the relative displacement of the device rather than the relative velocity as was the case for the visco-elastic devices. Since the device is subjected to yielding, its behavior is necessarily inelastic and the linear analysis method cannot be used to obtain the response of the structure installed with the yielding metallic devices.

The idea of using yielding metallic devices in a structure to absorb a large portion of the input seismic energy began with the work of Kelly et al. (1972) and Skinner et al. (1974). After these studies, a wide variety of efficient yielding metallic devices has been proposed. Among the various yielding metallic devices, the Added Damping and

Stiffness (ADAS) device and the Triangular-plate Added Damping and Stiffness (TADAS) device are the most popular and useful for the seismic retrofit of existing structures as well as in the seismic design of a new structure. These devices dissipate the seismic energy through yielding caused by bending. The ADAS device is made with an X-shaped mild steel plate that deforms in double curvature. TADAS is a variation of ADAS in shape with a triangular mild steel plate that deforms as a cantilever beam. Figure 5.1 shows a plate of the TADAS device. In a device there are usually several plates that are assembled in a base. The base is attached to a brace which is in turn supported on the floor beam. The top of the plates is attached to the beam above the floor. Because of their shapes, the metal plates in the ADAS and TADAS experience uniform flexural strains along their lengths. Thus, when the strain reaches the yield level, yielding occurs and spreads almost uniformly throughout the material.

In this chapter we present the details of calculating the optimal design parameters of the yielding metallic devices that would minimize the expected life-cycle cost of a structure. As mentioned previously, the hysteretic behavior of yielding metallic devices is strongly nonlinear accompanied by the abrupt changes in the element stiffness associated with loading and unloading of a yielding element. This hysteretic behavior of the yielding element of the device is explicitly considered in the analysis in this study. However, since an optimal installation of these devices will dissipate energy and reduce the dynamic response, the braces through which the device is attached to the structure and the structure itself may remain elastic while the deforming element of the devices goes into the nonlinear range. To calculate the response of such yielding elements, we have used the step by step analysis approach that uses the representative time histories of the input ground motion and considers yielding of the device as well as that of structural members.

5.2 Analytical Model of Yielding Metallic Device

A yielding metallic device is best characterized by the force-displacement hysteretic relationships of the yielding element. The nonlinear force-displacement relationship is usually represented by multi-linear models such as a simple elasto-plastic model, a bilinear model or a polynomial model with the bilinear model being the most common. Here in this study, a simple bilinear model is used to represent the hysteretic behavior of the devices.

Schematically, a structure with yielding metallic devices can be represented in terms of three elements that affect the stiffness of the system: the structural member, the yielding metallic element, and the brace that supports the device and connects it with the structure. For the mechanical modeling of the unit in the story of a shear building (which is the subject of this study in this chapter), the metallic device and the brace are in series. Figure 5.2 provides a schematic depicting these series and parallel components of the device-brace-structure unit in a building story. The stiffness contribution of the brace and device to the story stiffness can be represented in the following form:

$$k_{DB} = \frac{1}{\frac{1}{k_D} + \frac{1}{k_B}} = \frac{k_D}{1 + \frac{1}{r_{BD}}} \tag{5.1}$$

where k_D and k_B represent the stiffness of the plate of the yielding metallic device and the brace, respectively; r_{BD} represents the stiffness ratio of brace to device expressed as:

$$r_{BD} = \frac{k_B}{k_D} \tag{5.2}$$

Equations (5.1) and (5.2) show that the contribution of the brace stiffness to the structural system stiffness decreases as the brace stiffness increases. For very stiff braces, the total contribution of the device and brace assembly to the structural stiffness is the same as the stiffness of the device. The total story stiffness of a structure with yielding metallic device and brace assembly for the elastic and yielding phase of the device can be written in the following form:

$$\begin{aligned} k_{T,b} &= k_S + k_{DB,b} \\ k_{T,y} &= k_S + k_{DB,y} \end{aligned} \tag{5.3}$$

where $k_{DB,b}$ and $k_{DB,y}$ represent the total added stiffness due to the metallic device and the brace before and after yielding of the yielding element, respectively. Likewise, $k_{T,b}$ and $k_{T,y}$ represent the total stiffness of the unit structural system before and after yielding of the yielding metallic device. While tracing the path of the hysteretic loop, $k_{T,b}$ is used to represent the stiffness of the structure for the loading before yielding and

also unloading, and $k_{T,y}$ is used in the section of the loading after yielding. If the stiffness of the brace is large enough compared to the stiffness of the yielding metallic device, then the total stiffness of the structural system can be represented simply as the sum of k_S and k_D.

5.2.1 Mechanical Property of Yielding Metallic Device

It is assumed that the yielding metallic device in this study has the same material property as in the structural members of the building. The yielding metallic device increases the structural stiffness and dissipates the seismic energy in hysteresis when it yields. The stiffness and load capacity of a yielding metallic device depend on the stiffness of the bending plates and the yield displacement. In terms of the total number of linearly tapered plates used in a story, n_p, the elastic stiffness k_D of the devices in the story and the yield displacement δ_{Dy} can be expressed in the following forms:

$$k_D = n_p E \Big/ \left(\int_0^{h_p} \int_0^x \frac{x}{I(x)} dxdx \right) = \frac{n_p E b_p t_p^{\,3}}{6 h_p^{\,3}} \tag{5.4}$$

$$\delta_{Dy} = \frac{f_y}{E} \int_0^{h_p} \int_0^x \frac{1}{y(x)} dxdx = \frac{f_y h_p^{\,2}}{E t_p} \tag{5.5}$$

where E = Young's modulus, I = the second moment of area of the plate, y = half plate thickness, f_y = tensile yield stress of the plate, b_p = width of the plate, h_p = length of the plate, and t_p = thickness of the plate. The yield strength of the yielding element P_y can be defined with the yield displacement of the device δ_{Dy} and the stiffness of the device k_D in the following form:

$$P_y = k_D \delta_{Dy} = k_{DB} (1 + \frac{1}{r_{BD}}) \delta_y \tag{5.6}$$

where δ_y represents the yield displacement of the device-brace assembly. We express Eq. (5.6) in terms of the design parameters that will be used in the optimal design of yielding metallic devices in the following form:

$$P_y = SR\ k_S \left(1 + \frac{1}{r_{BD}}\right) \delta_{Dy} \tag{5.7}$$

where *SR* represents the stiffness ratio of the brace-device assemblage to the original structure without supplementary device, and can be expressed in the following form:

$$SR = \frac{k_{DB}}{k_S} \tag{5.8}$$

5.3 Optimization Problem

As shown in Equations (5.1) to (5.8), the force-deformation characteristics of a yielding metallic device in a structure generally depend on the following three parameters: the stiffness ratio of brace to device, the yield displacement of the metallic device, and the stiffness ratio of the brace-device assemblage to the corresponding structural members. Thus, the seismic response quantity of a structure with yielding metallic devices would depend on the value of the three parameters, and these parameters can be the mechanical variables of the optimization problem. In this study, the expected life-cycle cost is used to evaluate the performance of a structure, and this performance depends on how much the structure deforms. Therefore, the three parameters which determine the displacement response of the structure are directly related to the expected life-cycle cost analysis. For our optimization study, where we are interested in sizing (the dimensions and the number of yielding plates and the size of the braces) the yielding device, we need to express these three parameters in terms of these properties. Furthermore, it is necessary to reduce the number of design variables, since the computational effort needed to solve the optimization problem increases almost exponentially with the increase in the number of design variables, as it becomes difficult for the optimal solution to converge in a few iterations. The following presentation will address these aforementioned issues.

The studies by Xia et al. (1992) and Moreschi and Singh (2002) have shown that the stiffness ratio of the yielding device to the supporting braces r_{BD} does not influence much the response of the structural system. Thus, in this study it is assumed that the parameter r_{BD} has a constant value during the optimization procedure, and the stiffness of the bracing and device assembly can be defined in terms of the stiffness of the yielding metallic devices. With the assumption of a constant r_{BD}, the stiffness ratio of the brace-device assemblage to the structural member SR can be defined in terms of the stiffness of the device, which would depend on the stiffness of unit and the number of the units placed in a given story.

As shown in Equations (5.4) and (5.5), the yield displacement of yielding devices depends on the width b_p, thickness t_p, and length h_p of a yielding plate, and total story stiffness depends on the number of plates n_p and these parameters. Also, it is obvious from Eq. (5.4) that the stiffness of the yielding device is affected more strongly by the thickness and length of the plate than the width. Eq. (5.5) shows that the yield displacement depends on only the length and thickness of the plate. The yield strength P_y of the devices can be expressed in the following form by inserting Equations (5.4) and (5.5) in (5.6):

$$P_y = \frac{n_p f_y b_p t_p^{\,2}}{6h_p} \tag{5.9}$$

Eq. (5.9) shows that the yield strength of a yielding metallic device is affected more strongly by the thickness of the plate than the length. The cost of a plate, which depends on the volume of the plate, is, however, affected equally by the three dimensions. In this study, we will fix length and base width dimensions of a plate but leave the plate thickness t_p as a design variable along with, of course, the number of these plates n_p needed in a story to be optimized.

The cost optimization problem with yielding metallic devices can, thus, be stated in the following form:

$$
\begin{aligned}
&\textit{minimize} \quad && E\left[C\left(\mathbf{R}\left(\mathbf{x},t\right)\right)\right] \\
& && \mathbf{x} = \left\{\mathbf{n}_p, t_p\right\}^{\mathrm{T}} \\
&\textit{subject to} \quad && \mathbf{n}_p \le \mathbf{n}_p^t \\
& && t_{\min} \le t_p \le t_{\max}
\end{aligned} \tag{5.10}
$$

where $\mathbf{n}_p$ is the vector containing the number of yielding plates on a floor, $\mathbf{n}_p^t$ is the vector containing the maximum number of plates that can be put in different stories, and $t_{\max}$ and $t_{\min}$, respectively, represent the allowable maximum and minimum thickness values of a yielding plate in the device.

5.3.1 Selected Values of Design Parameters

As shown above, the stiffness, yield deflection and yield load for the device is a function of the width, length, thickness, Young's modulus and yield stress of the plate. The yield stress is of course determined by the material used. For mild steel we used the values of: Young's modulus E=200GPa, yield strength f_y=345MPa. One could, of course, use the plate dimensions such as width, length and thickness as the design variables as they all affect the stiffness and yield load differently. However, to reduce the number of design variables, we take the width and length as fixed quantities as the yield load depends on these variables relatively mildly (with the exponent 1) compared to the thickness which appeared with exponents 2. In terms of the stiffness, the plate length also seems to be relatively as important a variable as the thickness, as both appear in the equation with the power 3. However, to reduce the number of variables, the length was also fixed. These fixed values were taken as: b_p= 300mm and h_p= 400mm.

Another parameter that we need to select is the ratio of the brace stiffness to that of the device. As mentioned earlier, this parameter does not affect the response significantly, and thus it is assumed to be fixed at r_{BD}= 2. That is, the stiffness of the bracing members is assumed to be two times the stiffness of the device. This value is recommended by Xia et al. (1992) that is the most economical value considering the cost of bracing members and enough strength for the bracing to yield the metallic device.

The hysteretic behavior of the yielding metallic device is defined by a simple bilinear

model. In the bilinear model assumed here, the value of the post-yield stiffness of steel needs to be decided. This value usually varies from 0% to 5% of the initial stiffness, with a value of 1% being more commonly used. This value has also been used in some models such as the Menegotto-Pinto Model (1973). In our study, the post-yield stiffness of the steel plate of the TADAS device is taken to be 1.0% of the initial stiffness.

5.3.2 Unit Cost Values for TADAS Devices

The cost of a unit of a TADAS device can be divided into two component costs: the cost of the steel plates used in the device and the cost of the base where the plates are anchored and then connected to the brace. The cost of the base includes all other elements to connect the plates to the bracing system. The cost of the steel plate can be assumed to be proportional to the volume of the plate or the amount of material used in the plate. We do not know the thickness of the plate, which will be calculated by the optimization algorithm. However, since we know the length and the width of the plate, we define the unit cost for the plate in terms of cost per unit thickness. Based on the surface area of the plate, this cost has been estimated to be $5.0/mm. This cost includes the material cost, the cost of fabrication, and other costs such as contractor's margin, etc. To estimate the unit cost of the base to which the yield plates are attached, we determined the cost of a base unit in a typical TADAS device with 5 to 7 plates and then used this cost to determine the cost of the base per mm of the plate thickness used. This cost was estimated to be $7.0/mm. This cost included all costs associated with machining, cutting holes for bolts, bolting, and assembling onto the brace to produce a tight anchor to the yielding plates.

Unit Bracing Cost

The lateral stiffness of a chevron brace can be calculated using the following formula:

$$k_B = \frac{2EA_B \cos^2\theta \sin\theta}{h_S} \tag{5.11}$$

where A_B, h_S, and θ represent the cross sectional area of the bracing member, story height, and the angle between the bracing member and the horizontal structural member, respectively. In terms of the stiffness ratio r_{BD}, the stiffness of a yielding plate k_p and

the number of plates used in a device n_p, the stiffness of a brace can be expressed as

$$k_B = k_p n_p r_{DB} \tag{5.12}$$

Using Eqations (5.11) and (5.12) the required cross sectional area A_B of the bracing member can be calculated as follows:

$$A_{req} = \frac{h_S}{2E\cos^2\theta\sin\theta} r_{BD} k_D \tag{5.13}$$

The cost C_B for the bracing member can be calculated with the estimated cross-sectional area A_{req} and the unit cost of construction steel per cross sectional area C_{area} as follows:

$$C_B = C_{area} A_{req} l_B \tag{5.14}$$

where l_B represents the length of the bracing member. The unit cost C_{area} is estimated from the RS Means Open Shop Building Construction Cost Data (2009), and the estimated unit cost of the bracing member is \$3.5/cm^2/m.

5.3.3 Constraints on Design Variables

In previous chapters it is assumed that the number of available installation places for damping devices at each floor of the model buildings is limited to 9 and the maximum number of dampers that can be installed at each floor is 18 because two fluid viscous damper or two solid visco-elastic dampers can be installed in the same bay. Here in this chapter also we assume that 9 locations on each story are available to install TADAS devices. However, based on the size of a TADAS device with 5~7 triangular steel plates attached, we assume that only one TADAS device per location can be installed, limiting the number per story to 9. Assuming that a TADAS unit can accommodate 5 triangular steel plates, the total number of plates that can be installed in a story is limited to n_d^t=54.

We also placed constraints on the thickness of the plates to limit the search space for the optimization process. To arrive at this number we considered the suggestion made by

Xia et. al (1992). They suggested a plate yield displacement in the range of 0.0014H to 0.002H, where H is the story height. Thus, the design yield displacement of the plate for the model building is limited in the 5 mm to 8 mm range considering the story height of the model building. Using Eq. (5.5) the corresponding limits on the plate thickness can be calculated with the width, length and yield stress of the plate, and the estimated plate thickness range is t_{max}=55mm to t_{min}=35mm.

5.4 Response Calculations

The equations of motion of the structural system with yielding metallic devices can be written in standard form, realizing that such a device only affects the stiffness matrix, as follows:

$$\mathbf{M}\ddot{\mathbf{u}}(t)+\mathbf{C}\dot{\mathbf{u}}(t)+\mathbf{K}\mathbf{u}(t)=-\mathbf{M}\mathbf{u}\ddot{u}_g(t) \tag{5.15}$$

where $\mathbf{M}$ and $\mathbf{C}$ represent the mass and damping matrix of the original structure, respectively. $\mathbf{K}$ represents the total stiffness matrix of the structure with the supplementary yielding metallic devices, which can be written in the following form:

$$\mathbf{K}=\mathbf{K}_S+\mathbf{K}_{DB} \tag{5.16}$$

Where $\mathbf{K}_S$ and $\mathbf{K}_{DB}$ represent the stiffness matrix of the original structure and the stiffness matrix due to the supplementary yielding metallic devices, respectively. The entries of the stiffness matrix $\mathbf{K}$ vary during the response analysis as yielding occurs in the metallic plates and the structural members.

Eq. (5.15) is solved using the well-known Newmark-β method. The yielding in the elements is tracked and depending upon the loading and unloading phase, the stiffness matrix is modified. The response vector at time step $i+1$ is obtained as follows (Hart and Wong, 2000):

$$\mathbf{q}_{i+1}=\mathbf{R}_N\mathbf{q}_i+\mathbf{P}_G\mathbf{\iota}\left(\ddot{u}_g\left(t_{i+1}\right)-\ddot{u}_g\left(t_i\right)\right)+\mathbf{P}_N\Delta\mathbf{F} \tag{5.17}$$

where $\mathbf{q}_i$ is the state vector of the responses at time t_i written as follows:

$$\mathbf{q}_i = \begin{Bmatrix} \mathbf{x}_i \\ \dot{\mathbf{x}}_i \\ \ddot{\mathbf{x}}_i \end{Bmatrix} \tag{5.18}$$

The matrices $\mathbf{R}_N$, $\mathbf{P}_G$, and $\mathbf{P}_N$ are defined as:

$$\mathbf{R}_N = \begin{bmatrix} \mathbf{I} & (\Delta t)\mathbf{I} - \alpha(\Delta t)^3 \mathbf{B}^{-1}\mathbf{K} & \frac{1}{2}(\Delta t)^2 \mathbf{I} - \alpha(\Delta t)^3 \mathbf{B}^{-1}\mathbf{C} - \frac{1}{2}\alpha(\Delta t)^4 \mathbf{B}^{-1}\mathbf{K} \\ \mathbf{0} & \mathbf{I} - \beta(\Delta t)^2 \mathbf{B}^{-1}\mathbf{K} & (\Delta t)\mathbf{I} - \beta(\Delta t)^2 \mathbf{B}^{-1}\mathbf{C} - \frac{1}{2}\beta(\Delta t)^3 \mathbf{B}^{-1}\mathbf{K} \\ \mathbf{0} & -(\Delta t)\mathbf{B}^{-1}\mathbf{K} & \mathbf{I} - (\Delta t)\mathbf{B}^{-1}\mathbf{C} - \frac{1}{2}(\Delta t)^2 \mathbf{B}^{-1}\mathbf{K} \end{bmatrix} \tag{5.19}$$

$$\mathbf{P}_G = -\begin{bmatrix} \mathbf{B}^{-1}\mathbf{M}\alpha(\Delta t)^2 \\ \mathbf{B}^{-1}\mathbf{M}\beta(\Delta t) \\ \mathbf{B}^{-1}\mathbf{M} \end{bmatrix} \qquad \mathbf{P}_N = -\begin{bmatrix} \mathbf{B}^{-1}\alpha(\Delta t)^2 \\ \mathbf{B}^{-1}\beta(\Delta t) \\ \mathbf{B}^{-1} \end{bmatrix} \tag{5.20}$$

$$\mathbf{B} = \mathbf{M} + \beta\Delta t\mathbf{C} + \alpha(\Delta t)^2 \mathbf{K} \tag{5.21}$$

$\Delta\mathbf{F}$ represents the imbalance of forces on the members of the structural system between the forces $\mathbf{F}_{dynm}$ from the dynamic equilibrium equation of motion and the force $\mathbf{F}_{stat}$ from the static analysis due to the change of stiffness of the structural system that is caused by yielding of the metallic devices. This can be expressed in the following form:

$$\Delta\mathbf{F} = \mathbf{F}_{dynm} - \mathbf{F}_{stat} \tag{5.22}$$

The constant average acceleration method with $\alpha = 1/4$ and $\beta = 1/2$ is adopted as with these parameter values the Newmark-β method is known to be unconditionally stable. Geometric stiffness due to the $P-\Delta$ effect is not considered in this study.

The computer program written based on this formulation was validated with two examples. The first was a single degree of freedom problem for which the numerical results were available in a textbook. The second was a two degree of freedom problem which was solved in another textbook for which the response time history plot was available. These problems are shown in Appendix D.

Input Ground Motion

To calculate the response, synthetic time histories that are compatible with the design spectrum were used. In this study, 20 independent acceleration time histories were generated using SIMQKE-1 corresponding to all seven hazard intensities that define the seismic hazard on the site. Thus a total of 140 different synthetic ground motion accelerograms were generated and used for calculating the response for the life-cycle cost calculations. All time histories were generated at 0.01 second intervals with a total duration of 20 seconds. The envelope function shown in Chapter 2 was used to modulate the time history ordinates. One could use the response results obtained for the ensemble of time histories to calculate the mean and standard deviation values. However, it was observed that SIMQKE-1 generated time histories provide a good estimate of the mean response but the variation in the response (which defines the standard deviation) was more than the variation in the Newmark-Hall study on the basis of which the mean-plus-one-standard-deviation spectra were developed. Thus, to calculate the standard deviation, another set of time histories compatible with the mean-plus-one-standard-deviation spectrum was used to calculate the mean-plus-one-standard-deviation values of the response. The difference of the mean values calculated for the two sets was used to obtain the standard deviation of the response quantities of interest. The mean and standard deviation values calculated in this way were used to calculate the probabilities of the response being in different limit states which are needed for calculating the failure cost.

5. 5 Numerical Results

In this study we have generated numerical results only for the shear building, primarily because of the ease of calculating its response when the structural members and the device yield. An optimal design with yielding metallic devices is obtained to minimize the expected life-cycle cost. For the numerical calculations, TADAS devices are used as the yielding devices of choice. The TADAS device was developed in Taiwan, and it is one of the most widely used yielding metallic devices. Numerical results for the failure costs, object cost, and the response of the structure are obtained and compared with those for the structure without any device.

Again the genetic algorithm was used to calculate the optimal values of the design

variables of the plate thickness and the number of plates in each story. The individual design consisted of 10 genes representing the 10 variables representing the numbers of the yielding plates in the 9 stories of the frame and the plate thickness. The number of plate variables could be any number between the value of 0 and 54, and thus had 55 choices. There were 21 possible choices of the plate thicknesses between the limits of 35 mm to 55mm, increased at an interval of 1mm. The population in a generation consisted of 400 individual designs. The convergence to the optimal solution was assumed to have been achieved when the calculated object cost value remained the same for 40 generations. Figure 5.3 shows the evolution of the convergence where the optimal search was stopped after 172 generations of trial.

The optimum design called for a plate thickness of 0.05m (50mm) with a total of 215 plates. The distribution of these plates in different stories of the building is shown in Table 5.1 and Figure 5.4 where the percentage distribution of the total plates with the height of the building is plotted. We note that the algorithm requires relatively more plates in the lower stories. The contribution of the TADAS plates to the stiffness of different stories is also shown.

Table 5.2 shows the failure cost, the object cost and the life-cycle cost for this optimal design. These costs are also compared with the similar costs for the original building. We note that the failure cost is reduced by about 73%, whereas the object cost is reduced by about 45%. The reduction in the life-cycle cost is only 2.6%, mainly because the object cost is a small fraction of the initial cost. However, it is of interest to note that with a relatively very small investment in the improvements of installing yielding devices, the failure cost can be significantly reduced.

In Table 5.3 we show the distribution of the failure costs for different levels of hazard intensities. The failure costs for the original buildings are also shown. A better visual description of these costs and the percentage cost reductions are given in Figures 5.5 and 5.6. We observe, as was also observed with other dampers in the previous chapters, that most cost reductions occur for the lower levels of excitation intensity. The cost reductions vary between the value of about 91% for the lowest hazard intensity and 19% for the highest hazard intensity. As the lower levels of hazard intensities contribute the most to the failure cost, the optimization algorithm focuses on reducing these costs more to minimize the objective cost. However, this cost reduction at the lower intensities is not because of energy dissipation (as at these levels the system does not

yield), but primarily because of lower story drifts caused by increased story stiffness. At the higher intensities, the reduction in the cost is both due to the interplay of the stiffness enhancement as well as dissipation of energy in yielding which contributes to the overall reduction in the force response.

Figures 5.7 and 5.8 plot the hysteresis loops for a particular input motion for the device in the first and the fifth stories for two levels of hazard intensities of 0.5g and 0.88g. The difference in the sizes of the loops is an indication of the energy dissipation in yielding at these two intensity levels.

Next we show the effect of optimal TADAS design on various response quantities of interest. In Figures 5.9 through 5.11 we compare the response values of inter story drift ratios, floor accelerations and story shears for the original building and the building with TADAS devices. The percentage reductions in these response quantities for various stories are also plotted in Figure 5.12. These figures are for an excitation intensity level of 0.5g. From these figures, we observe that the inter-story drift ratios are significantly reduced, and these reductions are responsible for reducing the failure costs. The floor accelerations and story shears are not much reduced. Rather for some stories there is an increase in the floor acceleration. This is attributable to the contribution of the increased system stiffness due to the addition of TADAS devices. Some reductions are attributed to the dissipation of energy in the system. At the lower levels of excitation, the results for which are shown in Figures 5.13-5.16, we note that both the story shears and accelerations are increased and not decreased primarily because of the increased system stiffness and no dissipation of energy in yielding.

Effect on System Fragility

The effect of TADAS installations on the fragility of the system expressed in terms of maximum inter-story drift for the limit states of immediate occupancy, life-safety, and collapse limit states are shown in Figures 5.17. The figure compares the fragility curves of the original system with that those of the system with TADAS devices. The large improvements in the fragility are noted, especially for the lower intensity values. Figure 5.18 shows similar curves for the inter-story drift at the fifth story. Again when compared with the original building we note a dramatic improvement in the fragility values, and again more at higher intensity levels.

5.6 Chapter Summary

This chapter describes the application of the life-cycle based optimization methodology for optimal designs of TADAS devices. These devices add stiffness to the system and dissipate energy in hysteresis when they yield. The stiffness and yielding characteristics of the devices are described to identify the key design parameters that need to be considered in the optimal design search. The optimization search is again done using the genetic algorithm. The key variables of interest in the optimal design are chosen to be the thickness of the yielding plates and the number of them to be placed in different stories of the building to minimize the object cost. Again the object cost is defined as the sum of the cost of the devices plus the total cost of failure. The total cost of failure is obtained in seven limit states due to all seven earthquake motion intensities that define the seismic hazard at the site. To calculate the cost of failure, the response of the structural frame is obtained by the step-by-step Newmark-β approach. The numerical results indicated that the failure costs are significantly reduced. As was the case with other protective devices discussed in the previous two chapters, the optimization algorithm ensures the largest reduction in the failure cost for the more frequent but low intensity events primarily because these events, contribute most to the total failure cost. The numerical results are also obtained to examine the effect of the TADAS devices on other response quantities of interest such as story shears and floor accelerations. It is observed that although the inter-story drifts are significantly reduced by the installation of these devices, the other response quantities are not necessarily reduced, especially at the lower ground motion intensities, primarily because the system is made stiffen by the installation of these devices.

Tables 5

Table 5.1 Optimal Distribution of TADAS Plates in Shear Building

Story	Number of Plates	Added Stiffness ($\times 10^7 N/m$)	Distribution (%)
1	29	37.8	13.5
2	36	46.9	16.7
3	36	46.9	16.7
4	26	33.9	12.1
5	28	36.5	13.0
6	20	26.0	9.3
7	16	20.8	7.4
8	18	23.4	8.4
9	6	7.8	2.8
Total	215	279.9	100.0

Note: Added Stiffness represents the total stiffness by the metallic device and brace assembly.

Table 5.2 Results from the Optimization of TADAS for Shear Building Model

Costs (× $1,000)	Seismic Design Approaches	
	W/O Damper	Optimal TADAS
Initial Cost	15,700	15,700
Damper Cost	0	265
Failure Cost	955	260
Object Cost	955	525
Life-Cycle Cost	16,655	16,225
Mean Annual Failure Cost	50.2	13.7

Table 5.3 Expected Failure Costs of Shear Building Model with TADAS under Earthquake with Design Intensities

PGA(g)	Expected Failure Cost (× $1,000)		Cost Reduction Rate (%)
	W/O Damper	Optimal TADAS	
0.11	246	23	90.7
0.24	275	55	80.0
0.37	213	59	72.3
0.50	113	45	60.2
0.62	64	43	32.8
0.75	30	22	26.7
0.88	16	13	18.8
Total	955	260	72.8

Table 5.4 Mean Inter-Story Drift Ratios of Shear Building with Optimal TADAS

Story	PGA (g)		
	0.11	0.50	0.88
1	0.14	0.50	1.07
2	0.15	0.53	1.07
3	0.15	0.54	1.06
4	0.15	0.51	0.98
5	0.15	0.53	1.08
6	0.14	0.47	0.96
7	0.15	0.47	0.98
8	0.11	0.38	0.86
9	0.10	0.31	0.66

Table 5.5 Inter-Story Drift Ratios of Shear Building Model with TADAS (PGA=0.11g)

Story	Story Drift Ratio			Coefficient of Variation		
	W/O Damper	Optimal	% Change	W/O Damper	Optimal	% Change
1	0.19	0.14	23.5	0.27	0.24	12.0
2	0.19	0.15	22.9	0.29	0.21	27.6
3	0.19	0.15	22.2	0.31	0.17	44.0
4	0.17	0.15	10.7	0.31	0.16	49.5
5	0.18	0.15	19.3	0.28	0.22	23.6
6	0.16	0.14	10.6	0.29	0.23	20.2
7	0.17	0.15	11.4	0.26	0.29	-10.9
8	0.15	0.11	23.4	0.27	0.31	-13.4
9	0.10	0.10	-0.2	0.37	0.33	12.1

Table 5.6 Inter-Story Drift Ratios of Shear Building Model with TADAS (PGA=0.50g)

Story	Story Drift Ratio			Coefficient of Variation		
	W/O Damper	Optimal	% Change	W/O Damper	Optimal	% Change
1	0.80	0.50	37.8	0.37	0.47	-25.7
2	0.82	0.53	35.8	0.37	0.34	6.8
3	0.81	0.54	33.6	0.40	0.29	28.1
4	0.74	0.51	31.2	0.40	0.26	34.8
5	0.80	0.53	33.8	0.35	0.29	18.4
6	0.69	0.47	32.4	0.34	0.33	2.0
7	0.74	0.47	36.5	0.34	0.38	-12.3
8	0.72	0.38	46.7	0.34	0.38	-11.4
9	0.52	0.31	40.0	0.36	0.28	20.9

Table 5.7 Inter-Story Drift Ratios of Shear Building Model with TADAS (PGA=0.88g)

Story	Story Drift Ratio			Coefficient of Variation		
	W/O Damper	Optimal	% Change	W/O Damper	Optimal	% Change
1	1.39	1.07	22.7	0.25	0.20	18.6
2	1.45	1.07	26.1	0.23	0.20	12.3
3	1.49	1.06	28.8	0.23	0.22	4.7
4	1.36	0.98	28.2	0.23	0.21	8.7
5	1.45	1.08	25.7	0.27	0.12	54.2
6	1.24	0.96	22.1	0.30	0.07	77.7
7	1.32	0.98	25.6	0.27	0.06	77.3
8	1.20	0.86	28.5	0.24	0.12	51.9
9	0.90	0.66	26.8	0.20	0.20	-3.3

Figures 5

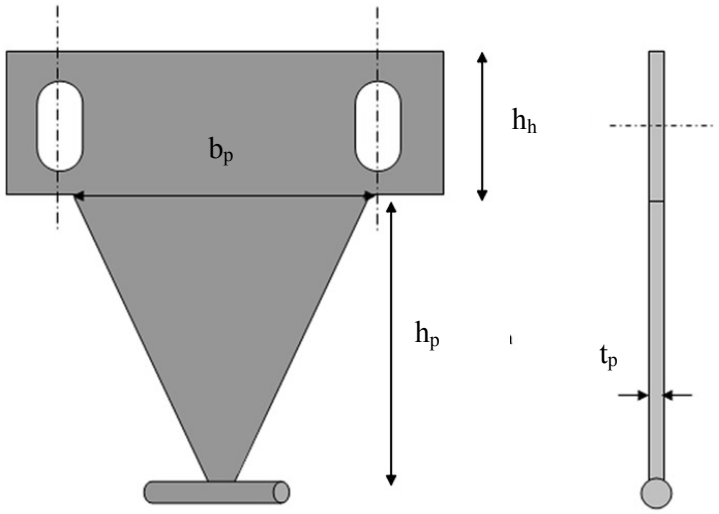

Figure 5.1(a) Triangular-plate Added Damping and Stiffness (TADAS) device

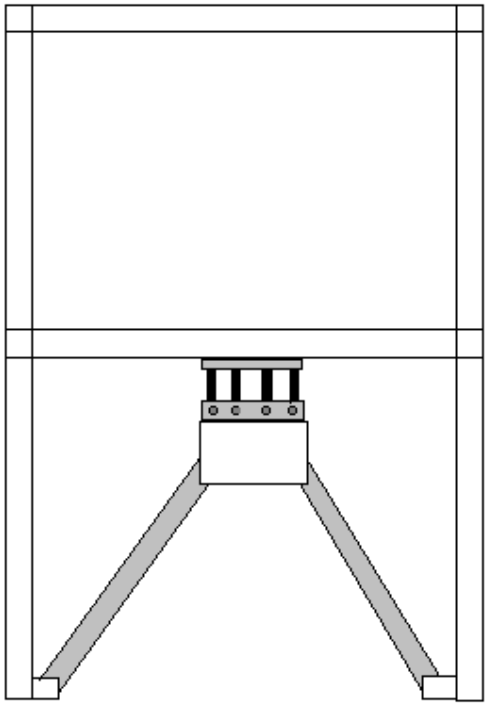

Figure 5.1(b) Typical Installation of TADAS Devices with Chevron Braces

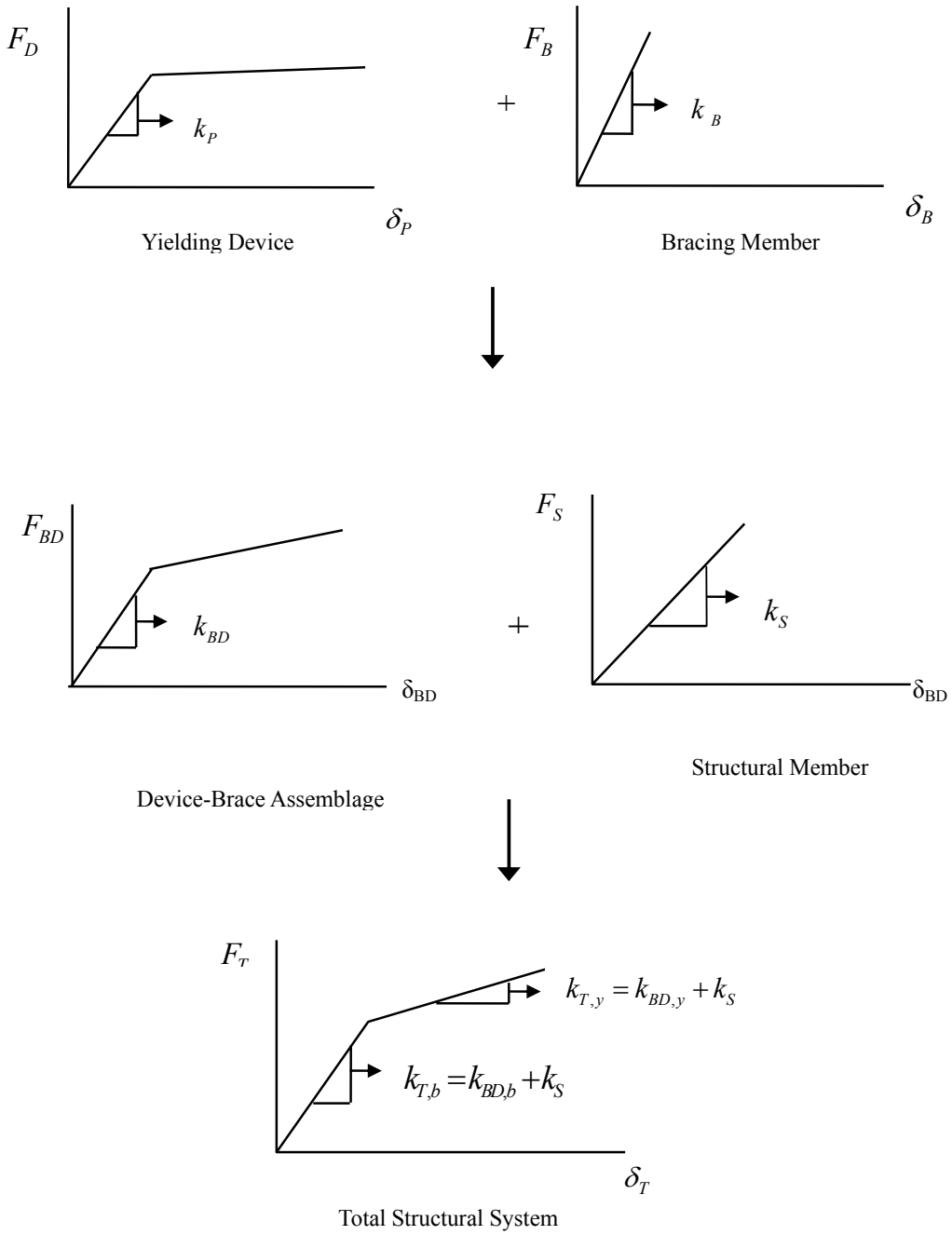

Figure 5.2 Force-Displacement Relationship of the Structural System with Yielding Metallic Device

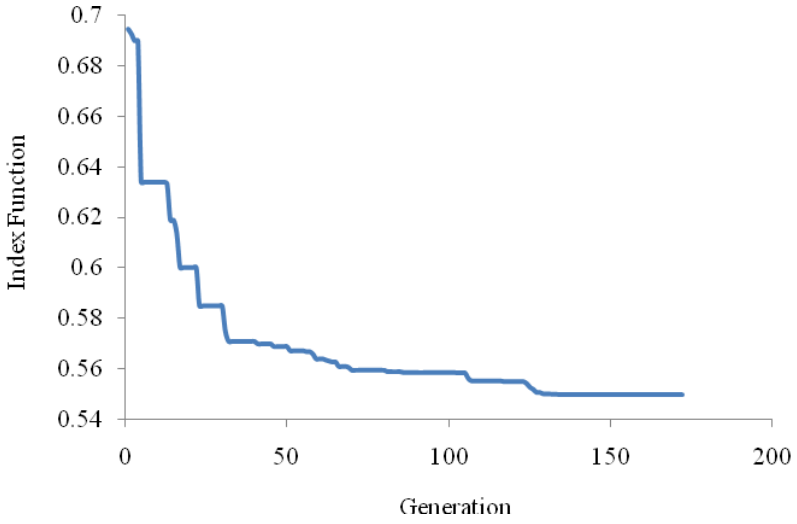

Figure 5.3 Convergence of GA for Shear Building Model with TADAS

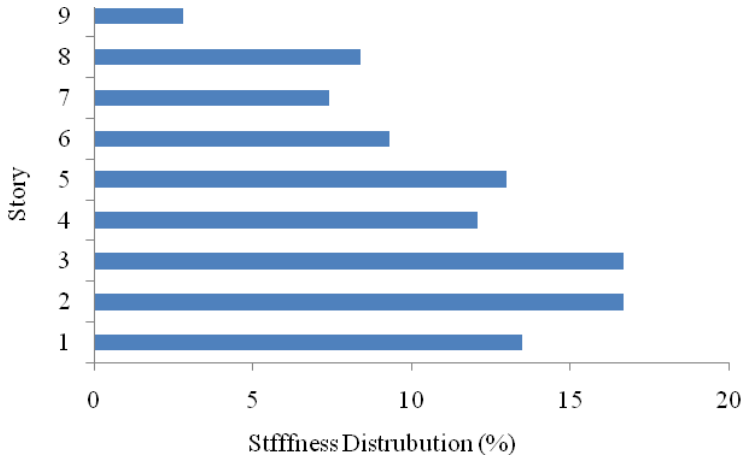

Figure 5.4 Comparison of the Percentage Distribution of Additional Stiffness

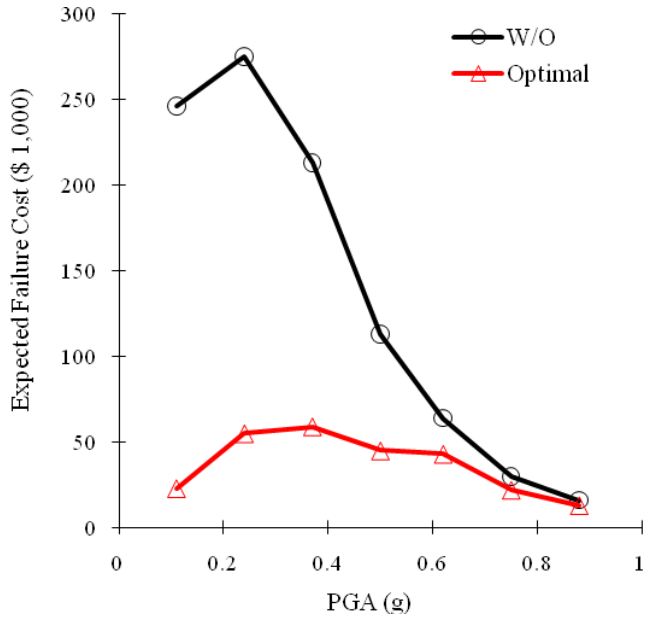

Figure 5.5 Expected Failure Costs of Shear Building Model with TADAS Under Various Earthquakes Intensities

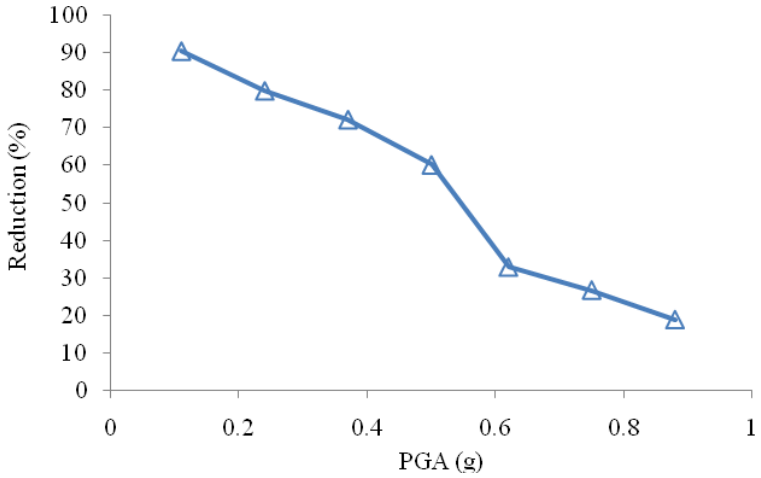

Figure 5.6 Percentage Failure Cost Reductions for Various Earthquake Intensities

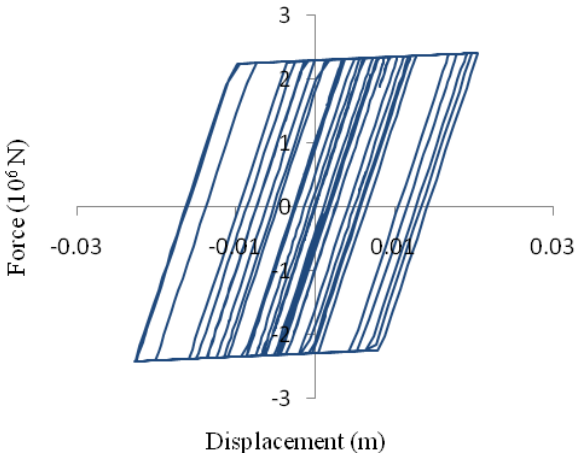

Figure 5.7(a) Hysteresis Loop of Device-Brace Assemblage at 1st Floor under the Design Earthquake with PGA=0.50g

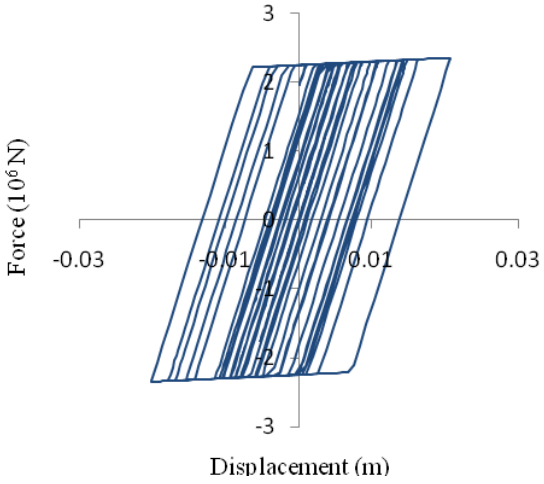

Figure 5.7(b) Hysteresis Loop of Device-Brace Assemblage at 5th Floor under the Design Earthquake with PGA=0.50g

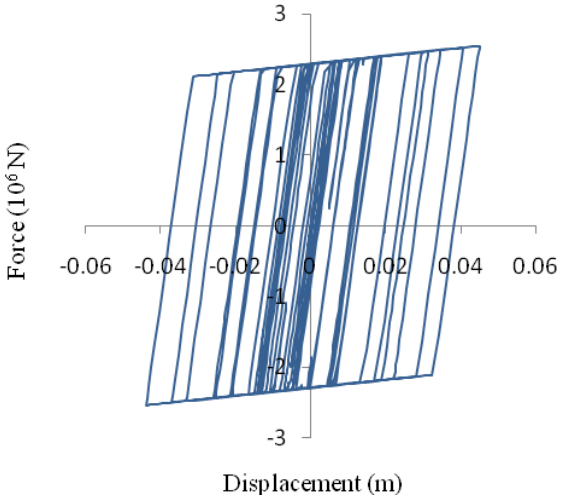

Figure 5.8(a) Hysteresis Loop of Device-Brace Assemblage at 1st Floor under the Design Earthquake with PGA=0.88g

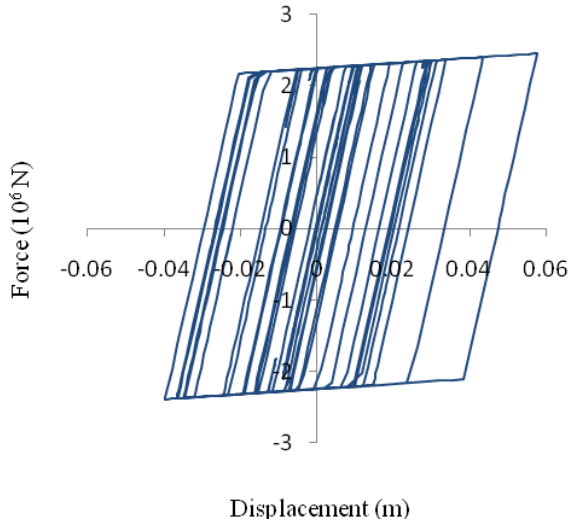

Figure 5.8(b) Hysteresis Loop of Device-Brace Assemblage at 5th Floor under the Design Earthquake with PGA=0.88g

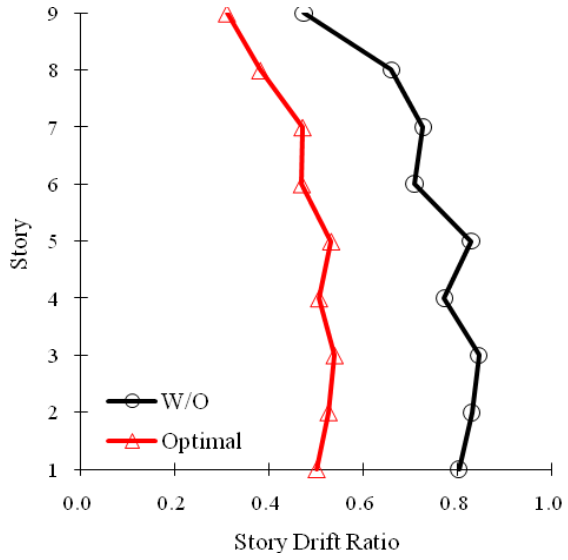

Figure 5.9 Comparison of the Mean Story Drift Ratios of the Original Building and the Building with TADAS Devices (Earthquake Intensity = 0.50g)

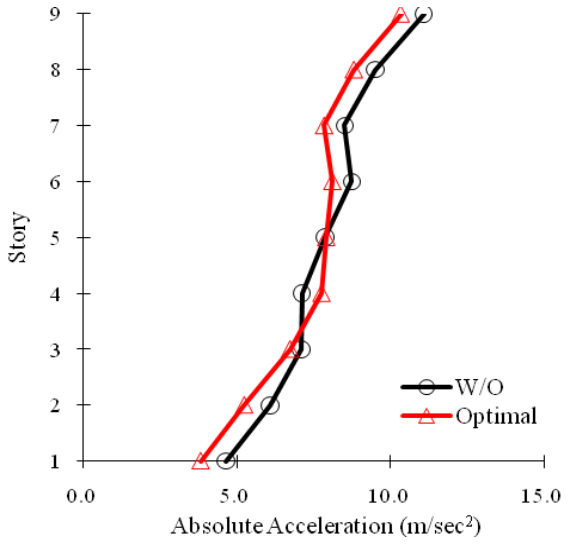

Figure 5.10 Comparison of the Average Floor Accelerations of the Original Building and the Building with TADAS Devices (Earthquake Intensity = 0.50g)

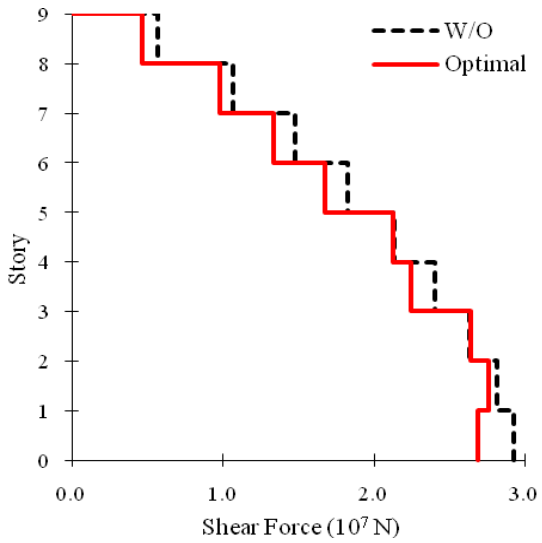

Figure 5.11 Comparison of the Mean Story Shear of the Original Building and the Building with TADAS Devices (Earthquake Intensity = 0.50g)

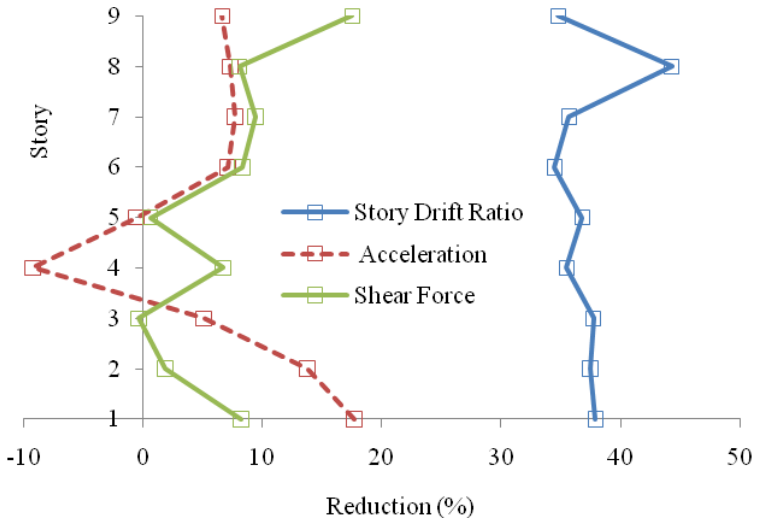

Figure 5.12 Percentage Response Reductions in story drifts, accelerations and story shears for Optimal TADAS Design

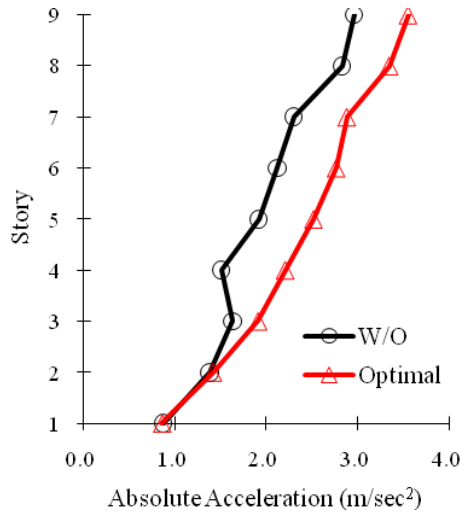

Figure 5.13 Comparison of the Average Floor Accelerations of the Original Building and the Building with TADAS Devices (Earthquake Intensity = 0.11g)

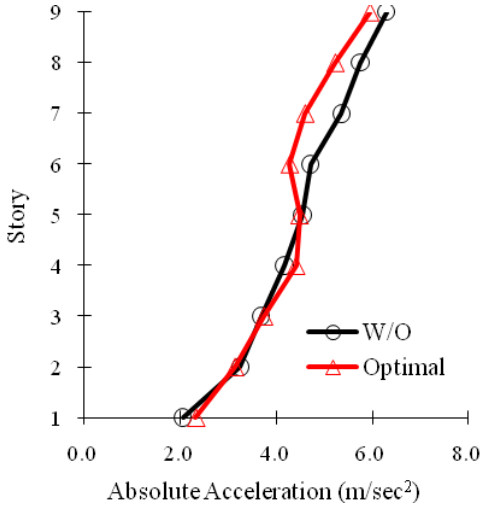

Figure 5.14 Comparison of the Mean Story Drift Ratios of the Original Building and the Building with TADAS Devices (Earthquake Intensity = 0.24g)

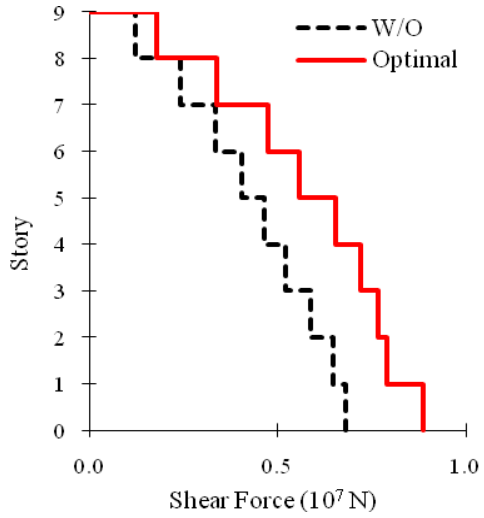

Figure 5.15 Comparison of the Mean Story Shear of the Original Building and the Building with TADAS Devices (Earthquake Intensity = 0.11g)

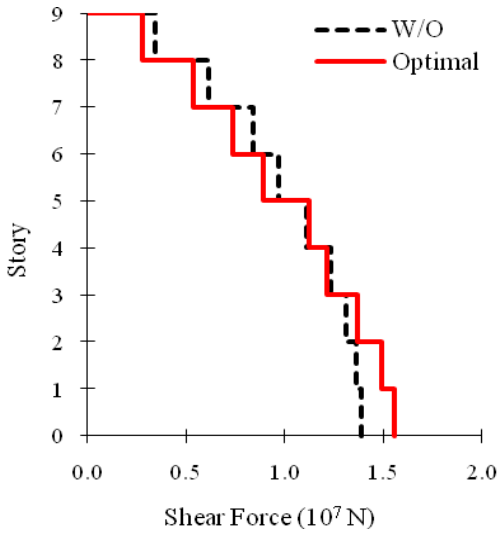

Figure 5.16 Comparison of the Mean Story Shear of the Original Building and the Building with TADAS Devices (Earthquake Intensity = 0.24g)

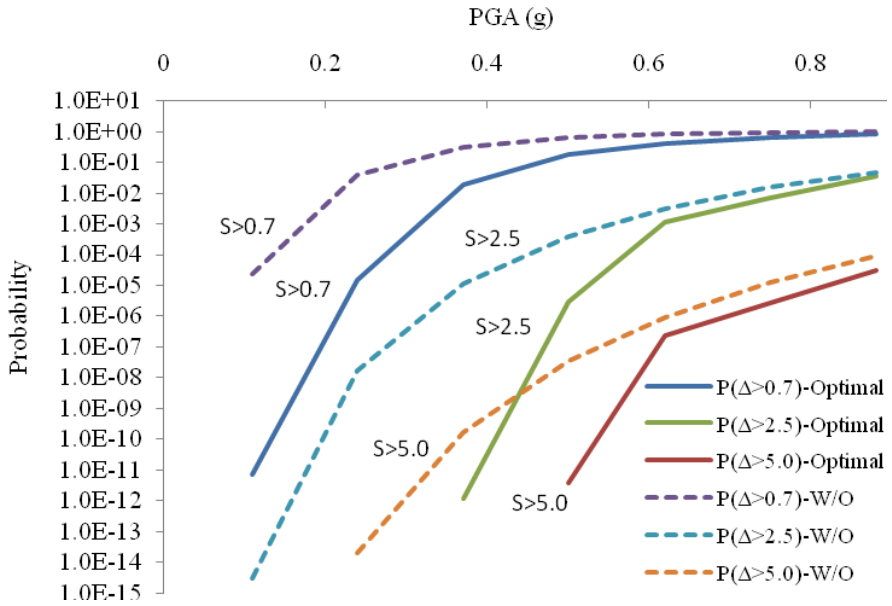

Figure 5.17 Fragility Curves with Maximum Story Drift Ratio of Shear Building Model

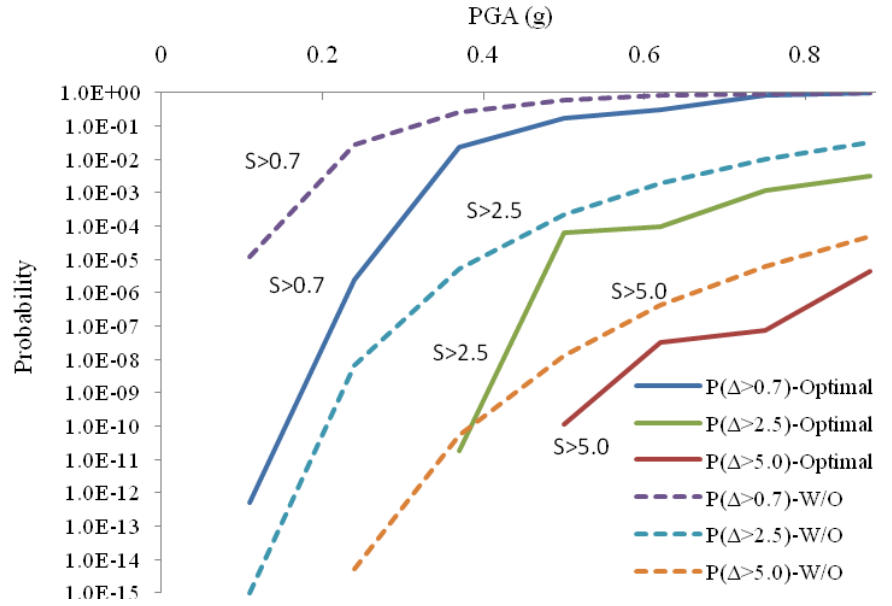

Figure 5.18 Fragility Curves with 1st Story Drift Ratio of Shear Building Model

CHAPTER 6

Damper Combination Designs

6.1 Introduction

Previous chapters presented the life-cycle cost–based optimization of structural systems installed with one of the three devices: fluid viscous dampers (FVD), solid visco-elastic dampers (SVD), or yielding metallic dampers (YMD). In this chapter we consider two combinations of two dampers to obtain cost-based optimal designs. The motivation is to check if any improvement is realized by considering dampers with two different characteristics and different cost structures. First we examine the combination of FVD and SVD and then we study the combination of FVD with YMD. The first combination we call, in short form, FVSV and the second combination we call FVMD. Again the objective in both combinations is to minimize the object cost which is the combination of the failure cost plus the cost of the damper including installation and maintenance. It is expected that combinations will improve the cost efficiency as these devices reduce the failure cost differently relative to their own cost.

In the following sections we briefly describe the optimization problem features that are special to these combinations. This is followed by the numerical studies for each combination where the results are obtained for different cost quantities and for the response reductions that are realized. These results are then compared with the similar results obtained for the original building model and also for the models enhanced with each device separately.

6.2 Designs with Combination of Fluid Viscous Damper (FVD) and Solid Visco-Elastic Damper (SVD): FVSV

As described in Chapters 3 and 4 earlier, FVD and SVD have some a similar as well as different characteristics. Their force characteristics were described by similar analytical model. In the model considered in earlier chapters, the FVD contributed only to the damping force which was directly proportional to the relative velocity and it did not add

any stiffness to the system. The SVD, on the other hand, contributed to both the damping as well as stiffness where the damping force was represented proportional to the relative velocity and the stiffness was proportional to the shear deformation. Thus a combination of the two installed in a structural system will modify both the stiffness and damping matrices of the system. The combined damping and stiffness matrices of the system can be described as follows:

$$\begin{aligned} \mathbf{C} &= \mathbf{C}_{\mathrm{S}} + \sum_{i=1}^{n_{\mathrm{F}}} \mathbf{r}_i \, n_i \, c_i^F \, \mathbf{r}_i^{\mathrm{T}} + \sum_{j=1}^{n_{\mathrm{S}}} \mathbf{r}_j \, n_j \, c_j^s \, \mathbf{r}_j^{\mathrm{T}} \\ \mathbf{K} &= \mathbf{K}_{\mathrm{S}} + \sum_{j=1}^{n_{\mathrm{S}}} \mathbf{r}_j \, n_j \, k_j^s \, \mathbf{r}_j^{\mathrm{T}} \end{aligned} \tag{6.1}$$

where $\mathbf{C}_{\mathrm{S}}$ and $\mathbf{K}_{\mathrm{S}}$ represent the generic damping matrix and generic stiffness matrix of a structure, respectively; $\mathbf{r}_i$ and $\mathbf{r}_j$ represent the influence vector of FVD and SVD to the main structure, respectively; c_i^F is the damping coefficient of the fluid viscous damper placed on the ith floor; c_j^s and k_j^s, respectively, are the damping coefficient and stiffness coefficient of the solid visco-elastic damper on the jth floor; n_i and n_j represent the total number of FVDs and SVDs at each floor.

Since the force-velocity and force-displacement relationships of these dampers are linear, the structural system installed with these devices can be assumed to be linear if the main structural elements do not yield. The response analysis of these systems can be carried out as explained in Chapters 3 and 4. We used the response spectrum approach for all lower intensities of ground motions for which the structural members remained within the elastic range. For the two higher intensities of ground motion, the modified response spectrum approach with deflection amplification factor C_d and response modification factor R from the 2009 NEHRP Provisions (2009) was used to calculate the story drift responses. The calculations of the limit state probabilities and the failure costs were based on the approach discussed in Chapters 3 and 4.

The optimization problem set up was similar to those discussed in Chapters 2 and 3, except that there were twice as many variables than before. These variables were the number of viscous dampers in different stories where they are placed. All seven FVDs

were considered, but one at a time, in combination with one SVD of visco-elastic layer of size 0.5 m^2 with a total area of 1.0m^2 in a damper. The cost optimization showed that the best performance was obtained again with the largest FVD, designated as Fv7. In the following, thus, the numerical results reported are for the combination of Fv7 with the SVD of the total visco-elastic area of 1.0m^2. The cost and mechanical properties of these two dampers that were used are shown in Table 6.1. For the SVD, the temperature effect was included according to the approach described in Chapter 4. The temperature range was divided into four equal intervals. The cost analysis was performed for the SVD properties for each interval, and the total cost was the sum of the cost for each temperature interval weighted by the probability that the temperature will be in that interval during the life of the structure. These temperature ranges and corresponding probabilities are given in Table 4.3. The constraint on the number of dampers that can be placed on a floor was the same; that is, the combined number of the FVD and SVD on a floor was limited to 18. The numerical results are obtained for both building models: shear building and the MRF building as considered before.

In the genetic algorithm, since there are twice as many variables in this case as in the cases of the FVDs or SVDs, the number of genes in a chromosome (or a design) were also twice as many. With this large size of the chromosome, a population of 600 different designs was selected to start the GA. These designs were rank ordered, paired for mating, mutated and elitists scheme applied as discussed in Chapter 2. Since there were more choices for the variables, the convergence took longer than when the FVD or SVD was individually considered. This convergence to final solution is shown in Figures 6.1 and 6.2, respectively, for the designs with the shear and MRF buildings.

Tables 6.2 and 6.3 give more details of the final designs for the shear building and the MRF building, respectively. The tables provide information about the distribution of damping and stiffness values in different stories. Comparing the results in the two tables with each other, we note that the shear building calls for a smaller amount of total damping than the more flexible MRF building. In addition, the MRF building is more flexible, and thus will deform more, so the optimization also requires significantly more stiffness contribution from the SVD than does the shear building. As a result, we note that the shear building just relies on using more FVDs for damping enhancement and much fewer SVDs as it has its own high stiffness compared to those needed by the MRF building. Figures 6.3 and 6.4 show the distributions of the two types of dampers in the two model buildings, clearly showing the much lower dependence of the shear building

on the SVDs. Table 6.4 shows the change in the modal properties of the two building because of the installation of the dampers. We note that there is much less change in the modal frequencies of the shear building compared to that of the MRF building. The fundamental frequency of the shear building is increased by about 1% whereas that of the MRF building is increased by about 11%. The modal damping ratios have also significantly increased for both buildings, with some of the modes becoming even over-damped in both cases. Thus, since the MRF building was deficient in stiffness (from the standpoint of failure cost), the optimization algorithm focused on increasing the stiffness and damping values in a balanced way to reduce the failure cost as well as the cost of the devices to reduce the object cost. In the case of the shear building, the stiffness was not an issue, and thus the optimization algorithm focused on adding more damping to reduce its failure costs. Tables 6.5 and 6.6 show the final cost results obtained for the two buildings, and compare them with the similar costs for the original building. We note that the failure costs are much more drastically reduced in the MRF building, primarily because this cost for the original building was very high, primarily attributable to its relatively large flexibility. However, to decrease this failure cost also required a relatively large damper cost investment compared to the shear building. Another comparison of interest is revealed here when the cost of dampers and corresponding level of reduction in the life-cycle cost are compared for the two buildings in these two tables. We observe that a small damper investment compared to the initial cost in a flexible building can improve its performance (expressed in terms of reduction in the life cycle cost) more than the performance of a stiffer building. This will be shown more explicitly later.

The results in Tables 6.7 and 6.8 show the effectiveness of the two optimal designs over the different ranges of the excitation intensities. The reductions in the costs are very high for the low intensity but more frequent excitations, as they contribute the most to the economic loss. In this respect, the optimization algorithm aptly responds to the main objective of the performance-based design concept, that is, to reduce the unusual high losses observed in earthquakes that were below the design intensity values.

Figures 6.5 and 6.6 show the percent reduction in the total limit state costs at different intensities for three different designs. Figure 6.5 is for the shear building and Figure 6.6 for the MRF building. For the shear building the combined damper design is between the two other cases, but it is close to the FVD curve, primarily because the contribution of the SVD in the shear building was almost nominal. See Figure 6.3. For the MRF

building, the design with the combined dampers provides a higher percent reduction, as they provide enhanced damping combined with enhancement of stiffness which is also needed by the more flexible MRF design. Figure 6.7 compares the percent reductions in the failure costs over different intensities of excitation for the two models, indicating that damping systems are relatively more effective in the flexible MRF building as they bring a larger level of reduction compared to that in the shear building.

Next we compare the cost efficiencies of the different designs, that is the designs made with individual dampers and with their combinations. Table 6.9 is created to show this for the two models. The upper part of Table 6.9 is for the shear building, whereas the lower part is for the MRF building. The values in columns 2, 3 and 4 show the percent reductions in the various cost values for the two buildings for the three designs: (a) design only with FVD (column 2), (b) design with only SVD (column 3) and (c) combination of FVD and SVD (column 4). We note that the level of reduction in the cost values for the combination are somewhere in between the values for the individual cases for the shear building. However, for the MRF building, the combined design is somewhat better than the two other designs. As alluded to earlier, it is because the MRF building, being more flexible and thus in need of stiffening, makes use of the stiffness enhancement characteristics of the SVD more effectively than the shear building which is already stiff. This also shows up when we compare the cost efficiency of the designs by the cost efficiency ratios shown in the next three columns. The cost efficiency ratio C_{eff} is defined as:

$$C_{\text{eff}} = \frac{\Delta C}{C^{\text{d}}} = \frac{\left(C_{\text{o}} - C_{\text{b}}\right)}{C^{\text{d}}} \tag{6.2}$$

where C_{o} and C_{b}, respectively, represent the expected cost (failure, object, or life-cycle) of the original building and the building with optimally configured dampers. C^{d} represents the damper cost of a given design. We note that the cost efficiency of the combined design, shown by the numbers in the last column of the table, is slightly higher than the numbers shown for the other designs. Thus the combination makes better use of the damper characteristics cost-wise. In the case shown here, the difference in these numbers is not very large, but it is likely to be larger if the cost differences of the two devices were higher. We also note, by comparing the numbers shown in the upper part with the corresponding numbers in the lower parts, that the cost efficiencies are in general higher for the MRF building. In the shear building, the number 3.5 in the

last column of the first row implies that these dampers are 3.5 times as effective in reducing the failure cost. The same number for the MRF building indicates that these dampers reduce the failure cost by about 7.6 times their own cost.

In Figures 6.8 and 6.9 we plot the distribution of the expected failure cost for different input intensities for three different designs. Figure 6.8 is for the shear building and figure 6.9 is for the MRF building. The comparison of the failure cost for the shear building for different damper device designs shows that the combined design costs are mostly between the costs associated with the other designs. For the MRF building, there is not a clear trend for all intensities. However, in both models and for all designs the maximum contribution to the total failure cost comes from the medium intensity earthquakes, in this case somewhere below the design intensity level (0.56g).

Figures 6.10 and 6.11 show the plot of the failure cost efficiencies for three different designs at different input intensities for the two building models. First we note that all designs are more efficient in reducing the lower intensity costs which contribute more to the failure cost. Second, we observe that, although the difference is not much, the combined design envelopes the other two designs. This was also observed for the total failure costs as well as for the object cost when the results in Table 6.9 were discussed.

In Figures 6.12 and 6.13 we compare the fragility curves for the limit state of immediate occupancy for the three designs for the two building models. Of course, all three designs improve the fragility. The fragility curve for the combined damper design is between the fragility curves for the other two designs for the shear building, whereas for the MRF building the combined design provides the most improvement in terms of reduced fragility. This observation is consistent with observations made earlier that the combined design provides a higher reduction in the response and also in the failure cost for the MRF building compared to the other two designs.

6.3 Designs with Combination of Fluid Viscous Damper (FVD) and Yielding Metallic Devices (YMD): FVMD

In this section we present the study on the combination of two very different devices. Out of all 7 choices for FVD we adopted Fv7 as it was found to be the most efficient in previous studies. This FVD is now combined with the TADAS devices, the details

about which were presented in Chapter 5. The same configuration as in Chapter 5 is also used here. The unit cost details and other mechanical properties of these devices needed for this analysis are given in Table 6.10. The variables for the TADAS devices are the number of plates in different stories, and thickness of the plate. In addition to these variables, there is a variable for the FVD, the number of devices in different stories. So in this case the chromosome will have more genes than in the previous problem. A population size of 600 designs is considered in the GA. The FVD only provides damping, whereas the YMD provides a large increase in the stiffness as well as energy dissipation for the higher levels of motion intensities. Thus the damping matrix of the system will consist of the damping matrix defined by Eq. (3.10) in Chapter 3. The stiffness matrix of the system is also changed according to the procedure described in Chapter 5, considering the stiffness of the plate, brace and the story. The analysis of this system will necessary be done using the time history analysis because of yielding of the YMD. Only the shear beam model is considered for this study as was done in Chapter 5. Thus, having defined the complete stiffness and damping matrices for the system, the Newmark-β time-stepping method described in Chapter 5 can be applied.

Figure 6.14 shows the convergence of the GA to the optimal designs. It took about 190 iterations. Thus the time required for these calculations was much larger than for the other cases. Table 6.11 shows the details of the final design, showing the total damping and stiffness added to the system and its distribution in different stories. The distribution shows that the design is more focused on using the viscous damper and less on the TADAS as only a few TADAS plates are needed in the upper stories. This is because this shear beam model is already stiff but lacks energy dissipation in damping. The addition of a few TADAS plates in the higher stories tries to re-adjust stiffness at higher levels to decrease the failure cost.

Table 6.12 shows the cost analysis results. Again the failure costs are significantly reduced. In Table 6.13 we show the failure costs for different hazard intensities, and their percent reductions. Figure 6.15 shows the percent reduction in the total limit state costs at various input intensities. This, when multiplied by the probability of the response being in the limit state, gives the reductions in the failure costs. We observe that the percent reductions in the limit state costs decrease with the intensity, meaning thereby that the relative reductions in the inter-story drifts at the higher intensities are not as much as at the lower stories. It is again because the algorithm focuses more in reducing the lower but more frequent intensities, as they contribute the most to the

failure costs. Figure 6.16 shows the failure cost values and Figure 6.17 shows the percent reductions in them at different input motion intensities. As we observed before, in all three optimum design cases the major share to the total failure cost comes from the medium intensity ground motions which are slightly below the design intensity level. Another observation we make from this figure is that the performance, measured in terms of the limit state cost reduction, failure cost and failure cost reduction, of the design with combined devices lies between those of the individual devices. In fact the performance of the combined design is closer to that of the FVD design as the combined design has a major contribution for the FVD as indicated by Table 6.11.

Table 6.14 compares the cost efficiencies of the combined design with those of the individual designs. This table is similar to Table 6.9 discussed earlier for the combined FVSV design. The columns 2, 3 and 4 show the percent reductions in the failure costs by the three designs. In this we observe that the combined design is just about the same as the FVD design, with just a point better. This, however, shows up relatively more in the cost efficiency ratio which are shown in columns 5, 6 and 7. The numbers in the last column pertaining to the design with combined devices are slightly higher than those for the other two designs. This observation is similar to the one made earlier for the FVSV combination, that the GA being more focused on the cost minimization tries to get the best performance out of the two alternatives when they are combined. The differences in these cost efficiency numbers of the combined design and the FVD design are not too large primarily because the system, being more rigid, did not depend more on the TADAS to provide stiffness but relied more on reducing the failure cost through viscous dampers. Figure 6.18 plots the cost efficiency values for the three designs as a function of the hazard intensity. We again observe that the combined design envelops the other two designs especially for the lower values where the failure costs are reduced the most. Figure 6.19 shows the fragility function plotted for the limit state of immediate occupancy for the three designs and the original buildings. The combined design is in between the other two designs. That is, it improves the fragility better than the TADAS design but not as well as the FVD design. This was also observed in the cost reductions and reduction in the response values where the response and cost reduction capability of the combined design were between those of the other two designs.

6.4 Chapter Summary

This chapter has presented a study examining the effect of using two or more devices on the system performance in terms of its capability in reducing the response and the failure and object costs. Two different combinations have been considered. The first combination consisted of the fluid viscous dampers and solid visco-elastic dampers, and the second one consisted of the fluid viscous damper and yielding metallic devices. For the first combinations both the shear building and MRF building were considered in the study, whereas for the second combination only the shear beam model was considered primarily for the convenience of nonlinear analysis by time stepping method.

It was observed that the GA took longer to converge in each case as there were more design variables compared to the case of a single device design. The response and cost reduction performance of the combined design were between the performances of the individual design for all cases and all systems. However, the cost efficiencies, which mean the cost per unit cost of the damper, was always greater for the combined design. It was because the focus of the optimization was to reduce the object cost and not directly the response values. The response values, especially the inter-story drifts, were, however, needed to be reduced to reduce the failure costs. But since the objective was to reduce the object cost which also contained the cost of the device, the GA also focused on reducing the device cost, and thus the higher cost efficiency.

While comparing the results for the shear building and MRF building designs, we observed that the cost efficiencies were much better for the MRF design. It was again due to the fact that the shear building being more rigid did not require the help from the SVD in enhancing its stiffness but relied more on the FVD, whereas the flexible MRF building could use both the enhancement in the damping as well as stiffness to reduce the failure cost, and thus this design was also influenced relatively more by the SVD. This offered the GA an opportunity to lower the device cost more in MRF building than the shear building and thus enhanced cost the efficiency.

Tables 6

Table 6.1 Dampers Used for the Combination Study

Damper Type	Unit Damper Cost ($)	Unit Bracing Cost ($)	Total Damping Coefficient (N-sec/m)
Fluid Viscous (Fv7)	10,800	430/m	9.8×10^6
Solid Visco-Elastic (Area=2×0.5 m^2)	1,440	85/m	8.9×10^5 (Shear) 11.3×10^5 (MRF)

Table 6.2 Optimal Distribution of Fluid Viscous and Solid Visco-Elastic Dampers for Shear Building Model

Story	Total Added Damping ($\times10^7$ N-sec/m)	Fluid Viscous Dampers		Solid Visco-Elastic Dampers		Total Added Stiffness ($\times10^7$ N/m)
		No. of Dampers	% of Total Damping	No. of Dampers	% of Total Damping	
1	4.90	5	28.8	0	0.0	0.00
2	3.92	4	23.0	0	0.0	0.00
3	2.94	3	17.3	0	0.0	0.00
4	2.94	3	17.3	0	0.0	0.00
5	2.05	2	11.5	1	0.5	0.72
6	0.00	0	0.0	0	0.0	0.00
7	0.26	0	0.0	3	1.5	2.16
8	0.00	0	0.0	0	0.0	0.00
9	0.00	0	0.0	0	0.0	0.00
Total	17.01	17	98.0	4	2.0	2.88

Table 6.3 Optimal Distribution of Fluid Viscous and Solid Visco-Elastic Dampers for MRF Building Model

Story	Total Added Damping ($\times 10^7$ N-sec/m)	Fluid Viscous Dampers		Solid Visco-Elastic Dampers		Total Added Stiffness ($\times 10^7$N/m)
		No. of Dampers	% of Total damping	No. of Dampers	% of Total Damping	
1	1.24	1	4.9	2	1.3	1.44
2	4.58	4	19.8	5	3.3	3.59
3	3.47	3	14.8	4	2.7	2.88
4	4.13	3	14.8	9	6.0	6.47
5	3.41	2	9.9	11	7.3	7.91
6	2.17	1	4.9	9	6.0	6.47
7	0.66	0	0.0	5	3.3	3.59
8	0.13	0	0.0	1	0.7	0.72
9	0.00	0	0.0	0	0.0	0.00
Total	19.80	14	69.3	46	30.7	33.06

Table 6.4 Modal Properties of Model Buildings with Optimal Design of FVSVs

Story	Shear Building Model			MRF Building Model		
	Frequency (Hz)		Damping Ratio	Frequency (Hz)		Damping Ratio
	Original	With FVSV		Original	With FVSV	
1	0.96	0.97	0.17	0.64	0.71	0.28
2	2.51	2.64	0.20	1.77	2.08	0.26
3	4.01	*3.68	1.01	2.95	*2.26	1.02
4	5.43	4.66	0.32	4.27	*4.46	1.00
5	6.64	5.82	0.29	5.72	4.48	0.43
6	7.77	6.67	0.55	7.37	6.52	0.48
7	8.99	7.56	0.16	9.09	7.62	0.30
8	10.01	7.65	0.98	10.90	*12.48	1.09
9	11.09	*26.62	1.04	12.80	*38.34	1.02

Note: Over-damped case indentified by *

Table 6.5 Comparison of Different Costs for the Original Building and Optimally Damped Building Using a Combination of Fluid Viscous and Solid Visco-Elastic Dampers: Shear Building Model

Costs (× $1,000)	Seismic Design Approaches	
	W/O Damper	Optimal
Initial Cost	15,700	15,700
Damper Cost	0	229
Failure Cost	955	155
Object Cost	955	384
Life-Cycle Cost	16,655	16,097
Mean Annual Failure Cost	50.0	8.2

Table 6.6 Comparison of Different Costs for the Original Building and Optimally Damped Building Using a Combination of Fluid Viscous and Solid Visco-Elastic Dampers: MRF Building Model

Costs (× $1,000)	Seismic Design Approaches	
	W/O Damper	Optimal
Initial Cost	12,900	12,900
Damper Cost	0	269
Failure Cost	2,255	215
Object Cost	2,255	484
Life-Cycle Cost	15,155	13,384
Mean Annual Failure Cost	115.0	11.0

Table 6.7 Expected Failure Costs and Cost Reductions at Different Ground Motion Intensities Due to Optimally Damped Combination of Fluid Viscous and Solid Visco-Elastic Dampers: Shear Building Model

PGA(g)	Expected Failure Cost (× $1,000)		Cost Reduction (%)
	W/O Damper	Optimally Damped FVSV	
0.11	246	0	100.0
0.24	275	41	85.0
0.37	213	36	82.9
0.50	113	37	67.0
0.62	64	24	62.2
0.75	30	10	68.3
0.88	16	6	59.7
Total	955	155	83.8

Table 6.8 Expected Failure Costs and Cost Reductions at Different Ground Motion Intensities Due to Optimally Damped Combination of Fluid Viscous and Solid Visco-Elastic Dampers: MRF Building

PGA(g)	Expected Failure Cost (× $1,000)		Cost Reduction (%)
	W/O Damper	Optimally Damped FVSV	
0.11	813	0	100.0
0.24	648	58	91.0
0.37	403	51	87.2
0.50	198	50	74.9
0.62	110	33	70.3
0.75	53	13	74.8
0.88	29	9	67.9
Total	2,255	215	90.5

Table 6.9 Comparison of Percentage Cost Reductions for Different Optimal Design Configurations and Their Cost Efficiency Ratios

Item	Percent Reductions			Cost Efficiency Ratios		
	FVD (2)	SVD (3)	FVSV (4)	FVD (5)	SVD (6)	FVSV (7)
Shear Building Model						
Failure Cost	85.2	75.6	83.8	3.3	2.8	3.5
Object Cost	59.3	48.3	58.4	2.3	1.8	2.5
Life-Cycle Cost	3.3	2.8	3.4	2.3	1.8	2.4
MRF Building Model						
Failure Cost	88.7	88.2	90.5	7.3	6.6	7.6
Object Cost	76.6	74.8	78.5	6.3	5.6	6.6
Life-Cycle Cost	11.4	11.1	11.7	6.3	5.6	6.6

Table 6.10 Characteristics of Fluid Viscous Dampers and TADAS Devices Used for Optimal Combination

Damper Type	Unit Device Cost ($)	Total Bracing Cost Bracing Cost ($)	Total Damping Coefficient or Total Stiffness
Fluid Viscous(Fv7)	10,800	430/m	9.8×10^{6} N-sec/m
TADAS*	2,760	308/m	1.52×10^{7} N/m

*plate width = 0.3 m ; Plate length= 0.4 m; Ratio of device to brace stiffness = 2; Number of plates per base = 5

Table 6.11 Optimal Distribution of Fluid Viscous Dampers and Metallic TADAS Devices for Shear Building Model

Story	Total Added Damping ($\times10^{7}$ N-sec/m)	Fluid Viscous Dampers		TADAS Devices		Total Added Stiffness ($\times10^{7}$ N/m)
		No.	% of Total damping	No. of Plates.	% of Total Stiffness	
1	4.90	5	31.3	0	0.0	0.00
2	3.92	4	25.0	0	0.0	0.00
3	2.94	3	18.8	0	0.0	0.00
4	1.96	3	12.5	0	0.0	0.00
5	1.96	2	12.5	6	42.9	0.72
6	0.00	1	0.0	4	28.6	0.00
7	0.00	0	0.0	4	28.6	2.16
8	0.00	0	0.0	0	0.0	0.00
9	0.00	0	0.0	0	0.0	0.00
Total	15.68	18	100.0	14	100.0	2.88

Table 6.12 Comparison of Different Costs for the Original Building and Optimally Configured Combinations of Fluid Viscous and TADAS Devices: Shear Building Model

Costs (× $1,000)	Seismic Design Approaches	
	W/O Damper	Optimally Configured System
Initial Cost	15,700	15,700
Damper Cost	0	221
Failure Cost	955	167
Object Cost	955	388
Life-Cycle Cost	16,655	16,088
Mean Annual Failure Cost	50.2	8.8

Table 6.13 Expected Failure Costs and Cost Reductions at Different Ground Motion Intensities Due to Optimally Configures Combination of Fluid Viscous and Metallic TADAS Devices: Shear Building Model

PGA(g)	Expected Failure Cost (× $1,000)		Cost Reduction (%)
	W/O Damper	Optimally Configured System	
0.11	246	4	98.4
0.24	275	33	88.0
0.37	213	44	79.3
0.50	113	33	70.8
0.62	64	24	62.5
0.75	30	20	33.3
0.88	16	10	37.5
Total	955	167	82.5

Table 6.14 Comparison of Percentage Reductions for Different Optimal Design Configurations and Their Cost Efficiency Ratios for Shear Buildings

Item	Percent Reductions			Cost Efficiency Ratios		
	FVD	TADAS	FVMD	FVD	TADAS	FVMD
	(2)	(3)	(4)	(5)	(6)	(7)
Failure Cost	85.2	72.8	82.5	3.3	2.6	3.6
Object Cost	59.3	40.0	59.4	2.3	1.6	2.6
Life-Cycle Cost	3.3	2.6	3.4	2.3	1.6	2.6

Figures 6

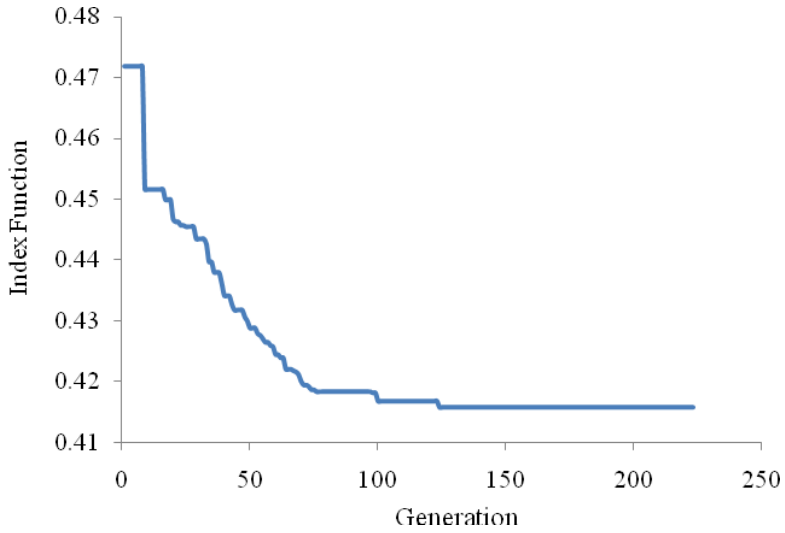

Figure 6.1 Convergence of Genetic Algorithm to Optimal Solution with Combinations of Fluid Dampers and Solid Visco-Elastic Dampers on Shear Building Model

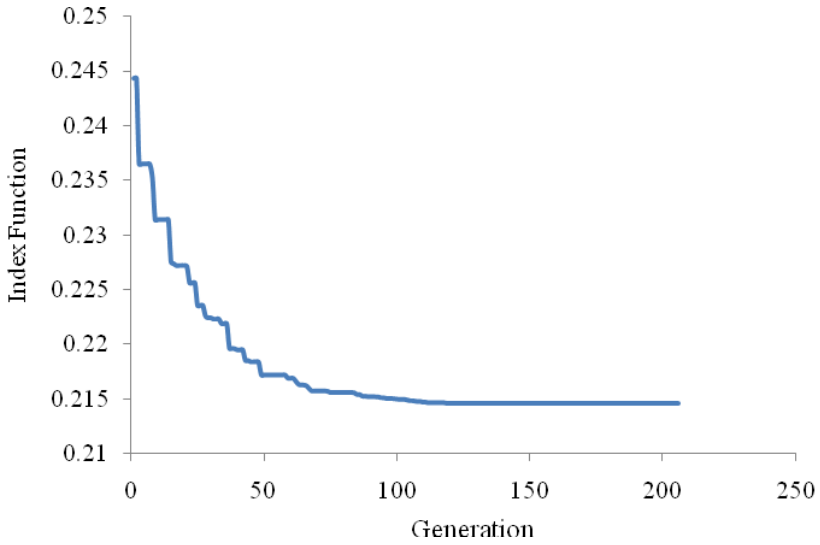

Figure 6.2 Convergence of Genetic Algorithm to Optimal Solution with Combinations of Fluid Dampers and Solid Visco-Elastic Dampers on MRF Building Model

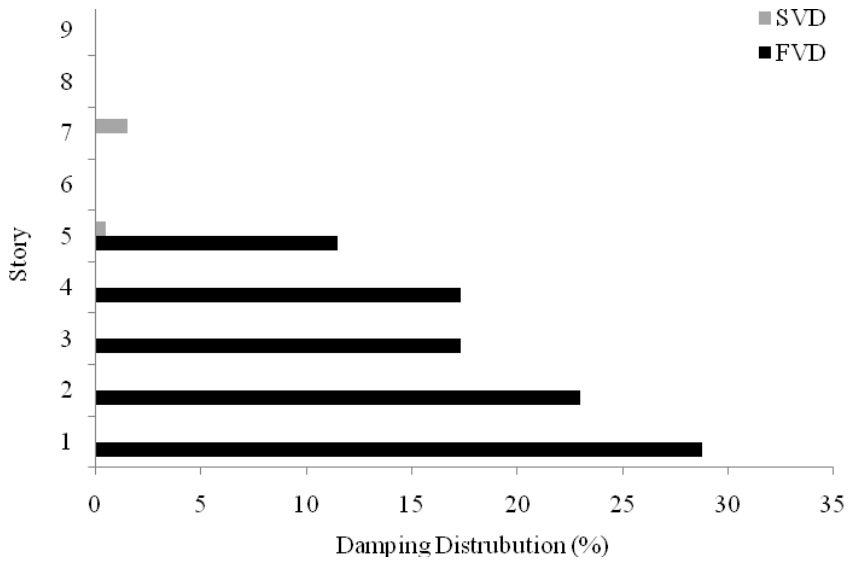

Figure 6.3 Percentage Distributions of Optimal Fluid and Solid Visco-Elastic Damping Coefficients in Shear Building Model

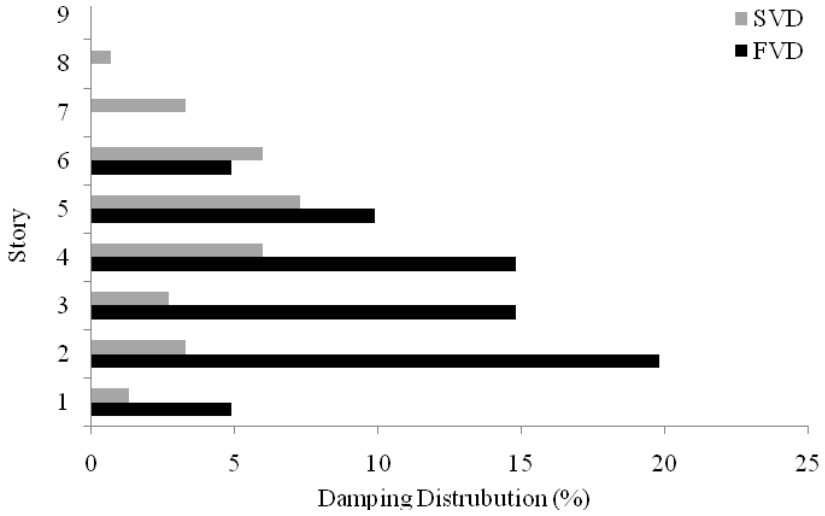

Figure 6.4 Percentage Distributions of Optimal Fluid and Solid Visco-Elastic Damping Coefficients in MRF Building Model

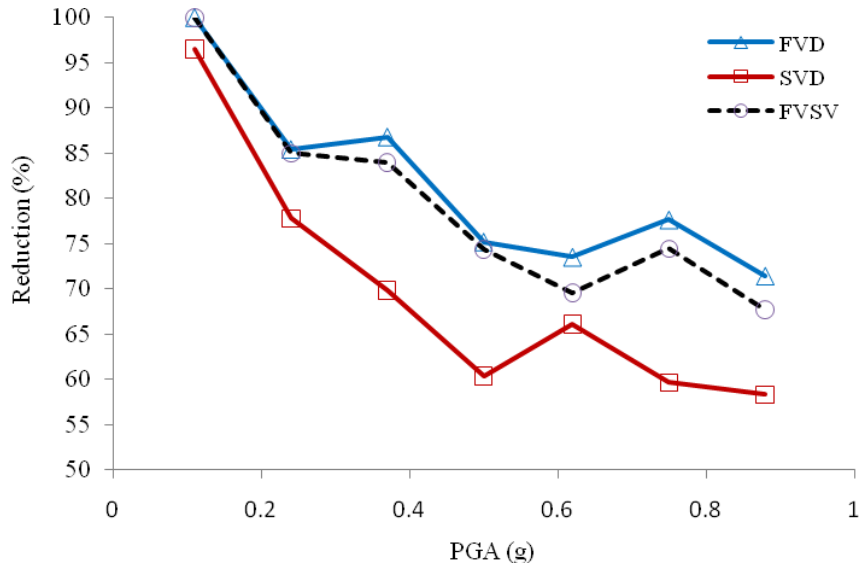

Figure 6.5 Percent Reduction in Total Limit State Cost at Different Earthquake Intensities due to Different Optimal Designs: Shear Building Model

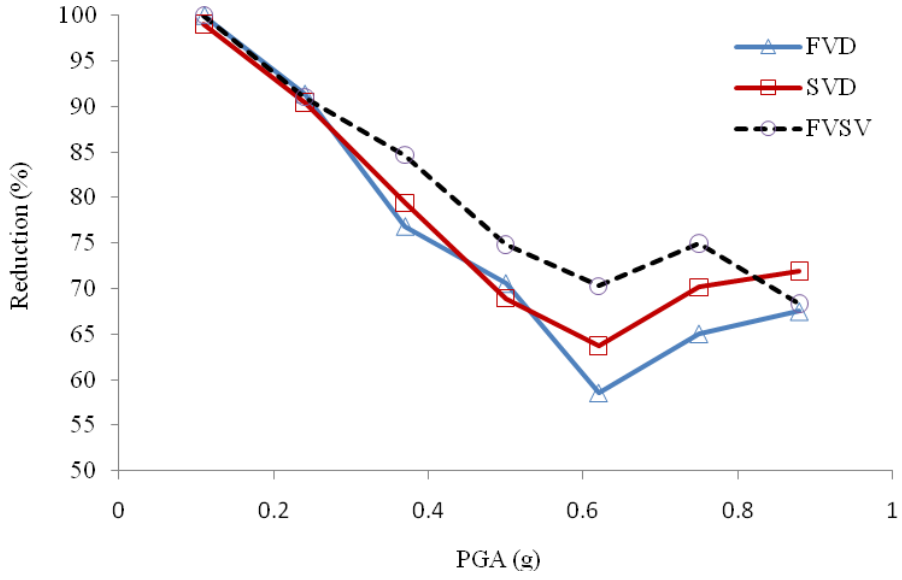

Figure 6.6 Percent Reduction in Total Limit State Costs at Different Earthquake Intensities due to Different Optimal Designs: MRF Building Model

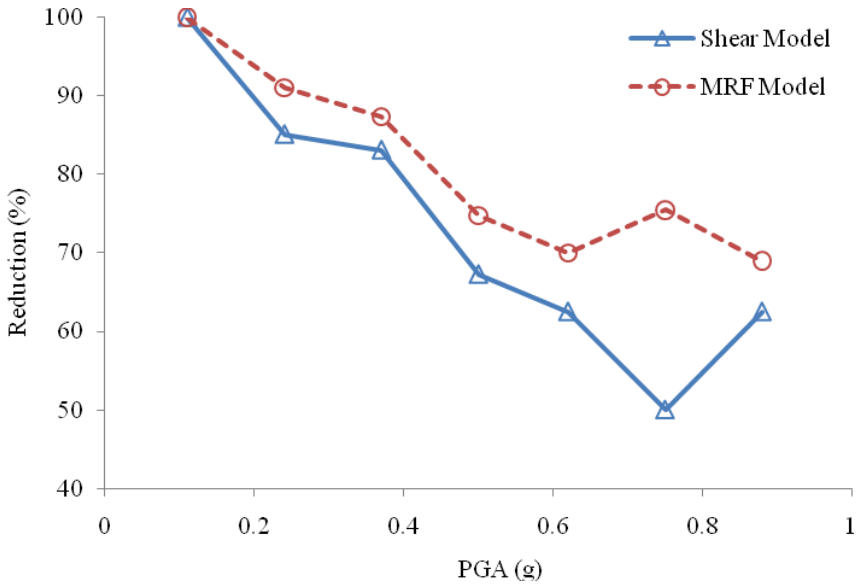

Figure 6.7 Percentage Reductions in the Failure Cost for Various Intensities of Ground Motions in Shear and MRF Buildings Due to Optimal Installation of FVSV

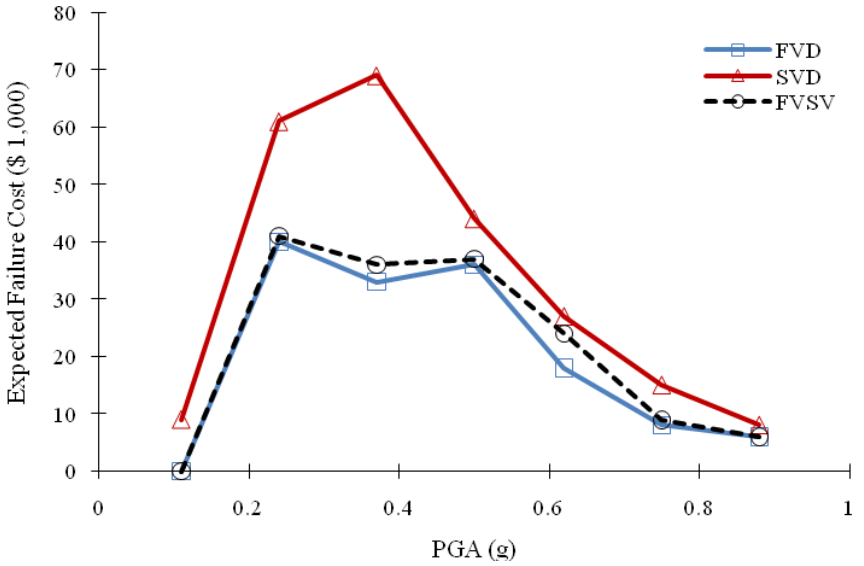

Figure 6.8 Comparison of Expected Failure Cost for Different Optimal Designs with Fluid Dampers only, Solid Visco-Elastic Damper only and FVSV for Various Earthquake Intensities: Shear Building Model

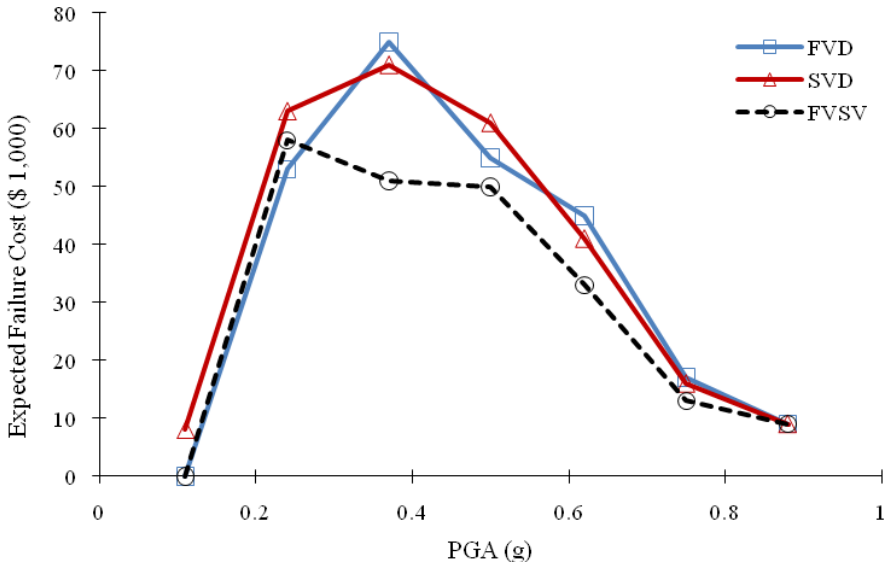

Figure 6.9 Comparison of Expected Failure Cost for Different Optimal Designs with Fluid Dampers Only, Solid Visco-Elastic Damper Only and FVSV for Various Earthquake Intensities: MRF Building Model

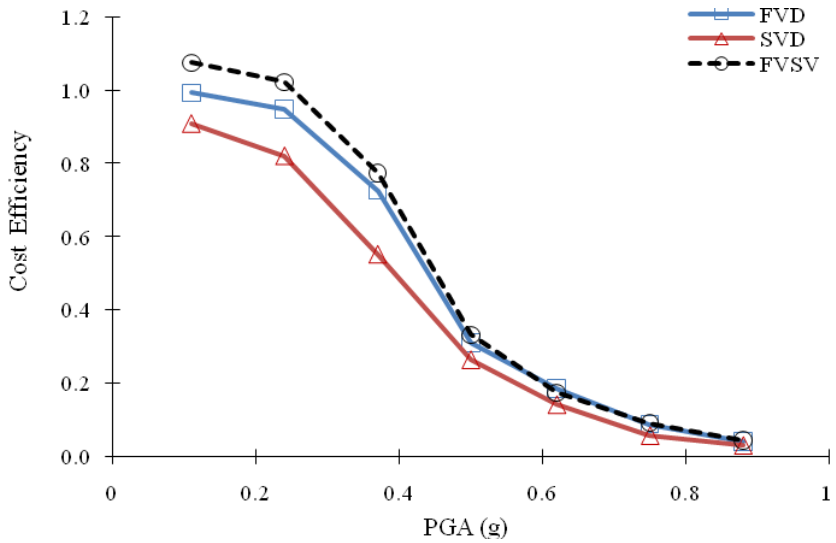

Figure 6.10 Comparison of Failure Cost Efficiency Ratios of Optimal Designs with Different Configurations of Dampers on Shear Building Model

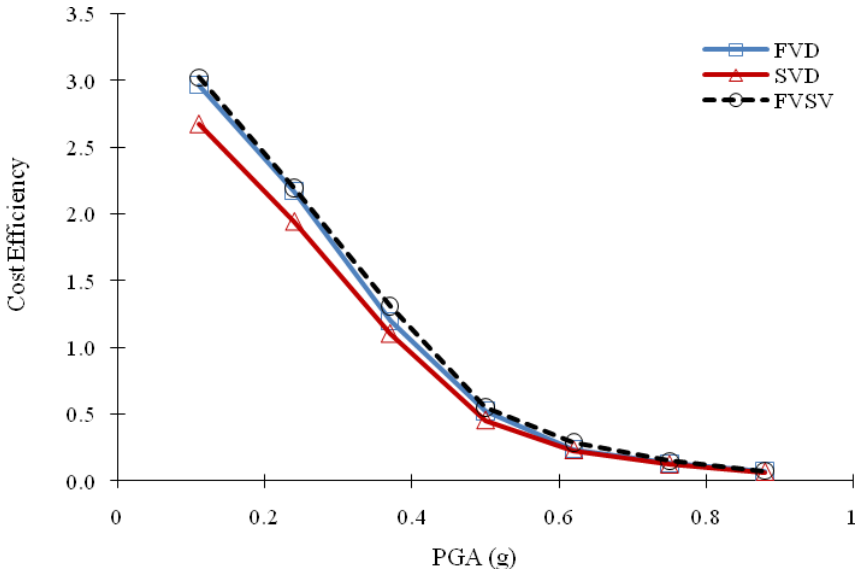

Figure 6.11 Comparison of Failure Cost Efficiency Ratios of Optimal Designs with Different Configurations of Dampers on MRF Building Model

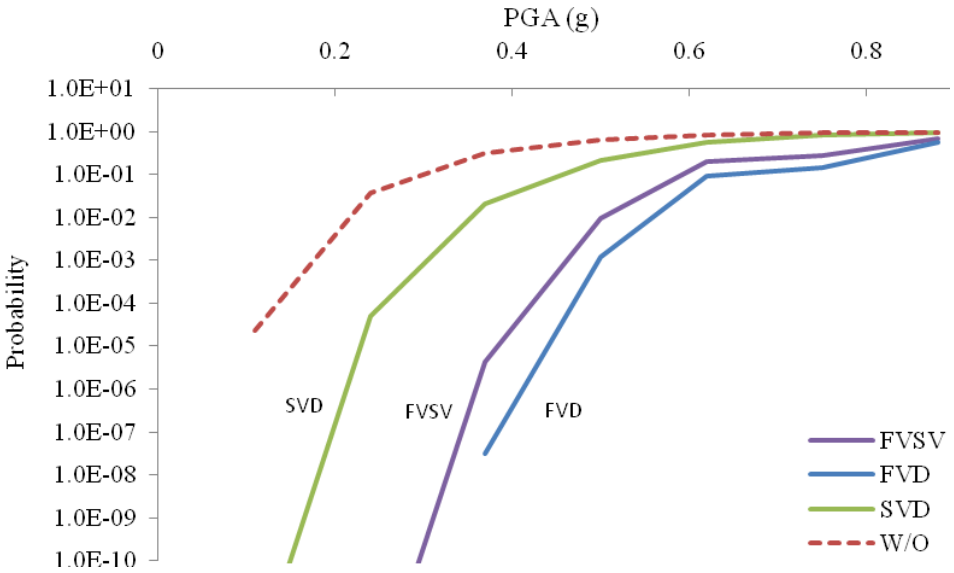

Figure 6.12 Comparison of Fragility at P(Δ>0.7) of Optimal Designs with Different Configurations of Dampers on Shear Building Model

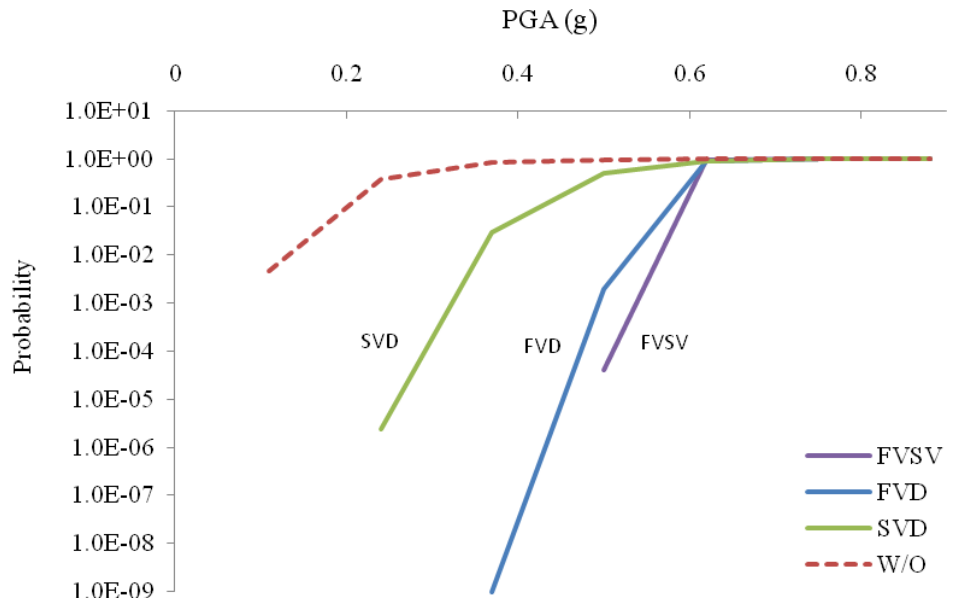

Figure 6.13 Comparison of Fragility at P(Δ>0.7) of Optimal Designs with Different Configurations of Dampers on MRF Building Model

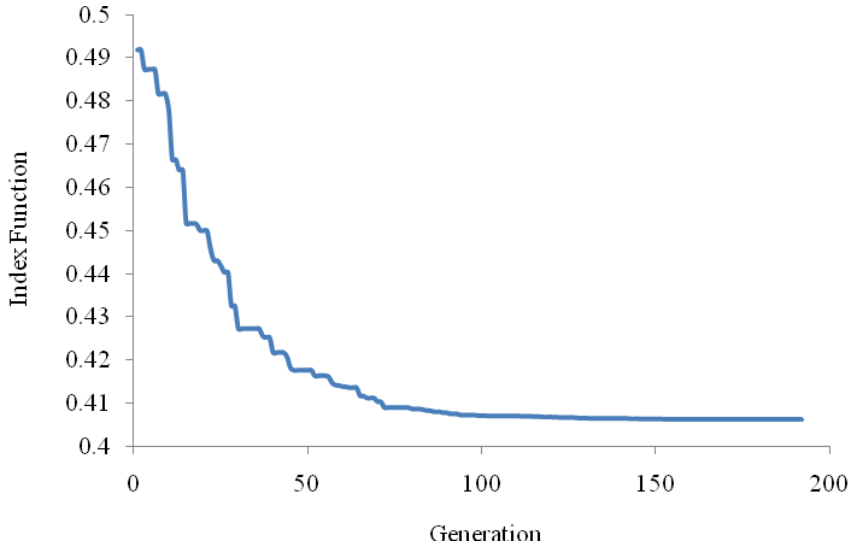

Figure 6.14 Convergence to Optimal Design with Combination of FVD and TADAS Devices in Genetic Algorithm

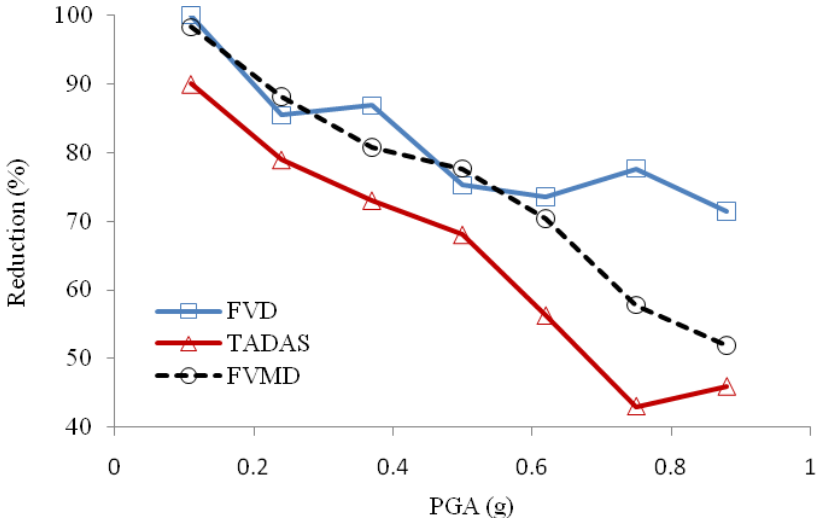

Figure 6.15 Percent Reduction in Total Limit State Costs at Different Earthquake Intensities due to Different Optimal Designs: Shear Building Model

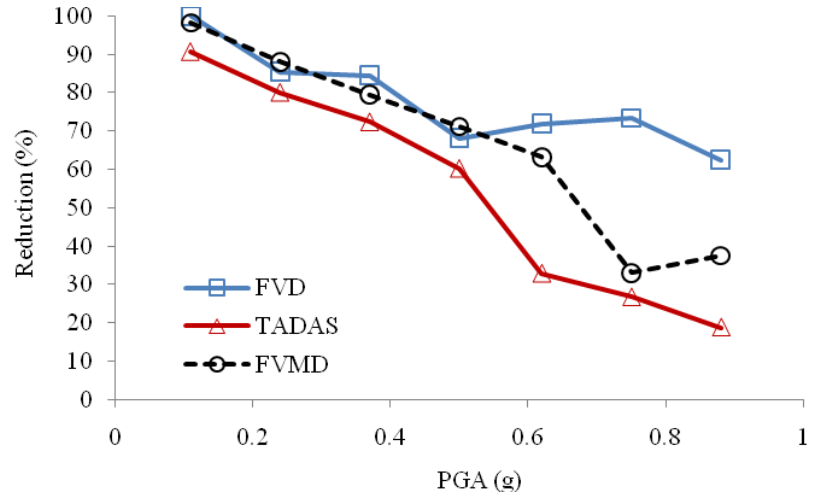

Figure 6.16 Percent Reduction in Failure Costs at Different Earthquake Intensities due to Different Optimal Designs: Shear Building Model

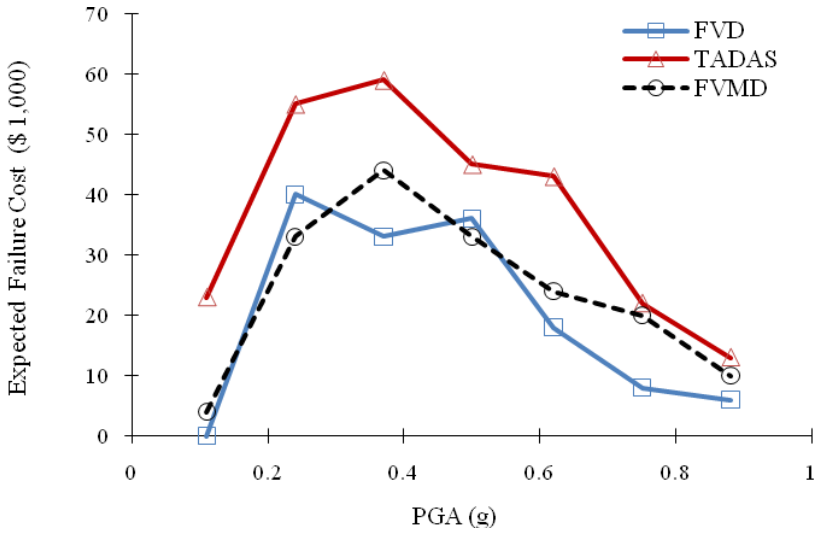

Figure 6.17 Expected Failure Cost on the Shear Building Model with Optimal Designs of Each Type of Dampers under Various Earthquake Intensity

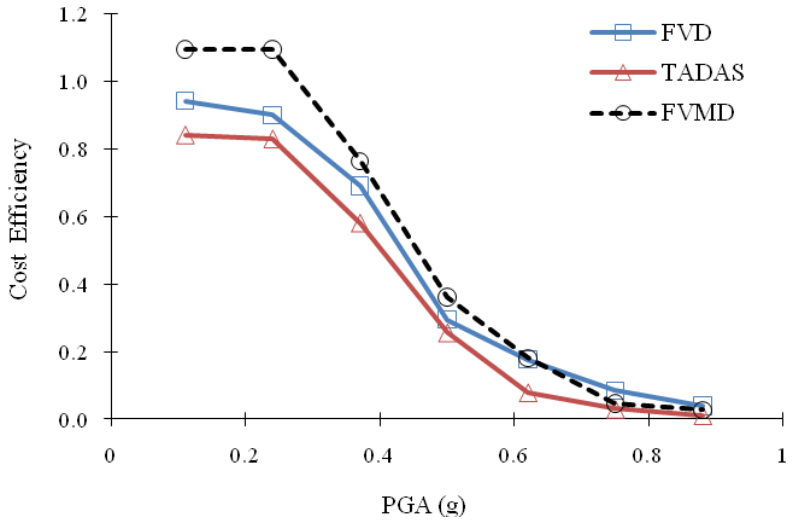

Figure 6.18 Efficiency of Each Optimal Design on the Reduction of the Expected Failure Cost of Shear Building Model

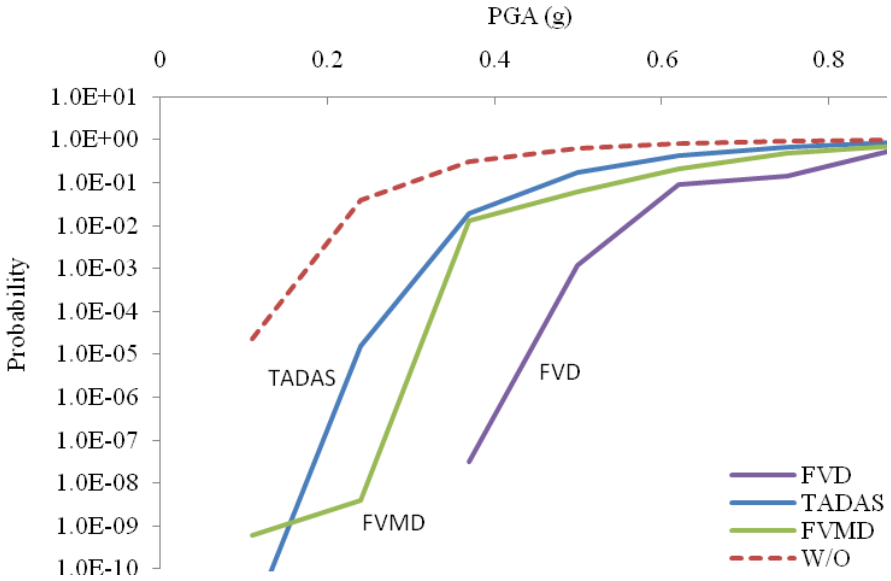

Figure 6.19 Comparison of Fragility at P(Δ>0.7) with Each Optimal Design for Shear Building Model

CHAPTER 7

Summary and Concluding Remarks

7.1 Summary

This work has focused on the study of methods to make optimal performance improvements in building structures exposed to seismic loads using energy dissipation devices. The structural design community in earthquake engineering is now moving towards performance-based design of buildings and other structures in which multiple performance objectives need to be considered. Earlier and current designs of building structures have been based on a single performance objective of life safety. Such designs have been shown to perform well according to the life-safety performance objective, but have not performed as well in satisfying the performance objective of mitigating large economic losses. The community is now moving towards prescribing three to four performance objectives. It is being realized that it would be very difficult to satisfy all prescribed performance objectives without incurring cost in either over- or under-design for some performance objectives if the current practice of proportioning structural elements is used. One can, however, achieve performance improvements across the specified spectrum of performance objectives by using energy dissipation devices. This has been the motivation behind this study as discussed in Chapter 1.

The effectiveness of the supplementary energy dissipation devices for reducing the seismic response of structural systems is now well known. Studies have, thus, been performed on optimal sizing and placement of the devices to achieve a reduction in some desired response quantities in an earthquake. In this study we broaden the scope by focusing not on reducing just some particular response quantity such as story drifts or acceleration that only satisfy narrowly focused needs but on a broad spectrum of performance objectives. To improve performance over a broad spectrum of objectives, it is necessary that the objective function that needs to be minimized must cover these desired performance objectives. For this, the life-cycle cost has been chosen as the objective function in this study. Thus, the main focus of this study has been to formulate a general framework for this life-cycle cost-based optimal use of passive energy dissipation devices for the application to seismic structures. To achieve this objective,

the research activities in this study have focused on the development of the reasonable cost estimating strategies considering the random and stochastic nature of the seismic hazard environment, the establishment of meaningful cost-based performance indices, the application of efficient analytical and numerical techniques for seismic response calculation including fragility functions and then the calculation of the damage cost, and the implementation of an appropriate optimization strategy. Life-Cycle Cost Analysis (LCCA) is used as an essential design process for controlling the initial cost of supplementary devices versus the benefit it brings in reducing the future cost of structures with those devices.

For optimization, a genetic algorithm approach is adopted to obtain the solution of problems with discrete variables such as the number of devices needed and placement location in the structure. Two basic structural models are considered to represent a relatively rigid shear beam structure and a more flexible intermediate moment frame structure. For the ease of calculating the response of these structural models repeatedly, it is initially assumed that the structural elements remain elastic. This is indeed the case for a major part of hazard intensity values, especially after the installation of the devices. However, if the structural elements in any story are stressed beyond the yield limit, then the approach prescribed in the 2009 NEHRP Provisions is used to account for the effect of yielding in calculating the deformation response. The impact of using this approach vis-a-vis a more accurate nonlinear time stepping approach on the cost analysis is evaluated and found to be not very significant. These aforementioned topics and research issues are presented in Chapter 2.

Chapters 3 and 4 have presented the approaches that have been used for achieving optimal designs with linear fluid viscous dampers and linear solid visco-elastic dampers for the model building structures. The fluid viscous dampers are considered in Chapter 3 and the solid visco-elastic dampers in Chapter 4. The mechanical characteristics of these two dampers could be modeled with linear velocity dependent dashpots in conjunction with linear displacement dependent springs. The optimal designs of each damper for the model buildings were obtained with the elastic behavior assumption about the main system. For linear systems with optimal placement of dampers, a non-classical response spectrum method was used for estimation of the maximum response quantities. However, as mentioned before, if the linear analysis showed some yielding in structural members, the deformation and other response values are calculated as prescribed in the 2009 NEHRP Provisions. The numerical results are obtained for the optimal damper

designs for the two model buildings to examine the effect of the damper installation on the failure cost, object cost, life-cycle cost, system fragility, and the response quantities that are of design interest. Comparison of the numerical results with the similar results for the original building model is made to quantitatively evaluate the improvement in the system performance. It is observed that there is an across the board improvement in the performance in terms of reduced failure cost, reduced dynamic response and reduced fragility for all levels of seismic intensities for both building models. The improvements in the more flexible intermediate moment resisting frame building are however more than in the relatively rigid shear building.

Chapter 5 has presented the optimal design with yielding metallic devices for the shear building model. The linearity of the system response facilitated the analysis and subsequent application of the optimization procedures in the previous chapters utilizing the fluid and visco-elastic dampers. However, the incorporation of devices with highly nonlinear hysteretic behavior introduces localized nonlinearities even if the main system remains elastic, which renders the overall structural system nonlinear. Consequently, a time domain method of analysis has to be used to calculate the required response quantities. A set of synthetic ground accelerograms was generated as the input ground motions for the time history analysis. The optimal design search in this case took much longer than in the previous cases simply because of many repeated time history analyses of the nonlinear structure. However, the genetic algorithm was able to converge to the optimal value. Numerical results similar to those in the previous chapters were also obtained here. They included the cost calculations, response calculation and fragility function calculations. The results again showed significant improvement in reducing the failure costs and the inter story drift response. However, since these devices introduce stiffness in the structure, the reduction in the acceleration and story shear force were not as large as with other dampers.

Chapter 6 has presented the optimal design with the combination of two different types of devices. The combinations of the fluid viscous dampers with the solid visco-elastic dampers and the metallic yielding dampers have been studied. The combination of two fluid viscous dampers and visco-elastic dampers essentially had two similar types of devices in their mechanical properties and operational characteristics. The response spectrum method used in Chapters 3 and 4 was used to calculate the response quantities for this combinational design. However, the combination of the fluid viscous dampers and the yielding metallic devices involved two totally different devices with different

mechanical characteristics. For this combination it was necessary to use the time stepping method to calculate the response. Cost-effectiveness of the combinations designs was evaluated compared with those of the single type of devices. It was observed that the performance was again improved across the board, but this performance improvement was somewhere between those of the two separate devices.

7.2 Conclusions

The specific conclusions of each chapter are presented in the chapter in somewhat more detail. The above summary also alludes to some of the broader conclusions. In the following we summarize separately these broad conclusions of this study.

- The expected life-cycle cost of a building structure can be conveniently used as a good measure to evaluate the overall performance of a building structure. The study also shows that it can be conveniently minimized to obtain optimum designs of different structural configurations as well as optimal placement and sizing of the protective devices such as the energy dissipation devices.
- Genetic algorithm is a very useful tool to search for the optimal solution for a problem with discrete design variables. The time required for convergence to the optimum can be reduced by careful selection of the variables and their limit values. Since the system with the linear devices could be analyzed much more easily, the time required for convergence was not an issue. For the nonlinear system, where it is necessary to use the time-stepping methods to calculate the response for input time history motions, and since it is necessary to consider a good sample of these motions to represent the stochastic variability of the ground motion, the time required for convergence was quite significant, being about 38 times that for the linear devices such as viscous and visco-elastic dampers.
- Numerical results obtained for the optimal design show that all energy dissipation devices are very effective in improving across-the-board performance. This was clearly shown by a large reduction in the failure cost, significant reductions in the structural responses, and reducing the fragility of the system for all seismic intensities. However, the relative efficiencies of different devices varied with the device itself and the structural characteristic of the building. All devices were effective in reducing the displacement and inter-

story drifts. The viscous and visco-elastic devices were more effective than the yielding metallic device in reducing the floor accelerations and story shears. In fact, the metallic devices were not effective in reducing the accelerations, which is of significance if the facility contains acceleration sensitive equipment. The performance improvement effectiveness of a combination of the different devices was observed to be between the effectiveness of the two individual devices.

- In general the results showed that the devices were relatively more effective with the flexible frame building than with the relatively rigid shear building.
- Although there was an across the board improvement in the performance with the intensity level, the results showed that the expected life-cycle cost and the corresponding cost-efficiency within the same device as well as across the devices was not uniformly the same with the intensity level of the design earthquake. The expected failure costs under the relatively lower intensity but more frequent earthquakes were larger than those under the higher but relatively less frequent earthquakes. Since the earthquake losses were more for the lower intensity but more frequent than for the higher but relatively less frequent, the optimization algorithm ensured that these high costs were reduced more. Therefore, the devices showed higher cost-efficiency under the relatively lower intensity levels of design earthquake than the relatively higher intensity levels.

7.3 Limitations of this Study and Future Work

Limitations

A preliminary study with nonlinear time stepping method was conducted to show that consideration of inelastic behavior in calculating the response did not significantly change the object cost, which was the function considered for minimization. It was because the nonlinear effects only appear when the earthquakes of higher intensity occur. However, the higher intensity earthquakes are also very infrequent with low probability of occurrence. Thus, although there was some difference in the response calculated by the inelastic time history analysis and by 2009 NEHRP Provision, the difference of the limit state cost when multiplied by the probability of the response being in the limit state, the net difference was not large. However, it will be more desirable if this conclusion is verified by a more thorough and accurate analysis of several structural systems. In such analyses, the effect of formation of plastic hinges, joint deformation,

and P-Δ effect may be also considered to calculate the failure cost. Although it is believed that this may still not impact the overall object cost simply because these effects are only important in more infrequent higher intensity motions, this can only be verified by more detailed analyses and thus this is suggested as an item of future study below.

In this study to conduct nonlinear analysis, we used the synthetically generated time histories using a known computer code SIMQKE-1. This allowed us to generate several sets of independent ground motion time histories for difference levels of seismic intensities represented by the hazard curve. However, it is generally felt that the simulated motions impose higher demand on the structures than the recorded ground motions, primarily because these time histories are richer in many frequencies that are represented by design spectrum than the recorded motions. It may, therefore, be of interest to study what difference it would make in the life-cycle cost analysis if recorded motions are used. This is thus suggested as a topic for future studies.

In this study no attempt was also made to optimize the original structure or the design of braces to which the dampers are connected. Among different types of frames that are considered in the design of structure, one could also optimize them by proper selection of the member sizes and perhaps connection details. This is thus also proposed as an item for a possible future study.

In view of the above discussion and consideration of some other issues not covered by this study the following are suggested as the possible of topics for future studies:

- More thorough collection of data on the fragility of nonstructural components – both displacement sensitive and acceleration sensitive – and their costs of repair and replacement for different levels of damage. This will allow a more accurate calculation of the failure cost using approaches such as assembly based methods where one calculates the response and fragility analysis of each component that is likely to get damaged or fail.
- Based on the framework developed here for the life-cycle cost-based optimization, consideration of different structural systems with different types of frames and material, considering nonlinearities in the system with more refined nonlinear analyses including P-Δ effects and hinge formations with recorded and synthetically generated ground motions will provide a more comprehensive

study of wider practical use on this subject.

- Integrated life-cycle cost-based optimization of initial structure and well as that of the structure with the devices since the installation of the devices affects the response of the structure which in turn can be used to modify the original design.
- Since it takes a major computational effort to calculate the response of nonlinear structures, especially for high intensity of ground motions, random vibration studies with use of statistical linearization in which the linearization point shifts with the intensity of the ground motion are needed for efficient calculation of the structural response and the probability of the response being in a limit state to calculate the failure cost.
- Development of simplified procedures, software tools, and design approaches for the direct use of practitioners and engineers.
- Study of the differences in the seismic performances of structures with response quantity-based (such as reduction of accelerations, reduction of an index based on acceleration and drifts, reduction in down time, etc.) optimal design and the cost-based optimal designs.

Appendix

Appendix A. Validation Test of the Genetic Algorithm

In this appendix, the code of the GA algorithm adopted in this study is validated by applying it to the Ackley's function described in Sec. 2.6.2. Two types of validation tests are conducted. In the first test, the number of variables is fixed (three) but the population size is varied with the values of 50, 100, and 200. In the second test, the size of the population is fixed at 100 but the number of variables in the problem varies from 5 to 20. The test results are compared with each other to check the effectiveness of the developed GA code. The theoretical optimal solution for the Ackley's function is $f(\mathbf{X}) = 0$ at $\mathbf{X} = \mathbf{0}$.

The result in Table A.1 and the plot in Figure A.1 show that the code converged to the global optimum quite well in each case. That is, the variable values as well as the function values are close to the theoretical values. In figure A.2 we plot the function values curves of Figure A.1 on a log-scale to accentuate the differences. The larger populations provide results closer to the theoretical values for the same number of iteration. However, the larger populations also require a larger number of calculations. No optimum number can be set as it will depend on the time it takes to evaluate a function. There is, however, a possibility of the lower population not reaching the final goal, and depending on the iteration termination criterion used, it may stop too early. However, the results will always improve monotonically with increasing iterations. In the smaller population, more mutations may also be needed to introduce the diversity in the population to scan a wider domain of possible values.

Table A.1 Result of the Validation Test with Various Sizes of Population

Size of Population	Optimal Vector			Value of Object Function
	x_1	x_2	x_3	
50	1.22×10^{-3}	-0.31×10^{-3}	1.49×10^{-3}	2.84×10^{-3}
100	2.61×10^{-5}	-2.37×10^{-5}	-0.73×10^{-5}	1.26×10^{-5}
200	2.77×10^{-11}	0.92×10^{-11}	1.48×10^{-11}	2.36×10^{-11}

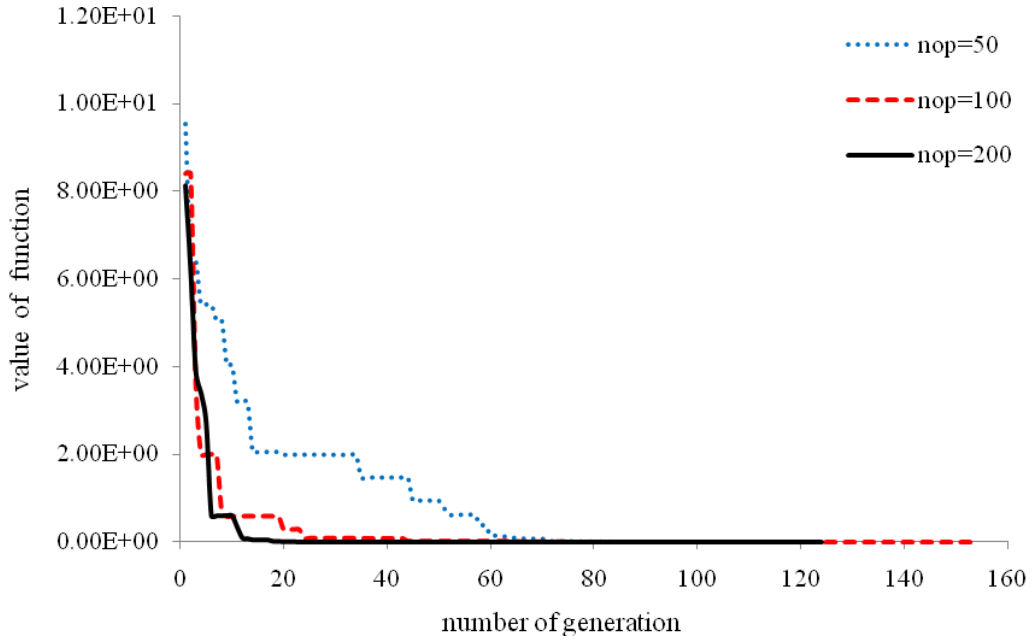

Figure A.1 Performance of GA Code with Various Sizes of Population (Natural Scale)

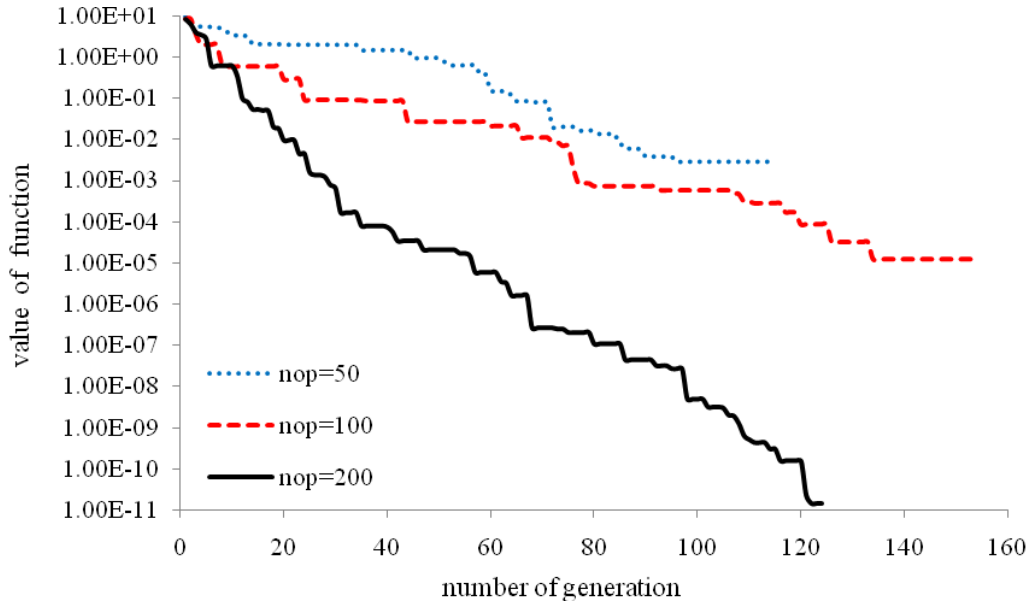

Figure A.2 Performance of GA Code with Various Sizes of Population (Log Scale)

Next we considered the effect of increasing the number of variables in the problem from 5 to 20 and used a population of size 100 for each case. For each variable case, the test was started with four different populations which were randomly created. Table A.2 shows the results after around 33000 iterations of function evaluation. The converged values are slightly different in each case; the average value is shown in the last column. These results indicate that the code does converge near the theoretical values in each case. Figures A.3 and A.4 show the time evolution of the convergence; the results in Figure A.3 are plotted on a natural scale whereas the function values in Figure A.4 are plotted on the log scale to accentuate the differences in the converged values. In each variable case, there are some differences in the values of the objective function and the computer time it takes to achieve these values. Of course, for the same number of iterations, one can obtain more accurate results with a smaller number of variables.

Table A.2 Result of the Validation Test with Various Numbers of Variables

Number of Variables	Optimum Value of Each Try (Elapsed Time)				Average Value (Time)
	1st	2nd	3rd	4th	
5	8.39×10^{-8} (2.84)	7.86×10^{-8} (2.93)	1.55×10^{-8} (2.83)	3.65×10^{-8} (2.99)	5.36×10^{-8} (2.89)
10	2.59×10^{-6} (4.74)	2.92×10^{-6} (4.76)	4.10×10^{-6} (4.70)	6.15×10^{-6} (4.66)	3.94×10^{-6} (4.71)
20	2.88×10^{-5} (9.13)	2.47×10^{-5} (9.00)	2.82×10^{-5} (9.07)	2.50×10^{-5} (9.03)	2.66×10^{-5} (9.05)

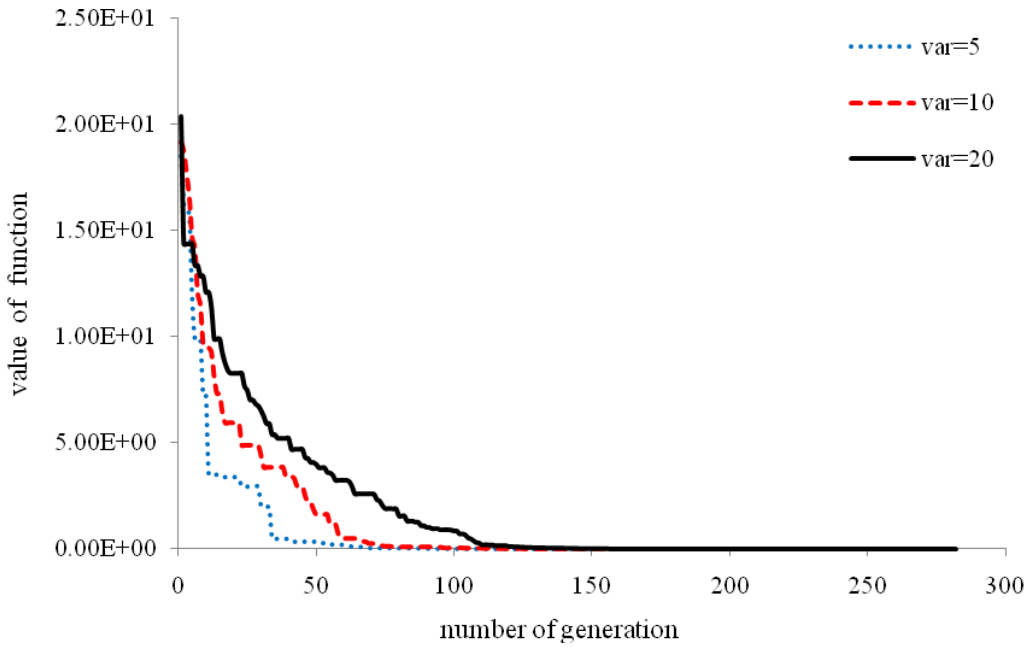

Figure A.3 Performance of GA with Various Numbers of Variables (Natural Scale)

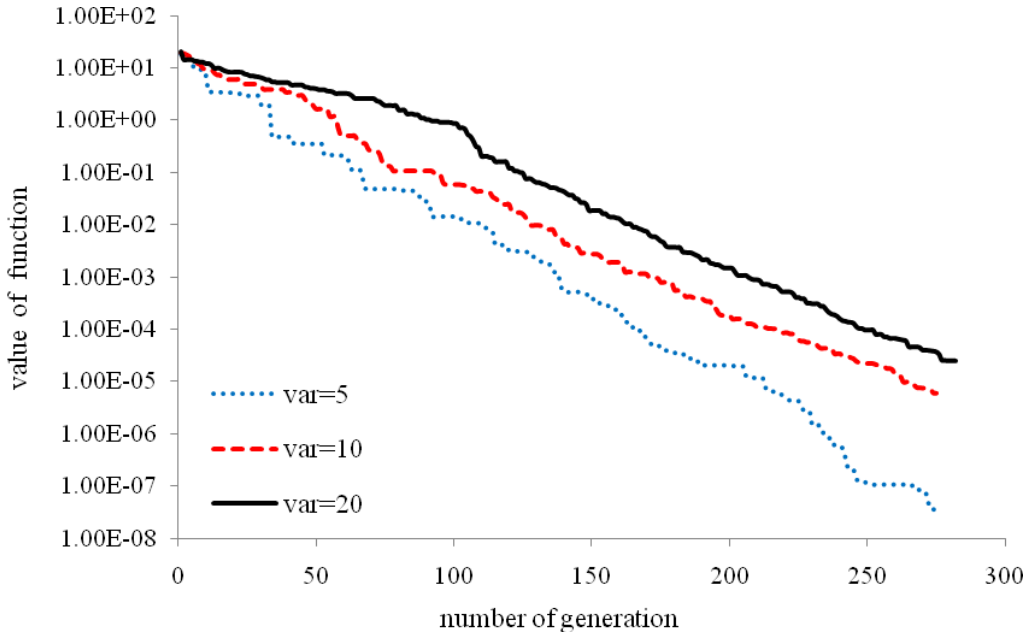

Figure A.4 Performance of GA with Various Numbers of Variables (Log Scale)

Appendix B. Initial Cost Estimation with Each Story

Table B.1 Initial Cost Estimation of Shear Building Model

Story	1	2	3	4	5	6	7	8	9
City Cost Index	1.08	1.08	1.08	1.08	1.08	1.08	1.08	1.08	1.08
Floor Area (m^2)	840	840	840	840	840	840	840	840	840
Story Height (m)	4.5	3.9	3.9	3.9	3.9	3.9	3.9	3.9	3.9
Column Weight (kg)	62472	46922	42069	42069	38262	38262	34733	28580	24517
Connection Weight (kg)	9371	7038	6310	6310	5739	5739	5210	4287	3678
Beam Weight (kg)	187099	187099	168309	168309	156617	156617	143255	143255	117607
Column Area (m^2)	282	239	235	235	232	232	230	230	217
Beam Area (m^2)	1436	1436	1432	1432	1428	1428	1424	1424	1293
Column Unit Cost (/kg)	2.78	2.78	2.78	2.78	2.78	2.78	2.78	2.78	2.78
Beam Unit Cost (/kg)	2.93	2.93	2.93	2.93	2.93	2.93	2.93	2.93	2.93
Column Fireproofing Unit Cost (/m^2)	18.9	18.9	18.9	18.9	18.9	18.9	18.9	18.9	18.9
Beam Fireproofing Unit Cost (/m^2)	24.2	24.2	24.2	24.2	24.2	24.2	24.2	24.2	24.2
Slab Unit Cost (/m^2)	46.7	46.7	46.7	46.7	46.7	46.7	46.7	46.7	46.7
Story Cost for Structural Elements	827232	776705	705965	705965	659382	659382	608814	589145	497591
Unit Cost for non-structural elements (/m^2)	1122.9	1122.9	1122.9	1122.9	1122.9	1122.9	1122.9	1122.9	1122.9
Story Height Adjustment (/m)	6.43	1.84	1.84	1.84	1.84	1.84	1.84	1.84	1.84
Story Cost for Non-structural Elements	948641	944780	944780	944780	944780	944780	944780	944780	944780
Sub-Total	1775873	1721486	1650745	1650745	1604162	1604162	1553595	1533925	1442372
Adjusted Total Cost for Location	**1917943**	**1859205**	**1782805**	**1782805**	**1732495**	**1732495**	**1677882**	**1656639**	**1557761**

Table B.2 Initial Cost Estimation of MRF Building Model

Story	1	2	3	4	5	6	7	8	9
City Cost Index	1.08	1.08	1.08	1.08	1.08	1.08	1.08	1.08	1.08
Floor Area (m^2)	840	840	840	840	840	840	840	840	840
Story Height(m)	4.5	3.9	3.9	3.9	3.9	3.9	3.9	3.9	3.9
Column Weight (kg)	68553	59413	51542	51542	43532	43532	35940	29671	20199
Connection Weight (kg)	10283	8912	7731	7731	6530	6530	5391	4451	3030
Beam Weight (kg)	63908	63908	60503	60503	56672	56672	59509	50287	35600
Column Area (m^2)	308	267	257	257	248	248	244	232	214
Beam Area (m^2)	1273	1273	1269	1269	1267	1267	1264	1260	968
Column Unit Cost (/kg)	2.78	2.78	2.78	2.78	2.78	2.78	2.78	2.78	2.78
Beam Unit Cost (/kg)	2.93	2.93	2.93	2.93	2.93	2.93	2.93	2.93	2.93
Column Fireproofing Unit Cost (/m^2)	18.9	18.9	18.9	18.9	18.9	18.9	18.9	18.9	18.9
Beam Fireproofing Unit Cost (/m^2)	24.2	24.2	24.2	24.2	24.2	24.2	24.2	24.2	24.2
Metal Deck/Concrete Fill Slab Cost (/m^2)	50.4	50.4	50.4	50.4	50.4	50.4	50.4	50.4	50.4
Story Cost for Structural Elements	485379	455382	419957	419957	382906	382906	366798	319415	238689
Unit Cost for non-structural elements (/m^2)	1122.9	1122.9	1122.9	1122.9	1122.9	1122.9	1122.9	1122.9	1122.9
Story Height Adjustment (/m)	6.43	1.84	1.84	1.84	1.84	1.84	1.84	1.84	1.84
Story Cost for Non-structural Elements	948641	944780	944780	944780	944780	944780	944780	944780	944780
Sub-Total	1434019	1400162	1364737	1364737	1327686	1327686	1311578	1264195	1183469
Adjusted Total Cost for Location	**1548741**	**1512175**	**1473916**	**1473916**	**1433901**	**1433901**	**1416504**	**1365330**	**1278147**

Appendix C. Partial Fraction Coefficients

The partial fraction coefficients required in Eqs. (3.20) to (3.22) are defined as:

$$W_{jk} = -\left\{\left(\Omega^2 - \Omega^{-2}\right)\mu_{jk} - 2\left[1 - \Omega^2 + 2\left(\beta_j^2\Omega^2 - \beta_k^2\right)\right]\eta_{jk}\right\} / \delta_{jk} \tag{C.1}$$

$$Q_{jk} = -\left\{\left(\Omega^2 - \Omega^{-2}\right)\eta_{jk} - 2\Omega^{-2}\left[1 - \Omega^2 + 2\left(\beta_k^2\Omega^2 - \beta_j^2\right)\right]\mu_{jk}\right\} / \left(\omega_j^2\delta_{jk}\right) \tag{C.2}$$

with

$$\Omega = \omega_j / \omega_k \tag{C.3}$$

$$\begin{aligned}\eta_{jk} = {} & \{\mathbf{g}_i\}_j \{\mathbf{g}_i\}_k \left(1 - 4\beta_j^2 + 4\beta_j\beta_k\Omega - \Omega^2\right) + \\ & 4\omega_j^2 \{\mathbf{a}_i\}_j \{\mathbf{a}_i\}_j \left(1 - \Omega^2\right) + 4\omega_j \left(\{\mathbf{a}_i\}_j \{\mathbf{g}_i\}_k - \{\mathbf{a}_i\}_k \{\mathbf{g}_i\}_j\right)\left(\beta_k\Omega - \beta_j\right)\end{aligned} \tag{C.4}$$

$$\begin{aligned}\mu_{jk} = {} & \{\mathbf{g}_i\}_j \{\mathbf{g}_i\}_k \left(\Omega^2 - 1\right) + 4\omega_j^2 \{\mathbf{a}_i\}_j \{\mathbf{a}_i\}_j \left[\left(1 - 4\beta_j^2\right)\Omega^2 + 4\beta_j\beta_k\Omega - 1\right] + \\ & 4\omega_j\Omega\left(\{\mathbf{a}_i\}_j \{\mathbf{g}_i\}_k - \{\mathbf{a}_i\}_k \{\mathbf{g}_i\}_j\right)\left(\beta_j\Omega - \beta_k\right)\end{aligned} \tag{C.5}$$

$$\begin{aligned}\delta_{jk} = {} & 16\left(\beta_j^2 + \beta_k^2 - \beta_j^4 - \beta_k^4\right) + \\ & 4\left(\Omega^2 + \Omega^{-2}\right)\left[1 - 2\left(\beta_j^2 + \beta_k^2 - 2\beta_j^2\beta_k^2\right)\right] - \Omega^{-4} - \Omega^4 - 6\end{aligned} \tag{C.6}$$

$$\gamma_{jk} = \omega_k^2 + \alpha_j^2 + 2\alpha_j\omega_k\beta_k \tag{C.7}$$

Appendix D. Validation Test of the Time History Analysis Procedure

In this appendix, the time history analysis procedure adopted in this study is validated by applying it to a simple single degree of freedom system presented in the book of Paz (1985).

The example problem represents a structure with a story height of 15ft. The post yield stiffness is assumed to be 0% of the original stiffness (elasto-plastic). The mass, damping, and stiffness of the system in this problem are as follows:

$$\begin{aligned} m &= 0.2 \text{ k-s}^2/\text{in.} \\ c &= 0.274 \text{ k-sec/in.} \\ k &= 12.35 \text{ k/in.} \end{aligned} \tag{D.1}$$

The yield strength of the spring element is assumed to be 15 kips. The input force in the problem varies from -10 to 18.46 kip within a duration of 1.5 sec and is specified with 0.1 sec time increment. The following tables show the results of the response analysis given in the book of Paz (1985) and the results obtained in this study. Figures D.1 and D.2 show the displacement response quantity and velocity response quantity obtained by the computer program written in this study and those obtained by Paz. The results are close to each other with some minor differences mainly because the book by Paz uses a slightly different numerical integration approach.

The time history analysis procedure adopted in this study is also validated by applying it to a simple two degree of freedom system presented in the book of Hart and Wong (2000).

For this problem the mass, damping, and stiffness matrix of the system are as follows:

$$\begin{aligned} \mathbf{M} &= \begin{bmatrix} 1.0 & 0.0 \\ 0.0 & 1.0 \end{bmatrix} \text{k-s}^2/\text{in.} \\ \mathbf{C} &= \begin{bmatrix} 2.0 & -1.0 \\ -1.0 & 1.0 \end{bmatrix} \text{k-s/in.} \\ \mathbf{K} &= \begin{bmatrix} 200 & -100 \\ -100 & 100 \end{bmatrix} \text{k/in.} \end{aligned} \tag{D.2}$$

The yield strength of the two spring elements is assumed to be 562.5 kips. The post yield stiffness is assumed to be 20% of the original stiffness. The North-South component of the El-Centro earthquake time history is used as the input ground motion

modified by a scale factor of 1.8. This modified El-Centro earthquake time history is shown in Figure D.3. Table D.2 gives the partial numerical results for the displacement and velocity response of the system calculated for a first few seconds of the motion by the computer program coded in this study and those provided by Hart and Wong (2000). The numerical values are very close to each other. In Figures D.4 to D.7 we show the displacement and velocity response quantities obtained by the computer program written in this study and those obtained by Hart and Wong for the entire earthquake motion duration. The two sets of plots are identical to each other, primarily because in this study the algorithm given in the book by Hart and Wong (2000) is used. This, thus, validates the computer program used in this study.

Table D.1 Results of Nonlinear Response for Single Degree of Freedom System

Time (sec)	Force (kip)	Result by Paz (1985)		Result by This Study	
		Displacement (in.)	Velocity (in/sec)	Displacement (in.)	Velocity (in/sec)
0.0	0	0	0	0	0
0.1	0 4.444	0.0316	0.9485	0.0316	0.9484
0.2	8.888	0.2326	3.1844	0.2326	3.1828
0.3	13.333	0.6669	5.3760	0.6668	5.3752
0.4	17.777	1.2681	6.3768	1.2678	6.3747
0.5	18.462	1.9358	7.0190	1.9541	6.8620
0.6	15.356	2.6505	7.0189	2.6610	6.8735
0.7	12.308	3.2916	5.5791	3.2937	5.4437
0.8	9.231	3.7244	2.8840	3.7190	2.7636
0.9	6.154	3.8319	-0.9054	3.8197	-1.0127
1.0	3.077	3.5397	-4.8048	3.4932	-4.8737
1.1	0	2.9268	-7.0295	2.8391	-7.0274
1.2	-10	2.1729	-8.0806	2.1334	-8.0157
1.3	-5	1.4211	-5.8177	1.3225	-5.7300
1.4	0	1.1739	1.3860	1.1227	1.4430
1.5	0	1.6619	8.2227	1.6506	7.5006

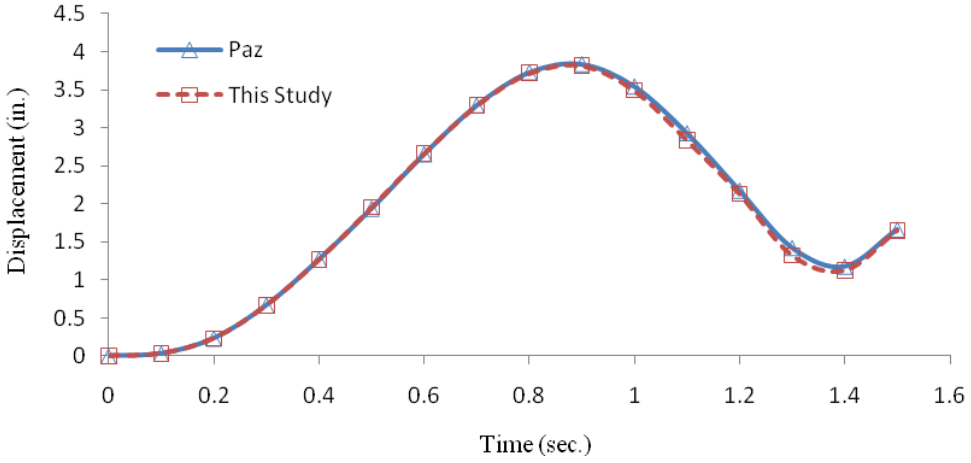

Figure D.1 Displacement Response Quantity Calculated by Paz and This Study

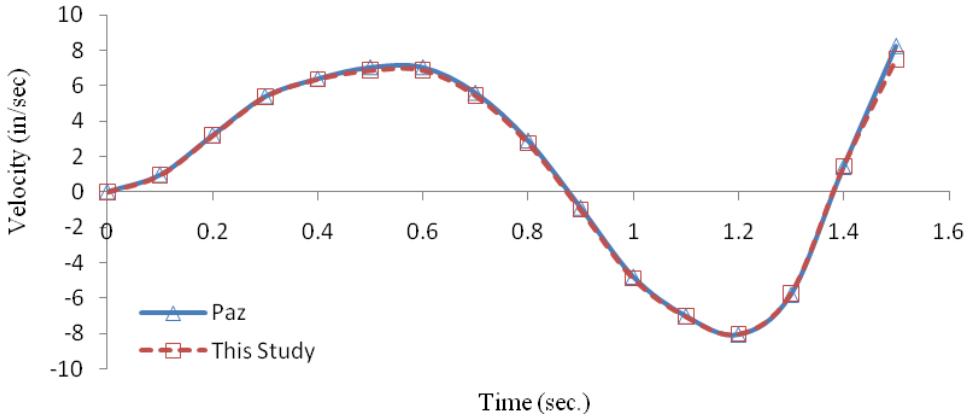

Figure D.2 Velocity Response Quantity Calculated by Paz and This Study

Table D.2 Partial Results of Nonlinear Response for Two Degree of Freedom System (Upper Floor)

Time (sec)	Ground Acceleration (g)	Result by Hart and Wang		Result by This Study	
		Displacement (in.)	Velocity (in/sec)	Displacement (in.)	Velocity (in/sec)
0.00	-0.00257	0	0	0	0
0.02	-0.01980	0.00086	0.0864	0.00086	0.0864
0.04	-0.01850	0.00407	0.2342	0.00407	0.2344
2.78	0.03450	6.62956	40.6829	6.62923	40.6861
2.80	-0.01740	7.38777	35.1381	7.38751	35.1415
2.96	0.03400	9.07667	-15.1666	9.07651	-15.1673
2.98	0.07710	8.71185	-21.3154	8.71168	-21.3160
3.30	0.24800	-4.90826	-44.7627	-4.90784	-44.7711
3.32	0.37500	-5.78253	-42.6641	-5.78226	-42.6704

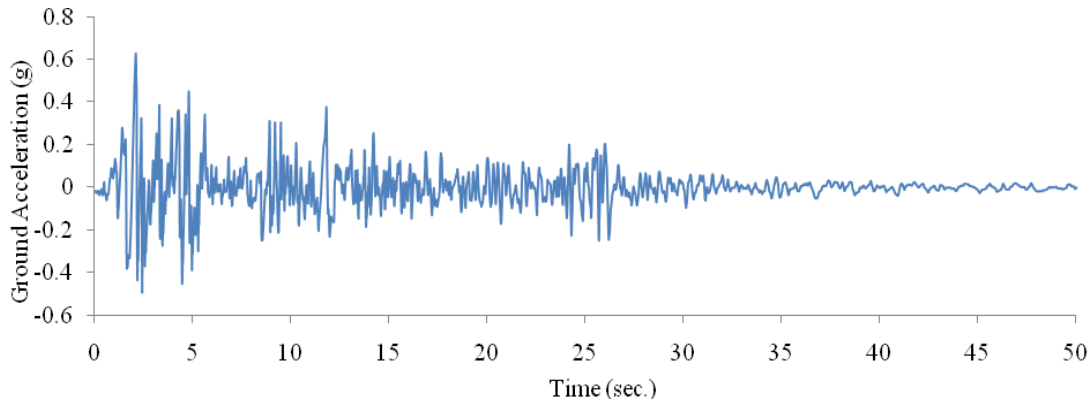

Figure D.3 Time History of El-Centro Earthquake

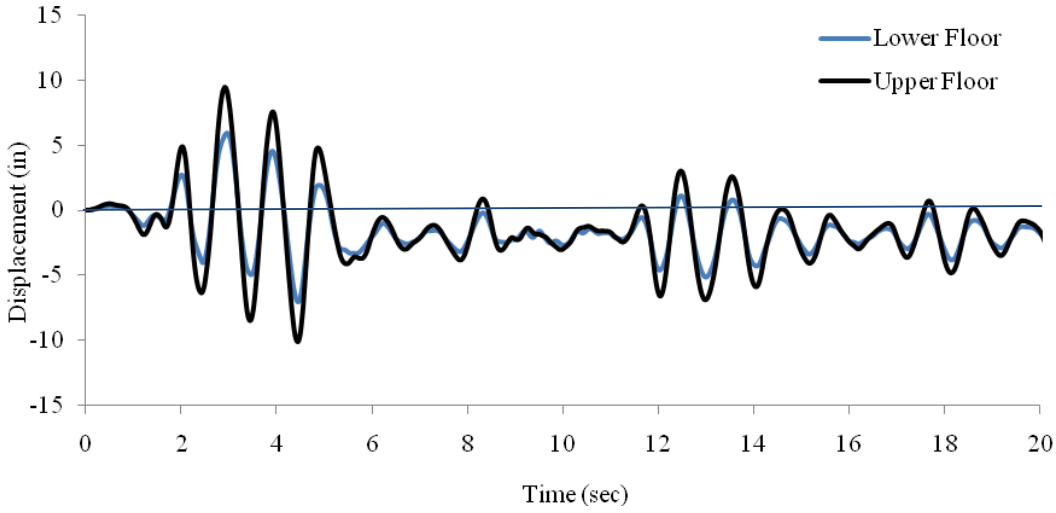

Figure D.4 Floor Displacement Response Calculated by This Study

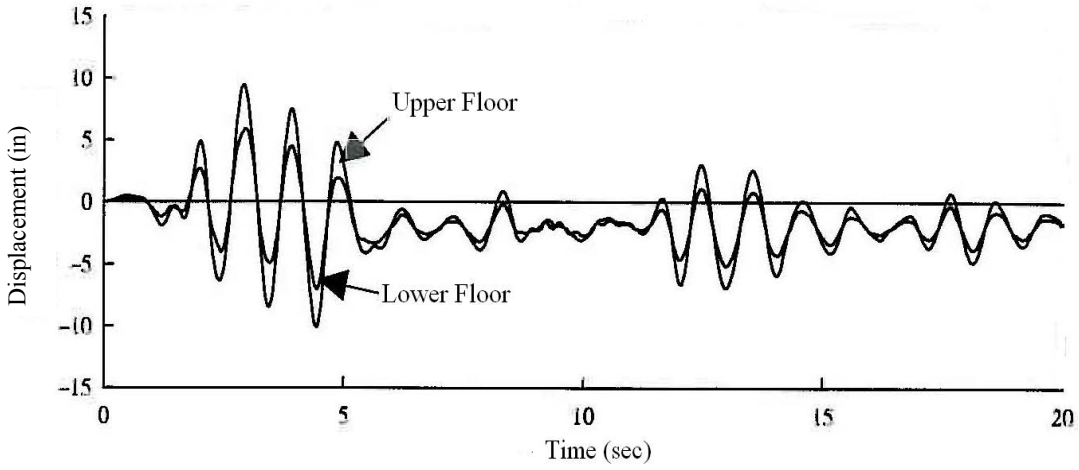

Figure D.5 Floor Displacement Response Calculated by Hart and Wong

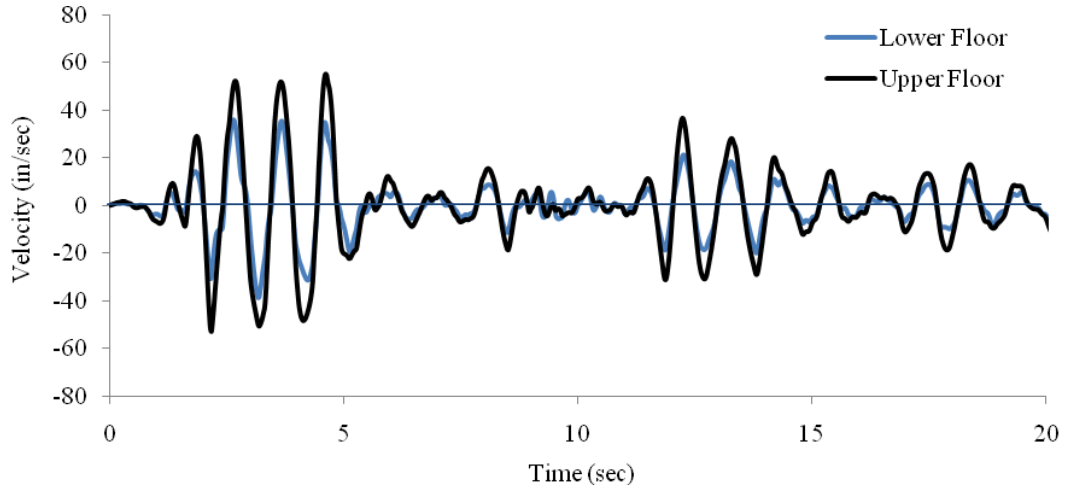

Figure D.6 Floor Velocity Response Calculated by This Study

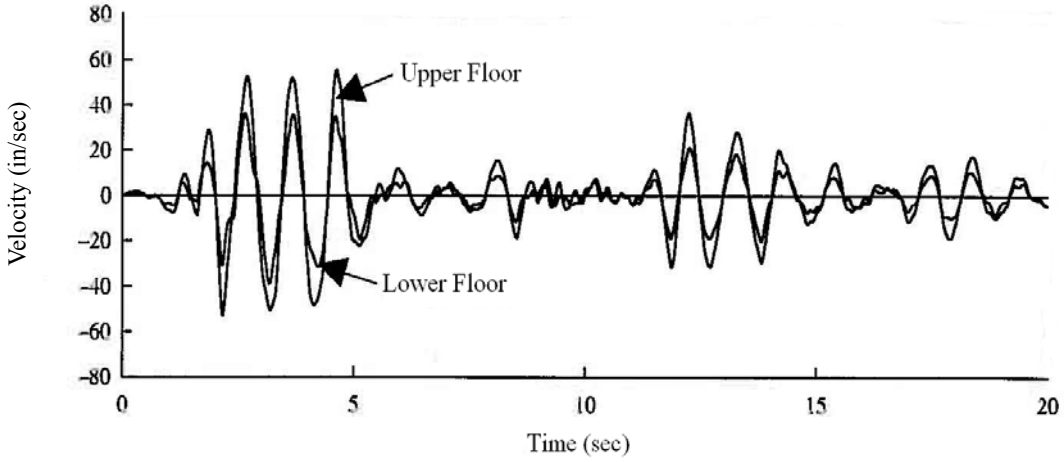

Figure D.7 Floor Velocity Response Calculated by Hart and Wong

References

Ackley, D. H., (1987) *A Connectionist Machine for Genetic Hillclimbing,* Kluwer Academic Publishers, Boston

Aiken, I. D. and Kelly, J. M., (1990). "Earthquake Simulator Testing and Analytical Studies of Two Energy-Absorbing Systems for Multistory Structures," *Report No. UCB/EERC-90/03*, *Earthquake Engineering Research Center*, University of California at Berkeley, Berkeley, CA.

Alaska Department of Education & Early Development (1999). *Life Cycle Cost Analysis Handbook*, *1st Edition*, Alaska

American Institute of Steel Construction Inc., (2001). *Manual of Steel Construction 3rd Edition*, *AISC*

Ang, A. H-S and Leon, D., (1997). "Development of Target Reliability for Design and Upgrading of Structures," *Structural Safety*, Amsterdam, 14(1), 91-103.

Applied Technology Council, (1985). "Earthquake Damage Evaluation Data for California," *ATC-13*.

Applied Technology Council, (2009). *Guidelines for Seismic Performance Assessment of Buildings*, *ATC-58 50% Draft*.

Aprile, A., Inaudi, J. A., and Kelly, J. M., (1997). "Evolutionary Model of Viscoelastic Dampers for Structural Applications," *Journal of Engineering Mechanics*, 123(6), 551-560.

Baker, J. E., (1985). "Adaptive Selection Methods for Genetic Algorithms," *Proceedings of an International Conference on Genetic Algorithms and Their Applications*, 101-111.

Barroso, L. R., (1999). *Performance Evaluation of Vibration Controlled Steel Structures under Seismic Loading*, Department of Civil and Environmental Engineering, Stanford University.

Beck, J. L., Chan, E., Irfanoglu, A., and Papadimitriou, C., (1999). "Multi-Criteria Optimal Structural Design under Uncertainty," *Earthquake Engineering and Structural Dynamics*, 28, 741-761.

Bergman, D. M. and Hanson, R. D., (1993). "Viscoelastic Mechanical Damping Devices

Tested at Real Earthquake Displacements," *Earthquake Spectra*, 9(3), 389-418.

Bommer, J. J. and Mendis, R., (2005). "Scaling of Spectral Displacement Ordinates with Damping Ratio," *Earthquake Engineering and Structural Dynamics*, 34, 145-165

Camp, C. V., Pezeshk, S., and Cao, G., (1998). "Optimized Design of Two-Dimensional Structures Using Genetic Algorithm," *Journal of Structural Engineering*, 124(5), 551-559.

Cardone, D., Dolce, M. and Rivelli, M., (2009). "Evaluation of Reduction Factors for High-Damping Design Response Spectra," *Bulletin of Earthquake Engineering*, 7, 273-291

Chan, E., (1997). "Optimal Design of Building Structures Using Genetic Algorithms," *Report No. EERL 97-06*, Earthquake Engineering Research Laboratory, California Institute of Technology, Pasadena, CA.

Chang, K. C., Soong, T. T., Lai, M. L., and Nielsen, E. J., (1993). "Viscoelastic Dampers as Energy Dissipation Devices for Seismic Applications," *Earthquake Spectra*, 9(3), 371-388.

Chang, K. C., Soong, T. T., Lai, M. L., and Nielsen, E. J., (1993). "Development of a Design Procedure for Structures with Added Viscoelastic Dampers", *ATC-17-1 Seminar on Seismic Isolation, Passive Energy Dissipation, and Active Control*, San Francisco, CA, 473-484.

Chang, K. C., Soong, T. T., Oh, S. T., and Lai, M. L., (1995). "Seismic Behavior of Steel Frame with Added Viscoelastic Dampers," *Journal of Structural Engineering*, 121(10), 1418-1426.

Chang, T.-S. and Singh, M. P. (2009). "Mechanical Model Parameters for Viscoelastic Dampers", *Journal of Engineering Mechanics*, 135(6), 581-584

Chen, Y. T. and Chai, Y. H. (2008). "Seismic Design of Structures with Supplemental Maxwell Model-Based Brace-Damper Systems," *The 14th World Conference on Earthquake Engineering*, October 12-17, Beijing, China

Cheng, F. Y. and Li, D., (1998). "Genetic Algorithm Development for Multiobjective Optimization of Structures," *AIAA Journal*, 36(6), 1105-1112.

Chopra, A. K. (2000). *Dynamics of Structures-Theory and Application to Earthquake Engineering; 2nd Edition*, Prentice Hall, NJ

Constantinou, M. C. and Symans, M. D., (1993). "Experimental and Analytical

Investigation of Seismic Response of Structures with Supplemental Fluid Dampers," *Report No. NCEER 92-0032*, National Center for Earthquake Engineering Research, University of New York at Buffalo, Buffalo, NY.

Constantinou, M. C. and Symans, M. D., (1993). "Experimental Study of Seismic Response of Structures with Supplemental Fluid Dampers," *The Structural Design of Tall Buildings*, 2, 93-132.

Constantinou, M. C. and Symans, M. D., (1993). "Seismic Response of Structures with Supplemental Damping," *The Structural Design of Tall Buildings*, 2, 77-92.

Constantinou, M. C., Symans, M. D., Tsopelas, P., and Taylor, D. P., (1993). "Fluid Viscous Dampers in Applications of Seismic Energy Dissipation and Seismic Isolation," *ATC-17-1 Seminar on Seismic Isolation, Passive Energy Dissipation, and Active Control*, San Francisco, CA, 581-592.

Constantinou, M. C., Soong, T. T., and Dargush, G. F., (1998). *Passive Energy Dissipation Systems for Structural Design and Retrofit*, Monograph No. 1, Multidisciplinary Center for Earthquake Engineering Research, Buffalo, NY.

De Leon, D. and Ang, A. H-S., (1994). "A Damage Model for Reinforced Concrete Buildings: Further Study with the 1985 Mexico City Earthquake," *Proceedings 6th International Conference on Structural Safety and Reliability*, 3, 2081-2087.

FEMA-178, (1992). *NEHRP Handbook for the Seismic Evaluation of Existing Buildings*

FEMA-227, (1992). *A Benefit-Cost Model for the Seismic Rehabilitation of Buildings*, Vol. 1.

FEMA-228, (1992). *A Benefit-Cost Model for the Seismic Rehabilitation of Building*, Vol. 2.

FEMA-273, (1997). *NEHRP Guidelines for the Seismic Rehabilitation of Buildings.*

FEMA-274, (1997). *Commentary on the Guidelines for the Seismic Rehabilitation of Buildings*

FEMA-310, (1998). *Handbook for the Seismic Evaluation of Buildings-A Prestandard.*

FEMA-343, (1999). *Case Studies: An Assessment of the NEHRP Guidelines for the Seismic Rehabilitation of Buildings.*

FEMA-350, (2000). *Recommended Seismic Design Criteria for New Steel Moment-Frame Buildings.*

FEMA-356, (2000). *Prestandard and Commentary for the Seismic Rehabilitation of Buildings*.

FEMA-445, (2006). *Next-Generation Performance-Based Seismic Design Guidelines; Program Plan for New and Existing Buildings.*

Fogel, D. B., (2006). "Evolutionary Computation: Toward A New Philosophy of Machine Intelligence," 3rd Edition, IEEE Press, Piscataway, NJ

Frangopol, D. M., (1985). "Multicriteria Reliability-Based Optimum Design," *Structural Safety*, 3(1), 23-28.

Furuya, O., Hamazaki, H., and Fujita, S., (1998). "Proper Placement of Energy Absorbing Devices for Reduction of Wind-Induced Vibration in High-Rise Buildings," *Journal of Wind Engineering and Industrial Aerodynamics*, 76, 931-942.

Fujita, K., Moustafa, A., and Takewaki, I., (2010). "Optimal Placement of Viscoelastic Dampers and Supporting Members under Variable Critical Excitations," *Earthquake and Structures*, (1), 43-67

Gasparini, D. A. and Vanmarcke, E. H., (1976). "Simulated Earthquake Motions Compatible with Prescribed Response Spectra," *Department of Civil Engineering, Report No. 2*, MIT, Cambridge

Gen, M. and Cheng, R., (1997). *Genetic Algorithms and Engineering Design*, John-Wiley & Sons, New York, NY.

Goldberg, D. E., (1989). *Genetic Algorithms in Search, Optimization and Machine Learning*, Addison-Wesley, Reading, MA.

Goldberg, D. E., (2002). "The Design of Innovation: Lessons from and for Competent Genetic Algorithms," Addison-Wesley, Reading, MA.

Gupta A. K., (1990). *Response Spectrum Method in Seismic Analysis and Design of Structures*, Blackwell Scientific Publications, London, UK.

Gürgöze, M. and Müller, P. C., (1992). "Optimal Positioning of Dampers in Multi-Body Systems," *Journal of Sound and Vibration*, 158(3), 517-530.

Hadi, M. N. and Arfiadi, Y., (1998). "Optimum Design of Absorber for MDOF Structures," *Journal of Structural Engineering*, 124, 1272-1280.

Hanson, R. D. and Soong, T. T., (2001). *Seismic Design with Supplemental Energy Dissipation Devices*, EERI, MNO-8.

Hanson, R., (1993). "Supplemental Damping for Improved Seismic Performance," *Earthquake Spectra*, 9(3), 319-334.

Holland, J. H., (1975). “Adaptation in Natural and Artificial Systems,” University of Michigan Press, Ann Arbor, MI.

Igusa, T., Kiureghian, A. D. and Sackman, J. L., (1984). “Modal Decomposition Method for Stationary Reponse of Non-Classically Damped Systems,” *Earthquake Engineering and Structural Dynamics*, 12, 121-136.

Inaudi, J. A. and De la Llera, J. C., (1993). “Dynamic Analysis of Nonlinear Structures Using State-Space Formulation and Partitioned Integration Schemes,” *Report No. UCB/EERC-92/18*, Earthquake Engineering Research Center, University of California at Berkeley, Berkeley, CA.

Jenkins, W. M., (1997). "On the Application of Natural Algorithms to Structural Design Optimization," *Engineering Structures*, 19(4), 302-308.

Jennings, P. C., Housner, G. W. and Tsai, N. C., (1968). “Simulated Earthquake Motions,” *Earthquake Engineering Research Laboratory*, California Institute of Technology, Pasadena, CA.

Kanai, K., (1961). “An Empirical Formula for the Spectrum of Strong Earthquake Motions,” Bulletin of the Earthquake Research Institute, University of Tokyo, 39, 85-95.

Kargahi, M. (2009). “Structural Optimization of Viscous Damper Using Genetic Algorithms for Improving Seismic Performance of Existing Buildings,” *Proceedings of the 2009 ATC & SEI Conference on Improving the Seismic Performance of Buildings and other Structures*, San Francisco, CA, Innovative Approaches to Rehabilitation 1, 955-966

Kasai, K., Fu, Y., and Watanabe, A., (1998). “Passive Control Systems for Seismic Damage Mitigation,” *Journal of Structural Engineering*, 124(5), 501-512.

Kasai, K., Munshi, J. A., Lai, M. L., and Maison, B. F., (1993). "Viscoelastic Damper Hysteretic Model: Theory, Experiment, and Application", *ATC-17-1 Seminar on Seismic Isolation, Passive Energy Dissipation, and Active Control*, San Francisco, CA, 521-532.

Keel, C. J. and Mahmoodi, P., (1986). "Designing of Viscoelastic Dampers for Columbia Center Building", *Building Motion in Wind*, Eds. Isyumov, N. and Tschanz, ASCE, New York, NY, 66-82.

Kelly, J. M., Skinner, R. I., and Heine, A. J., (1972). "Mechanism of Energy Absorption

in Special Devices for Use in Earthquake Resistant Structures," *Bulletin of the New Zealand Society for Earthquake Engineering*, 5(3).

Kim, Y. and Ghaboussi, J., (1999). "A New Method of Reduced Order Feedback Control Using Genetic Algorithms," *Earthquake Engineering and Structural Dynamics*, 28, 193-212.

Kircher, C. A., Nassar, A. A., Kustu, O. and Holmes, W. T., (1997). "Development of Building Damage Functions for Earthquake Loss Function," *Earthquake Spectra*, 13, (4), 663-682.

Kjellstrom, G., (1991). "On the Efficiency of Gaussian Adoption," *Journal of Optimization Theory and Application*, 71(3), 589-597.

Lavan, O. and Levy, R. (2006). "Optimal Design of Supplemental Viscous Dampers for Linear Framed Structures," *Earthquake Engineering and Structural Dynamics*, 35(3), 337-356.

Lundén, R., (1980). "Optimum Distribution of Additive Damping for Vibrating Frames," *Journal of Sound and Vibration*, 72, 391-402.

Mahmoodi, P., (1969). "Structural Dampers," *Journal of the Structural Division ASCE*, 95, 1661-1672.

Maison, B. F. and Bonowitz, D., (1999). "How Safe are Pre-Northridge WSMFs? A Case Study of the SAC Los Angeles Nine-Story Building," *Earthquake Spectra*, 15(4), 765-789

Makris, N. and Constantinou, M. C., (1991). "Fractional Derivative Model for Viscous Dampers," *Journal of Structural Engineering*, 117(9), 2708-2724.

Makris, N. and Constantinou, M. C., (1993). "Models of Viscoelasticity with Complex-Order Derivatives," *Journal of Engineering Mechanics*, 119(7), 1453-1464.

Makris, N., (1998). "Viscous Heating of Fluid Dampers, I: Small-Amplitude Motions." *Journal of Engineering Mechanics*, 124(11), 1210-1216.

Makris, N., (1998). "Viscous Heating of Fluid Dampers, II: Large-Amplitude Motions." *Journal of Engineering Mechanics*, 124(11), 1217-1223

Makris, N., Constantinou, M. C., and Dargush, G. F., (1993). "Analytical Model of Viscoelastic Fluid Dampers," *Journal of Structural Engineering*, 119(11), 3310-3325.

Makris, N., Dargush, G. F., and Constantinou, M. C., (1993). "Dynamic Analysis of Generalized Viscoelastic Fluids," *Journal of Engineering Mechanics*, 119(8), 1663-1679.

Makris, N., Dargush, G. F., and Constantinou, M. C., (1995). "Dynamic Analysis of Viscoelastic Fluid Dampers," *Journal of Engineering Mechanics*, 121(10), 1114-1121.

Maldonado, G. O. and Singh M. P., (1991a). "An Improved Response Spectrum Method for Calculating Seismic Design Response. Part-1: Classically Damped Structures," *Earthquake Engineering and Structural Dynamics*, 20, 621-635.

Maldonado, G. O. and Singh M. P., (1991b). "An Improved Response Spectrum Method for Calculating Seismic Design Response. Part-2: Non-Classically Damped Structures," *Earthquake Engineering and Structural Dynamics*, 20,637-649.

Malushte, S. R., (1987). *Prediction of Seismic Design Response Spectra Using Ground Characteristics*, Thesis (M.S.), VPI & SU, Blacksburg, VA

Michalewicz, Z., (1992). *Genetic Algorithms + Data Structures = Evolution Programs*, Springer-Verlag, New York, NY.

Milman, M. H. and Chu, C. C., (1994). "Optimization Methods for Passive Damper Placement and Tuning," *Journal of Guidance, Control and Dynamics*, 17, 848-856.

Miyamoto K., Determan, L. M. and Cilani, A., (2003). "Seismic Rehabilitation of Historic Concrete Structure with Fluid Visco-Elastic Dampers," *10th U.S.-Japan Workshop on Improvement of Structural Design and Construction Practices*, Maui, Hawaii.

Moreschi, L. M., and Singh, M. P., (2003). "Designs with Yielding Metallic and Friction Dampers for Optimal Seismic Performance", *Earthquake Engineering and Structural Dynamics*, 32(8), 1291-1311.

National Construction Estimator 2009 (2008). Craftsman Book Company.

National Earthquake Hazard Reduction Program, (2009). "2009 NEHRP Recommended Seismic Provisions for New Buildings and Other Structures," NEHRP.

Newmark, N. M. and Hall, W. J., (1982). "Earthquake Spectra and Design," *Engineering Monograph on Earthquake Criteria, Structural Design, and Strong Motion Records*, 3, Earthquake Engineering Research Institute, Oakland, CA

Newmark, N. M., Blume, J. A. and Kapur, K. K., (1973). "Seismic Design Spectra for Nuclear Power Plants," *Journal of the Power Division,* ASCE 97.

Onoda, J. and Hanawa, Y., (1993). "Actuator Placement Optimization by Genetic and Improved Simulated Annealing Algorithms," *AIAA Journal*, 31, 1167-1169.

Park, K.-W. and Koh, H.-M., (2004). "Preference-Based Optimum Design of an

Integrated Structural Control System Using Genetic Algorithms," *Advances in Engineering Software*, 35, 85-94.

Patil, V. B. and Jangid, R. S., (2009). "Response of Wind-Excited Benchmark Building Installed with Dampers," *The Structural Design of Tall and Special Buildings*, DOI: 10.1002/tal.523.

Paz, M., (1985), *Structural Dynamics: Theory and Computation*, Van Nostrand, New York.

Porter, K. A., (2007). "Fragility of Hydraulic Elevators for Use in Performance-Based Earthquake Engineering," *Earthquake Spectra*, 23(2), 459-469.

Porter, K. A., Beck, J. L., and Shaikhutdinov, R. V., (2004). "Simplified Performance-Based Earthquake Engineering Estimation of Economic Risk for Buildings," *Earthquake Spectra*, 20(4), 1239-1263.

Porter, K. A., Kiremidjian, A. S., and LeGrue, J. S., (2001). "Assembly-Based Vulnerability of Buildings and Its Use in Performance Evaluation," *Earthquake Spectra*, 17(2), 291-312.

Porter, K. A., Mirtrani-Reiser, J., Beck, j. L., and Ching J. Y., (2006). "Near-Real-Time Loss Estimation for Instrumented Buildings," *The Structural Design of Tall and Special Buildings*, 15(1), 3-20.

Ribakov, Y. and Gluck, J., (1999). "Optimal Design of ADAS Damped MDOF Structures," *Earthquake Spectra*, 15(2), 317-330.

RS Means, (2008). *2009 RS Means Building Construction Cost Data*, 67th Annual Edition, Reed Construction Data.

RS Means, (2008). *RS Means Square Foot Cost 2009*, Reed Construction Data.

SAC Joint Venture Guidelines Development Committee, (1995). *Interim Guidelines: Evaluation, Repair, Modification and Design of Steel Moment Frames, Report No. SAC-95-02*, Sacramento, CA, 6-52.

Segui, W. T., (2003). *LRFD Steel Design*, 3rd Edition, Thomson Brooks/Cole.

Seleemah, A. A. and Constantinou, M. C., (1997). "Investigation of Seismic Response of Buildings with Linear and Nonlinear Fluid Viscous Dampers," *Report No. NCEER 97-0004*, National Center for Earthquake Engineering Reserch, University of New York at Buffalo, Buffalo, NY.

Shinozuka, M. and Deodatis, G., (1991). "Simulation of Stochastic Process by Spectral

Representation," ASME, Vol. 44(4), 191-203.

Shinozuka, M., Zhong, R. H. and Wen, Y., (1992). "Cost-Effectiveness Consideration in Structural Control," *Proceeding of the Japan National Symposium/Workshop on Structural Response Control*, Japan

Shukla, A. K. and Datta, T. K., (1999). "Optimal Use of Viscoelastic Dampers in Building Frames for Seismic Force," *Journal of Structural Engineering* 125, 401–409.

Singh M. P., and Moreschi L. M., (2002). "Optimal Placement of Dampers for Passive Response Control," *Earthquake Engineering and Structural Dynamics*, 31, 955-976.

Singh, M. P. and Chu, S. L., (1976). "Stochastic Considerations in Seismic Analysis of Structures," *Earthquake Engineering and Structural Dynamics*, 4, 295-307.

Singh, M. P., (1980). "Seismic Response by SRSS for Nonproportional Damping," *Journal of the Engineering Mechanics Division*, ASCE, 106(EM6), 1405-1419.

Singh, M. P. and Moreschi, L. M., (1999a). "Genetic Algorithm-Based Control of Structures for Dynamic Loads," *Proceedings of IA-99*, Osaka University, Japan.

Singh, M. P. and Moreschi, L. M., (1999b). "Genetic Algorithm for the Optimal Passive Response Control for Seismic Structural Design," *Proceedings of the International Conference on Health Monitoring of Civil Infrastructure Systems, ICHMCIS'99*, On Board of Ship on Yangtze River, China, 237-242

Singh, M. P., and Moreschi, L. M., (2001). "Optimal Seismic Response Control with Dampers", *Earthquake Engineering and Structural Dynamics*, 30, 553-572

Singh, M. P., and Moreschi, L. M., (2002). "Optimal Placement of Dampers for Passive Response Control", *Earthquake Engineering and Structural Dynamics*, 31, 955-976

Singh, M. P., Singh, S., and Moreschi, L. M., (2002). "Tuned Mass Dampers for Response Control of Torsional Buildings", *Earthquake Engineering and Structural Dynamics*, 31, 749-769

Singh, M. P., Verma, N. P., and Moreschi, L. M., (2003). "Seismic Analysis and Design with Maxwell Dampers", *Journal of Engineering Mechanics*, 129(3), 273-282.

Skinner, R. I., Kelly, J. M., and Heine, A. J., (1974). "Hysteretic Dampers for Earthquake Resistant Structures," *Earthquake Engineering and Structural Dynamics*, 3(3), 287-296.

Soong, T. T. and Dargush, G. F., (1997). *Passive Energy Dissipation Systems in Structural Engineering*, John-Wiley & Sons, New York, NY.

Spanos, P. D. and Vargars L. M., (1985). “A Statistical Approach to Generation of Design Spectrum Compatible Earthquake Time History,” *Soil Dynamics and Earthquake Engineering*, 4(1)

Stender, J., Hillebrand, E. and Kingdom, J., (1994). “Genetic Algorithms in Optimization, Simulation and Modeling,” IOS Press, Amsterdam

Structural Engineers Association of California, (1996). “Conceptual Framework for Performance-Based Seismic Design,” *Appendix B to Recommended Lateral Force Requirements and Commentary*, 6th Edition, SEAOC.

Syswerda, G., (1989). “Uniform Crossover in Genetic Algorithms,” *Proceedings of the 3rd International Conference on Genetic Algorithms*, Morgan Kamfman.

Tajimi, H., (1960). “A Statistical Method of Determining the Maximum Response of a Building Structure During an Earthquake,” *Proceeding of 2nd World Conference on Earthquake Engineering*, Tokyo, 781-797.

Takewaki, I., (1997). "Optimal Damper Placement for Minimum Transfer Functions," *Earthquake Engineering and Structural Dynamics*, 26, 1113-1124.

Takewaki, I., (1999). "Optimal Damper Placement for Building Structures Including Surface Ground Amplifications", *13th ASCE Engineering Mechanics Division Conference*.

Tsai, C. S. and Lee, H. H., (1993). "Applications of Viscoelastic Dampers to High-Rise Buildings," *Journal of Structural Engineering*, 119(4), 1222-1233.

Tsai, C. S. and Tsai, K. C., (1995). "TPEA Device as Seismic Damper for High-Rise Buildings," *Journal of Engineering Mechanics*, 121, 1075-1081.

Tsai, C. S., (1993). "Innovative Design of Viscoelastic Dampers for Seismic Mitigation," *Nuclear Engineering and Design*, 139, 165-182.

Tsai, C. S., (1994). "Temperature Effect of Viscoelastic Dampers During Earthquakes," *Journal of Structural Engineering*, 120(7), 394-409.

Tsai, K. C., Li, J-W., Hong, C. P., Chen, H. W., and Su, Y. F., (1993). "Welded Steel Triangular-Plate Device for Seismic Energy Dissipation", *ATC-17-1 Seminar on Seismic Isolation, Passive Energy Dissipation, and Active Control*, San Francisco, CA, 687-698.

Tsai, K., Chen, H., Hong, C., and Su, Y., (1993). "Design of Steel Triangular Plate Energy Absorbers for Seismic-Resistant Construction," *Earthquake Spectra*, 9(3), 505-528.

Tsai, K., Chen, H., Hong, C., and Su, Y., (1993). "Design of Steel Triangular Plate Energy Absorbers for Seismic-Resistant Construction," *Earthquake Spectra*, 9(3), 505-528.

Tsuji, M. and Nakamura, T., (1996). "Optimum Viscous Dampers for Stiffness Design of Shear Buildings," *The Structural Design of Tall Buildings*, 5, 217-234.

Tversky, A. and Kahneman, D., (1974). "Judgment under Uncertainty: Heuristics and Biases," *Science*, 185, 1124-1131.

Wang, X. Y., Ni, Y. Q., Ko, J. M., and Chen, Z. Q., (2005). "Optimal Design of Viscous Dampers for Multi-Mode Vibration Control of Bridge Cables," *Engineering Structures* 27, 792-800.

Warszawski, A., Gluck, J. and Segal, D., (1996). "Economic Evaluation of Design Codes-Case of Seismic Design," *Journal of Structural Engineering* , 122(12), 1400-1408.

Wen, Y. K. and Ang, A. H-S, (1992). "Reliability and Cost-Effectiveness of Structures with Active Control," *Intelligent Structures-2, Monitoring and Control*, Elsevier, 63-71.

Wen, Y. K. and Shinozuka, M., (1998). "Cost-Effectiveness in Active Structural Control," *Engineering Structures,* 20(3), 216-221.

Wen, Y. K. and Kang, Y. J. (2001a). "Minimum Building Life-Cycle Cost Design Criteria. I: Methodology." *Journal of Structural Engineering*, 127(3), 330-337.

Wen., Y. K., Kang, Y. J. (2001b). "Minimum Building Life-Cycle Cost Design Criteria. II: Application." *Journal of Structural Engineering*, 127(3), 338-346.

Whiteman, R.V., Hong, S. T. and Reed, J. W., (1973). "Damage Statistics for High-Rise Buildings in the Vicinity of the San Fernando Earthquake" *Department. of Civil Engineering, Report No. 7, R73-24*, MIT, Cambridge, MA.

Whitney, A., (2002). "Cost of Demolition of Downtown's Dirty Dozen," Cityscape, Detroit.

Wongprasert, N. and Symans, M. D. (2004). "Application of a Genetic Algorithm for Optimal Damper Distribution within the Nonlinear Seismic Benchmark Building," *Journal of Engineering Mechanics,* 130(4), 401-406.

Wu, B., Ou, J. P., and Soong, T. T., (1997). "Optimal Placement of Energy Dissipation Devices for Three-Dimensional Structures," *Engineering Structures*, 19, 113-125.

Xia, C. and Hanson, R., (1992). "Influence of ADAS Element Parameters on Building

Seismic Response," *Journal of Structural Engineering*, 118, 1903-1918.

Yun, S. Y., (2000) “Investigation on Performance, Prediction and Evaluation of Low Ductility Moment Frames.” *Ph.D. thesis*, University of Illinois at Urbana-Champaign, Urbana, IL

Zalzala, A. M. S. and Fleming P. J., (1997). “Genetic Algorithms in Engineering Systems,” Institute of Electrical Engineers, London

Zhang, R. H. and Soong, T. T., (1989). "Seismic Response of Steel Frame Structures with Added Viscoelastic Dampers," *Earthquake Engineering and Structural Dynamics*, 18, 389-396.

Zhang, R. H. and Soong, T. T., (1992). "Seismic Design of Viscoelastic Dampers for Structural Applications," *Journal of Structural Engineering*, 118(5), 1375-1392.